WARWICK
THE UNIVERSITY OF WARWICK

ANALYSIS OF COHESIVE SUBGRADE SUBJECT TO LONG TERM CYCLIC LOADING

Natalie Wride

A thesis submitted in partial fulfilment of the requirements for the degree of Doctor of Philosophy

School of Engineering, University of Warwick

April 2022

Contents

List of Figures

List of Tables

In loving memory of

James Taylor (1926 - 2017)

and

Betty Taylor (1930 - 2021)

Acknowledgements

Firstly, my sincere gratitude goes to my supervisor Dr. Xueyu Geng for her support during my PhD. For the opportunities she has given me, the advice, reviews and feedback she has provided throughout this process and the encouragement I have received. I would also like to thank my second supervisors, Dr. Stefano Utili and Prof. Toby Mottram for their contributions to my studies, since I first appeared as an undergraduate.

I wish to thank the students and staff at Zhejiang University of Technology and Tongji University for welcoming me during my secondment. This opportunity was an incredible experience that would not have been possible without funding from the Marie Curie research and innovation exchange programme, for which I am extremely grateful. In particular, I would like to extend my thanks to Dr. Zhen-yu Yin, Dr. Ni Jing and Dr. Li Shi for their support and advice during my time abroad.

I would also like to express my gratitude to my employers during my studies, Arup and Rendel, for encouraging me to pursue my studies, especially to Sachin Kumar for supporting me through my professional Chartership.

This research was funded by EPSRC and I am grateful for the feedback I have received from HS2 Ltd., particularly providing soil samples for my research.

Finally, my greatest gratitude goes to my family and friends for their support on this journey. To my Mum, my motivation, my Uncle Nigel and my Brother Sam, for your love and support, without which this would not have been possible. I am extremely fortunate to have you. To Annie and Harriet for always being there and to the memories we have created along this journey. To Luc, Hannah, Shelby and Raman, your company has kept me going when I have struggled and I am forever grateful for your friendship. And finally to Paul, your support means more than you will ever know.

Declaration

I declare that this thesis has been composed solely by myself and that it has not been submitted, in whole or in part, in any previous application for a degree. Except where states otherwise by reference or acknowledgment, the work presented is entirely my own.

I confirm that this thesis presented for the degree of Doctor of Philosophy, has been composed entirely by myself, is solely the result of my own work and has not been submitted for any other degree or professional qualification

I declare that this thesis was composed by myself, that the work contained herein is my own except where explicitly stated otherwise in the text, and that this work has not been submitted for any other degree or processional qualification except as specified.

Parts of this work have been published by the author:

Wride N.M., Geng X-Y. (2018) Analysing the Permanent Deformation of Cohesive Subsoil Subject to Long Term Cyclic Train Loading. *Proceedings of China-Europe Conference on Geotechnical Engineering, pp. 628–631.*

Wride N.M, Geng X-Y. (2019) Analysis of preloaded cohesive subgrade soils subject to cyclic loading. *15th International Conference on Railway Engineering.*

Wride N.M. Geng, X-Y. Zhou, W.H. Cui, Y-J. (2016) Partially drained response of cohesive soils subjected to cyclic loading. *Proceedings of XVII European Conference on Soil Mechanics and Geotechnical Engineering.*

Abstract

Rail transportation is a key consideration for the future of sustainable cities. As cities develop and grow, greater demands are placed on existing infrastructure, and as rail networks expand, the construction of new routes will be governed by land availability. In this case, it is likely these routes will transit soft clay subgrade material. Quantifying the response of cohesive subgrades under repeated loading is therefore important for both the design and construction of future rail links and the maintenance of existing routes.

A body of triaxial test data is presented examining the performance of reconstituted kaolinite samples to cyclic loading. Reconstituted Gault clay samples, obtained from bulk samples, where also tested. In total, 20 monotonic tests, 59 cyclic triaxial tests and 12 post-cyclic triaxial tests were performed in this study. These tests examined the influence of load frequency and load magnitude, defined in terms of a cyclic stress ratio, to characterise the cyclic behaviour. Further studies demonstrated the performance of cohesive subgrade material considering preloading and examined the response of a sample under partial drainage. The laboratory tests were complimented by an undrained cyclic numerical model, extended to consider vertical drainage. Finally, the influence of various factors on cohesive subgrade beneath slab track were analysed and design charts presented to determine the cyclic stress for input to the numerical model.

Findings of this study highlighted some of the key considerations for cohesive subgrade soils when subjected to cyclic loading and the influence on the strain accumulation and excess pore pressure response. For the Gault clay, the difference in response with respect to the compressibility of the samples was investigated considering the plasticity of the clay. The results from this study provided further validation data for the existing undrained cyclic model, and predictions of partially drained soil response are in good agreement with the case studies analysed.

Chapter 1

Introduction

1.1 Background and Objectives

In the UK, a report released by the Department for Transport reported transportation was responsible for 27% of the UK's total emissions in 2019 (Department of Transport (2021)), greater than any other sector. Of this proportion, over 90% was due to road transport. With the current climate emergency, an increasing population and therefore the expansion of towns and cities creating a greater need for interconnectivity, it is important to focus on more sustainable transportation solutions and public transport.

Railways have been a form of land transport used for both the transportation of goods and people across the UK for over 180 years. Over the years, demands on the rail network coupled with improvements and advances in engineering and technology have resulted in increased train speeds and train loading, presented in Figure 1.1.

For existing rail infrastructure, increasing passenger numbers could result in an increasing frequency of train passage, expansion of train lengths resulting in increased rail traffic duration or adaptation of carriages resulting in greater train loading. Under these conditions, more stringent conditions are being placed on existing infrastructure. Several of the key transportation links, such as the West Coast Main Line (WCML), a key railway corridor in the UK connecting major cities between Glasgow and London, are ageing pieces of infrastructure

that were not designed to accommodate these increases in loading and speed (Woodward et al. (2014)).

Another option is therefore the creation of new rail links, capable of accommodating increased passenger demands, such as High Speed Two. As advances in track and rail technology have meant increasing speeds can be achieved, this becomes a key benefit to encourage a shift from road to rail transport. However, new lines are governed by the availability of land for construction and in some cases are trafficking soils that would have previously been avoided for development, characterised by their high compressibility and low strength. These clay subgrades can therefore cause problems for rail lines where the linearity of the system is a key requirement.

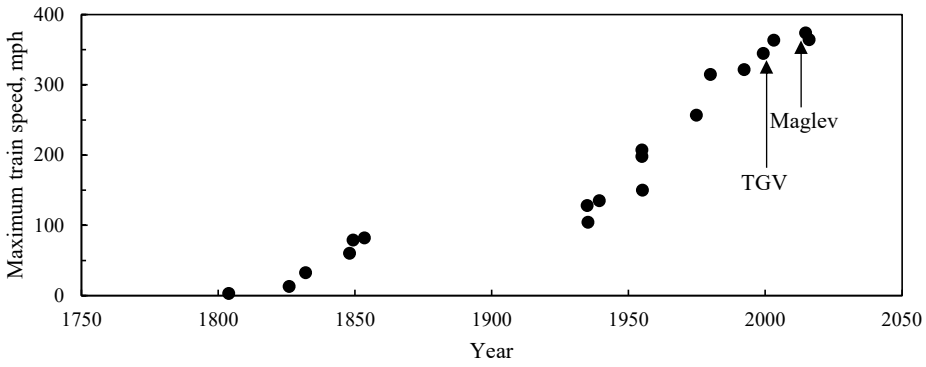

Figure 1.1: The evolution of train speed

Over the last 20 years, new rail systems, particularly those of high-speed lines, have began to adopt concrete slab track systems rather than traditional ballasted track. The rigidity of the slab system reduces the effect of train passage on the underlying clay subgrade soil, however the continuity of this system means settlement tolerances are more onerous than for ballasted track. Furthermore, when clay subgrade deterioration under cyclic loading occurs, subsequent train passages result in concentrated load that can lead to slab cracking.

Maintenance and repairs of this slab system are more costly and time consuming compared to ballast track and due to this, in the short term, result in speed restrictions should undesirable settlements occur. If the full benefits of a slab track high speed rail system are to be realised, it is therefore important to understand the response of underlying clay subgrade soils under repeated

loading. To meet this purpose the following research objectives were set:

- Establish a limiting strength that could be considered for a clay soil to remain in-situ without excavate and replace. Considering this limit, undertake a series of undrained monotonic and cyclic triaxial tests on laboratory prepared kaolin samples to propose a reference framework for the influence of load magnitude and load frequency on the samples and develop an empirical relationship for the strain and excess pore pressure accumulation under cyclic load. Establish the post-cyclic response and strength attainment as a result of cyclic loading.

- Perform monotonic and cyclic triaxial tests to investigate factors that influence the performance of a clay subgrade soil in the field. In the first instance, examine the influence of preloading considering the framework of kaolin tests performed. Determine the effect of preload on the post-cyclic strength of the sample and develop an empirical relationship. Another in-situ consideration is that of partial drainage, therefore investigate cyclic triaxial tests on the kaolin samples under partial drainage and establish a series of recommendations for performing tests using standard cyclic triaxial equipment.

- Validate an existing undrained cyclic model, extending the previous assessments to consider it's performance with respect to overconsolidated samples representative of treated soft subgrade layers. Extend the analysis of the model to consider the case of partial drainage under vertical drainage exhibited by the triaxial tests.

- Perform monotonic, cyclic and post-cyclic triaxial tests to assess the performance of high plasticity Gault clay samples obtained from bulk samples excavated in Oxford. Expand the cyclic assessment on kaolin clay to high plasticity site-won samples, representative of cohesive subgrades.

- Validate the performance of the cyclic model considering partial drainage using existing case studies for traffic loading, adopting a 2D FE model to determine stress influence at subgrade level due to rail track interaction.

Through the above research objectives, a body of undrained monotonic, cyclic and post-cyclic triaxial tests are presented. The conditions and geotechnical parameters analysed have practical implications for the stability of cohesive subgrades underlying rail track systems and recommendations can be made with respect to the design life of transportation infrastructure.

1.2 Thesis Structure

This thesis comprises 8 Chapters, inclusive of this introduction. Chapter 2 provides an overview of the relevant literature related to the response of clay soils when subjected to cyclic loading. Chapter 3 introduces the cyclic triaxial cell apparatus, presenting a study of the performance of reconstituted kaolin samples subject to monotonic and cyclic undrained triaxial tests. The influence of the load magnitude and frequency of loading is examined and the post-cyclic response presented. Chapter 4 summarises a suite of cyclic triaxial tests that have been performed considering conditions that could be more applicable to the in-situ condition of a clay subgrade. The influence of preloading is presented, focussing on the degree of improvement with respect to the economic considerations of soft soil treatment. The influence of partial drainage has also been examined. Chapter 5 sets out the cyclic model developed by Ni (2012), extending the solution to consider vertical drainage. Chapter 6 synthesises the conclusions on the cyclic performance of clay soils based on the kaolin studies, examining the response of Gault clay. Chapter 7 subsequently presents a series of design charts for the stress influence beneath rail track systems and the sensitivity of typical soil types under partial drainage. Finally, conclusions on the cyclic performance of clays are presented and recommendations for future work are summarised in Chapter 8.

Chapter 2

Literature Review

There are several influence factors that influence the cost of a new rail route which can subsequently affect the soil subgrade response to high speed train loading. Lichtberger (2005) considers the key cost factors for a high-speed rail line to be the selection of the rail route and therefore governing soil lithologies and topography of the area, weather conditions of the region under development, the type of track and the desired speed of the new line. Herein, this study will focus predominately on the influence of soft lithologies whereby at high speeds, the linearity of the system, and as such vertical differential tolerances of the system are an important feature. When tolerances are exceeded, this can lead to;

- Passenger discomfort due to undesirable train motions.
- Potential concentrated zones of track deformation that are further enhanced with routine train passage,
- That in turn lead to increased track repairs and maintenance, reduced operational line speed, or,
- Potential train derailment

Existing projects worldwide have acknowledged the contribution of repeated loading to the overall settlement of soft deposits. The soft marine Ariake clay of the Saga Plain, Japan, has been an area of interest for a number of researchers (Hyodo et al. (1992); Miura and Hayashi (1995); Yasuhara et al. (1982)). In

2002, the subsoils beneath shallow embankments situated at Saga airport were analysed by Chai and Miura (2002) where the 20.0m thick Ariake clay sublayer documented in the area underwent significant vertical settlements both during and post embankment construction, experiencing 38mm settlement in the first 56 days of construction and approximately 0.7 m vertical settlement 4 years after the construction of the 3.0m high embankments. Previously, Fujikawa et al. (1996) had found traffic induced settlement had accounted for 50% of the total vertical settlement measured (approximately 400 – 600mm) on the Saga airport expressway. It was concluded traffic loading could be apportioned to the settlements experienced where Chai and Miura (2002) estimated the depth of influence of traffic loading for shallow embankments could be up to 6.0m below the base of the embankment, shown in Figure 2.1(a), whilst Samang et al. (2005) concluded traffic loading induced settlement could account for 20% of the total settlement, lower than previously established by Fujikawa et al. (1996). Similar conclusions on the influence of traffic loading on the vertical settlement of the Saga site have been documented by Hu (2010) using an analytical solution.

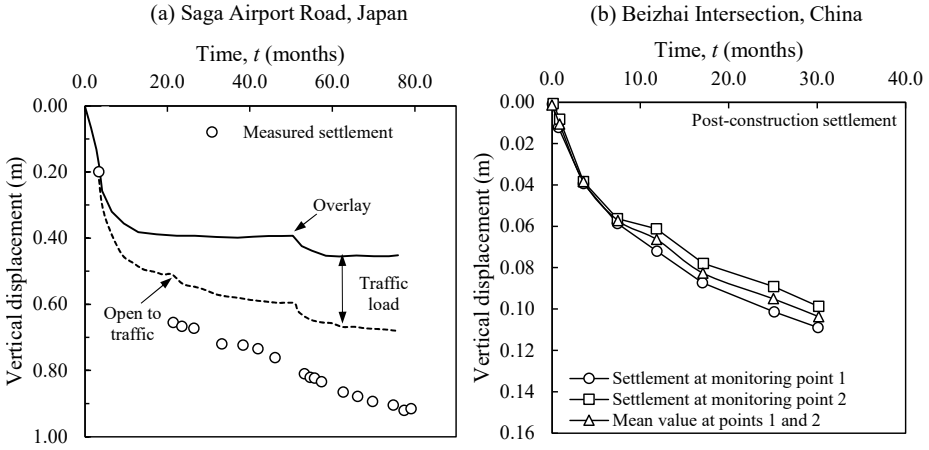

Figure 2.1: Vertical settlements from case studies at Saga Airport, reproduced from Chai and Miura (2002) and Beizhai Intersection, reproduced from Cui et al. (2014)

Although significant interest has been paid to the soils of the Saga Plain, further case studies examining transportation earthworks settlements have also been documented in China. Ling et al. (2002) reported cumulative pavement settlement of over 100mm after 2.5 years at the Beizhai Intersection of the Outer-Ring line in Shanghai which opened to traffic in January 1999 to

approximately 1500 vehicles a day (Cui et al. (2014)), shown in Figure 2.1(b). Whilst He (2005) reported traffic-induced settlement of approximately 300 mm on the Shenzhen-Shantou Expressway, even after surcharge preloading of the subgrade prior to construction.

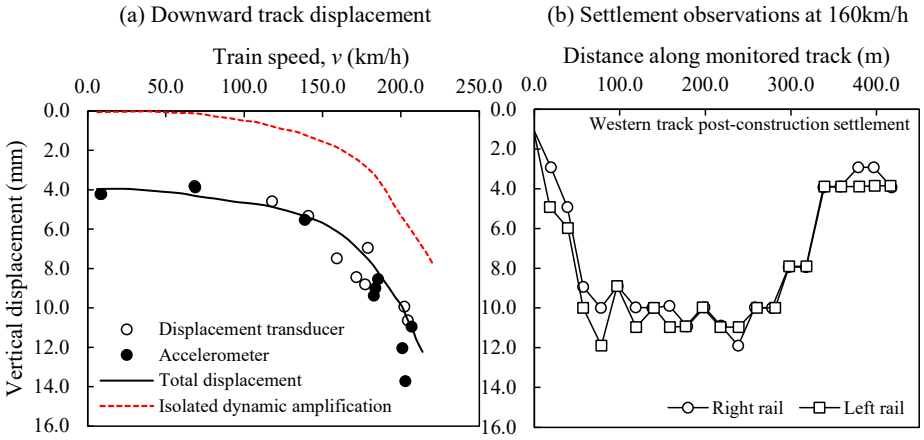

Figure 2.2: Dynamic amplification and measured vertical settlement at Ledsgård, reproduced from Banverket (1999) and Holm et al. (2002) respectively

Considering the influence of train passage rather than vehicle passage however, dynamic amplification of displacements has been shown to occur at high train speeds, due to the influence of the soft soil. In the early 1990's, the West Coast Rail Line of Sweden was upgraded with the placement of new UIC (International Union of Railways) track to facilitate the introduction of high-speed commuter trains with a maximum speed of 200km/h.

Ledsgård, 25.0km south of Gothenburg in Sweden, is situated along the West Coast railway line and comprises approximately 3.0m of organic soil close to ground level with an undrained shear strength of approximately 15kPa to nearly 8.0m depth (Holm et al. (2002)), defined as 'very low' strength material in accordance with BS EN ISO 14688-2 (2018). Initially, the vibrations generated at 200km/h were nearly 10 times greater than those under previous traffic and the speed was subsequently reduced to 160km/h, and then further to 130km/h (Banverket (1999)). Monitored settlements from 1998 to 1999 under a train speed of 160km/h demonstrated significant settlements in the zone of the organic, soft, highly compressible gyttja formation, presented in Figure 2.2(b) when compared to the last 50.0m of monitored track (between 350 and 400m increments).

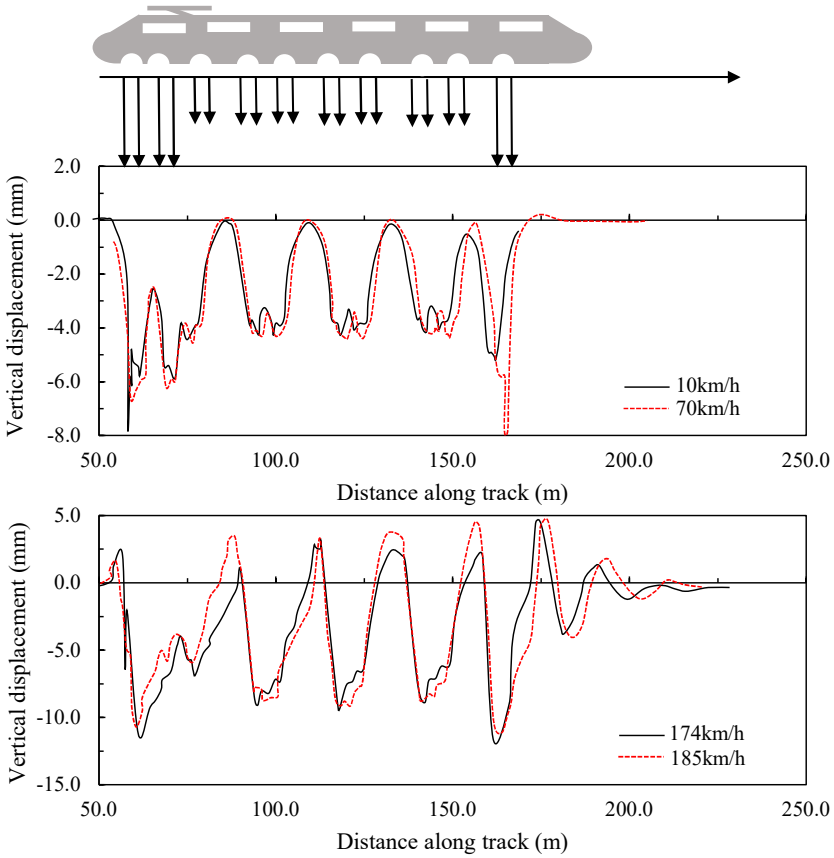

Figure 2.3: Increase in displacements with train speed at Ledsgård, reproduced from Holm et al. (2002)

Furthermore, Banverket (1999) demonstrated that as the velocity of the train increased, the dynamic amplification of the displacements increased such that at 200km/h, shown in Figure 2.2(a) the displacements were over 10mm in amplitude. This can be seen more clearly in Figure 2.3, presenting the vertical track displacements at various different speeds. Subsequently, the site as Ledsgård was remediated by dry deep mixing with lime-cement columns (Holm et al. (2002)).

Similar observations have been found at Stilton Fen, in the United Kingdom, whereby the high speed rail line transitted the Thames Marshes, and in Holland, considering the displacements of the Amsterdam-Utrecht line over soft clay and peat layers. Woldringh and New (1999) examined all three ballasted track case studies, shown in Figure 2.4 where Carchiolo et al. (2017) subsequently

proposed the dynamic amplification as a result of the introduction of a concrete slab track system would reduce. This slab track dynamic amplification factor aligns closely with the findings of Song et al. (2011). In China however, there have since been cases of significant settlements beneath slab track systems of the high speed rail network and evidence of slab cracking (Zhai and Zhao (2014)), since whilst the displacements are reduced, the tolerances for adjustment of such a system is also limited.

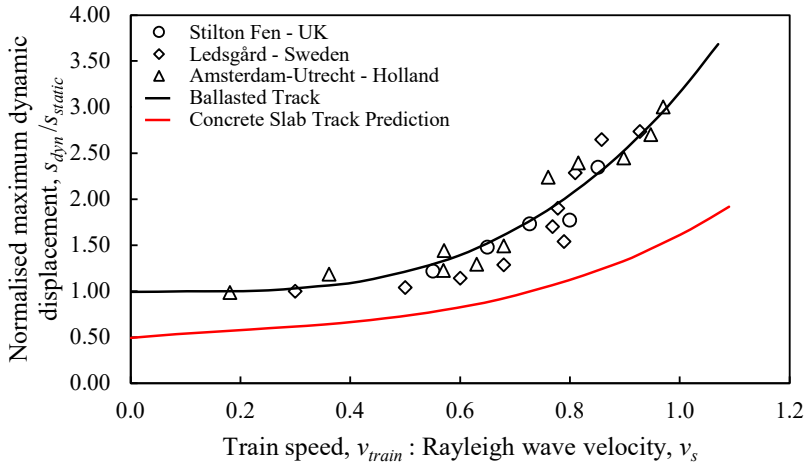

Figure 2.4: Relationship between normalised maximum dynamic displacement, otherwise defined as dynamic amplification, and normalised train speed, reproduced from Carchiolo et al. (2017)

2.1 Rail Systems

As presented in Chapter 1 Figure 1.1, the speed of rail traffic and rail loadings have continually increased with the chronological development of rail technology. Most notably, in the last 30 years, the development of high-speed rail has continued to push the boundaries and capabilities of rail infrastructure. In order to consider the influence of train passage on a soft lithology, it is however important to consider the interactions that lead to the distribution of load to the subgrade layers. Examining the response of a soft soil, the interaction between three different components should be considered; the source of the load and vibration, the transmission or passage of the load and the response of the soil and track systems to the load, shown in Figure 2.5.

The passage of a train results in a series of forces transmitted to the track via the train wheelsets. Vertical and horizontal forces comprise both quasi-static and dynamic components of low and high frequency, transferred from vehicle eventually through to subgrade and subsoil level. As shown in Figure 2.5, from vehicle to bogie and to wheel set, these behaviours can be characterised mathematically where both elastic and damping elements, k and c in Figure 2.5, are acknowledged. Below this, at permanent way and subsequently track system level, the purpose of the system is to distribute these transmitted forces such that permissible limits of the system are not exceeded. There are commonly two forms of track system for this purpose, summarised in the following subsections. Section 2.1.1 explores the construction of permanent way infrastructure and the advantages and disadvantages of two forms of track system, whilst Section 2.1.2 presents a review of train loading.

2.1.1 Track Components

As technology has advanced, track infrastructure has had to adapt. Higher speeds and greater track loading discussed above have led to developments in track technology. Whilst ballast track is prevalent across the word, in recent decades ballastless technology has been used in newly built lines, particularly for high-speed rail links. As of 2012, across the world over 10,000km of slab track has been constructed. Figure 2.6 presents both ballast and slab track system arrangements alongside the track bed terminology adopted for High Speed Two in the UK.

2.1.1.1 Ballast Track

Ballast track, shown in Figure 2.6(a), comprises wooden, or more typically concrete, sleepers that rest on a ballast bed. Beneath the ballast, a sub-ballast layer forms the transition to formation whilst also acting as a protection layer to the underlying subgrade soil. The ballast takes the compressional forces imparted on it by the sleepers that subsequently generate the compressional strain in the underlying subgrade soil. Due to the presence of the granular ballast layer, voids will inherently exist beneath the sleeper-rail permanent way system. In this case, it is considered to be a floating support and as a result,

under the repetition of dynamic forces, the geometry of the system can begin to deteriorate, sometimes known as the 'churning' of ballast. The solution and repairs required for this system are however low cost.

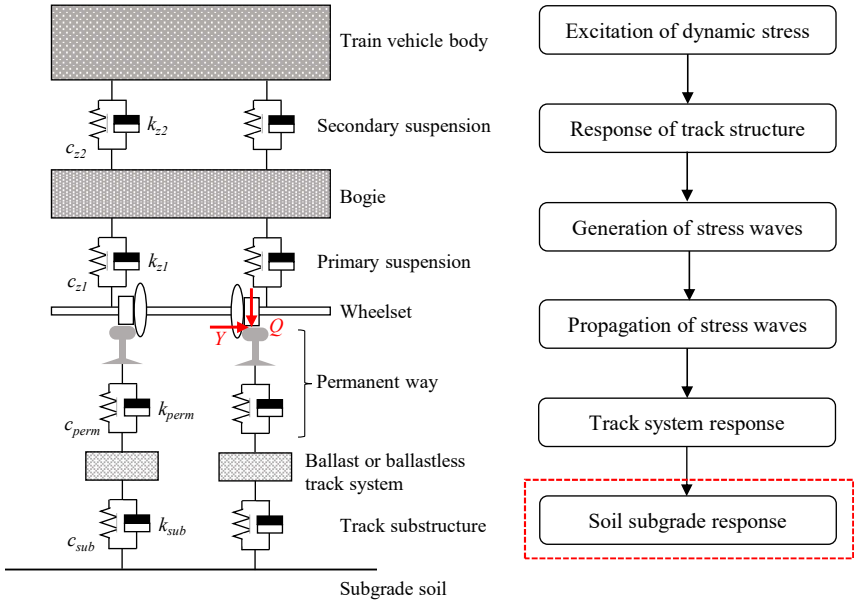

Figure 2.5: Schematic representation of the wheel-track system, after Esveld (2001) and Lichtberger (2005) and the generation of interactions between components for soil subgrade response

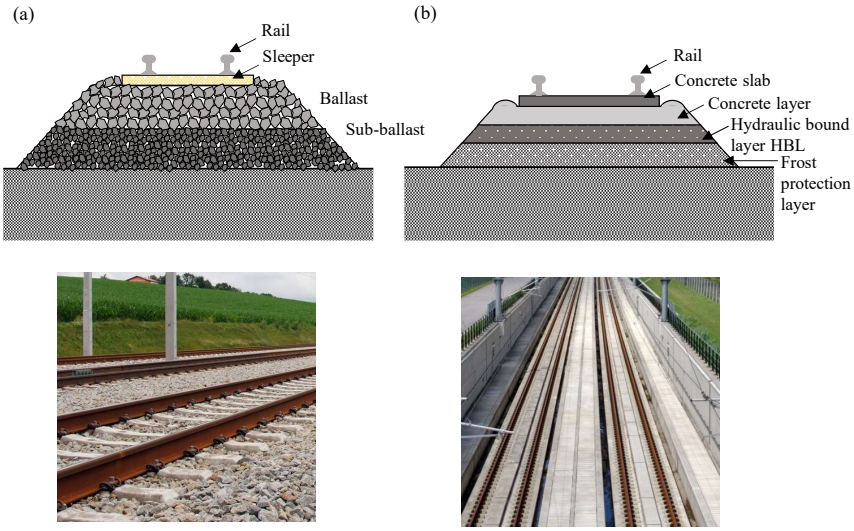

Figure 2.6: Schematic diagram of (a) Ballast track formation and (b) Slab Track Formation

2.1.1.2 Ballastless Track

Ballastless track, more specifically slab track systems as shown in Figure 2.6(b), have become more prevalent with higher operational speeds of rail lines across the world. In such a system, reinforced concrete slabs replace the ballast as the component of load bearing of the transmitted static and dynamic forces. This slab system rests on a concrete layer, hydraulic bound layer (HBL) otherwise known as a cement-bound base layer and a frost protection layer. It is much more rigid than a granular ballast system, therefore reducing the effect of the loading on the subgrade system. However, the linearity and continuity of a slab system means the sensitivity to settlement increases, dependent on the slab system selected. A summary of ballastless systems is presented in Table 2.1. As of 2012, over 4391km of track had been constructed using the Bögl system which has been adopted on the Beijing to Shanghai high-speed line, whilst over 3000km had been constructed with Shinkansen and 2205km with Rheda systems (Michas (2012)).

Table 2.1: An overview of ballastless track systems, adapted from Casal (2010)

Discrete rail support				Continuous rail support	
With sleepers		Without sleeper			
Embedded	Non embedded	Prefabricated concrete slabs	Direct rail fastenings	Embedded rails	Clamped rails
Rheda® (Germany)	FFYS®* (Germany)	Shinkansen® (Japan)	Civil structures (Netherlands)	Embedded rail structure (ERS) EDILON corkelast ®	Cocon ®
Züblin® (Germany)	SATO®* (Germany)	Bögl® (Germany)	Monolithic in-situ slabs		ERL ®

* indicates the use of ashphalt layers

Slab track systems have a number of benefits over the traditional ballast track, namely;

- Reduced maintenance due to lack of ballast churning and inability for rails to buckle due to their vertical and lateral confinement in the slab. Esveld (2001) estimated this reduction to be in the order of 70-90% in comparison with ballasted track.
- In turn, in comparison with ballasted track, the life-time operational and

maintenance costs have been estimated by Casal (2010) to be around 20-30% due to reduced maintenance and increased service life of the slab system. Balfour Beatty Rail Technologies (2003) estimate this service life increase to be in the order of up to 50%.

- Reduced weight and height of track, resulting in more permissible uses than ballasted systems, such as tunnels and viaducts.

The cost of a slab track system is however initially greater than that of ballast and due to the continuous nature of many slab systems, repairs are more costly and require significant more time than that of the more familiar ballast track system. Therefore, in order to realise the benefits of slab track, particularly with regards to the reduced maintenance that is crucial for the operation of rail infrastructure, the subgrade layers must be capable of withstanding the loads imposed on them by the overlying train-rail-slab track system.

2.1.2 Train Load Component

Section 2.1 demonstrated the importance of considering the stability of the subsoil beneath the track system, particularly considering slab track systems, with respect to maintaining a rail line at optimal performance. However, a key input to the problem of ensuring the load bearing capabilities of a subsoil, is the magnitude of the load applied to the system. Section 2.1.2.1 explores the options for the load model to represent a train passage whilst Section 2.1.2.2 considers the magnitudes of loading that are typical of trains from around the world. Section 2.1.2.3 subsequently presents the attempts to classify this load for industry purposes.

2.1.2.1 Load Models

The application of load, and subsequently the applied cyclic stress to the soil subgrade, has been modelled using a range of time varying load profiles. Andersen et al. (1980) and Moses et al. (2003) concluded the shape of the load pulse, a range of variations of which are presented in Figure 2.7, had a negligible affect on the overall soil behaviour, although the profile considered in the studies was trapezoidal; a close fit to the sinusoidal profile that is most

commonly adopted. A sinusoidal profile has been adopted by a number of authors (Suiker et al. (2005), Erken and Can Ulker (2007), Ni (2012), Cai et al. (2013), Lei et al. (2016), Guo et al. (2018), Wang et al. (2021)), whilst Andersen et al. (1980) considered a trapezoidal cyclic stress profile such that the profile was approximated to that of an equivalent sinusoidal profile. This was applied for 5000 load cycles to undrained samples by the authors. Later, Miller et al. (2000) and Pillai et al. (2014) also examined trapezoidal waveforms when undertaking cyclic triaxial tests, discussed further in Section 2.3, on Vicksburg clay and kaolinite respectively. Similarly, based on numerical analyses to determine stresses in the ground in response to train passage, Powrie et al. (2007) recommended undertaking Hollow Cylinder Apparatus (HCA) tests in which either the trapezoidal or sinusoidal stress paths, presented in Figure 2.8, could be superimposed to reflect the application of a stress state induced by a train wheel load.

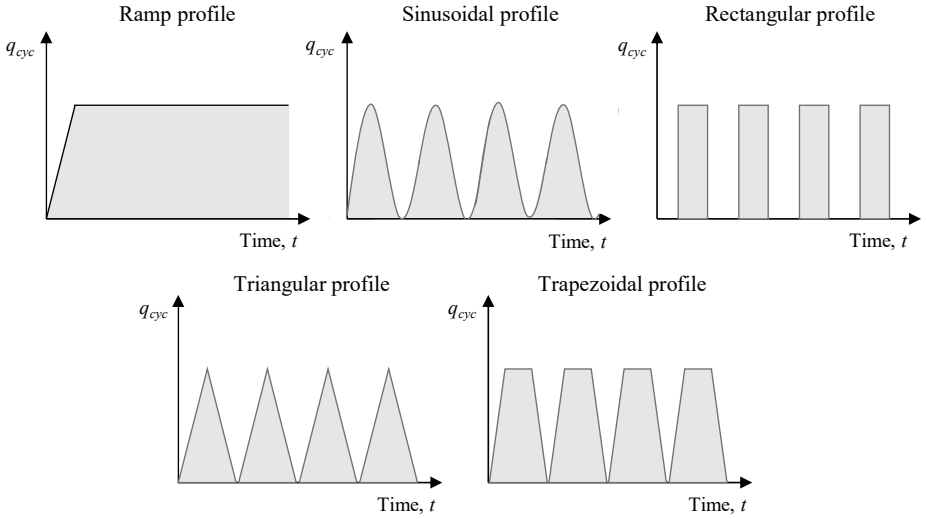

Figure 2.7: Time varying load profiles

A triangular profile was considered at high frequencies of cyclic triaxial tests conducted by Procter and Khaffaf (1984), however this was a function of the pneumatic system used for the application of cyclic load, limited by the frequencies in which a 'degraded square waveform' was initially adopted. Similarly, the system appeared to apply a rectangular waveform at the other end of the freqeuncy range, at low frequencies, enabled by the pneumatic

apparatus. Fujikawa et al. (1996) and Huang et al. (2006) also proposed a triangular profile based on field measurements of the Saga Airport site on Ariake clay. Hu (2010) considered a rectangular profile, later extending the analysis to a semi-sinusoidal profile when determining an analytical solution to assess the settlement of the same case history. A rectangular stress profile has also been examined by Fu et al. (2016) and Frost et al. (2004), in which over 60 repeated load tests were performed on samples obtained from various sites in the UK. Frost et al. (2004) concluded pavement subgrade could remain stable provided it had sufficient stiffness and strength, and given consideration for the applied cyclic load which is discussed in greater detail in Section 2.3. The application of a specific stress profile, presented in Figure 2.7, did not contribute to the conclusions of the study.

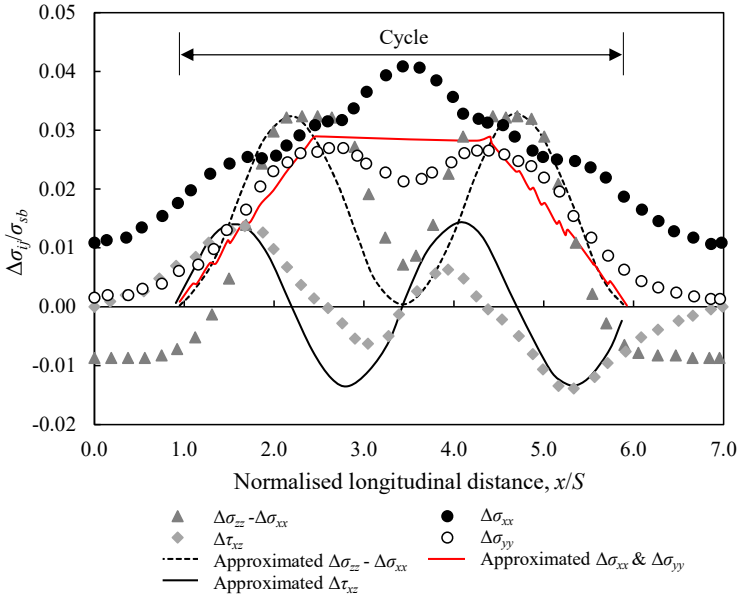

Figure 2.8: Stress path subject to train loading where S is the sleeper length, σ_{ij} represents the normal stress in x,y,z directions and σ_{sb} is the maximum surface stress (axial load/sleeper area), reproduced from Powrie et al. (2007)

2.1.2.2 Train Loads

The loading induced as a result of the passage of a train typically comprises two parts, namely the cyclic vertical component and a lateral moving load. This study focusses on the cyclic loading component, determined from the

self-weight of the vehicle, distributed to the track and substructure through the wheels of the vehicle. For the purpose of the determination of loading for laboratory tests, this is typically assumed to act as a point load located at the centre of each wheel axle of the train. A review of high speed train parameters is presented in Table 2.2. This creates a cyclic load as the train transits over a specified location, with the frequency of this load governed by the speed and total length of the train carriages and also the spacing between bogies, as defined in Figure 2.9. A range of high speed train dimensions and loads are presented in Table 2.3, described according to Figure 2.10.

Based on the high speed train dimensions described in Table 2.2, Table 2.3 presents the average and peak train speeds for each vehicle and the corresponding total train length. Assuming the loading as a result of axle load, P, at each wheel axle location can be represented by dynamic load, q, with the simplified profile shown in Figure 2.11 by the solid line on the load time graph, for laboratory testing the loading profile can be simplified to different load patterns, as discussed above. In this case; trapezoidal, represented by the blue dashed line, and semi-sinusoidal, shown by the red dashed line in Figure 2.11. Based on these profiles and assuming the interval between loads is described by the bogie spacing, b, the cyclic load frequency of each train can be determined. In each calculation, the bogie spacing for the passenger carriages has been used as this is the most frequent carriage component.

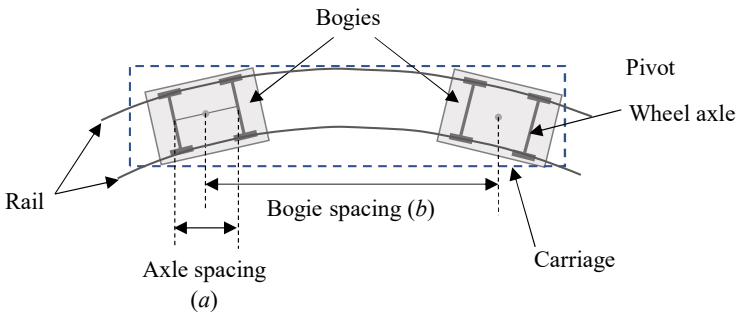

Figure 2.9: Definition of terms

The frequency associated with the high speed trains listed in Table 2.2 is presented in Table 2.3 for both the average and top speeds of each route listed. The frequencies range from 1.6Hz (Amtrak Acela) to 6.5Hz (CRH2 and CRH3)

calculated using the bogie spacing. The high speed train routes listed in Table 2.3 comprise a range of routes of varying lengths from across the world that are either built on slab track or ballast track. It should be noted slab track is now the standard in high speed rail track construction in Japan (Miura et al. (1998)). Whilst it is noted European train lines have typically used ballasted track, many lines have implemented areas of slab track. For instance, the Channel Tunnel section of the Eurostar line between London and Paris implemented slab track in order to provide overheard clearance for larger trains (Bonnett, 2005). Some newer European lines such as the Frankfurt to Cologne link constructed in 2002, have since been totally constructed using slab track.

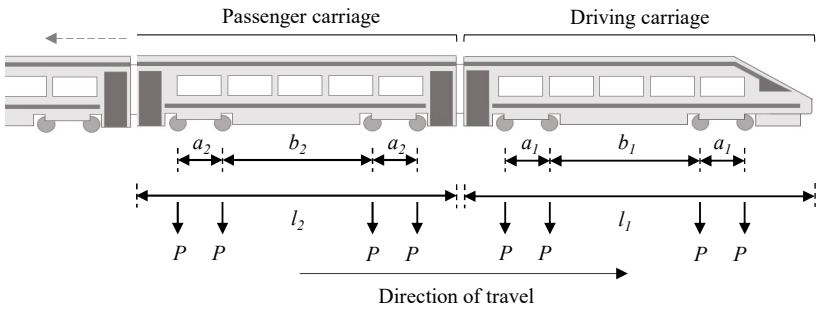

Figure 2.10: Definition of vehicle loads

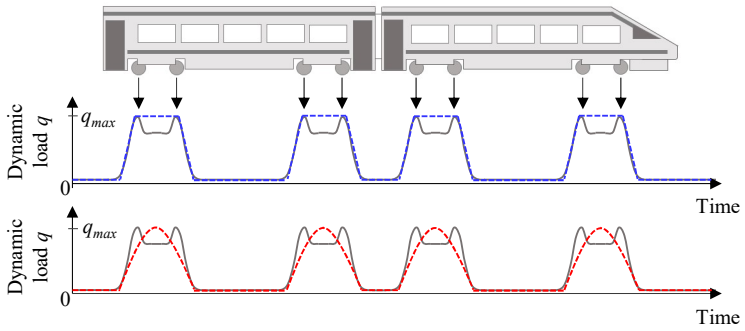

Figure 2.11: Simplified train loading patterns

The load, determined above as P in Table 2.3 generates a stress in the underlying subgrade as it is transmitted via the bearing of the slab or ballast system. Most commonly in practice, this load is modified, described in Section 2.1.2.3, however an initial design chart was presented by Heath et al. (1972), otherwise known as the British Rail Method (Burrow et al. (2007)) to define the

required subgrade soil modulus capable of withstanding the applied static axle load. The initial chart is presented in Figure 2.12.

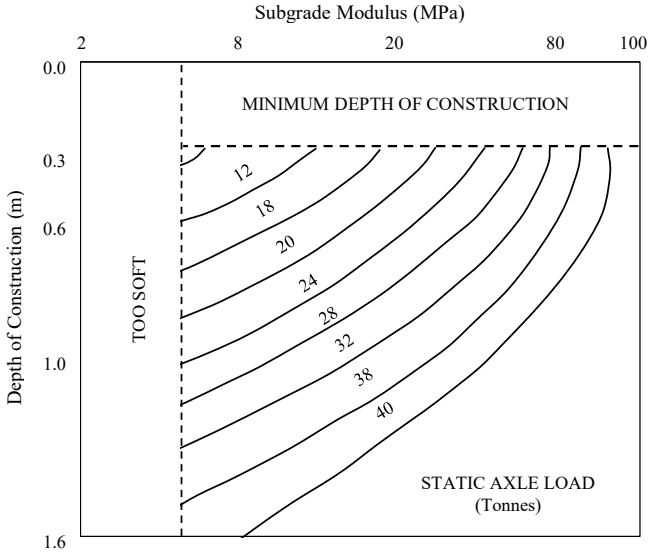

Figure 2.12: The British Rail Method, reproduced from Heath et al. (1972)

Table 2.2: Summary of train vehicle parameters

Reference	Train	Driving carriage			Passenger carriage			Maximum axle load
		Axle spacing a_1	Bogie spacing b_1	Carriage length l_1	Axle spacing a_2	Bogie spacing b_2	Carriage length l_2	P
Jiang et al. (2016) Pandrol UK (2014)	CRH2	2.50m	17.50m	25.00m	2.50m*	17.50m*	25.00m*	167kN
Bian et al. (2015) Pandrol UK (2014)	CRH3	2.50m	14.88m	25.00m	2.50m*	14.88m*	25.00m*	167kN
Connolly et al. (2014) ALSTOM (2016)	TGV	3.00m	11.00m	22.15m	3.00m	15.70m	21.84m	167kN
Connolly et al. (2014) ALSTOM (2016)	Thalys	3.00m	11.00m	22.15m	3.00m	15.70m	18.70m	167kN
Kawasaki (2010)	ICE-1	3.00m	11.46m	20.56m	2.80m	17.00m	26.40m	191kN
Kawasaki (2010)	ICE-3	3.00m	17.00m	25.84m	2.80m	17.00m	24.78m	157kN
ALSTOM (2016)	NTV AGV	3.00m	17.10m	22.80m	3.00m	15.70m	17.30m	167kN
Cahill et al. (2015) UIC (2004)	Shinkansen	2.50m	17.50m	27.35m	2.50m*	17.50m	25.00m	130kN
Siemens AG (2013)	Siemens Velaro	3.00m	17.38m	25.54m	3.00m	17.38m	24.18m	167kN
Siemens AG (2016)	Eurostar	3.00m	11.00m	22.15m	3.00m	15.70m	18.70m	167kN
Amtrak (2013)	Amtrak Acela	3.00m	10.74m	21.21m	3.00m	18.10m	26.64m	159kN

* denotes assumed values from the available data described in the referenced paper.

Table 2.3: Derivation of high-speed train frequency

Country	Train	Route	Track Type	Route length	Total train length	Bogie spacing	Average speed	Load duration	Frequency	Top speed	Load duration	Frequency
				km	m	m	km/h	s	Hz	km/h	s	Hz
China	CRH3	Wuhan to Guangzhou	Slab	1068	401.4	14.88	299.3	4.8	5.6	349.2	4.1	6.5
China	CRH2	Beijing to Shanghai	Slab	1318	399.3	17.5	235	6.1	3.7	329.9	4.4	5.2
France	TGV	Paris to Lyon	Ballast	425	394	15.7	225.3	6.3	4	299.3	4.7	5.3
France	Thalys	Paris to Brussels	Ballast	333	200.2	15.7	300	2.4	5.3	320	2.3	5.7
Germany	ICE-1	Hannover to Würzburg	Ballast	327	410.7	17	280	5.3	4.6	363	4.1	5.9
Germany	ICE-3	Köln to Frankfurt	Slab	177	400	17	320	4.5	5.2	330	4.4	5.4
Italy	NTV AGV	Milan to Naples	Ballast	205	200	17.1	300	2.4	4.9	360	2	5.8
Japan	Shinkansen	Osaka to Hakata	Slab	554	425	17.5	235.8	6.5	3.7	299.3	5.1	4.8
Spain	Siemens Velaro	Barcelona to Madrid	Ballast	621	200.3	17.4	350	2.1	5.6	403	1.8	6.4
UK	Eurostar	London to Paris	Ballast	113	394	15.7	218.9	6.5	3.9	299.3	4.7	5.3
USA	Amtrak Acela	New York City to Boston MA	Ballast	369	202.9	18.1	101.4	7.2	1.6	241.4	3	3.7
China	Maglev*	Shanghai intercity airport connection	Slab	30	153	-	431.3	1.3	-	498.9	1.1	-

* The Shanghai Maglev has been included for comparison of the vehicle speed. As the Shanghai intercity connection relies on magnetic levitation rather than traditional wheel-rail connection, the dynamics of the train and therefore the frequency differ in calculation and have been neglected in this table.

2.1.2.3 Train Load Factors

Whilst the static load determined from the axles, as summarised in Section 2.1.2.2, generates a stress in the underlying subgrade as it is transmitted via the bearing of the slab or ballast system, the design axle load that is considered in practise is one in which the movement of the vehicle at speed, acknowledged by authors in the case histories presented earlier in this chapter, is accounted for. The dynamic stress under these conditions is enhanced as a result of the speed of a passing train and when considered for application in industry, the design axle load to induce this dynamic stress, P_{design}, can be defined by the empirical equation in Equation 2.1.

$$P_{\text{design}} = \Phi P \tag{2.1}$$

where P is the static wheel load defined in Figure 2.10 and Φ is the dynamic load factor

Doyle (1980) and Sadeghi and Barati (2010) have summarised various approaches adopted worldwide on railway infrastructure in industry as well as definitions adopted within research to determine an expression for the load factor, presented in Table 2.4. Considering the dynamic load factors summarised, the range of derived factor magnitudes calculated with respect to the speed of the train under consideration are shown in Figure 2.13.

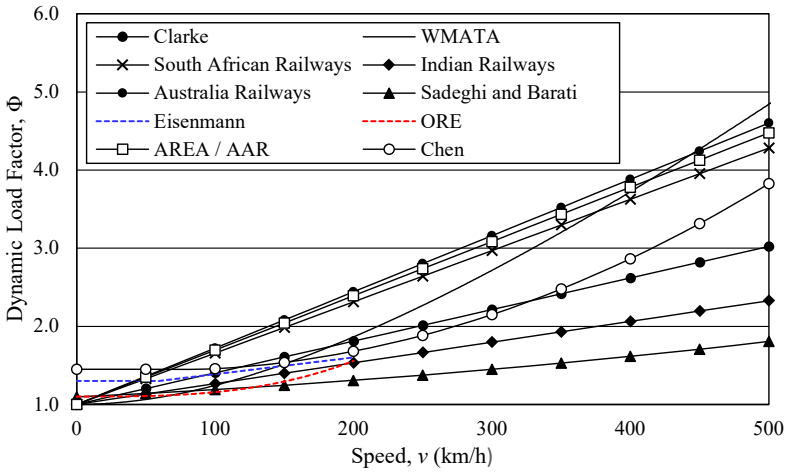

Figure 2.13: Dynamic load factor, Φ, with increasing speed

Table 2.4: Dynamic load factor, Φ (adapted from Doyle (1980) and Sadeghi and Barati (2010))

Dynamic factor		Load factor expression, Φ	
Clarke	Clarke (1957)		$1 + \frac{19.65v}{D\sqrt{K}}$
German Railways	Schramm (1961)	$v \leq$ 100km/h	$1 + \frac{v^2}{30000}$
		$v >$ 100km/h	$1 + \frac{4.5v^2}{10^5} - \frac{1.5v^3}{10^7}$
ORE[a]	ORE (1965) UIC (2004)[b]		$1 + \alpha' + \beta' + \gamma'$
Eisenmann	Eisenmann (1972)		$1 + \delta\eta t$
AREA[c] / AAR[d]	Prause et al. (1974) AREMA (2006)[e]		$1 + 5.21\ \frac{v}{D}$
South African Railways	Lombard (1978)		$1 + 4.92\ \frac{v}{D}$
Indian Railways	Agarwal (1974)		$1 + \frac{v}{58.14\sqrt{K}}$
WMATA[f]	Prause et al. (1974)		$(1 + 3.86 \text{ x } 10^{-5}v^2)^{\frac{2}{3}}$
British Railways	Fredrick and Newton (1977)		$1 + \frac{8.784(\alpha_1 + \alpha_2)v}{P}\sqrt{\frac{D_j P_u}{g}}$
Australia Railways	Ni (2012)		$1 + 5.4\ \frac{v}{D}$
Sadeghi	Sadeghi (2008)		$1 + 4.73\ \frac{v}{D}$
Sadeghi & Barati	Sadeghi and Barati (2010)		$1.098 + 8 \text{ x } 10^{-4}v + 10^{-6}v^2$
Chen	Chen et al. (2013)	$v \leq$ 60km/h	1.45
		$v >$ 60km/h	$1.48 - 1.46 \text{ x } 10^{-3}v + 1.23 \text{ x } 10^{-5}v^2$

Note: [a] ORE is the abbreviation for the Office of Research and Experiments; [b] UIC is the abbreviation for the Union Internationale des Chemins de Fer; [c] AREA is the abbreviation for the American Railroad Engineering Association; [d] AAR is the abbreviation for the Association of American Railroads; [e] AREMA is the abbreviation for the American Railway Engineering and Maintenance-of-way Association and [f] WMATA is the abbreviation for Washington Metropolitan Transit Authority.

Where v represents the train speed (km/h); D represents the wheel diameter (mm); K represents the modulus of the rail support system (MPa); α' and β' relate to the mean value of the impact factor; γ' represents the standard deviation of the impact factor; δ is a factor dependent on track conditions; η is a speed factor; t is a factor related to the selected upper confidence limits; k represents the track modulus (MPa); $(\alpha_1 + \alpha_2)$(represents the total rail joint dip angle (radians) ; P represents the static wheel load (kN); D_j represents the track stiffness at the joints (kN/mm); P_u represents the unsprung weight at one wheel (kN); g represents the gauge width (mm).

The results demonstrate the greater the speed of train considered, the greater the amplification of the load adopted in analytical and empirical design methods. Subsequently, considering the design load, the dynamic stress at top of subgrade level can be considered. However, it is further important to consider the depth of influence of such a load on the subgrade. Figure 2.14 presents the analysis of various authors that demonstrate the attenuation of this dynamic load with respect to depth of subgrade layer for both ballast and ballastless track. As such, the zone of influence for this dynamic stress is shown to reduce to decrease by approximately 50% at between 3.0m and 4.0m depth for ballastless track.

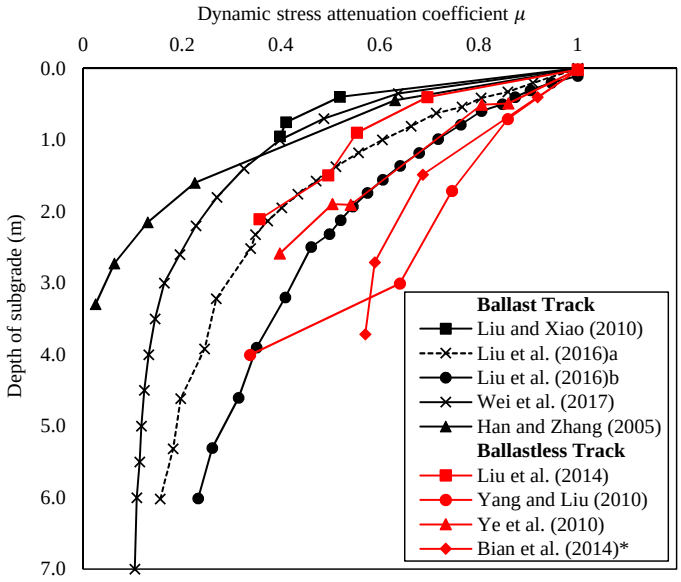

Note: a denotes results for a 23t vehicle; b denotes results for a 30t vehicle.
*(Bian et al. 2014) undertook full scale ballastless experimental tests.

Figure 2.14: Attenuation of dynamic stress with depth of subgrade

2.2 Subgrade Performance

Whilst soft ground conditions typically present problems for any construction due to their high compressibility, as recognised and examined by a number of researchers (Leroueil et al. (1985), Leroueil (2006), Karstunen and Yin (2010), Yin et al. (2011), Nash and Brown (2013) Yin et al. (2015)), the behaviour of soft ground is a significant concern for transportation infrastructure such as

highways, railways and airport runways due to the tolerances on settlement limits and the enhanced strain accumulation that has been shown to occur as a result of cyclic load application, as noted earlier in this Chapter. Under repetitive loading, the development of excess pore pressures and strains continues with an increasing number of cycles of applied load. For transport loading, this number of cycles is significant and occurs over many years of operation, and can result in a decreased subgrade bearing capacity, subsequently leading to differential settlements or impact to the overlying track system (Hyodo et al. (1992), Miller et al. (2000), Chai and Miura (2002)).

This Section examines the key components of cyclic soil behaviour for soft cohesive soils.

2.2.1 Strain Accumulation and Cyclic Strain Thresholds

Under the impact of traffic loading, soils are subjected to a continuous series of rapid stress applications and subsequent stress releases (Seed et al. (1955)). In traditional design methods, empirical correlations based on the interpretation of static soil tests has often been preferred for determining the long term deformation behaviour of a soil. One reason for this is the complex behaviour of cyclically loaded soils and therefore the required sensitivity of instrumentation within the laboratory to examine this behaviour. In the past, cyclic loading test frequency has been limited by the response time of pore pressure transducers to capture the cyclic shear induced excess pore pressure (Sangrey et al. (1969)), discussed in greater detail in the subsequent sections, however the application of loading has been shown to have an impact on the strain rate of cyclic tests. With advances in equipment, particularly the ability to test at higher frequency ranges (Liu and Xiao (2010), Sun et al. (2016) and Wichtmann and Triantafyllidis (2018)), these developments have resulted in a detailed examination of the response of cohesive soils under cyclic loading conditions.

The strain response under cyclic loading has been shown to be closely linked to the application of load, whereby the trend in strain accumulation is highly dependent on the magnitude load application relative to the strength of the

sample, discussed in greater detail in Section 2.2.2. Focussing on the accumulation of permanent strain of cohesive soils, Brown et al. (1975) demonstrated for low cyclic stress applications, the strain accumulation between 100 and 1000 load cycles was low, thus implying for low magnitudes of load applied cyclically to cohesive deposits, the irrecoverable strain developed is negligible as the number of load cycles increases. At higher magnitudes of cyclic stress application, the plastic strain was shown to continue to accumulate even beyond 100,000 load cycles. Whilst the accumulation of strain at low levels of applied cyclic stress was considered to be negligible, Brown et al. (1975) and later Yasuhara et al. (1982), Hyodo et al. (1992), Zergoun and Vaid (1994), Li and Selig (1996) and Huang et al. (2006) all demonstrated the cohesive samples under consideration did not attain equilibrium, such that there was no limit to the axial strain accumulated, and instead excess pore pressures and axial strain still continued to accumulate.

Considering high levels of applied cyclic stress however, rapid accumulation of the axial strain was shown to occur for the majority of samples tested by various authors. Seed et al. (1955) concluded failure of a sample could occur with no apparent sign and a sample could undergo sudden failure following a number of stress applications, due to the rapid trajectory of axial strain to failure that can develop over a small number of applications. This vertical strain behaviour has often been defined in terms of an exponential function (Singh and Mitchell (1968), Hyde and Brown (1976), Ullditz (1993)).

One power model to determine the long term deformation of a fine grained subsoil under repeated cycles of loading, based on the cumulative plastic strain, $\epsilon_{a,p}$ (%) and the number of cycles of loading N was proposed by Monismith et al. (1975):

$$\epsilon_{a,p} = AN^b \tag{2.2}$$

where A and b are defined as regression coefficients, initially proposed based on repeated load triaxial tests of coarse grained material. In agreement with the results of laboratory tests undertaken by Seed et al. (1955) the deviator stress has a significant effect on the development of plastic strains and subsequently affects

the variation of coefficient A (Monismith et al. (1975)). Coefficient b however is independent of the deviator stress (Li and Selig (1996)). Whilst the deviator stress is the most important influence on the exponential model, the tests of Seed and McNeill (1956) and Larew and Leonards (1962) also acknowledged moisture content and dry density to have an influence the accumulation of plastic strains. A number of modifications have since been proposed to the power model. Li and Selig (1996) accounted for the physical state of the soil, Chai and Miura (2002) accounted for the effect of the initial static deviator stress, whilst Luo et al. (2011) considered the compaction of the soil subgrade. The extensions of the exponential accumulation model are summarised in Equations 2.3 to 2.5 below.

Li and Selig (1996)
$$\epsilon_{a,p} = A\left(\frac{q_{cyc}}{q_s}\right)^m N^b \tag{2.3}$$

where q_{cyc} represents the cyclic deviator stress and q_s defines the static soil strength

Chai and Miura (2002)
$$\epsilon_{a,p} = A\left(\frac{q_{cyc}}{q_s}\right)^m \left(1 + \frac{q_0}{q_s}\right)^n N^b \tag{2.4}$$

where q_0 represents the initial static deviator stress

Luo et al. (2011)
$$\epsilon_{a,p} = A\left(\frac{q_{cyc}}{\sigma_c}\right)^m K^n N^b \tag{2.5}$$

where σ_c represents the confining stress of the sample and K represents the relative compaction of subgrade soils

Li and Selig (1996) proposed the value of exponent b was not dependent on deviatoric stress q of the soil, whilst Korkiala-Tanttu (2009) proposed the value was dependent on the stress ratio of the sample, where q_s represents the static deviatoric stress of the sample at failure.

$$\epsilon_{a,p} = CN^b \frac{q_{cyc}/q_s}{1 - q_{cyc}/q_s} \tag{2.6}$$

where

$$b = d\left(\frac{q_{cyc}}{q_s}\right) + c' \tag{2.7}$$

Paute et al. (1996) proposed the accumulation of strain to be dependent on both the number of cycles of load and also the stress level of the sample, shown in Equation 2.8. This Equation incorporated a stabilisation prediction (Ling et al. (2017)) accounting for the accumulated strain in the first 100 cycles of loading. In this manner, the prediction of axial strain is shown to eventually tend to an equilibrium value as the number of load cycles increases significantly towards infinity, a point that was not demonstrated by the findings above, including those of Brown et al. (1975). However it should be noted in practice this prediction is limited by the abilities of laboratory equipment to perform over a significantly high number of load cycles. Further, Equation 2.8 also accounted for the deviator stress of the sample and p^*, defined as the intersection of the failure line with the p-axis (Ling et al. (2017)). The value of coefficient A has however been disputed by Lekarp et al. (2000) (Gluchowski and Sas (2020)) where the limit of accumulated plastic strain did not agree with the results of laboratory tests performed on unbound aggregates, instead proposing Equation 2.14.

$$\epsilon_{a,p} = \epsilon_{a,p,100} + A\left[1 - \left(\frac{N}{100}\right)^{-B}\right] \tag{2.8}$$

where

$$A = \frac{q_{max}/(p_{max} + p^*)}{a - b(q_{max}/(p_{max} + p^*))} \tag{2.9}$$

$$\frac{\epsilon_{a,p}}{L/P_0} = A\left(\frac{q}{p}\right)_{max}^{b} \tag{2.10}$$

where

$$L = \sqrt{(q_{max} - q_{min})^2 + (p_{max} - p_{min})^2} \tag{2.11}$$

Several authors have since proposed empirical models where the deformation during the initial cycles, $\epsilon_{a,p,100}$ in the case of Paute et al. (1996) and $\epsilon_{a,p,1}$ in

the case of Qiu and Sun (2000), is calculated independently of the plastic strain subsequently accumulated whilst Wang et al. (2021) defined the permanent axial strain and normalised pore pressure after 1,000 cycles for soft Wenzhou clay as;

$$\epsilon_{a,p,1000} = 0.0936e^{0.0437q_{cyc}} \tag{2.12}$$

$$\frac{\Delta u}{p'_{c0}} = 0.1175e^{0.0227q_{cyc}} \tag{2.13}$$

Gu et al. (2016) subsequently proposed the accumulation of axial strain could instead be represented by an exponential function considering the overconsolidation ratio, OCR, of the sample and the mean cyclic principal stress. p_{ampl}.

$$\Delta\epsilon_{a,p} = \frac{0.00023\Delta p_{ampl} OCR^{-0.91}}{1\text{kPa}} \tag{2.14}$$

The above equation demonstrated even when a sample does not undergo shearing, permanent axial strains will still develop. The authors concluded irrespective of drainage conditions of the sample, the variation in confining pressure applied to the sample, in the case of triaxial testing an increase in σ_1 or vertical pressure, would result in an excess pore water pressure response that would subsequently lead to accumulation of axial amd volumetric strain upon dissipation.

The empirical equations proposed above for the accumulation of axial strain have mostly focussed on the response of a soil with respect to the number of cycles of load, and the stress of the sample - both the consideration of the soil stress state and the application of the cyclic stress to the sample itself, discussed in the following section. The consideration has predominately been the permanent strain of the cohesive soil since the key application is the deformation and settlement in the field. The total strain response of the sample under cyclic loading has generally been separated by authors to comprise of two components, defined as; (i) the resilient strain, or elastic strain of a sample, and (ii) the permanent irrecoverable strain. Ansal et al. (2001) proposed there were three stages when considering the strain response of a sample subjected to

cyclic loading. These three consecutive stages that occurred during a period of cyclic load were;

1. Soil behaviour is elastic - the strain developed under the applied load is recoverable and subsequently the induced strain of a sample is negligible;
2. Soil behaviour is elasto-plastic - the load application results in excess pore pressure accumulation and the induced strain results in softening of the sample resulting in deterioration of the 'stress-strain-shear strength' characteristics of the sample;
3. Soil behaviour is plastic - rapid strain accumulation occurs due to degradation of the dynamic shear modulus of the sample

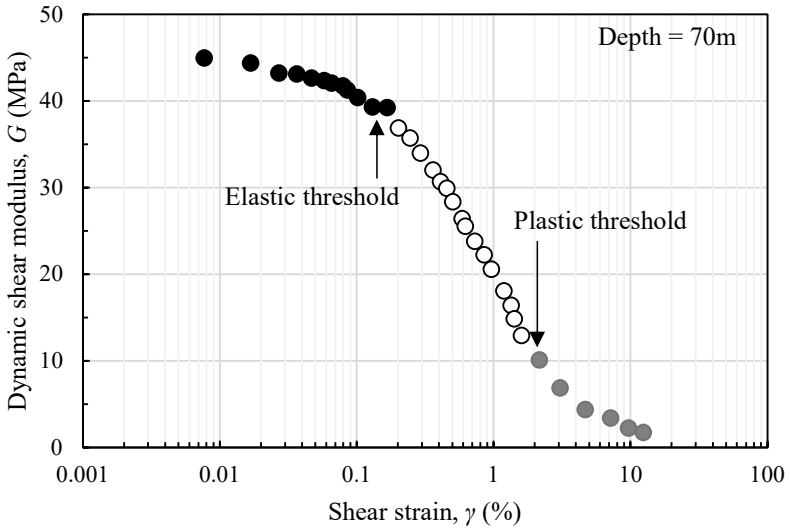

Figure 2.15: Definition of elastic and plastic thresholds, after Ansal and Tuncan (1989)

These three stages of loading are demonstrated in Figure 2.15, whereby the elastic strain threshold exists as the upper limit of elastic soil response and the plastic strain threshold defines the limit beyond which plastic flow of a sample occurs. Authors undertaking strain controlled cyclic tests including Ladd et al. (1989), Vucetic and Dobry (1988) and Hsu and Vucetic (2006), reported the cyclic shear strain threshold to be the differentiator between no excess pore pressure accumulation and rapid accumulation, shown in Figure 2.16; equivalent to the elastic threshold defined by Ansal and Tuncan (1989).

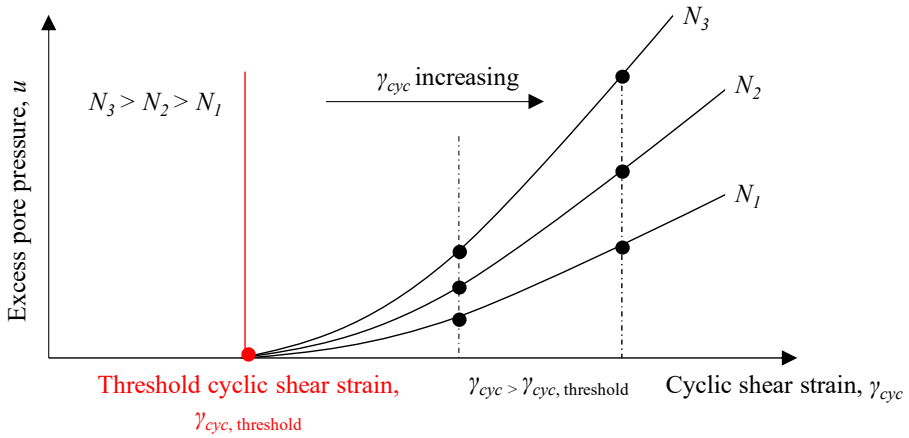

Figure 2.16: Definition of cyclic shear strain threshold, after Hsu and Vucetic (2006)

Okur and Ansal (2007) demonstrated the threshold cyclic strain increased with plasticity considering samples of Turkish Clay. The authors demonstrated a higher plasticity index resulted in less degradation of the sample at large strains. Subsequently, Bhattacharya (2019) presented the threshold shear strain values for 18 clays, shown in Figure 2.17, considering data from authors including Vucetic and Dobry (1988) and Okur and Ansal (2007). The analysis demonstrated a linear correlation exists between the plasticity index of a clay and the threshold shear strain value that could be scalable to different sites.

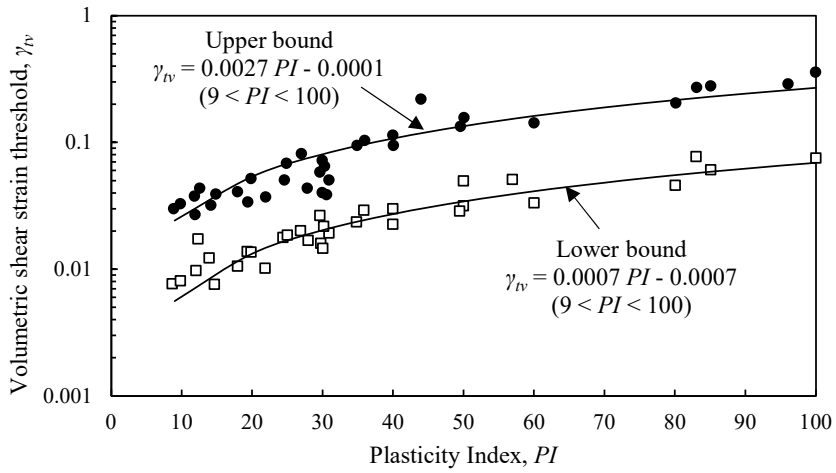

Figure 2.17: Relationship between shear strain threshold and plasticity index, after Bhattacharya (2019)

2.2.2 Cyclic Stress Ratio and Cyclic Stress Thresholds

As demonstrated in Section 2.2.1, the accumulation of strain under cyclic load is dependent on the stress of the sample, and the applied cyclic stress in the case of stress-controlled triaxial tests. This stress state governs the distinction of failure for a sample, whilst the strain threshold distinguishes between the stage of excess pore pressure accumulation. Brown et al. (1975) demonstrated the axial strains accumulated with an increasing number of load cycles were greater for high cyclic stress levels when compared to the static strength of a sample. Typically, the response of soils under cyclic triaxial test conditions is represented and discussed in terms of the cyclic stress ratio and loading frequency of the sample. The cyclic stress ratio (CSR) was defined by Brown et al. (1975) as the ratio of the applied cyclic deviator stress (q_{cyc}) to the static deviator stress at failure (q_s), presented in Equation 2.15. As such there exists a critical cyclic stress ratio, defined by Larew and Leonards (1962) and Seed et al. (1955) and supported by the work of Sangrey et al. (1969), at which failure will occur within a number of cycles of load repetition.

$$\text{CSR} = \frac{q_{cyc}}{q_s} \tag{2.15}$$

Under this framework of analysis, for a low cyclic stress ratio such that the applied cyclic stress to the sample is much lower than the static failure stress, the sample is anticipated to remain stable after a significant number of cycles of loading. Hyde and Brown (1976) defined this criteria that separated a sample that tends towards a stable strain accumulation or that which accumulates rapidly, to be the threshold CSR. For the silty clay samples of Yew York Clay under consideration by the authors, the value was determined to be approximately 0.5. Seed et al. (1955) demonstrated significant additional deformation occurred as a result of repeated loading on the samples, recording significantly lower levels of applied stress (60 – 70 % of the stress recorded for static tests) during the repeated load tests to achieve 5% strain. Sangrey et al. (1969) proposed the critical value of stress ratio was approximately 0.66, above which a sample tended towards failure, concluding this threshold existed for all samples of the same clay, irrespective of the initial stress conditions of the

sample. This is presented in Figure 2.18 showing the existence of a threshold cyclic stress ratio that exists as the value of q applied in the cyclic test increases relative to the monotonic, continuous load test. In the case of Figure 2.18(a) the sample remains stable at the end of the cyclic loading whilst in Figure 2.18(b) the hysteretic loops are shown to be more open, signifying the accumulation of plastic strain.

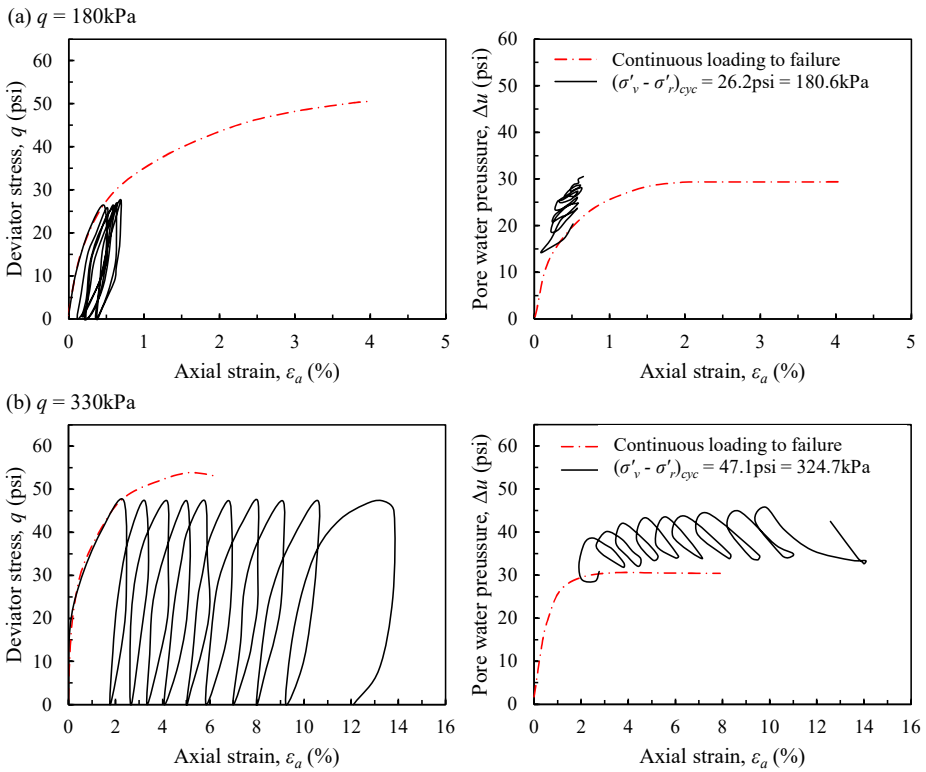

Figure 2.18: Stress strain curves and pore pressure evolution for (a) CSR < $CSR_{threshold}$ and (b) CSR > $CSR_{threshold}$, after Sangrey et al. (1969)

Subsequent studies have further confirmed the existence of a threshold cyclic stress ratio. France and Sangrey (1977) and Sangrey et al. (1978) concluded the cyclic stress ratio existed between 0.5 and 0.8. Ansal and Tuncan (1989) demonstrated for the organic Golden Horn Clay and Baltalimani Clay samples under consideration, a semi-logarithmic relationship existed between the cyclic stress ratio and settlement. The limit of this response was at a cyclic stress ratio of just under 70%, in agreement with the proposed threshold of 0.66 by Sangrey et al. (1969). Zhou and Gong (2001) reported the threshold cyclic stress ratio to

be between 0.5 and 0.6 for Hangzhou clay, Frost et al. (2004) reported a value of 0.5 for fine-grained subgrade soils, whilst Indraratna et al. (2021) determined for kaolinite samples, the threshold or critical cyclic stress ratio varied from 0.3 to 1.0. This was influenced by the initial void ratio and subsequent degree of compaction achieved prior to testing. For a very dense sample, achieving a compaction of 99.2%, the cyclic stress ratio was 1.0.

Zergoun and Vaid (1994) presented triaxial tests examining the response of marine clays at low frequencies, demonstrating a similar trend in the hysteretic loops presented by Sangrey et al. (1969) for two-way loading. The results indicate the existence of a threshold cyclic stress ratio between 0.54 and 0.57 based on the change in residual, plastic axial strain accumulation that occurs between these values, presented in Figure 2.19.

Examining the response to pore pressure in Figure 2.18, as reported by Andersen et al. (1980) for Drammen clay, at a low cyclic stress ratio, the pore pressure increment will be small due to the equilibration of pore pressures being achieved, leading to a stable sample over a significant number of cycles. In these conditions, the resilient strain will initially increase and then reach a steady value whilst the permanent strain will increase throughout the loading, shown in the axial strain response for the sample. Wang et al. (2013) examined the response of soft marine clays from Wenzhou over 50,000 cycles of loading. The authors concluded for stable samples that beyond 1000 cycles, the resilient strain of the sample remained constant whilst the permanent strain continued to gradually increase with a decreasing rate, similar to the findings of Zergoun and Vaid (1994). At high cyclic stress ratios beyond the defined threshold value of 0.3 however, both the resilient and plastic strain increased rapidly and exponentially with respect to the number of cycles of load. It was further acknowledged that the pore pressure response and accumulation increase with respect to cyclic stress ratio, whereby the greater the cyclic load applied, the greater the excess pore pressure response. In parallel, as the number of load cycles increases, degradation of the sample occurs and a greater number of cycles are subsequently required to dissipate the excess pore pressure generated in each load application (Moses et al. (2003)). The threshold CSR value of 0.3 reported is considerably lower than other authors have documented.

Subsequently, Ni (2012) and Indraratna et al. (2015) concluded for kaolinite samples, the threshold value existed between 0.6 and 0.8 based on the observed accumulation of axial strain from triaxial tests performed at a range of frequencies between 0.1Hz and 5.0Hz, demonstrating the independence of this threshold with respect to load frequency. However, as noted when considering cyclic threshold shear strains, the distinction of failure from excess pore pressure response of the sample alone was not possible.

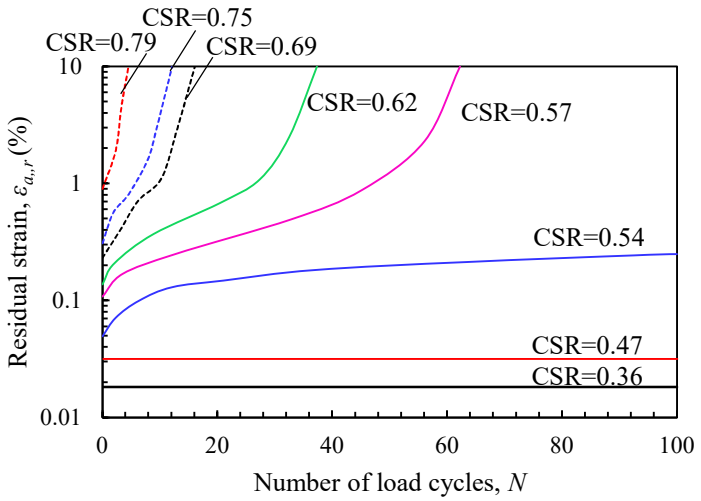

Figure 2.19: Residual strain curves, after Zergoun and Vaid (1994)

2.2.3 Excess Pore Pressure Development

Whilst the accumulation of excess pore pressure can be used to define the cyclic shear strain threshold, and therefore elastic threshold of a sample (Ansal and Tuncan (1989)), the response of pore pressure is independent from the determination of a failed or stable sample when considering stress controlled tests and the application of a cyclic stress ratio. As summarised in Section 2.2.1, dependent on the cyclic stress ratio during cyclic triaxial testing, the strain accumulated during loading can tend towards an equilibrium such that for subsequent load cycles, the resilient strain component dominates and accumulation of permanent plastic strain is negligible.

For these samples, at low cyclic stress ratios, Sangrey et al. (1978) proposed the total pore pressure response under cyclic loading was a summation of the pore

pressure response, Δu_q, generated as a result of the deviatoric stress of a sample, the pore pressure generated as a result of the cyclic load applied to the sample, Δu_{cyc}, and the pore pressure response due to sample creep, Δu_p, dependent on both time and mean effective stress of the sample. Upon correction of the total excess pore pressure for creep, the following relationship presented in Figure 2.20 was therefore proposed whereby for all soils that tended to equilibrium rather than failure, their corrected excess pore pressure responses would form straight lines in q,p' space.

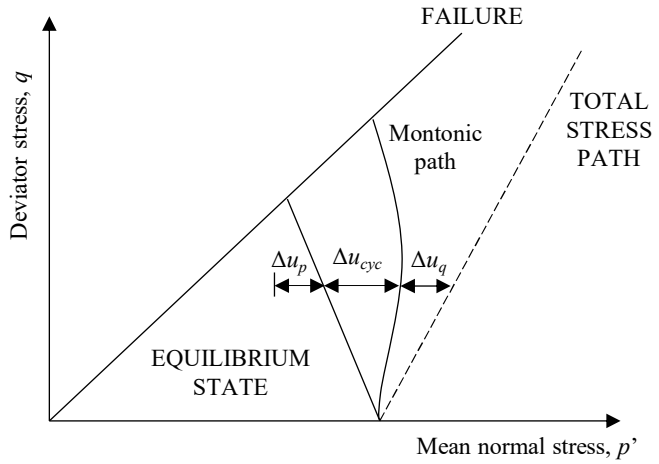

Figure 2.20: Effect of creep correction on equilibrium states, reproduced from Loach (1987) after Sangrey et al. (1978)

Examining the excess pore pressure of normally consolidated samples, normalised with respect to the confining cell pressure in the triaxial, Yasuhara et al. (1982) proposed a hyperbolic function related the response of the normalised excess pore pressure to the axial strain accumulation of the soil that was independent of the loading type adopted in the triaxial test, presented in Equation 2.16, whilst Hyde (1974) examined the response of Keuper Marl samples, showing the accumulation of pore pressure continued to develop for up to 10,000 cycles, particularly for highly overconsolidated samples, discussed further in Section 2.3.2. Thammathiwat and Chim-oye (2004) similarly concluded the accumulation of excess pore pressure continued with increasing cycles of load.

$$\frac{\Delta u}{p'_{c0}} = \frac{\epsilon}{a + \beta\epsilon} \tag{2.16}$$

At low cyclic stress ratios, Ohara and Matsuda (1988), Moses et al. (2003) and Prakasha and Chandrasekaran (2005) demonstrated the rate of increase in excess pore pressure under cyclic loading was low, increasing with increasing cyclic stress applied to the sample in accordance with Skemptons rule. Ohara and Matsuda (1988) reported at high cyclic stress ratios, the excess pore pressure generated in response to the applied load was four times greater than observed for the equivalent monotonic load path, a finding not supported by Lo (1969) and Yasuhara et al. (1982) whom concluded the accumulation of pore pressure was independent of the time of sustained applied cyclic stress. Importantly, Yasuhara et al. (1982) found no relationship between the accumulation of axial strain and the generation of pore pressure. This statement appears to hold true for cyclic stress controlled tests, in agreement with the conclusions of Ni (2012).

Similarly Thian and Lee (2017) did not identify a difference in the trend of excess pore water pressures for samples of Malaysian clay obtained from offshore that failed following a cyclic load stage when compared to samples with low cyclic stress ratios, other an an increase in the total excess pore pressure for samples with higher CSR. The authors noted the rapid growth in pore pressure during the initial load cycles (less than 100) followed by continued accumulation of pore pressure at a lower rate either to a failed or stable end state, in agreement with Hanna and Javed (2008).

2.2.4 Post-Cyclic Behaviour

When examining the response of a soft soil to cyclic loading, the previous sections have classified the response of the samples in terms of a 'failed' state, identified by the rapid accumulation of axial strain over a relatively small number of load cycles, or 'stable' state whereby the strain accumulation tends towards an equilibrium value such that negligible strain is developed over subsequent cycles. However, a 'stable' sample will have still experienced loading such that the stress path of the soil sample has been altered from its' initial state.

Seed et al. (1955) loaded samples to failure following a number of stress applications whilst permitting drainage. It was shown that the strength of the

specimens following a number of repeated load applications was greater than the strength of an the equivalent sample sheared under monotonic loading (shown in Figure 2.21 (a)). The authors reported a strength increase of 35%, irrespective of the load frequency adopted when considering the same test duration, however it was also demonstrated the strength of the sample under axial compression increased with respect to a greater number of applications, shown in Figure 2.21 (b). Seed et al. (1955) demonstrated for soils where greater axial strain had accumulated during cyclic loading, the subsequent strength of the sample upon monotonic shearing was greater. It was concluded that this response was a result of two factors; the particle rearrangement and densification of the sample and also an increase in strength with time as a result of sample consolidation due to the partially saturated nature of the Vicksburg clay examined.

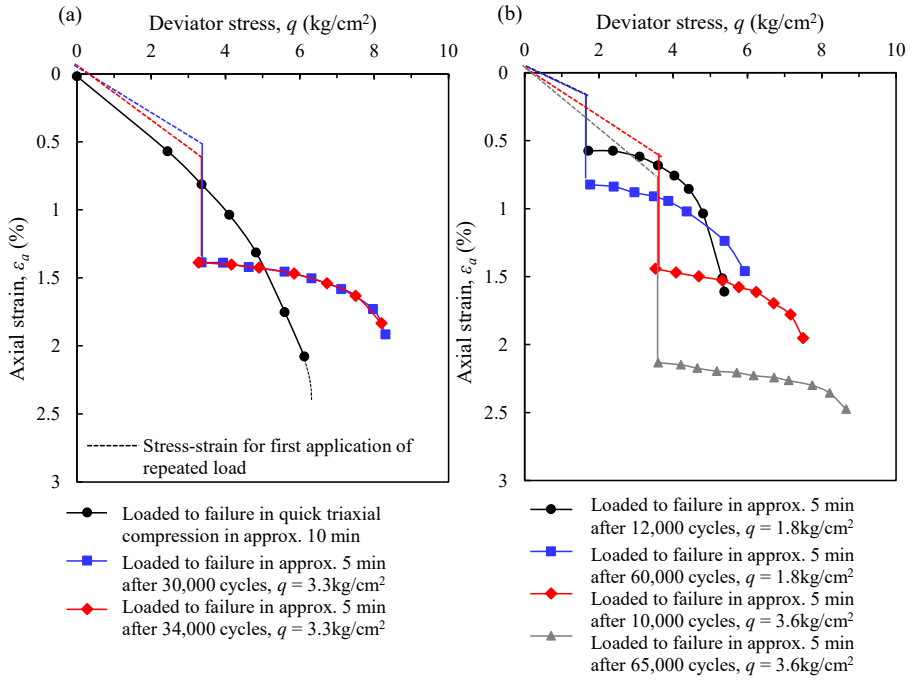

Figure 2.21: Effect of repeated loading on the strength of Vicksburg clay, after Seed et al. (1955)

Based on the above, even for an equivalent or similar number of load cycles, the magnitude of applied cyclic axial stress is demonstrated to contribute to the post-cyclic strength of the sample. The strengths of the samples presented in

Figure 2.21 (b) are summarised in Table 2.5, where the axial strain represents the accumulated strain under repeated loading prior to shearing.

Table 2.5: Results of post-cyclic monotonic shearing tests by Seed et al. (1955)

Deviator stress, q	Number of load cycles, N	Axial strain, ϵ_a	Strength
1.8kg/cm^2, 176.5kPa	12,000	0.55%	5.48kg/cm^2, 529.6kPa
1.8kg/cm^2, 176.5kPa	60,000	0.80%	5.9kg/cm^2, 578.6kPa
3.6kg/cm^2, 353.0kPa	10,000	1.45%	7.5kg/cm^2, 735.5kPa
3.6kg/cm^2, 353.0kPa	65,000	2.12%	8.75kg/cm^2, 858.1kPa

These early findings by Seed et al. (1955) indicate that under repeated loading, a sample exhibits an apparent overconsolidation. As proposed by Hyde (1974), this degree of apparent overconsolidation increases with the number of cycles of repeated load applied to a sample, shown in Figure 2.22. This response during cyclic loading results in an accumulation of excess pore pressure and subsequent decrease in the effective stress of the sample such that when the material is subsequently sheared under monotonic load conditions, the sample will exhibit similar behaviour to an overconsolidated one. The stress paths shown in Figure 2.22(a) demonstrate the path associated with a monotonic load test whilst Figure 2.22(b) presents the stress path following cyclic load. Based on tests conducted on the Keuper Marl formation by Hyde (1974), post-cyclic monotonic shear tests were performed on samples following 10,000 cycles of load. Unlike the tests performed by Seed et al. (1955), drainage was not permitted between the cyclic test and subsequent monotonic shear. This resulted in the opposite conclusions to those of Seed et al. (1955) such that a decrease in undrained shear strength was attained. The authors proposed this strength reduction was most marked for normal or lightly overconsolidated samples as for overconsolidated samples, the excess pore pressure accumulation under cyclic loading was less than normally consolidated samples.

Yasuhara et al. (1981) examined a series of normally consolidated cyclically loaded clay samples, proposing the degree of consolidation of the sample increased with the excess pore water pressure generated as result of cyclic loading. In this way, as the excess pore pressure of the sample increased and the effective stress of the soil subsequently decreased, leading to a reduction in undrained strength upon shearing under undrained conditions. For

overconsolidation ratios ranging between 1 and 10, the post-cyclic undrained shear strength decreased by up to 20% of the strength established from undrained monotonic tests on equivalent samples of Ariake clay. Similar findings were concluded by Andersen et al. (1980), demonstrating a reduction in post-cyclic strength of clay samples of approximately 25%. The authors demonstrated that the post-cyclic stress paths of normally consolidated cyclically loaded soils tended towards a similar stress path of that given by an overconsolidated monotonic test with an OCR of 4, presented in Figure 2.23 and subsequently a similar response existed for overconsolidated cyclic tests.

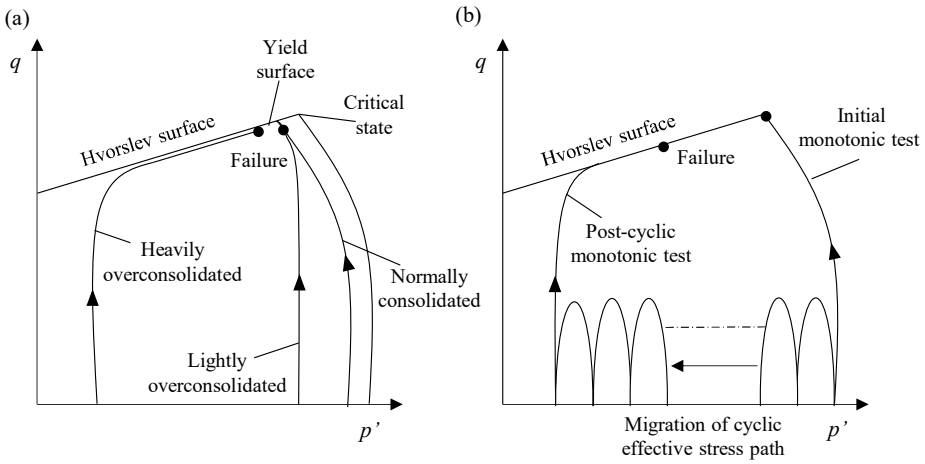

Figure 2.22: Effective stress paths for normally consolidated samples under (a) Monotonic loading and (b) after cyclic loading, reproduced from Hyde and Ward (1985)

Meimon and Hicher (1980) subsequently examined the post-cyclic reduction in sample strength in terms of sample structure, proposing the reduction in strength could be attributed to the destruction of the initial clay structure under cyclic loading. The authors proposed that for low strain levels attained during cyclic loading, less than 5%, the reduction in strength could be limited to approximately 8% of the monotonic strength. The maximum strength reduction observed however was much greater than that observed by Yasuhara et al. (1981), reaching a reduction of 40% when strain under cyclic loading reached 15%. Drumm et al. (1997) and Zergoun and Vaid (1994) similarly reported both higher strength and stiffness degradation with respect to higher cyclic strain accumulation. Suiker et al. (2005) also demonstrated the strain corresponding

to the post-cyclic peak strength decreased when the cyclic stress level increases. The authors concluded this strain response implied there would be less warning for the occurrence of post-cyclic failure observed in the laboratory tests and rapid strain would develop.

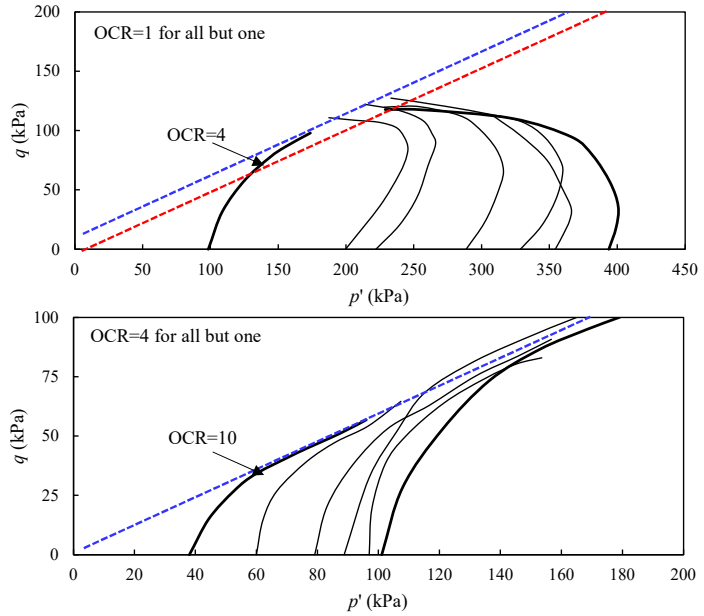

Figure 2.23: Post-cyclic response of normally consolidated and overconsolidated samples, after Andersen et al. (1980)

$$\text{POCR} = \frac{p'_0}{p'_{c0}} = \frac{p'_0}{p'_0 - \Delta u_{cyc}} \tag{2.17}$$

Guo et al. (2020) further examined the stress paths, and apparent overconsolidation of cyclic samples, reporting the greater the cyclic stress ratio during cyclic loading, the greater the apparent overconsolidation. This supported the findings of Pillai et al. (2014) on kaolin clay samples. Furthermore, the authors demonstrated the greater the initial confining pressure of the sample, the more marked the increase in apparent overconsolidation, shown in Figure 2.24, however a significant reduction in undrained shear strength was not observed. Guo et al. (2020) considered the apparent overconsolidation after Azzouz et al. (1989), presented in Equation 2.17, reporting the normalised stress and excess pore pressure curves

considering the apparent overconsolidation of the cyclic loaded samples, was similar to the behaviour of more overconsolidated samples. For instance, Guo et al. (2020) established for an POCR of 2.1 from cyclic tests, the observed post-cyclic monotonic response was more similar to that of a monotonic sample with an OCR of 4, governed by the excess pore pressure response. As such, the authors proposed the following relationship existed between POCR and OCR based on the swelling and compression indexes of the soil, C_s and C_c respectively;

$$\log \text{POCR} = \left(1 - \frac{C_s}{C_c}\right) \log \text{OCR} \tag{2.18}$$

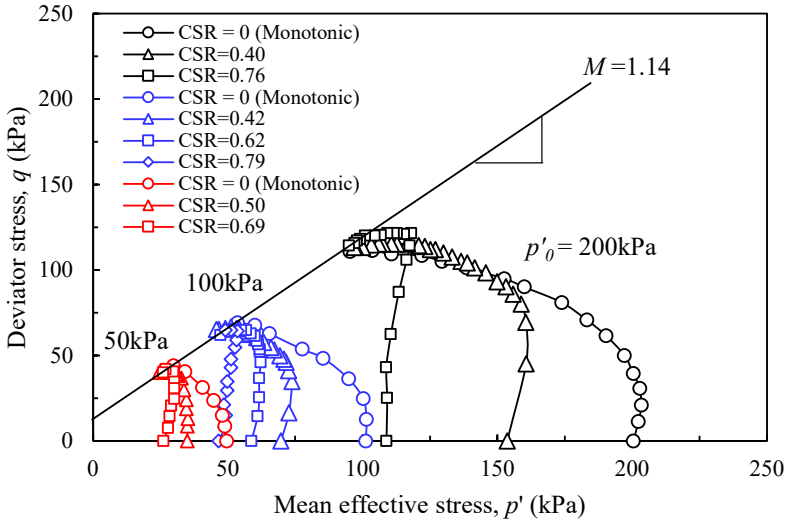

Figure 2.24: Effective stress paths from post-cyclic monotonic shear tests, reproduced from Guo et al. (2020)

As noted above, the tests performed by Seed et al. (1955) considered drainage, whilst Procter and Khaffaf (1984) concluded if sample densification was permitted with respect to cyclic loading, the weakening of the sample was inhibited. Yasuhara and Toyota (1997) performed post-cyclic shear tests permitting drainage on Ariake clay, concluding the change in void ratio associated with the drainage period included in the test regime resulting in volumetric hardening of the sample instead of a significant increase in sample strength. Wang et al. (2015) and Wang et al. (2019) further considered the effect of drainage on post-cyclic response of marine clay samples, citing the cyclic

loading applicable to traffic and storm loading was intermittent and the period between loadings would permit some reconsolidation of the soil to occur. Lu et al. (2021) recently examined the microstructure response of Pearl River Estuary clay after permitting sample reconsolidation using scanning electron microscope technologies. The authors observed the number of pores in post-cyclic samples was greater than undisturbed samples, noting subsequently the greater reconsolidation that occurred, the smaller the void ratio and subsequent reduction in pores.

Indeed, the most notable effect on the sample appeared to be the stiffness and elastic modulus of the sample, rather than strength, also identified by Thiers and Seed (1968), Matsui et al. (1992) and Zergoun and Vaid (1994). More recently however, Hyde et al. (2007) considered a drainage period between cyclic load and subsequent monotonic shearing, demonstrating an increase in the post-cyclic strength of silty soil under these conditions due to the permissible reconsolidation of the sample that occurs during the rest period prior to monotonic load. The authors also concluded the strength increase following a drainage period was greater for an increasing magnitude of deviator stress applied to the sample. Suiker et al. (2005) further reported the cyclic loading process could increase the peak strength the sample attains, also demonstrating it would increase the material stiffness, as embodied by the increase of the initial slope of the stress-strain curves.

The relationship between the applied stress with respect to the strain accumulated under each load application can be defined as the modulus of resilient deformation. Brown et al. (1975) showed the resilient modulus of Keuper marl was independent of the overconsolidation ratio and attained an equilibrium after 100,000 cycles, whilst Frost et al. (2004) demonstrated that under undrained conditions, cohesive pavement subgrades exhibited inverse stress dependency. As such, the value of CSR increases towards the threshold value, whilst the resilient modulus decreases, tending to a constant value. Yasuhara et al. (2003) proposed the secant stiffness modulus could be determined from a straight line extrapolated from the origin in stress-strain

space;

$$E_s = \frac{\Delta(\sigma_1' - \sigma_3')}{\Delta\epsilon_a} = \frac{q'}{\epsilon_a} \tag{2.19}$$

Guo et al. (2020) concluded the response of the stiffness observed in monotonic tests was different to that presented in post-cyclic monotonic tests, noting a point of inflection existed in the post-cyclic tests such that during the initial stages of post-cyclic shearing, the degradation observed is less than for an equivalent static test, shown in Figure 2.25. Subsequently, beyond this point of inflection, the stiffness degradation with respect to increasing strain for both monotonic and post-cyclic monotonic tests are the same. The authors identified the cyclic stress ratio of the sample was important when considering the degradation of a sample, governing the point of inflection such that at high CSRs, the inflection occurs at higher levels of axial strain.

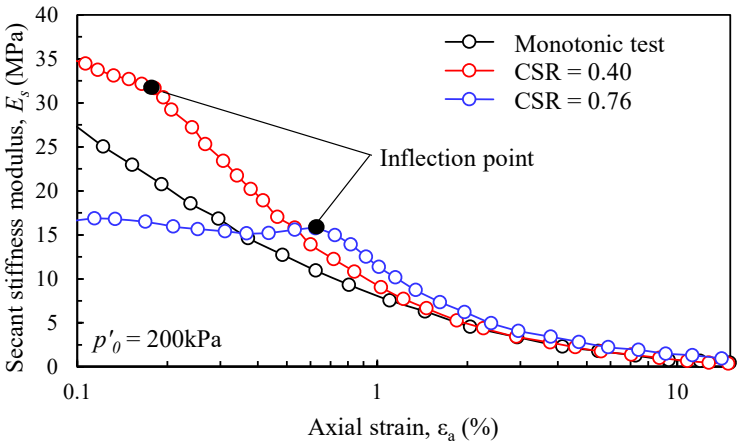

Figure 2.25: Degradation in post-cyclic secant stiffness with respect to axial strain, reproduced from Guo et al. (2020)

Thiers and Seed (1968) first completed cyclic strain controlled direct simple shear tests. The authors observed during the initial accumulation of strain, the elastic shear modulus of the sample decreased by approximately 50% to 80% upto a strain of 2%. Subsequently beyond this strain level, as observed later by Brown et al. (1975) for a significant number of load cycles in stress-controlled tests, the shear modulus reached an equilibrium and no further degradation was observed. Focussing on stress-controlled tests, Andersen et al. (1980) reported

the decrease in shear modulus of Drammen Clay, G, was greatest for higher cyclic stress ratios, concluding the degradation in elastic shear modulus was also dependent on the number of load cycles. Later, Thammathiwat and Chim-oye (2004) concluded this decrease in shear modulus could be in part attributed to the deterioration of soil particle bonding as well as an accumulation of strain.

Vucetic and Dobry (1988) quantified the degradation in shear modulus by proposing a degradation index, δ, a ratio between the secant shear modulus at a given number of cycles, N, and the initial shear modulus for the first cycle of loading given strain-controlled conditions. In this manner, the higher the ratio, the smaller the stiffness degradation of the sample. Furthermore, Okur and Ansal (2007) subsequently concluded the stiffness degradation was most noticeable at the elastic threshold, defined by Ansal and Tuncan (1989) in Section 2.2.1.

$$\delta = \frac{G_{s,N}}{G_{s,1}} \tag{2.20}$$

Idriss et al. (1978) and Zhou and Gong (2001) have since proposed the degradation index could instead be written in terms of the cyclic stress ratio and overconsolidation ratio. Similar to the definition by Vucetic and Dobry (1988), for greater degradation at higher values of CSR, the degradation index was small. The authors further concluded that for overconsolidated samples, the degradation in stiffness was less than for that of normally consolidated samples.

$$\delta = \frac{G_{sN}}{G_{s1}} = \frac{\frac{\sigma_d}{\epsilon_{a,N}}}{\frac{\sigma_d}{\epsilon_{a,1}}} = \frac{\epsilon_{a,1}}{\epsilon_{a,N}} \tag{2.21}$$

2.3 Laboratory Tests

Experimental investigations have been used to examine the performance of cohesive soils under cyclic loading, examining the strength of soils in response to various loadings conditions, whilst others have considered the post-cyclic performance of a soil, considering the subsequent consolidation of a clay sample as a result of the dissipation of generated excess pore pressures and strength

under shearing.

The loading applied to a cohesive soil governs its' response, namely;

- The frequency of load,
- The cyclic stress level or cyclic strain amplitude and the stress conditions of the cohesive sample, and
- The application and type of cyclic loading, discussed in the following sections.

The loading frequency of a sample can be applied under either stress or strain controlled conditions whilst the application of load itself can be performed using either a one way or two way loading approach. In the case of one way loading, there is no load reversal when applied to the sample, whilst for two way loading, full stress reversal, and therefore both compression and extension, are applied to the sample. Yasuhara et al. (1982) demonstrated two-way loaded samples failed at lower cyclic stress ratios for the same number of load cycles at failure when compared to one-way loaded samples. As such, the strength of the sample under cyclic loading was greater for one-way loading. One-way loading has been examined predominately within this review of literature as it has been demonstrated to best represent the loading a sample experiences due to traffic passage (Hyodo et al. (1992), Hyde et al. (1994), Cai et al. (2013), Wang et al. (2017), Sun (2021)).

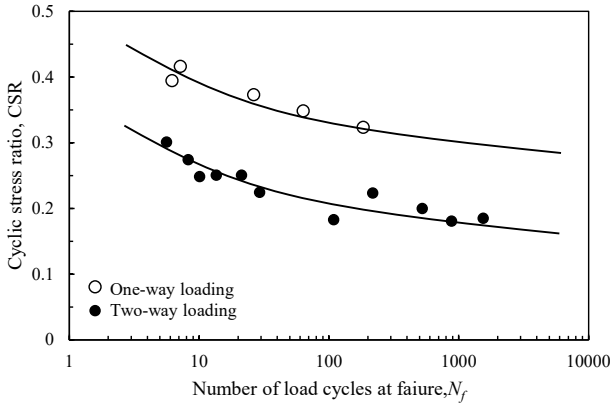

Figure 2.26: Cyclic response of samples under one-way and two way cyclic loading, after Yasuhara et al. (1982)

The identification of failure of a sample, as discussed in Section 2.2, has predominately been attributed to the rapid accumulation of strain with respect to a relatively low number of load cycles, such that the load hysteresis loops are open and plastic strain rapid accumulates at an upwards trajectory, shown in Figure 2.27. This can either be due to early softening of the clay sample, resulting in a fluidised sample, or due to the cyclic undrained failure. If a sample remains stable, shown by Case 1 in Figure 2.27, the strain gradually tends to a stable value.

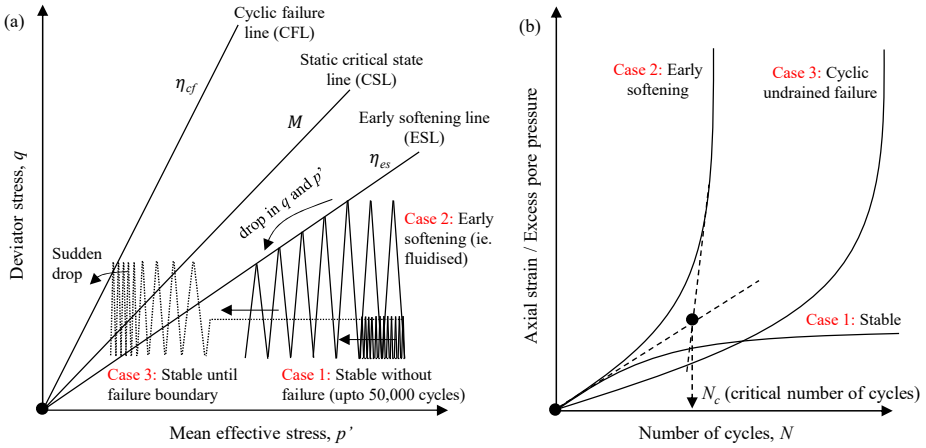

Figure 2.27: Kaolin sample failure mechanisms, after Indraratna et al. (2010)

Both the response attributed to stress and strain-controlled triaxial testing and shear testing has been summarised in consideration of both threshold cyclic shear strain and threshold cyclic stress values. These tests have typically been performed using three main types of equipment;

- Cyclic direct simple shear tests, adopted by Thiers and Seed (1968), Vucetic and Dobry (1988), Yasuhara and Andersen (1989), Lefebvre and Pfendler (1996), Yildirim and Erşan (2007) and Mortezaie and Vucetic (2013);
- Cyclic triaxial tests, examined by authors including Meimon and Hicher (1980), Yasuhara et al. (1982), Hyodo and Yasuhara (1988) Lefebvre and LeBoeuf (1987), Li et al. (2011); and
- Hollow cylinder apparatus, performed by Ansal et al. (2001), Powrie et al. (2007), Yang et al. (2019), Wang et al. (2021)

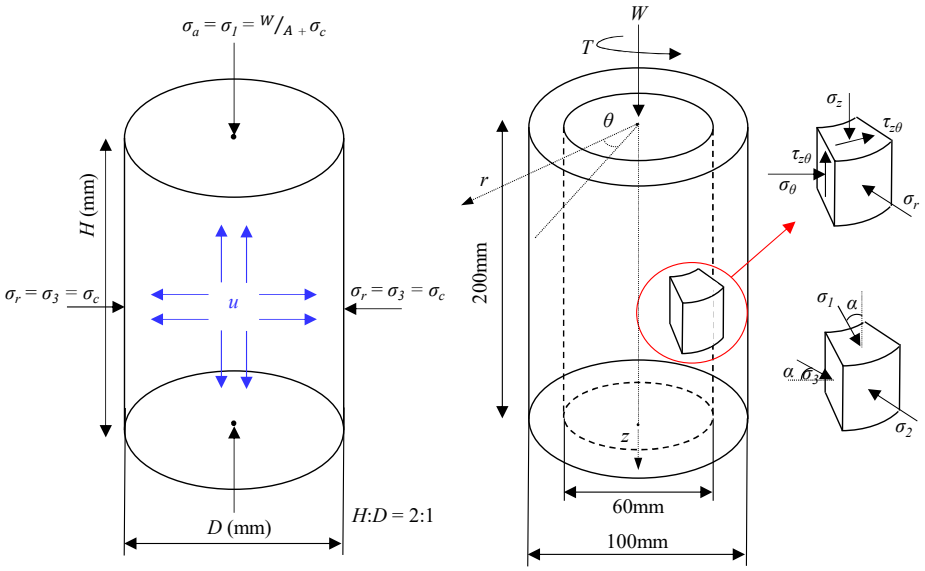

(a) Triaxial specimen (b) Hollow cylinder specimen

Figure 2.28: Stress state of a soil sample, after Wang et al. (2021)

The difference in conditions experienced by a soil sample is presented in Figure 2.28 for (a) a triaxial sample and (b) a hollow cylinder specimen. Several authors have suggested the hollow cylinder apparatus, such that the principal stress rotation that occurs under cyclic traffic loading can be replicated, to be more representative of the in-situ stress state a sample undergoes. The influence of load application will be reviewed further in Section 2.3.3.

This section reviews the influence of the various factors summarised above on the response of soft clay subsoils under cyclic loading.

2.3.1 Influence of Loading Frequency and Number of Load Cycles

Early repeated load tests performed by Seed et al. (1955) concluded soil deformation was dependent on the number of stress applications to the sample and independent of the frequency of stress application. Further load controlled cyclic triaxial tests undertaken by Procter and Khaffaf (1984), indicated that for a similar weakened condition, the soil behaviour observed was independent of the load frequency, performed at between 1/20Hz and 1/50Hz, instead depending on the number of load applications. However Graham and Houlsby

(1983) examined reconsolidated natural clay samples at different effective stresses in cyclic triaxial tests. Under these conditions, considering variations in both overconsolidation ratio and mean effective stress, a range of yield surfaces were obtained, however when normalised with respect to the pre-consolidation pressure of the sample, the yield surfaces converged to a single yield surface where the position of the yield locus was dependent on the loading rate applied to the sample. Matsui et al. (1992) further demonstrated at low frequencies, greater degradation of the sample occurred, whilst Zhou and Gong (2001) and Li et al. (2011) both concluded similar effects when examining the response of samples at low frequencies. However, importantly, considering the duration of the tests rather than the number of load cycles, the test duration prior to failure was greater for tests at lower frequencies

The effect of frequency on overall soil response has been shown to reduce with respect to an increased number of cycles of load (Ishihara and Yasuda (1980), Procter and Khaffaf (1984), Ansal and Tuncan (1989)). As such the frequency of load has generally been studied with respect to seismic analysis whereby a short number of load cycles are adopted. Furthermore, the threshold cyclic stress ratio has been demonstrated to be independent of the frequency of loading. As technology has improved with respect to equipment and instrumentation capable of achieving high frequency loading (60Hz tests performed by Sun et al. (2016)), and measuring the subsequent sample response, particularly pore pressure response, the frequency independence of cyclic tests has been further demonstrated by Ni (2012) and Indraratna et al. (2015).

2.3.2 Influence of Load History

The pre-existing stress conditions of soil samples have long been understood to play an important factor in the behaviour of cohesive soils under static and cyclic loading conditions. Singh and Mitchell (1968) highlighted the effective stress response of a soil was governed by the build-up of pore pressure under repeated loading, shown by Hyde and Ward (1985) to cause normally and lightly overconsolidated soils to become more overconsolidated under undrained cyclic loading. No matter the stress history of a clay soil, the cyclic effective stress paths converge on the Hvorslev surface at failure (Parry (1960), Hyde (1974)),

Matsui et al. (1980)) however clearly the initial stress of the sample governs its' initial position in q/p' space and can therefore affect the how quickly the sample fails.

2.3.2.1 Stress Ratio

Chen et al. (2018a), Huang et al. (2006) and Hyodo et al. (1999) all proposed the introduction of an initial static deviatoric stress, q, would result in a peak deviator stress, the combination of both the cyclic and static deviatoric stresses, that moved the sample closed towards its' failure state, shown in Figure 2.29. As such greater strain accumulation would therefore be observed when a large initial static deviatoric stress was applied to the sample. Considering the initial static deviatoric stress of the sample prior to the application of a cyclic load, Huang et al. (2006) determined for soft, and organic samples in the case of Chen et al. (2018a), that the application of a large initial stress resulted in greater axial strain and excess pore water pressure accumulation. Similar findings were presented by Liu et al. (2010) for cyclic simple shear tests performed on Wenzhou clay. Further extensive studies by Wichtmann and Triantafyllidis (2018) on kaolin samples considered the effects of initial stress ratio (q/p') on the accumulation of axial strain and excess pore water pressure. For an increase in stress ratio, the rate of accumulation of axial strain was shown to increase, whilst as highlighted by previous findings presented in Section 2.2.3, the response of pore pressure accumulation was moderate. Furthermore, the increase in stress ratio, and therefore increase in initial static deviatoric stress in relation to p', was shown to result in a decrease in the number of cycles to failure.

The findings also demonstrated that there existed a stress ratio for the sample such that only deviatoric strain accumulated and no excess pore pressures were generated. This value of cyclic stress ratio was found to be equivalent to the gradient, M, within the modified Cam Clay (MCC) model, where the friction angle, ϕ_c is defined as the mobilised friction angle in Equation 2.22, shown in Figure 2.29.

$$\mathrm{M} = \frac{6 \sin \phi_c}{3 - \sin \phi_c} \tag{2.22}$$

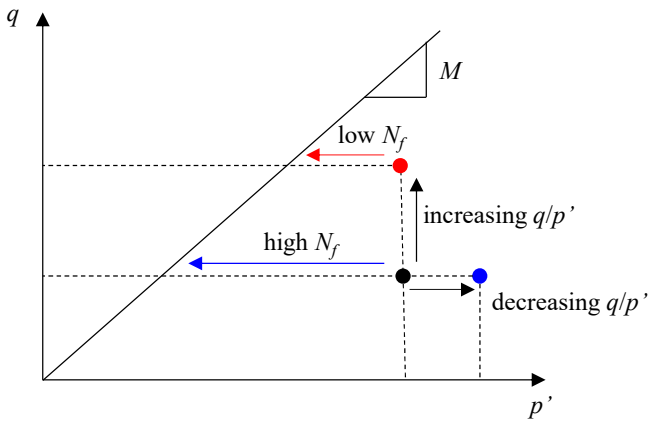

Figure 2.29: Influence of stress ratio

With respect to the initial anisotropy of a soil sample, the in-situ stress ratio or K_0 consolidated samples, a number of authors have performed cyclic triaxial tests on undisturbed and remoulded samples (Sakai et al. (2003), Samang et al. (2005), Hendry et al. (2013) Indraratna et al. (2015)). Ni (2012) conducted cyclic triaxial tests on remoulded kaolin samples consolidated with an initial in-situ stress ratio K_0=0.6, when extending the cyclic numerical model of Carter et al. (1982) to consider variation in anisotropy, the model suggested the generation of pore pressures during testing moves the effective stress state of the sample towards the failure criterion. The number of cycles of applied loading required for failure decreases with an increased level of cyclic deviator stress, and therefore CSR. However the number of cycles also decreases dependent on the initial stress state and therefore proximity to the failure surface.

Similarly, Cai et al. (2013) examined the undrained behaviour of Wenzhou clay and established for different initial consolidation stress paths, an increase in the vertical stress in relation to the horizontal stress, and therefore K_0 in-situ stress ratio of the sample, resulted in the excess pore pressure coefficient, Skempton's A defined in Equation 2.23 as the ratio between excess pore pressure developed as a result of deviatoric stress q and the change in deviatoric stress itself, decreasing. As such, the stress state of the sample converges away from the failure line, remaining stable under loading.

$$\mathrm{A} = \frac{\Delta u_q}{\Delta\sigma_1 - \Delta\sigma_3} \tag{2.23}$$

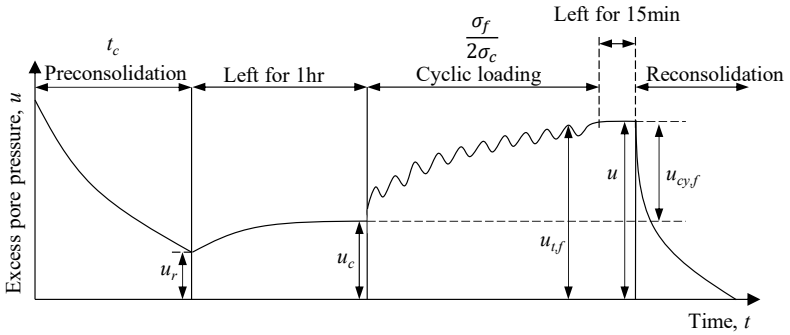

Figure 2.30: Loading scheme adopted for cyclic loading of preconsolidated Ariake clay samples, reproduced from Hirao and Yasuhara (1991)

Hirao and Yasuhara (1991) examined reconstituted Ariake clay samples under various durations of preconsolidation upto 24 hours. The loading scheme performed in cyclic stress controlled tests is shown in Figure 2.30. As concluded by Cai et al. (2013) with respect to sample K_0, Hirao and Yasuhara (1991) observed the longer the duration of preconsolidation, and therefore greater dissipation of excess pore pressure, the greater the gain in sample effective stress and therefore cyclic strength. The authors attributed the decrease in void ratio during the initial consolidation stage to influence the overall sample response, reporting similar findings to those discussed in Section 2.2.4.

2.3.2.2 Over-consolidation Ratio

Fujiwara and Ue (1990) cited the settlement of soil subject to surcharge preloading was dependent on the soil overconsolidation ratio, the degree of consolidation at the time of unloading, the magnitude of static load and the magnitude of repeated load during the service life of the preloaded subgrade. Considering the previous load history of the sample, such that some soils may have previously experienced a higher load to that at the present day, known as the over-consolidation ratio, OCR, the response of to cyclic load has been examined by a number of authors. OCR, defined as the ratio between the pre-consolidation pressure, p'_{c0}, or maximum stress experienced historically, and the existing consolidation stress of the sample, p'_0 is given by;

$$\text{OCR} = \frac{p'_{c0}}{p'_0} \tag{2.24}$$

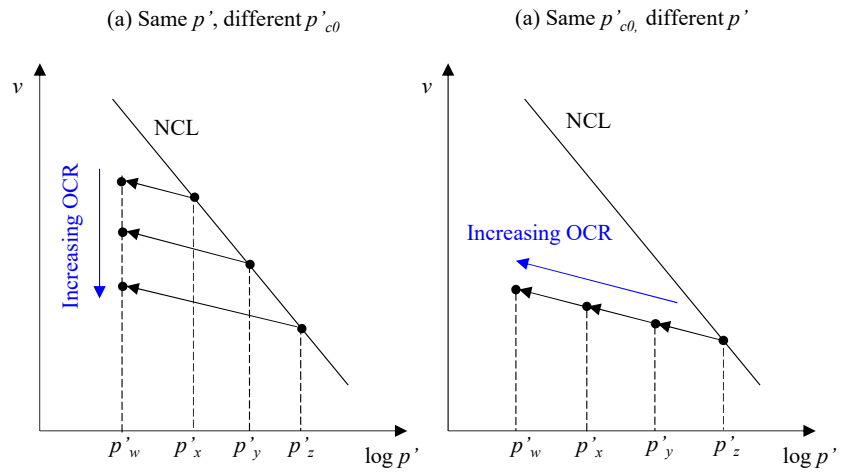

Figure 2.31: Over-consolidation ratio, (a) with the same existing stress (p') and (b) with the same pre-consolidation pressure (p'_{c0})

For an overconsolidation ratio of 1, the current stress experienced by the soil is also the maximum stress the soil has experienced in the past. For an OCR of greater than 1, the soil would have previously experienced a greater stress to that of it's current state. One common method of ground improvement of soft cohesive deposits prior to construction, particularly for new and existing transportation scheme developments, is the use of preloading whereby the soil is over-consolidated prior to construction, shown in Figure 2.31(a). In this case, the load applied to the sample, increases p'_{c0}, and when removed returns the soil to a value of p'. Under this condition, when samples swell upon unloading, for the sample value of p' attained, the monotonic undrained shear strength, c_u, of the sample is increased considering Equation 2.25. However, if instead the sample is loaded to the same value of p'_{c0} and upon unloading attains different values of p', the opposite conclusion with respect to Ladd et al. (1977) is established.

$$\frac{c_u}{\sigma'_v}_{\text{OC}} = \text{OCR}^m \frac{c_u}{\sigma'_v}_{\text{NC}} \tag{2.25}$$

where m can be defined as 0.8 for the majority of clay soils with a plasticity index of less than 60% (Jamiolkowski et al. (1985)).

Brown et al. (1975) examined the response of Keuper Marl silty clay subjected to cyclic loading of frequencies upto 10Hz. The undrained repeated load triaxial

testing performed on the samples considered overconsolidation ratios ranging from 2 to 20. Examining the pore pressure response, the cyclic triaxial tests showed as the overconsolidation ratio of the sample increased, the pore pressure development goes from positive to negative, shown in Figure 2.32. Further studies by Andersen et al. (1980) performed on Drammen Clay showed a similar response, whereby the initial pore pressure accumulation of all samples was positive, other than for an overconsolidation ratio of 10. This response was further demonstrated by the findings of France and Sangrey (1977) where for an overconsolidated clay with an OCR of 8, negative pore pressures accumulated, whilst Matsui et al. (1980) later demonstrated that whilst for an increase in overconsolidation ratio, the initial normalised excess pore pressure reduced. It eventually became negative for an OCR of greater than 3, whilst as the number of cycles increases, the excess pore pressure begins to become positive, shown in Figure 2.33.

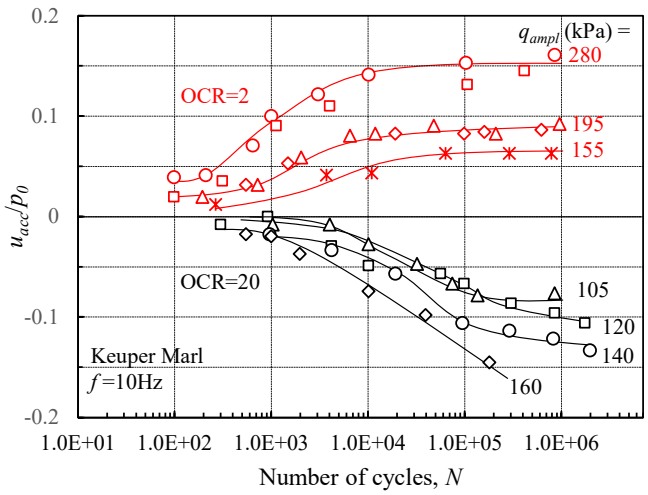

Figure 2.32: Normalised excess pore pressure development for overconsolidated Keuper Marl, after Brown et al. (1975)

Yasuhara et al. (1981) demonstrated the larger the degree of consolidation achieved prior to unloading, therefore greater the magnitude of p'_{c0} and OCR, the smaller the post construction settlements. Supported by Aboshi et al. (1981), the peak shear stress of a soil was shown to increase with the degree of consolidation achieved at the removal of the preload. The results of Sangrey et al. (1969) demonstrated the greater the degree of overconsolidation, the

greater the threshold cyclic stress ratio, whilst demonstrating similar findings with respect to excess pore pressure accumulation. Considering the results comparing an OCR of 1.0 and an OCR of 6, the results appear to contradict the conclusions of Yasuhara et al. (1981) however it should be noted in these tests, samples started from similar initial pressures p'_{c0} prior to being unloaded.

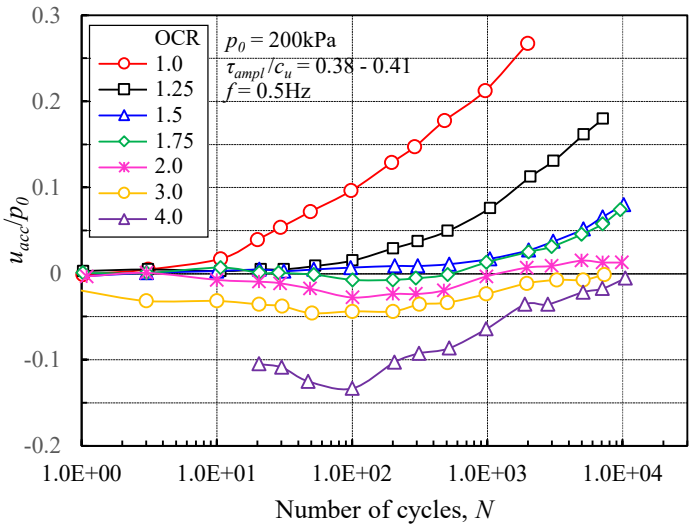

Figure 2.33: Normalised excess pore pressure development, after Matsui et al. (1980)

2.3.2.3 Unloading

Significantly, most studies (Brown et al. (1975), Andersen et al. (1980), Vucetic and Dobry (1988), Matsui et al. (1999), Zhou and Gong (2001), Qian et al. (2018)) presented have considered the application of an initial static deviatoric stress that represents the application of load to a soil, such that the sample is considered to be a better representation of the conditions it would experience following construction, for instance of an embankment or track structure. Liu et al. (2021) instead examined the response of kaolin samples to cyclic loading considering unloading, as shown in Zone 3 in Figure 2.34 reproduced from Liu et al. (2021), where Zone 1 represents the majority of studies presented so far in Section 2.3.2. Under the conditions reflective of Zone 3 in the study, a cyclic stress ratio of 0.2 was adopted. As a result of unloading, and various stages of unloading, reflected by Figure 2.31(b), the axial deformation experienced by the sample was greater due to the position of the stress state relative to failure. The

authors demonstrated that for samples unloaded by a larger $\Delta p'$, thus resulting in a smaller p' with respect to the initial p'_{c0} (a higher OCR) the axial strain accumulation was smaller.

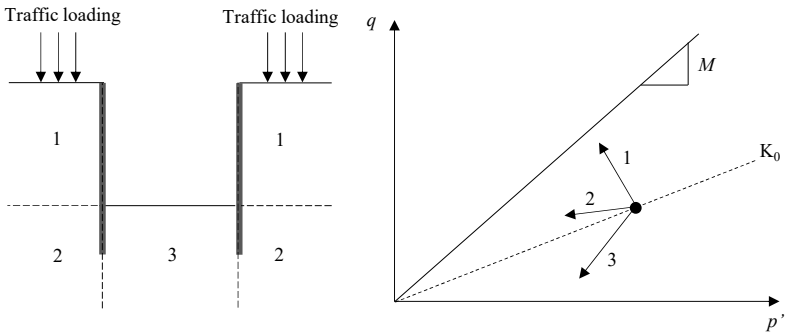

Figure 2.34: Stress zones under consideration during excavation, reproduced after Liu et al. (2021)

2.3.2.4 Partial drainage

Whilst the effect of drainage with respect to post-cyclic response has been reviewed, such that the facilitation of drainage following cyclic loading permits the dissipation of excess pore pressures and subsequent consolidation of the sample, in reality the cyclic load - drainage relationship is more complex with a number of authors adopting partially drained conditions during cyclic tests. Initial early studies by Knight and Blight (1965) commented the total load duration for which a soil subgrade is exposed to traffic load pulses is generally short. As such it would therefore be appropriate to consider a scenario where the loading occurs under undrained conditions whilst subsequently some drainage is then able to occur. Yasuhara and Andersen (1989) performed partially drained tests defined in terms of an undrained test followed by a drainage period., shown in Figure 2.35. For a normally consolidated sample, the drainage period permitted a reduction in void ratio such that the subsequent excess pore pressure accumulation in further periods of loading was repeatedly less. As discussed in Section 2.3.2.2, for an overconsolidated soil, Figure 2.35(b) shows the opposite effect whereby subsequent series of loading resulted in greater excess pore pressure generation.

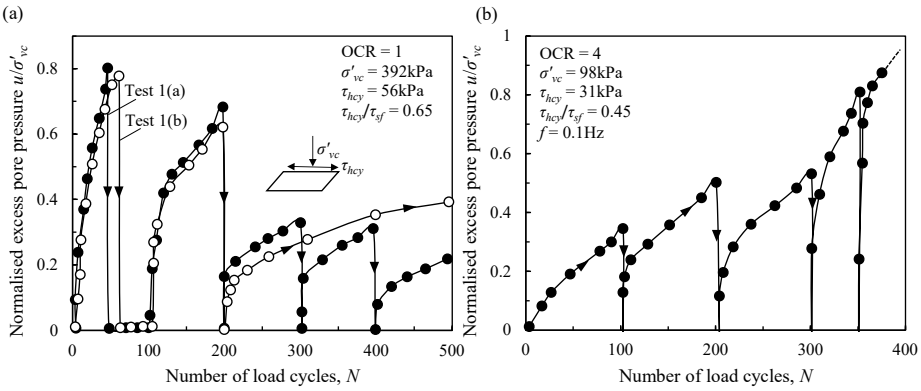

Figure 2.35: Excess pore water pressure accumulation for partially drained tests, reproduced from Yasuhara and Andersen (1989) for (a) Normally consolidated sample (b) Overconsolidated sample

However, for the consideration of a true partially drained condition, as proposed by Hyodo and Yasuhara (1988), Asaoka et al. (1992) and Sakai et al. (2003), it is proposed that whilst excess pore pressures accumulate during cyclic loading, at the same instance they are also permitted to dissipate thus creating a condition of partial drainage. In this way, the condition can be achieved by performing cyclic tests with drainage lines open on cohesive samples. Therefore, not only is there accumulation of axial strain, but also volumetric strain, proposed by Sakai et al. (2003) to generate in response to the excess pore pressure generated under these conditions, shown in Figure 2.36.

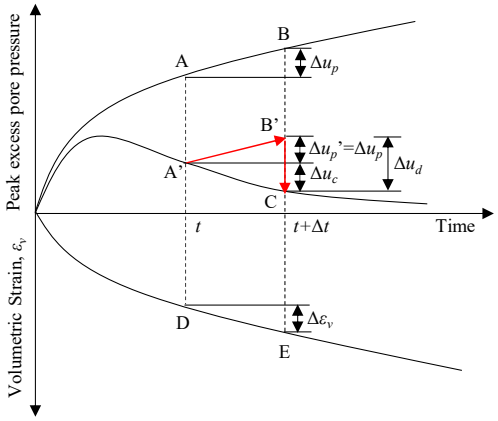

Figure 2.36: The behaviour of soil under partially drained conditions of cyclic loading, reproduced from Sakai et al. (2003)

Examining Ariake clay, and considering the case history and settlement data

obtained from the Saga Airport in Japan, the authors concluded the evolution of volumetric strain was dependent on the cyclic stress ratio, defined as q_{cyc}/p'_{c0}. In the subsequent model development, the compressibility of the sample was accounted for;

$$m_{vr} = \frac{0.44\alpha_c C_s}{(1+e_c)(1-u_p/p'_{c0})p'_{c0}} \tag{2.26}$$

where C_s is the swelling index of the soil and u_p is the peak excess pore pressure.

There have been limited studies examining the partially drained conditions of a sample, more recently Ni (2012) considered the effects of partial drainage with respect to the condition achieved via the introduction of prefabricated vertical drains. Sun et al. (2015a) subsequently considered partially drained conditions when examining the variation of confining pressure with respect to constant and variable confining pressures on Wenzhou clay.

2.3.3 Influence of Load Application

Whilst most cyclic triaxial tests have used the application of purely compressive cyclic deviatoric stress, various researchers have demonstrated this method could be insufficient for the simulation of traffic load (Powrie et al. (2007), Grabe (2009), Cai et al. (2013)). Lekarp et al. (2000) acknowledged the simulation of traffic loading constituted simultaneous variation of confining pressure and shear stress; requiring rotation of principal stress axes, presented in Figure 2.37. A number of authors have utilised hollow cylinder apparatus (Miura et al. (1986), Tong et al. (2010), Ishikawa et al. (2011), Xiao et al. (2014), Sun et al. (2015a)) to couple the cyclic vertical normal stress, horizontal normal stress and shear stresses however variable confining pressure (VCP) triaxial tests have also been employed for coarse soils, for example by Wichtmann et al. (2007), Gu et al. (2012) and Gu et al. (2016).

Cai et al. (2013) compared the response of saturated remoulded clays obtained from Wenzhou City in China to both constant and variable confining pressure, demonstrating the cyclic varying pressures had a greater effect on the pore pressure and axial strain response of the samples for VCP tests when considering the equivalent CCP (constant confining pressure) sample. Sun et al. (2015a)

extended this study further to consider natural soft clay samples cut from block samples at slightly deeper depths of 11m below ground level.

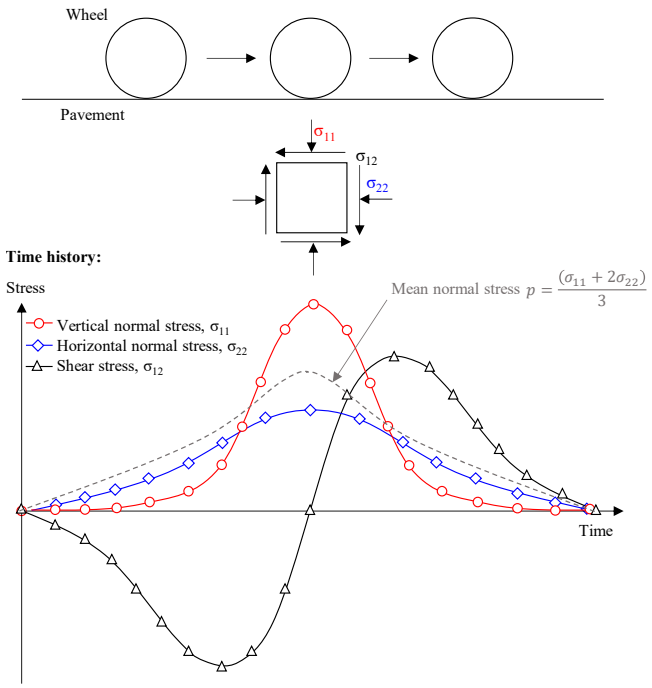

Figure 2.37: Stress distribution under a moving load, after Lekarp et al. (2000)

The authors performed both VCP and CCP triaxial tests with the drainage lines open, examining a range of stress ratios. In such tests, the cyclic stress ratio was defined as the ratio between the cyclic deviator stress applied to the sample and the initial mean effective confining pressure of the sample, p_{c0}. To define the stress paths in VCP and CCP tests, the stress ratio, defined as η was employed, defined in terms of the magnitude of cyclic deviator stress, q_{ampl}, equivalent to q_{cyc} in cyclic triaxial tests, and p_{ampl}, the cyclic mean principal stress, shown in Equation 2.27. Therefore, for CCP drained triaxial tests, η is equivalent to 1/3, whilst the other values of η examined by the authors considered larger ratios such that the magnitude of p_{ampl} in relation to q_{ampl} was greater, shown in Figure 2.38.

$$\eta = \frac{p_{ampl}}{q_{ampl}} \tag{2.27}$$

Considering the response of strain, the greater the stress ratio applied, the

greater the accumulation of both permanent volumetric and axial strains. As reported for partially drained tests, at commencement of the tests the excess pore pressures initially generated faster than they were dissipated. The greater the excess pore pressure generated, the greater the volumetric strain accumulation, noting the confining pressure played a significant role in the development of volumetric strains, irrespective of the CSR considered. For undrained tests, Cai et al. (2013) concluded the excess pore pressure were significantly influenced by the stress path considered, whilst the axial strain determined from CCP was greater than that of VCP tests. This was further demonstrated by Huang et al. (2020) whom demonstrated the ratio between the plastic strain under both types of confining pressure was a function of the stress ratio considered, shown in Figure 2.39. Considering drained conditions however, CCP tests under estimated the rate of displacement, further supported by Sun et al. (2015b).

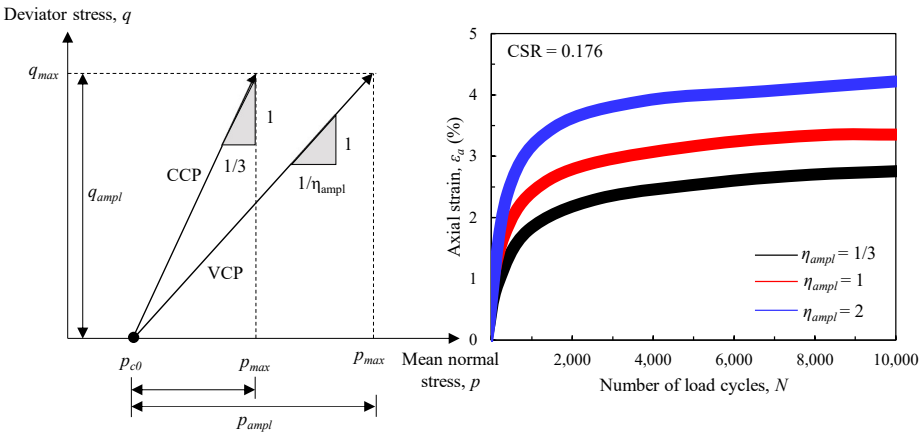

Figure 2.38: Assessment of CCP and VCP triaxial tests, reproduced after Sun et al. (2015a)

Guo et al. (2018) examined the undrained response of soft clay using cyclic hollow cylinder apparatus in which cyclic vertical and torsional shear were controlled. The authors concluded the stress path, and therefore rotation of principal stresses during testing, governed the excess pore pressure response, as per Cai et al. (2013) further noting the difference between the responses observed in cyclic triaxial and HCA tests increases as the cyclic stress ratio increased. Yang et al. (2019) and Wang et al. (2021) further reported that whilst the increase in axial strain arose with respect to number of principal stress rotation cycles,

the permanent axial strain for a stable sample could be determined based on the cyclic deviator stress applied during cyclic loading, irrespective of their confining pressure.

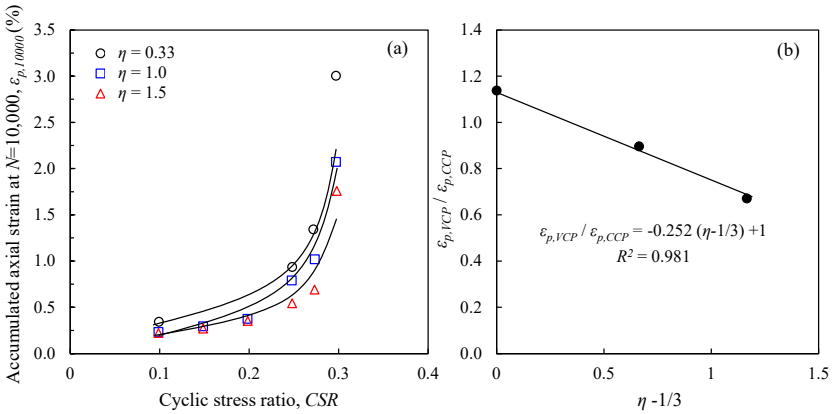

Figure 2.39: Response of axial strain with respect to cyclic stress ratio for different stress paths, reproduced after Huang et al. (2020)

2.4 Field Tests

Whilst the response of soil strain and excess pore pressures has been demonstrated with various forms of laboratory testing and described using empirical and numerical solutions, the exploration of the response in the field, particularly with respect to slab track systems has generally been limited to case histories where, as such, the assessment is post-event and significant or unexpected displacements have accumulated that have approached or reached the serviceability limit state of the system (He (2005), Cui et al. (2014)). Extensive field tests are costly and obtaining complete results in the field is extremely difficult (Bian et al. (2016)) owing to the numerous external factors influencing such a system, including but not limited to track substructure information and weather and climate information. As a result, large scale physical model tests and instrumented trial areas, such that certain external factors can be closely controlled and monitored provide a more economically viable solution for assessing the dynamic performance of rail track systems, bridging the gap between small-scale laboratory testing and numerical models and case histories.

2.4.1 Ballast Track Tests

Ballasted track system scale model tests were performed by Brown et al. (2007) with a model size of 4.1m x 2.1m x 1.9m, applying sinusoidal loads directly to the arrangement of three sleepers to determine the response of the underlying ballast at a train speed of 28km/h. As demonstrated by hollow cylinder tests, Section 2.3.3, not only was the speed important to the response observed, but also the movement and therefore principal stress rotation of a soil element, termed by the authors as the 'moving effect'.

Indraratna et al. (2021) recently undertook full scale 1:1 ballast track modelling with a test size of 6.0m x 6.0m x 2.3m for the assessment heavy haul freight train passages, considering a speed of between 60 and 80km/h and a maximum load of 125kN. The vertical settlements, for upto 550,000 load cycles, are presented in Figure 2.40 and compared to that of laboratory tests and field measurements. The authors noted the discrepancy between the field test and instrumented scale model, attributing the greater vertical displacement in the field to the construction of the track on an alluvial flood plain (Indraratna et al. (2010)).

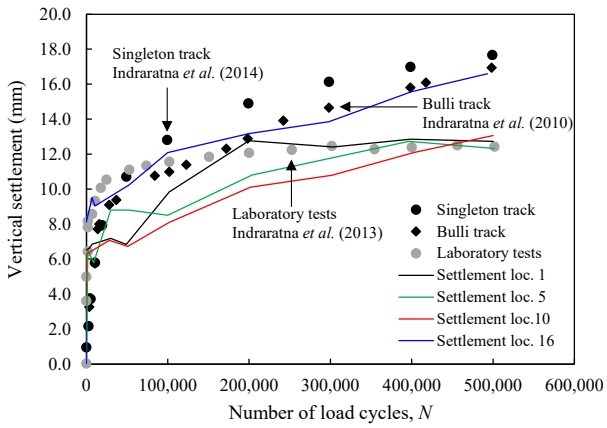

Figure 2.40: Response of full scale ballast track modelling, after Indraratna et al. (2021)

Unlike the scale tests above, Connolly et al. (2014) reported the results of three field experiments in Belgium, examining the effects of train passage on different earthwork geometries; at-grade, embankment and cutting sections, presented in Figure 2.41. These tests were achievable due to the distance of geophones from the track location to measure the influence of vibration, rather

than instrumentation directly beneath the track. As such, displacements at the track location were not measured however the results for vertical shear strain provide an indication of the distance from the track that such dynamic loads can influence, shown in Figure 2.41. Later, Connolly et al. (2015) reviewed cases from across Europe, concluding the influence of the passage of a high speed train can be significantly affected by the underlying soil subgrade properties.

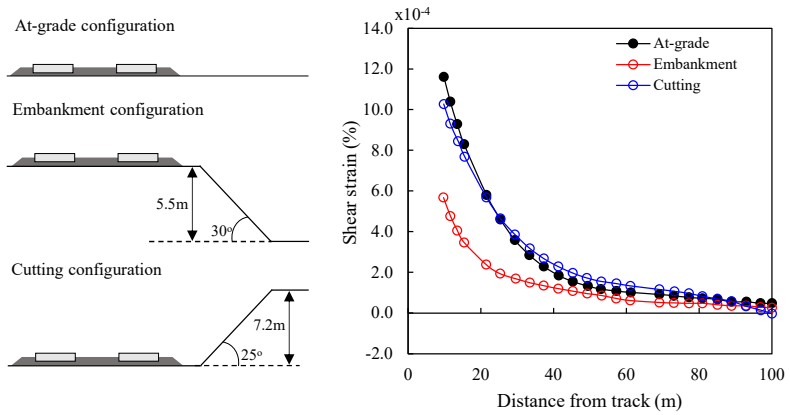

Figure 2.41: Results of field experiments in Belgium, after Connolly et al. (2014)

2.4.2 Slab Track Tests

A full-scale physical model test apparatus for slab track systems was performed by Bian et al. (2016). The results of the full scale test at 15m x 5m x 6m demonstrated close agreement with the field tests undertaken during test runs of the Wuguang and Jingjin high-speed tracks undertaken by Fan (2010) whilst achieving loading representative of train speeds between 180 and 360km/h with 8 load actuators.

Čebašek et al. (2018) contrasted the response of two test sections of track, a ballasted section under three concrete sleepers and a slab track section constructed with three in-built sleepers. Phased loading was adopted to simulate the passage of a train, applying loads of 58kN at 5.6Hz and 83kN at 2.5Hz based on the frequency calculated based on bogie distance, as per Table 2.3 and the optimum performance of the test rig respectively. In turn, a frequency of 5.6Hz corresponds to approximately 100m/s when applied in

phase by three actuators, shown in Figure 2.42(a). The settlement of both track forms under these frequencies are presented in Figure 2.42(b).

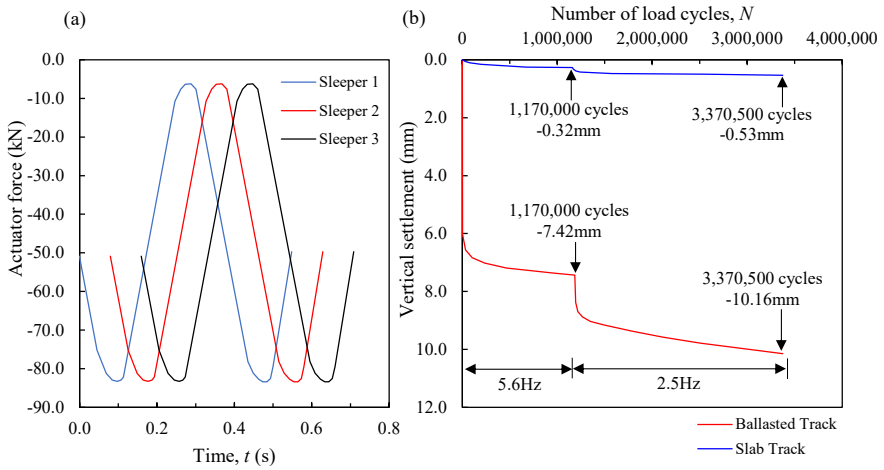

Figure 2.42: Settlement of ballast and slab track, after Čebašek et al. (2018)

Similarly, Zhai et al. (2020) also analysed both ballasted and slab track systems in their test rig, detailing the assessment to explicitly consider 5 track structures commonly adopted in rail track construction in China. This rig was larger than other rigs at 72.5m x 6m x 5.87m however housed all 5 track variations under consideration. Each track formation had a length of between 8.125m (Double-block track) and 16.35m (CRTS III track), both forms of slab track that vary with respect to reinforcement arrangements. Results demonstrated that when constructed according to Chinese high-speed rail standards, the vertical displacements after over 4 million train load cycles were still tolerable with respect to the operational allowances of the network. However, consideration was not given to soft subgrade soils for which may not, or be borderline, when satisfying the initial subgrade stiffness requirements of a design standard.

Considering subgrade stiffness, Xiao et al. (2016) undertook field tests in China subjecting constructed formations to a series of pulses generated at subgrade level with a dynamic stress amplitude of 92kPa ranging in frequency between 3 and 22Hz. Due to the high liquidity limits of the natural formations, lime stabilisation was used to improve the subgrade stiffness in order to satisfy the design standard adopted. Under these conditions, the tests on various sections resulted in displacements of less than 5mm for both embankment and cutting

sections. As demonstrated by Connolly et al. (2014), cutting settlements under dynamic load were less than those experienced due to dynamic loading of an embankment. Similarly, the results of Xiao et al. (2014) on treated subgrade presented elastic, recoverable, displacements in the order of approximately 0.3mm. It was noted under a period of significant rainfall this increased to 0.45mm. Liu et al. (2020) examined the operational line of Shanghai-Nanjing, 5 years post-construction, that had been constructed on a piled embankment platform for improved subgrade properties. In this case the elastic displacements were observed to be approximately 0.22mm, demonstrating that provided the underlying subgrade soils have sufficient strength and stiffness, achieved by various improvement methods, the dynamic elastic displacements observed in the field are low.

The findings in the field, from both instrumented full scale ballasted and slab track tests and instrumentation measurements of live track systems exhibit the same responses to the experimental studies in the laboratory; a rapid accumulation of strain during the initial stages of loading, followed by attaining a stable level of strain after subsequent repeated cycles of loading.

2.5 Conclusions

A detailed review of the response of cohesive soils subjected to cyclic loading has been presented considering factors that influence the performance of clay subgrade soils, particularly for the consideration of traffic loading.

- An examination of the rail track structure and range of frequencies associated with train loading is presented, considering how this loading has been studied in the laboratory and in empirical calculations to anticipate subgrade performance.
- Clay soils subjected to cyclic loading exhibit a response under undrained conditions that is influenced by the cyclic stress ratio of the sample, governed by the magnitude of applied cyclic load in relation to the static strength of the soil.

- The rate of applied loading, the frequency of the load, has also been shown to influence the response of soil however this influence diminishes with an increasing number of cycles that is more representative of traffic loading conditions.
- Considering in-situ conditions representative of traffic loading in particular, the accumulation of strain is influenced by the loading history of the soil, the initial stress conditions of the sample and in-situ stress ratio and the overconsolidation ratio.
- The settlement of soils are influenced by the accumulation of excess pore pressures and their subsequent dissipation, when permitted. As such, the response of a soil is also influenced by the drainage conditions under consideration, both during and after cyclic loading.
- Limited field tests exist to examine this behaviour, due to the difficulties in instrumenting operational track, however the axial strain development of subgrade soils beneath both ballast and slab track have been shown to demonstrate a similar response to that examined in the laboratory.

Chapter 3

Undrained Loading Behaviour of Soils

3.1 Introduction

To determine the long-term cyclic response of clay soils, it is important to consider the properties and initial conditions of the samples, ensuring they are representative of the in-situ conditions of subgrade soils. This Chapter presents the results of one dimensional compression tests to establish the deformation characteristics of the kaolinite samples tested. Subsequently, undrained monotonic triaxial tests describe the strength properties and define the in-situ conditions to be adopted in cyclic tests. Undrained cyclic triaxial tests have been performed considering a range of frequencies and cyclic stress ratios. The response of axial strain and normalised excess pore pressure have been examined considering the duration of loading as well as the number of cycles of loading to subsequently determine the effects of cyclic loading on the stability of the samples. A reduction in the strength of samples following undrained cyclic loading was identified, influenced by the magnitude of cyclic load applied to the sample. Similarly, as the cyclic load approached that of the monotonic deviatoric stress at failure, such that the cyclic stress ratio tends towards one, a threshold stress ratio was determined where cyclic tests attained failure irrespective of the frequency of loading applied to the sample. The results of undrained cyclic triaxial tests have also been used as a reference for

further cyclic triaxial testing presented in Chapter 4.

3.1.1 Soil Properties

Reconstituted kaolinite specimens were used for the undrained one dimensional compression tests and the static and cyclic triaxial tests. The samples were 70mm diameter and 20mm height for the one dimensional tests and 38mm diameter and 76mm height for the triaxial tests and had the following properties:

- A specific gravity of G_s= 2.68.
- A plastic limit of w_p = 25%. The plastic limit is defined as the moisture content at which a soil transitions between brittle and plastic behaviour. The plastic limit can be determined from the moisture content whereby a soil thread begins to crumble when rolled to a 3mm diameter. The results of three plastic limit tests are given in Table 3.1. The plastic limit is calculated as the average of the moisture contents reached in the tests: $w_p = (0.26 + 0.25 + 0.24)/3 = 0.25$.

Table 3.1: Moisture content data for determination of plastic limit

Container Name:	A01	A02	A03
Mass of container (g)	4.28	5.34	8.77
Mass of container and wet sample (g)	5.92	6.93	9.70
Mass of container and dry sample (g)	5.58	6.61	9.52
Moisture loss (g)	0.34	0.32	0.18
Mass of solid particles (g)	1.30	1.27	0.75
Moisture content (%)	0.26	0.25	0.24

- A liquid limit of w_L = 55%. The liquid limit w_L is defined as the moisture content at which a soil begins to behave as a liquid, transitioning from plastic behaviour to liquid behaviour. The liquid limit has been determined using Casagrande Apparatus, defined in the laboratory as the moisture content at which two sides of a 12.7mm groove close under 25 drops of the cup. Under a closure of between 15 and 30 cup drops, the results can be factored using the following equation:

  $f = (\frac{N}{25})^{0.12}$

  The results of 3 liquid limit tests are given in Table 3.2, where the average of the three tests gives the liquid limit of the soil in the tests of 0.55.

Table 3.2: Moisture content data for determination of liquid limit

Container Name:	B01	B02	B03
Mass of container (g)	4.76	4.97	4.52
Mass of container and wet sample (g)	21.32	14.55	20.64
Mass of container and dry sample (g)	15.39	11.18	14.86
Moisture loss (g)	5.93	3.37	5.78
Mass of solid particles (g)	10.63	6.21	10.34
Moisture content (%)	0.56	0.54	0.56
Number of cup drops, N	26	24	21
Factor, f	1.005	0.995	0.979
Liquid limit (%)	0.56	0.54	0.55

- A plasticity index of $I_p = 0.30$. The plasticity index is defined as the range of moisture contents where a soil exhibits plastic behaviour and is determined as $I_p = w_L - w_p = 0.55 - 0.25 = 0.30$.

3.2 Compression Properties

An important consideration in the design and engineering of transportation schemes over clay deposits is the consolidation of clay subsoil layers underlying the route. Both the strength and deformation characteristics of the soil to be used in design are affected by the compressibility of the soil, which for a clay soil is heavily influenced by the rheological properties of the soil. Considering the design of trackbeds and embankments and the design life of these structures, it is important to determine the compression response of these clay layers.

The deformation response of the soil can generally be defined in two phases; primary and secondary whereby the creep behaviour of the soil dominates the secondary phase. The oedometer enables the evaluation of both phases of compression response of the soil. The one dimensional (1D) compression test developed by Terzaghi, also known as the oedometer test, represents simple consolidation conditions whereby it is assumed the soil is subjected to loading only in the direction of maximum principal stress and the subsequent lateral expansion of the soil is prohibited by the confining ring of the sample.

In order to examine the compression, and the subsequent swelling response as a result of unloading of a clay sample, four one dimensional compression tests

are presented. Tests were undertaken using lever arm oedometer apparatus with incremental loading. The samples were confined laterally by a steel ring with a 70mm diameter and 20mm height. This sample size resulted in a diameter:height ratio of 3.5, satisfying British Standards BS 1377 (British Standard (1990)). Under an applied load, it is accepted there will be small variations in the stress state within the sample, whereby the greatest soil density is expected to be at the top of the sample and in the centre directly beneath the load piston application, however the use of a diameter:height ratio of between 3 and 4 is accepted to minimise the potential creation of a non-homogeneous stress state under the applied load. The inside of the confining ring was lined with a thin layer of silicone grease in order to inhibit the surface friction between the ring and the sides of the sample, further reducing the potential of uneven stress distributions within the sample. The sample was placed between two porous plates with filter paper placed on the top and bottom surfaces of the sample preventing particle migration into the porous stones. In order to ensure the samples remained fully saturated, the compression cell was filled with water and the laboratory environment maintained to a constant temperature.

3.2.1 One Dimensional Compression Tests

Oedometer tests were conducted using laboratory prepared remoulded kaolinite samples, where kaolinite powder was mixed to a slurry at a water content of 150% before applying a static load to achieve a pre-consolidation pressure of 10 kPa. A low pre-consolidation pressure was used for the oedometer tests in order to characterise the initial load response of the soil without a significant amount of initial recompression of the sample. Four one dimensional compression tests are presented that each aim to address a different objective with respect to the compressive (loading) and swelling (unloading) response of the kaolinite soil. A summary of the tests undertaken with respect to the cycles of load and unload of the samples and their duration are presented in Tables 3.3, 3.4 and 3.5.

Initial test C01 investigates the influence of the unload-reload cycle number on the response of the soil which is similar to a soil element being subjected to a number of train or vehicle passages. Test C02 is intended to address the

effects of loading history on the properties of the soil during recompression of the kaolinite samples. Test C03 aims to investigate the influence of load duration on the compression and swelling response of the soil subjected to increased increments of loading whilst test C04 is intended to analyse the effect of unloading amplitude on the soil sample and subsequently the swelling response of the kaolinite samples.

Table 3.3: Test schedule for one dimensional compressions tests C01 and C02

Sample Name:	Stage	Load (kPa)	Stage	Load (kPa)	Stage	Load (kPa)
C01 and C02	1	5	9	20	17	80
	2	10	10	40	18	40
	3	20	11	80	19	20
	4	40	12	40	20	10
	5	80	13	20	21	20
	6	40	14	10	22	40
	7	20	15	20	23	80
	8	10	16	40		

where the load stage duration for C01 is 1 day (total test duration of 23 days) and the load stage duration for C02 is 7 days per stage (total test duration of 155 days).

Table 3.4: Test schedule for one dimensional compressions tests C03

Sample Name:	Stage	Load (kPa)	Stage	Load (kPa)	Stage	Load (kPa)
C03	1	5	12	160*	23	80
	2	10	13	80	24	40
	3	20	14	40	25	20
	4	40	15	20	26	10*
	5	80*	16	10*	27	20
	6	40	17	20	28	40
	7	20	18	40	29	80
	8	10*	19	80	30	160
	9	20	20	160	31	320
	10	40	21	320*		
	11	80	22	160		

where the load stage duration for C03 is 1 day for each load increment. Load was held constant for 7 days for the final load stage and unload stage, denoted by * (total test duration of 67 days).

Table 3.5: Test schedule for one dimensional compressions tests C04

Sample Name:	Stage	Load (kPa)	Stage	Load (kPa)	Stage	Load (kPa)
C04	1	5	10	40	19	80
	2	10	11	20*	20	160
	3	20	12	40	21	320*
	4	40	13	80	22	160
	5	80	14	160	23	80*
	6	160	15	320*	24	160
	7	320*	16	160	25	320
	8	160	17	80		
	9	80	18	40*		

where the load stage duration for C03 is 1 day for each load increment. Load was held constant for 7 days for the final load stage and unload stage, denoted by * (total test duration of 61 days).

The loading pattern is maintained during cycles of load and unload such that the same load increment is applied in the reverse order for the unloading of the kaolinite samples for a time duration of either 1 day or 7 days. A load duration of 1 day was selected to permit the equilibration of pore pressures within the kaolinite sample.

The loading profiles of the four consolidation tests summarising the change in vertical strain with respect to vertical pressure are presented in Figure 3.1 alongside the corresponding compression parameter, λ/V, and rebound parameter, κ/V, for each unload-reload cycle. The compression parameter, λ/V, is described by the gradient of the line describing the virgin compression response of the sample, defined by the increment of vertical strain ($\Delta\epsilon_z$) as a result of a change in the vertical stress ($\Delta\ln(\sigma'_z)$) considering an ln scale. The rebound parameter, κ/V, is defined via the same procedure for the unload-reload response of the sample.

$$\frac{\lambda}{V} = \frac{\Delta\epsilon_z}{\Delta\ln(\sigma'_z)} = \frac{\epsilon_{z2} - \epsilon_{z1}}{\ln(\sigma'_{z2}/\sigma'_{z1})} \tag{3.1}$$

Conversely, the compression index, C_c, and swelling index, C_s, of the sample can be determined:

$$\frac{C_c}{V} = \ln(10)\frac{\lambda}{V} = 2.3\frac{\lambda}{V} \tag{3.2}$$

$$\frac{C_s}{V} = \ln(10)\frac{\kappa}{V} = 2.3\frac{\kappa}{V} \tag{3.3}$$

The values of compression index range from 0.39 to 0.42 whilst the values for rebound index range between 0.073 and 0.109. This range of values is in agreement with values obtained on kaolinite clay according to Banerjee and Yousif (1986) and values calculated using the Wroth and Wood (1978) relationship for remoulded normally consolidated clays. A summary of these values determined for each test is presented in Table 3.6 alongside the determined creep parameters ψ^c/V and $C_{\alpha e}$, defined by Yin and Graham (1989) and Yin and Graham (1994).

Table 3.6: Compression and viscous parameters for kaolinite samples

Sample Name:	λ/V	κ/V	C_c	C_s	ψ^c/V	$C_{\alpha e}$
C01	0.184	0.047	0.424	0.109	0.0019	0.011
		0.042		0.098		
		0.035		0.081		
C02	0.169	0.040	0.389	0.093	0.0014	0.008
		0.038		0.087		
		0.037		0.084		
C03	0.176	0.039	0.406	0.091	0.0010	0.007
		0.043		0.100		
		0.045		0.103		
C04	0.180	0.037	0.415	0.084	0.0013	
		0.035		0.080		
		0.032		0.073		

The creep coefficient, ψ_c^0 is defined from the linear response of vertical strain with respect to the natural logarithm of time, shown in Equation 3.4. t_c^e is defined as the equivalent time with respect to creep, determined by Yin and Graham (1994) and discussed in Chapter 2, whilst t_0^c defines the beginning of creep time and is related to the strain rate of the reference time line, determined from Figures 3.9 and 3.10 for 1 day and 7 day load durations respectively.

$$\epsilon_z = \epsilon_{z0} + \frac{\psi^c}{V}\ln\left(\frac{t_0^c + t_e^c}{t_0^c}\right) \tag{3.4}$$

where the secondary compression index, $C_{\alpha e}$, defined by Mitchell and Soga

(2005) after Lambe and Whitman (1969), can be expressed;

$$\frac{\psi^c}{V} = \ln(10)\frac{C_{\alpha e}}{V} = 2.3\frac{C_{\alpha e}}{V} \tag{3.5}$$

Examining each individual test in detail, test C01, with a load duration of 1 day for each increment of applied load, demonstrates that the soil exhibits a viscous response during loading. Shown in Figure 3.2, a strain increment still continues following the end of primary consolidation. Using Casagrande's log t method, it is determined that t_{EOP} is between 31 and 82 minutes. The creep parameter, ψ^c/V, is 0.0019 for test C01. For the unloading response of the soil, the t_{EOP} of an unloading reloading stage occurs earlier than for virgin loading, at a t, previously demonstrated by Feng et al. (2017), whilst ψ^c/V of the reloading stage following t_{EOP} is 0.011, less than for the same load increment considering virgin consolidation.

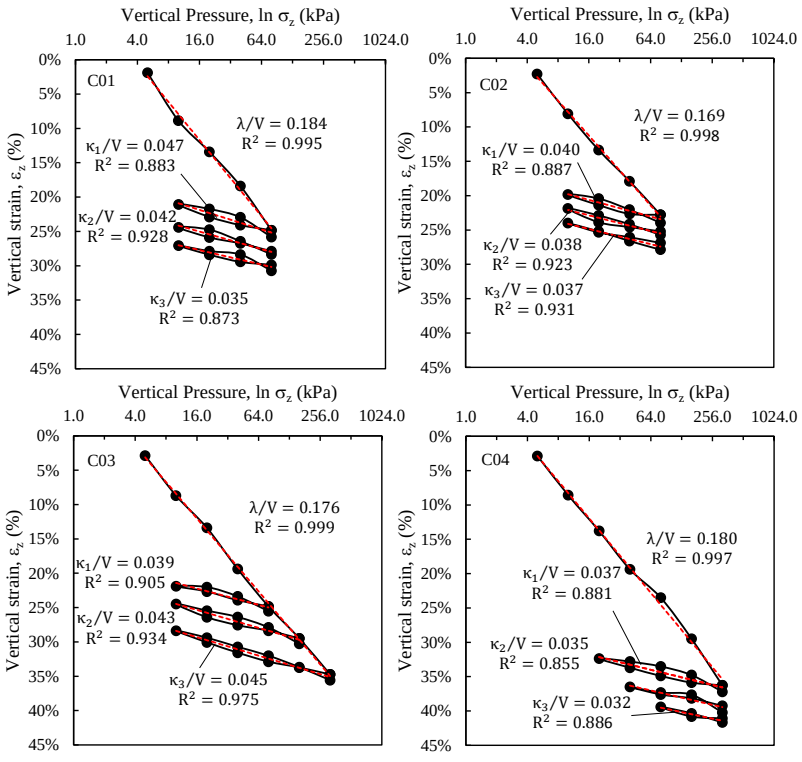

Figure 3.1: Relationship between vertical strain and logarithm of vertical effective stress for samples C01 to C04

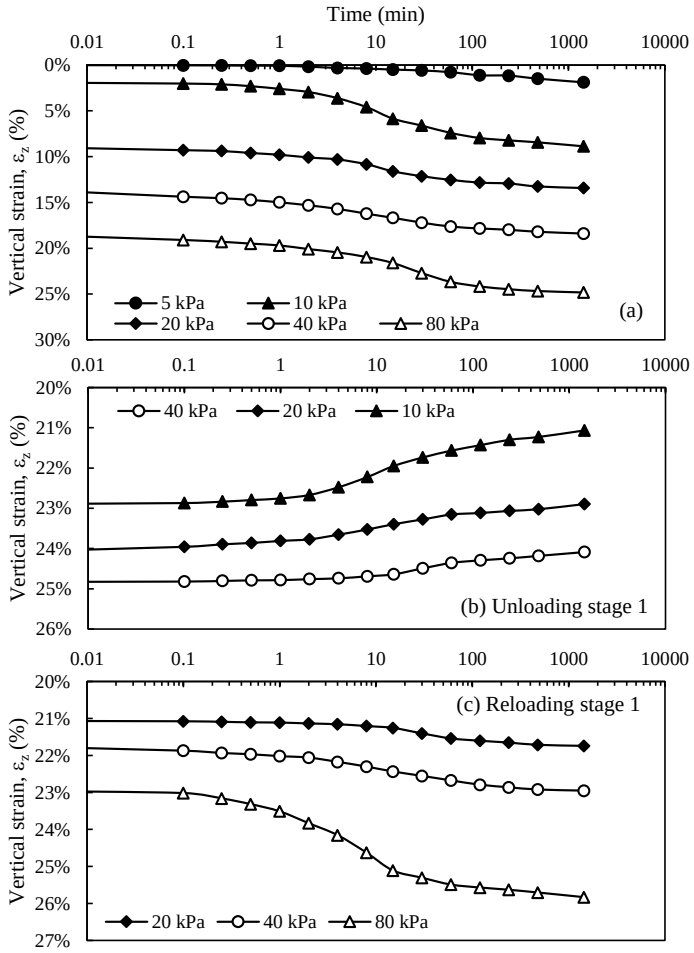

Figure 3.2: Relationship between vertical strain and log time for sample C01 (a) Loading stage (b) First unloading stage (c) First reloading stage

Soil creep deformation is characterised as time-dependent stress-strain behaviour that is dependent on the rate of loading (Yin et al. (2010)). The results of test C02, subjecting the sample to a load duration of 7 days, are presented in 3.3. Examination of the creep parameter gives a value of ψ^c / V of 0.0014, less than for test C01.

Examining the load response of test C01 and C02 subjected 80 kPa load in more detail, presented in Figure 3.6, it can be demonstrated that different values of $C_{\alpha e}$ are determined as a result of 1 day load increments compared to 7 day increments. The secondary compression index is significantly lower for the results of a 7 day load stage, demonstrating creep is a time dependent response

that will eventually tend to a finite limit Yin and Graham (1994).

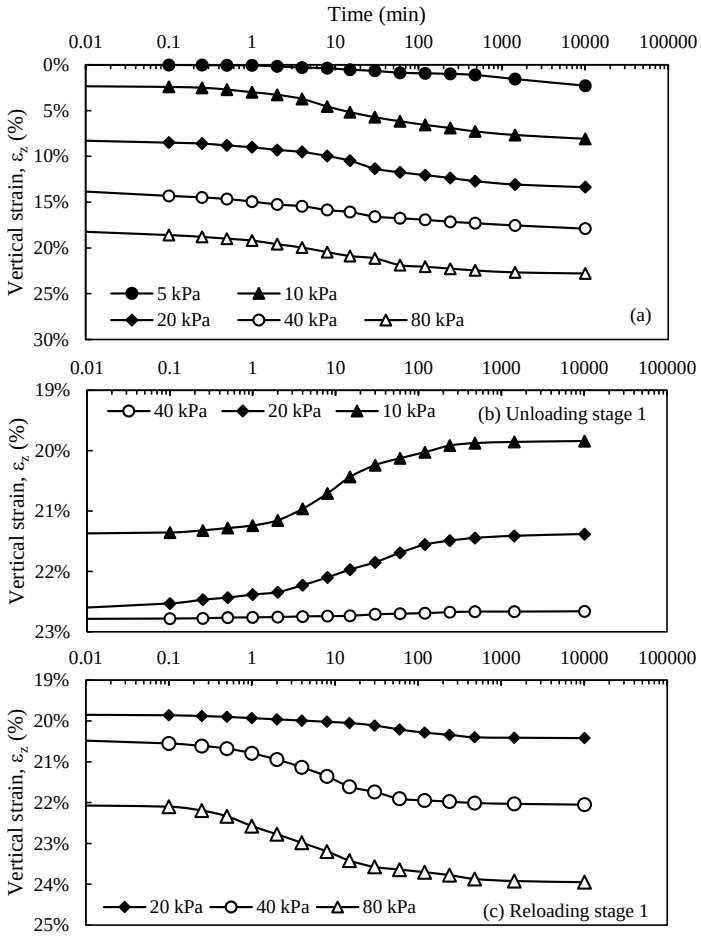

Figure 3.3: Relationship between vertical strain and log time for sample C02 (a) Loading stage (b) First unloading stage (c) First reloading stage

Considering the long term response of the sample the results demonstrate that using the value of secondary compression determined from a one day test could overpredict the amount of creep settlement a soil layer would exhibit subject to an applied static load. Feng et al. (2017) previously acknowledged that the use of a value of $\frac{\psi^c}{V}$ fitted based on test data with 7 day increments would reduce the difference between the observed and predicted results. However, the body of test results demonstrate that with an increase in load, the creep parameter reduces and subsequently, considering the design life of an engineering scheme, avoiding an over prediction of the creep settlement of clay sublayers can be

difficult. Whilst in practise this is a conservative approach, the determination of parameters based on 7 day increments could reduce the over-design of projects.

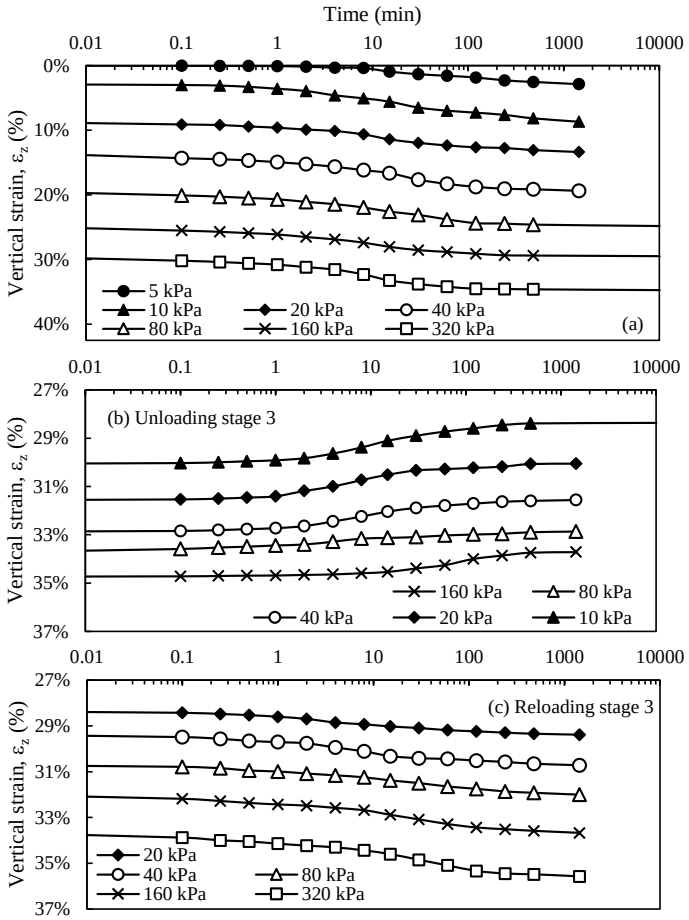

Figure 3.4: Relationship between vertical strain and log time for sample C03 (a) Loading stage (b) Final unloading stage (c) Final reloading stage

The influence of loading increment is examined in test C03, presented in 3.4. Considering the full loading profile, ψ^c/V of the final loading step of 320 kPa is 0.0010. The creep parameter is noted to progressively decrease with each increase in load increment. Upon examination of the reload phase 3 also presented, there is an increase in the value of ψ^c/V from 0.005 at 20 kPa to 0.009 at 160 kPa before a decrease to a value of 0.007 when the load is increased further to 320 kPa. Whilst these values, particularly during the reload cycle are low, it is important to acknowledge that a variation in the amount of creep

anticipated not only varies with respect to the amount of loading but also the previous loading history of the soil.

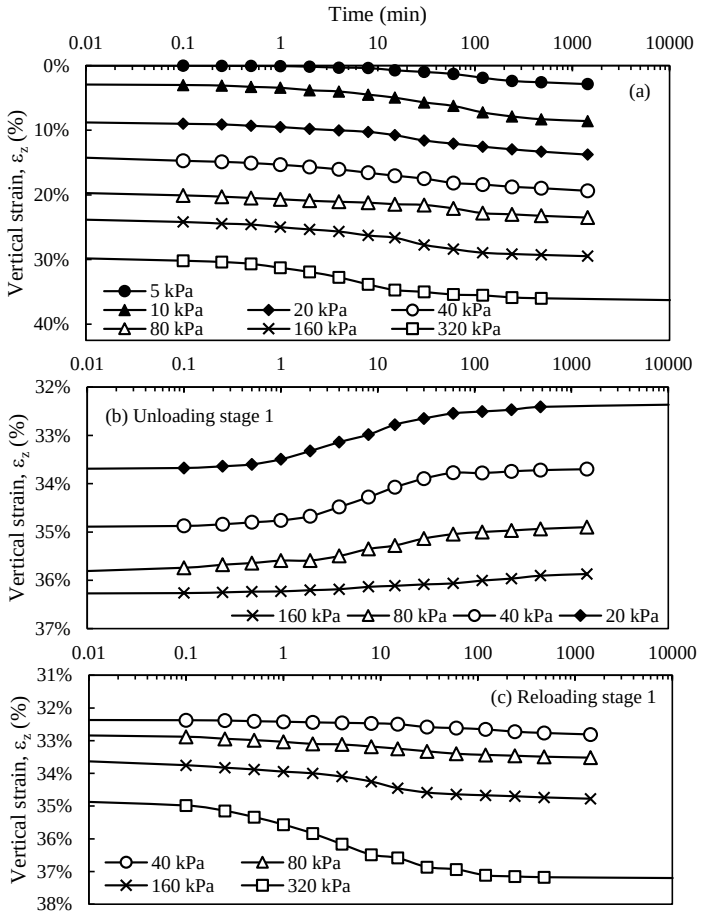

Figure 3.5: Relationship between vertical strain and log time for sample C04 (a) Loading stage (b) First unloading stage (c) First reloading stage

Further examining the loading history, the influence of the unload period is examined in test C04, Figure 3.5. Considering the reload phase to a vertical stress of 320 kPa, the value of ψ^c / V is 0.003, significantly less than the same reload increment in test C03. In test C04, the full reload path of the soil is reconsolidated following unloading from 320 kPa, unlike in test C03 where a reload increment of 320 kPa is within the normally consolidated behaviour of the soil, further demonstrating the importance of the stress history of the soil.

Considering normally consolidated samples, Feng et al. (2017) demonstrated

that the value of $C_{\alpha e}$ decreased with an increase in vertical stress for Hong Kong Marine Deposits (HKMD). Takeda et al. (2012) also demonstrated this for Hitachi clay. However at stresses below the preconsolidation pressure, such that the sample is overconsolidated, Takeda et al. (2012) noted a rapid increase in $C_{\alpha e}$. This has been demonstrated by plotting the values of $C_{\alpha e}$ for the reloading cycle of test C03, shown in Figure 3.7. It should be noted that the results are plotted against average vertical effective stress, σ'_z as there is likely to be some variation in the stress response throughout the sample due to the apparatus used, as noted above.

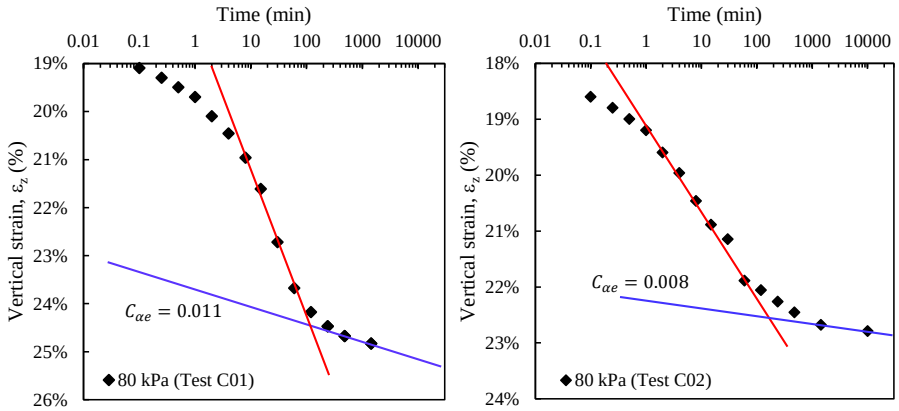

Figure 3.6: Determination of $C_{\alpha e}$ for 80kPa load increment

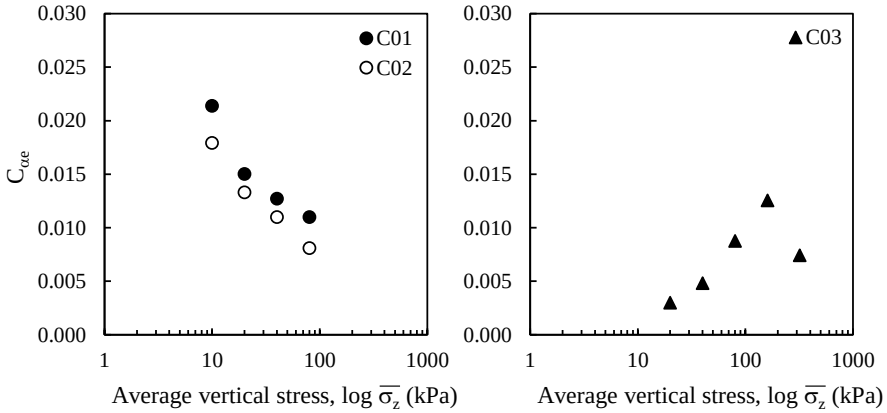

Figure 3.7: Variation of $C_{\alpha e}$ with vertical effective stress

The creep response of overconsolidated soils can be explained using Bjerrum's

equivalent time line concept Bjerrum (1967). Considering Figure 3.8(a) after Takeda et al. (2012), the authors demonstrated that during virgin compression of the sample under an applied vertical stress increase of σ_c, the response of a soil is typically assumed to follow a line of gradient C_c. The actual response of the soil comprises an initial elastic component, such that the void ratio of the sample immediately decreases to a value, e_i. After this immediate response to a change in effective stress, the soil then undergoes secondary compression until the void ratio has decreased to e_f. Along this path, a number of equivalent time lines (t_1, t_2, t_3 and t_4) are transcended by the soil element. Each line represents the time required for a soil element to creep to a specific void ratio under constant effective stress, where an increase in the subscript number represents a larger time period. As such, a vertical path through lines t_1 - t_2 - t_3 - t_4 results in a decrease in the creep rate of the soils, demonstrated by the results of C01 and C02 in Figure 3.7.

When examining the response of an overconsolidated soil, the actual path a soil element experiences in laboratory testing as a result of unloading and reloading is a hysteretic loop described by Figure 3.8(b). Typically the path of a soil element is described by the line of gradient C_s such that reconsolidation of the sample is assumed to be elastic. However if we use the same approach as Takeda et al. (2012) to explain the response of an overconsolidated soil , reloading a soil from σ_a to σ_b results in an initial response, described by the black point followed by creep to the final void ratio at σ_b. At this point, the amount of creep is extremely small, noted at low vertical effective stresses for test C03 in Figure 3.7, as the soil element moves between equivalent time lines t_2 and t_3. This was acknowledged by Feng et al. (2017) based on the model proposed by Yin and Graham (1990) whereby for an overconsolidation ratio of 4, the stress-strain state of a soil exists in a neutral zone such that the time-dependent behaviour of the soil can be neglected as it is extremely small. However, if a greater amount of reloading occurs, such that the soil element is lightly overconsolidated, we obtain a greater amount of creep in this region as the soil element transcends shorter durations of equivalent time. This explains the peak in $C_{\alpha e}$ for test C03 in Figure 3.7 at the point where the soil reloads beyond 160 kPa; the vertical stress the sample was previously unloaded at.

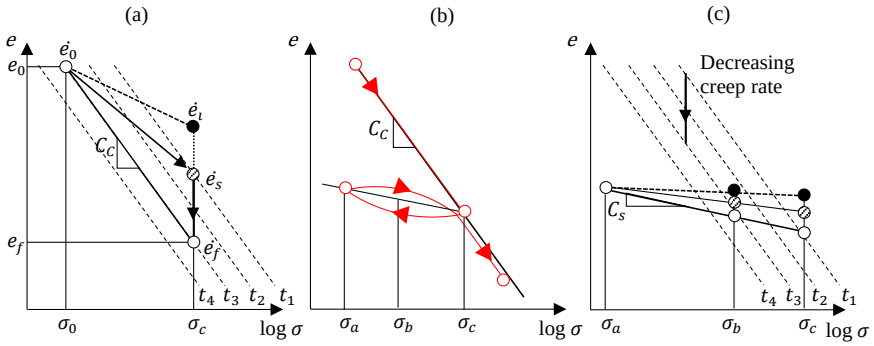

Figure 3.8: Creep behaviour of overconsolidated samples

The equivalent time lines for both load duration increments of 1 day and 7 days are presented in Figures 3.9 and 3.10. Using the determined values for t_e^c and t_0^c, the results of 1 day tests and 7 days have been fitted with the relationship defined by Yin and Graham (1989) in Equation 3.4. The coefficient of regression, R^2, shown in Figure 3.11 demonstrates both the results of one day and 7 day load increments fit the creep behaviour, however an improved fit of the results, and therefore an R^2 value closer to 1, was obtained using the 7 day loading increment oedometer tests, supporting the findings demonstrated in Figure 3.6.

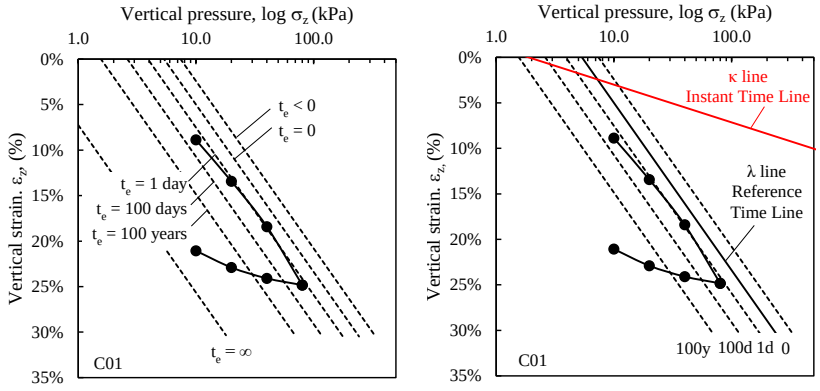

Figure 3.9: Determination of equivalent time lines and value of t_e for C01 (load increment duration of 1 day

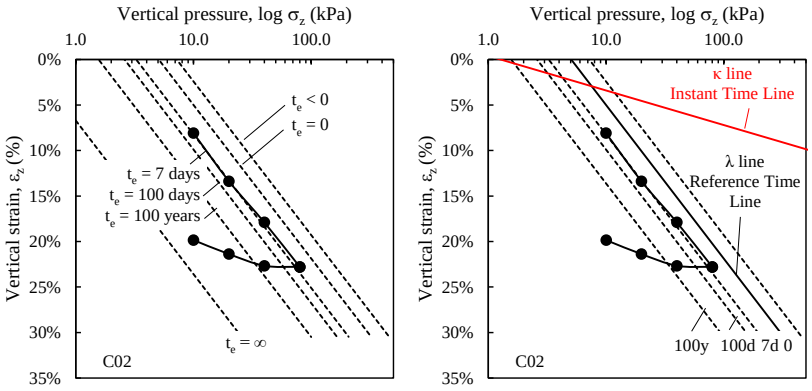

Figure 3.10: Determination of equivalent time lines and value of t_e for C02 (load increment duration of 7 days)

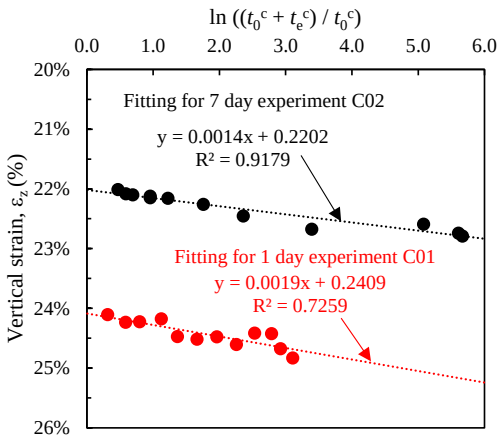

Figure 3.11: Curve fitting of long term creep behaviour for oedometer tests C01 and C02

The oedometer test results present a number of important findings with respect to construction of linear transport systems;

- Examination of the duration of applied load suggests that for a longer duration of load, a smaller degree of creep settlement is observed. With respect to infrastructure with a significant design life, it is anticipated that ultimately the settlement of the soil will tend to a finite value where there is negligible creep behaviour. Using oedometer tests to determine the amount of settlement anticipated will likely result in an conservative estimate of the soil response. Some improvement in this calculation can be achieved by using 7 day loading durations for each load increment

applied in the test.

- Examining the normally consolidated response of a soil, an increase in applied load and subsequently the vertical effective stress of the sample results in less secondary consolidation. As the vertical stress of the sample increases, the rate of creep decreases. This process occurs with respect to surcharging or preloading of ground prior to embankment construction.
- Furthermore, subsequent removal of the applied load results in significantly less creep response of the soil when reloaded due to overconsolidation of the sample. However, as the soil is reloaded and begins to approach the value of previous applied load, a rapid increase in the amount of creep experienced by the soil occurs. It is important therefore that the soil either remains in an over consolidated state or the loading is such that by the time the infrastructure is in use, the soil is normally consolidated with an increased load beyond the previous loading experienced by the soil layer. In industry, the treatment of the ground via surcharge loading typically results in the soil layer being lightly over-consolidated for the design life of the system.

Based on the results of the oedometer tests, a series of cyclic triaxial tests have been proposed. One consideration for triaxial tests to be undertaken is the initial confining pressure of the samples proposed for cyclic testing, whereby a higher confining pressure would result in a reduced value of creep coefficient. Section 3.4.1 describes the triaxial equipment arrangement used in the analysis of kaolinite that has been undertaken and the sample preparation adopted for monotonic (M) and cyclic (C) tests performed.

3.3 Triaxial Test Equipment

The undrained static and cyclic responses of the Kaolinite samples were examined using GDS Instruments cyclic triaxial equipment, shown in Figure 3.12, whereby the load ram applies a constant axial load for a static test and a varying axial load for cyclic tests.

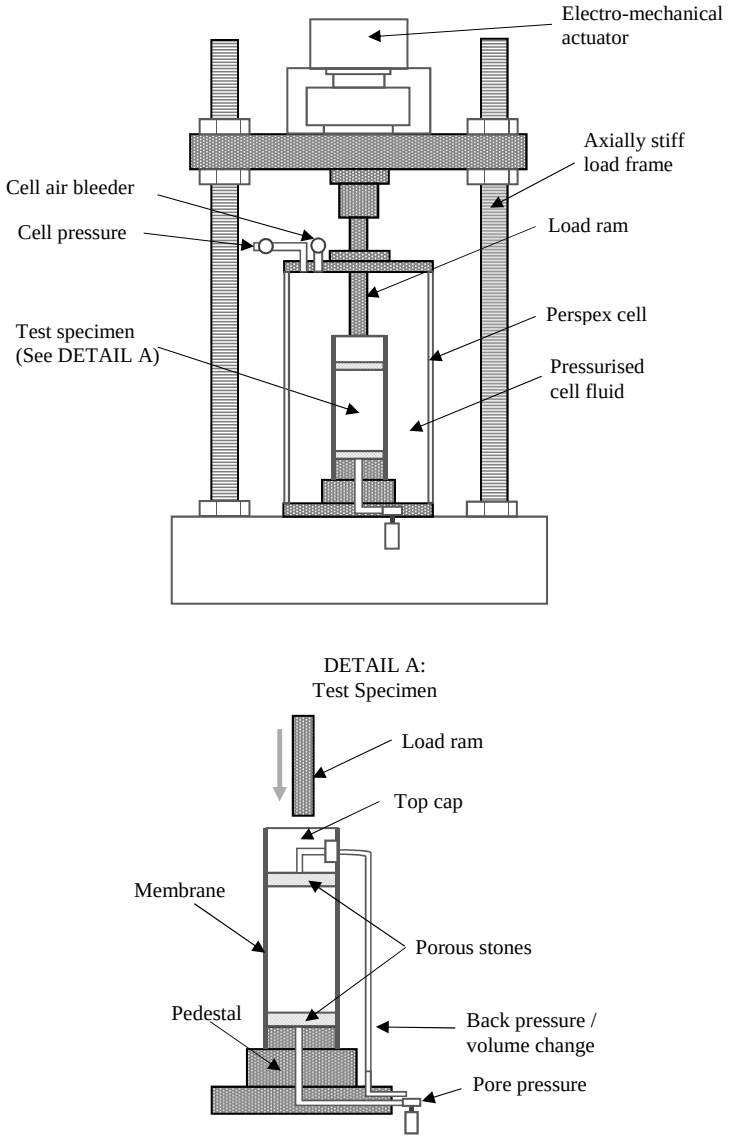

Figure 3.12: Triaxial cell equipment

The triaxial machine comprises an electro-mechanical actuator supported on an axially stiff load frame. The actuator controls a load ram which applies a static, or dynamic force, to the top cap of the test specimen situated in a pressurised cell. The fluid filled cell applies a confining cell pressure to the test specimen that replicates the in-situ conditions experienced by the soil elements. The test specimen is situated on a pedestal within the triaxial cell, shown in Detail A. It is encased in a membrane between two porous stones at either end of the specimen to permit drainage throughout the sample. Drainage is controlled by the application of back pressure to the specimen and the change in pore pressure due to load application with time can be measured through the pore pressure transducer at the base of the sample.

3.3.1 Loading Conditions

Preconsolidated samples were made mixing kaolinite to a slurry at a water content of 150%. This was allowed to settle and consolidate under a preliminary uniform confining pressure of 40kPa. When inserted into the triaxial cell, the sample was saturated, increasing the cell pressure and back pressure over a period of time, maintaining a small effective stress. In order to check the samples were fully saturated, a B-check was performed whereby the cell pressure is ramped up and the corresponding reaction of the pore pressure measured. A B check ratio of greater than 0.97 ensured samples were close to fully saturated.

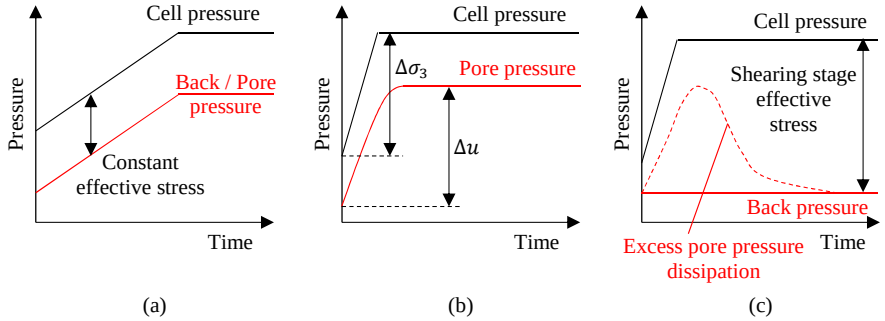

Figure 3.13: Triaxial test procedure (a) Saturation (b) B-check (c) Consolidation

To simulate the in-situ confining stress, the sample was isotropically consolidated to an initial stress, defined in the Section 3.4.1. The consolidation

stage typically lasted longer than 24 hours, applying a stress increase at a constant rate of 2.5 kPa per hour to reach the required initial confining stress for each sample.

3.4 Undrained Monotonic Triaxial Tests

3.4.1 Consideration of Soil Consolidation and Confining Pressure

Undrained Monotonic (UM) stress-controlled triaxial tests were performed on kaolinite samples in order to determine the influence of the initial confining pressure on soil response and propose an initial confining pressure representative of in-situ subgrade conditions to be adopted for cyclic triaxial tests. The five tests summarised in Table 3.7 were performed on kaolinite samples prepared in accordance with Section 3.3, examining an isotropic initial confining pressure ranging between 50kPa and 400kPa.

Table 3.7: Summary of undrained monotonic (UM) triaxial tests undertaken on kaolinite samples

Sample ID	p'_{c0}	q_{max} at failure
UM_{01}	50kPa	35.8kPa
UM_{02}	100kPa	65.2kPa
UM_{03}	200kPa	132.2kPa
UM_{04}	300kPa	169.7kPa
UM_{05}	400kPa	208kPa

The stress state of a soil is characterised by the mean effective stress of the sample;

$$p' = \frac{1}{3}\left(\sigma'_1 + \sigma'_2 + \sigma'_3\right) \tag{3.6}$$

And the deviatoric stress of the sample;

$$q = \frac{1}{\sqrt{2}}\sqrt{\left(\sigma_1' - \sigma_2'\right)^2 + \left(\sigma_2' - \sigma_3'\right)^2 + \left(\sigma_3' - \sigma_1'\right)^2} \tag{3.7}$$

For the triaxial cell arrangement whereby the consideration of cell pressure is such that $\sigma_2' = \sigma_3'$, p' and q can be rewritten;

$$p' = \frac{1}{3}\left(\sigma_1' + 2\sigma_3'\right) \text{ and } q = \sigma_1' - \sigma_3' \tag{3.8}$$

The results of the undrained monotonic tests UM_{01} to UM_{05} considering the relationship between the mean effective stress of the sample, p', and the deviatoric stress of the sample, q are shown in Figure 3.14(a). The failure envelope of the samples, plotted along the peak deviatoric stress of the samples at failure is shown, from which the results of the monotonic tests in the p'-q space show that the kaolinite samples have an effective friction angle, ϕ', of 23°. Similar values of effective friction have been established by Rossato et al. (1994) for artificial kaolinite soils.

The development of deviatoric stress, q, with respect to the axial strain of the sample, ϵ_a, is presented in Figure 3.14(b). During the early stages of sample shearing, at the initial compression of the sample, there is a rapid accumulation of deviatoric stress with respect to the strain developed in the specimen. Sample UM_{05}, considering the highest initial confining pressure applied to the kaolinite samples, demonstrated a greater rate of increase in deviatoric stress when compared to samples consolidated at lower pressures. Whilst some authors such as Chen et al. (2018b) have observed strain-softening behaviour, particularly in samples with low initial confining pressures, as discussed in Chapter 2, test UM_{01} did not show fluctuations in deviatoric stress with increasing axial strain that would be typical of this behaviour, associated with particle movement and convergence to a stable sample structure.

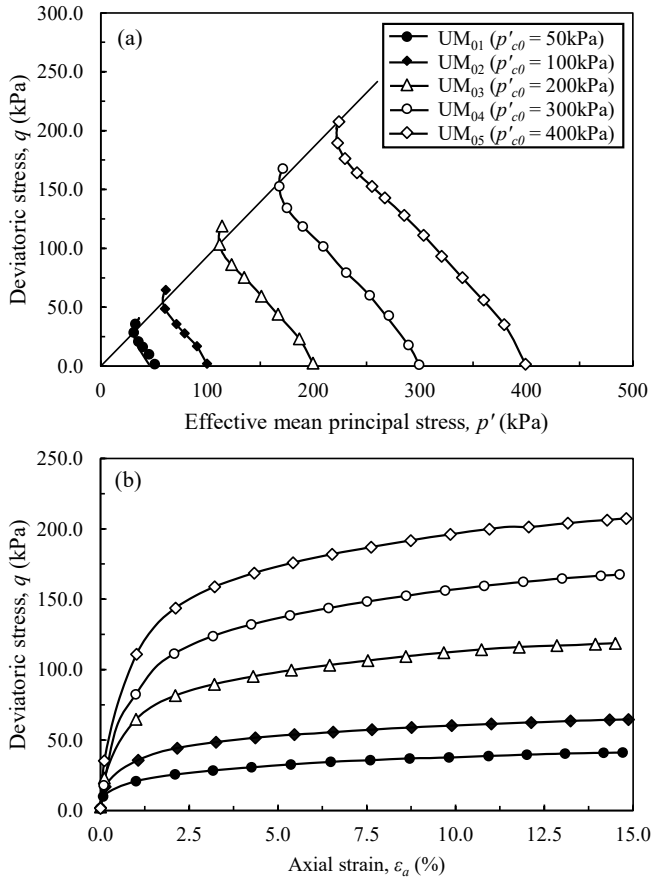

Figure 3.14: (a) p'-q space plot (b) Development of deviatoric stress with respect to axial strain

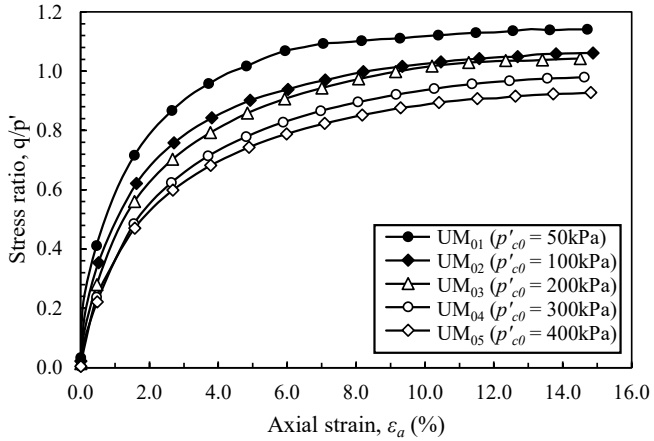

Figure 3.15: Plot of stress ratio, q/p', with respect to development of axial strain

Normalising the deviatoric stress of the sample during monotonic shearing with respect to the effective mean principle stress of the sample, the change in

stress ratio of samples UM_{01} to UM_{05} with respect to the accumulation of axial strain is presented in Figure 3.15. For the 5 confining pressures considered in the monotonic triaxial tests shown, the stress ratios converge between 0.9 and 1.1. Whilst there is some variation in convergence of stress ratio, the results suggest the samples all approach a constant value irrespective of their initial confining pressure, approaching a constant value at between 8 to 10% axial strain. As such, the samples have reached critical states by 10% strain.

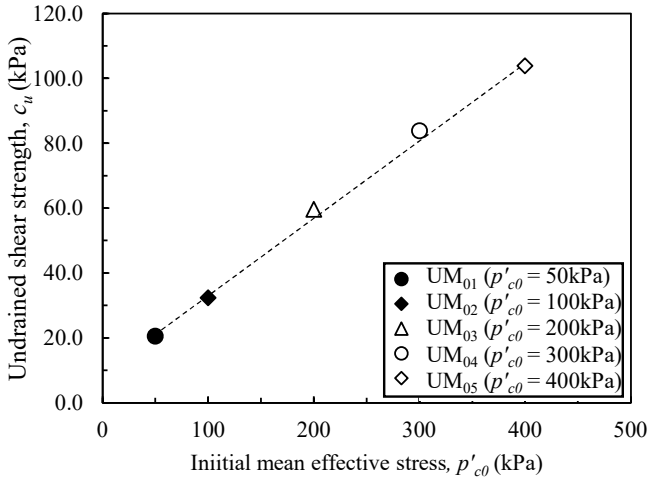

Figure 3.16: Relationship between undrained shear strength at failure with respect to initial confining pressure

The undrained monotonic tests will be used as a comparison against cyclic tests, presented in Section 3.5, however the results show a higher value of stress at failure, and therefore greater shear strength, for samples with a higher initial confining pressure. Examining the undrained shear strength of samples UM_{01} to UM_{05}, Figure 3.16 demonstrates samples with a higher initial confining stress attain a higher strength. Figure 3.17 further supports the increase in shear strength demonstrated in the monotonic triaxial tests with respect to increasing initial stress conditions, showing a reduction in the coefficient of volume compressibility with respect to increase confining pressure. The volume compressibility reported from the monotonic triaxial tests is in close agreement with the values of m_v determined by Karunaratne et al. (2000) for pure kaolinite when considering a range of Bentonite-Kaolinite mixes tested. In Sections 3.4.2 and 3.4.3, consideration of both the confining stress and undrained strength will be considered in detail in order to subsequently determine the value of p'_{c0} to be

adopted in the cyclic triaxial testing undertaken.

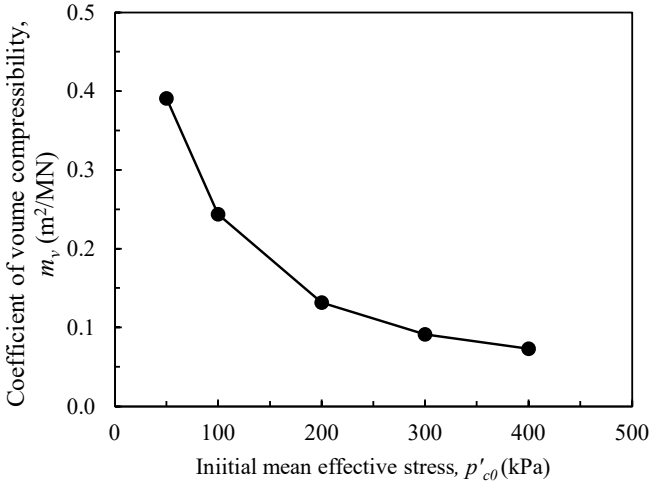

Figure 3.17: Relationship between coefficient of volmue compressibility with respect to initial confining pressure

3.4.2 Consideration of Track Subgrade Requirements

To determine the initial confining stress to be adopted in the analysis of cyclic soil response for the kaolinite samples, it is important to consider not only the stress conditions of the track subgrade but the practical design aspects of railways when assessing track subgrade performance. With respect to the latter consideration, the undrained shear strength of a clay soil is often assessed in terms of its' performance for both satisfying settlement limits and stability criteria.

For the consideration of the soft clay soils under examination, the strict differential settlement criteria imposed on high-speed rail lines, discussed in Chapter 2, can be difficult to achieve due to the low bearing capacity of these soils, unless additional mitigation measures are introduced. However, in addition to the settlement criteria, the analysis of subgrade soils for rail track structures also requires that a threshold value of shear wave velocity for the soil is satisfied. As a result, considering these two components of the design of slab track systems over soft deposits, soft clay deposits would be treated if their undrained shear strength falls below a certain threshold value such that the

static settlement condition governs the design case.

In order to assess the performance of clay subgrade using cyclic triaxial tests it is therefore important to consider soils underlying high speed rail tracks that satisfy both static and dynamic design criteria; satisfying both shear wave and undrained shear strength threshold values, such that the soils are of a minimum criteria that would permit their in-situ placement without treatment.

The shear wave velocity of the soil specifies the speed at which the generated impulses from the vibrations and passage of trains on the overlying tracks pass through the soil. For stiff soils, the shear wave velocity is generally much higher than the speed at which the train is travelling and therefore the soil movement induced by the shear waves is negligible. However, for softer soils, the shear wave velocity is typically less. In comparison with the speed of the train transiting the tracks this can therefore result in the movements of the track being reinforced by the deformation caused by the shear waves and result in significant track displacements, exceeding the displacement criteria, identified by Krylov (1994) and demonstrated by Connolly (2013) in Chapter 2.

The design shear wave velocity has been assumed to be 1.7 x the design speed of the vehicle such that the shear wave velocity for a train speed of 100m/s (close to the proposed speed of HS2 trains (HS2 Ltd., 2016) is 170m/s. This shear wave velocity would ensure the generated impulses in the soil strata sufficiently exceed the speed of the train. The shear wave velocity of a soil, V_s, can be related to the small strain shear modulus, G_0, of a soil using Equation 3.9, whilst the short-term strength of a clay soil, governing the static settlement criteria, is categorised by the undrained shear strength.

$$G_0 = \rho V_s^2 \tag{3.9}$$

Within literature, a minimum value for G_0/c_u of 300 has generally been proposed. Vardanega and Bolton (2013) summarised the material properties of various clays measured during analysis of the small strain stiffness. A statistical summary of their analysis is presented in Table 3.8. For the firm, stiff and very stiff clays where both c_u and G_0 were given, the normalised small strain

stiffness with respect to undrained shear strength, G_0/c_u, generally ranged from 280 to 2350. Weiler (1988) noted the ratio G_0/c_u reduced with increasing Plasticity Index with a minimum value of G_0/c_u = 300 might be expected for PI of around 40%. Larsson and Mulabdic (1991) suggested G_0/c_u of between 300 and 1200 for PI = 40%, shown in Figure 3.19.

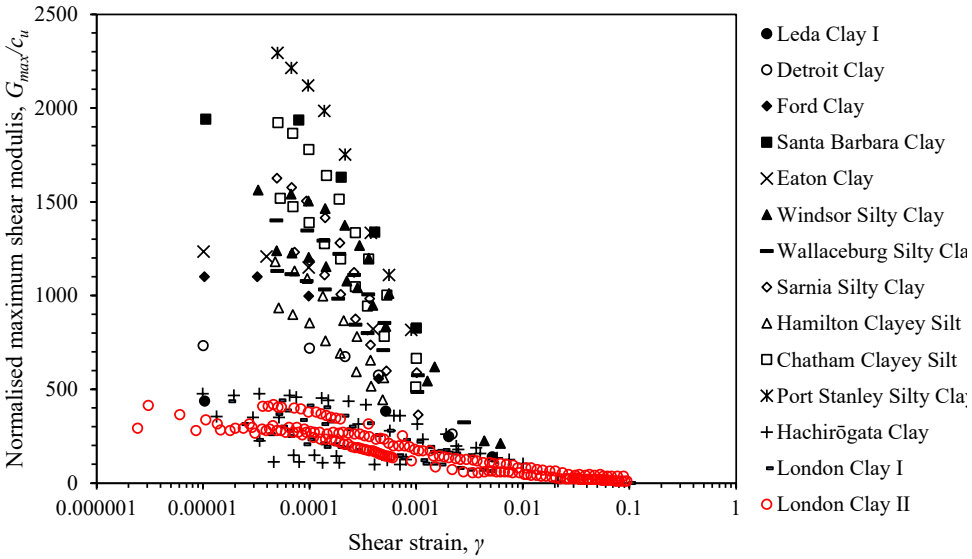

Figure 3.18: G_0/c_u against shear strain, after Vardanega and Bolton (2013)

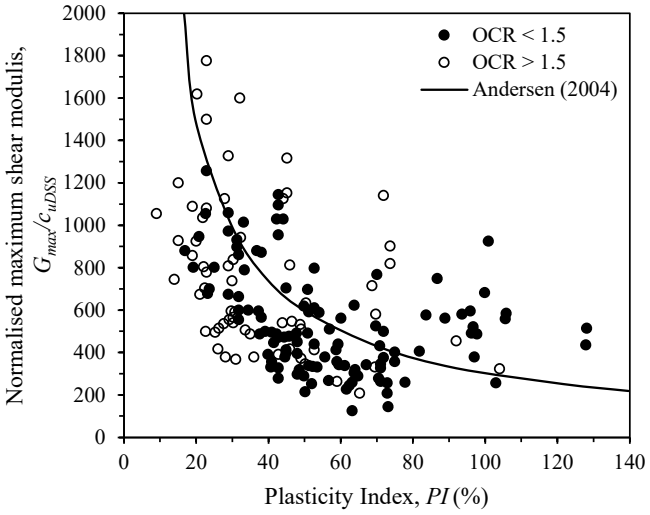

Figure 3.19: Relationship between G_0/c_u with plasticity index, after Larsson and Mulabdic (1991)

Table 3.8: Summary of Statistics for 21 fine-grained soils examined by Vardanega and Bolton (2013)

	w	e_0	w_L	w_p	I_p	p' (kPa)	c_u (kPa)	G_0 (MPa)	OCR
Maximum Value	2.50	6.15	2.39	0.89	1.50	5.70	470	179	17
Minimum Value	0.17	0.48	0.25	0.13	0.10	23	11	2	1
Mean Value, ρ	0.52	1.40	0.70	0.32	0.39	209	126	68	3
Study, n	67	67	67	67	67	62	35	67	42
Standard Dev., σ	0.39	0.99	0.35	0.14	0.23	149	119	47	3
COV	0.75	0.71	0.50	0.45	0.60	0.71	0.95	0.71	1.10

COV - coefficient of variation

Considering a shear wave velocity $V_s > 170$ m/s, the small strain shear modulus G_0 should be at least 52-64 MPa depending on the density and Poisson's ratio of the sample. For clays presented by Vardanega and Bolton (2013), all soils that did not achieve the specified range of G_0 had undrained shear strengths of less than 60 kPa, except for two samples of "London Clay II" with c_u values of 158 and 187 kPa. The data for London Clay II is identified in Figure 3.18 by the red data points. This was further demonstrated by Dickenson (1994) who proposed Equation 3.10 for the relationship between V_s and c_u;

$$V_s = 23 c_u^{0.475} \tag{3.10}$$

Based on this equation, a c_u value of less than 70kPa would result in shear wave velocities of approximately 170m/s. Furthermore, Black et al. (2009) showed that laboratory prepared kaolin samples with low shear strengths would also have shear wave velocities, examined using bender element measurements, of less than 170m/s. The results of the shear wave measurements, presented in Figure 3.20, showed a c_u of 66kPa resulted in a shear velocity of 140 to 160m/s, supporting the use of Equation 3.10 for determining the undrained shear strength criteria for kaolin.

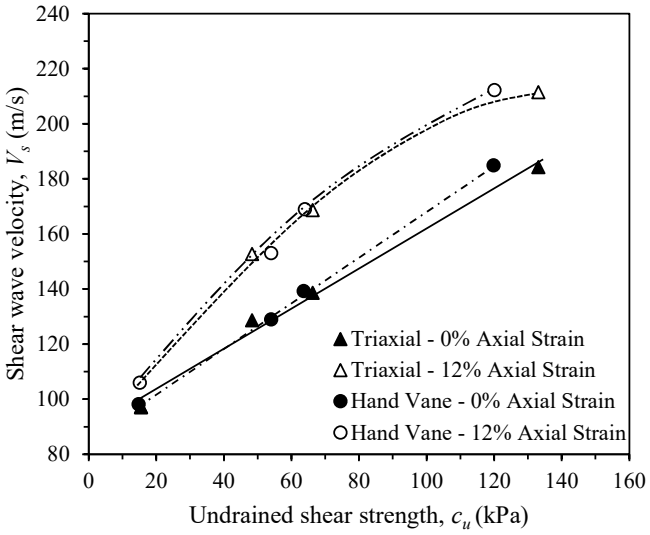

Figure 3.20: Relationship between shear wave velocity and undrained shear strength, after Black et al. (2009)

3.4.3 Consideration of Track Structure Components

Further to considering the undrained shear strength of the soil with respect to static and dynamic settlement conditions, it is also important to consider the corresponding confining pressure of the sample is representative of the in-situ conditions a soil element experiences beneath the slab track structure. The components of the track structure and sub-structure overlying the soil strata are given in Figure 3.21.

Ni (2012) previously determined the vertical stress for soil elements beneath ballasted track, demonstrating a depth of 4m should be adopted in cyclic triaxial tests such that additional dynamic stress attenuation induced as a result of train passage could be neglected. The complete derivation considering slab track components is summarised in Appendix A. Using the same principle for consideration of slab track structures, the vertical stress applied to the soil element under consideration, shown in Figure 3.21 as A, comprises three components; the additional stress from the slab track, the underlying sub-base material, and the embankment. The applied vertical stress can subsequently be calculated based on the principle of superposition and elastic theory by sectioning the embankment, sub-base and slab into the following components

below and assuming the embankment slopes are at a distance such that they do not influence the stress distribution as a result of the track and sub-base structure. The influence factor, I for each section whereby the vertical stress experienced is determined based on the factored pressure a section contributes:

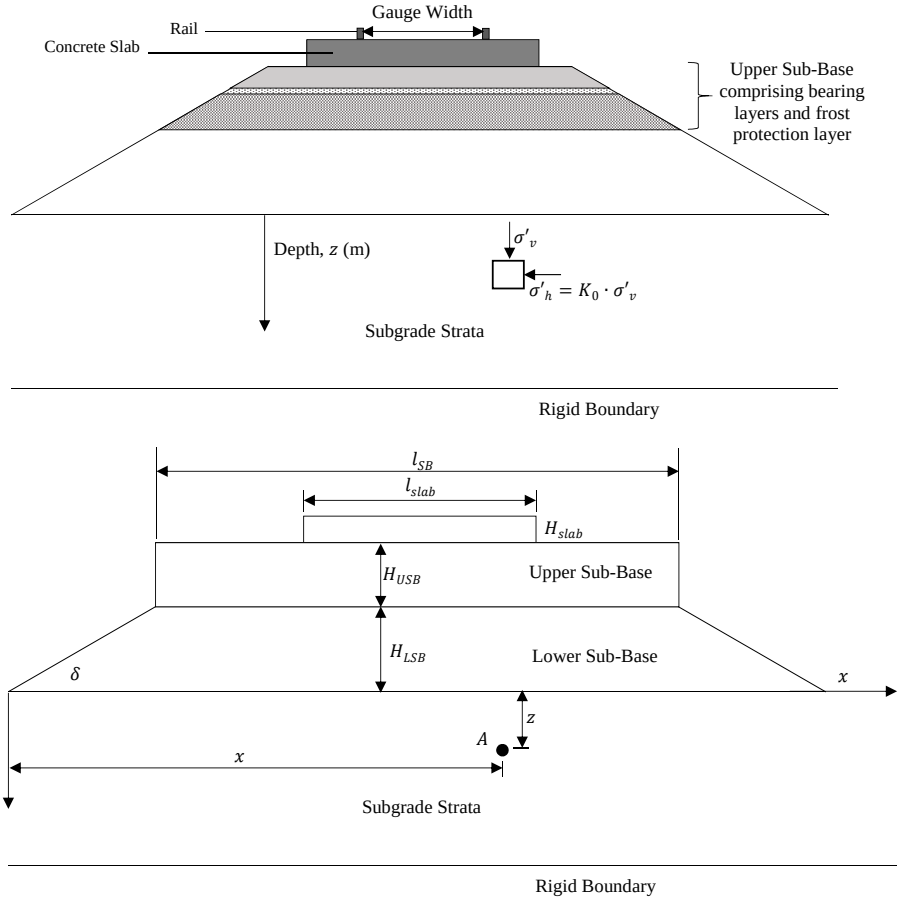

Figure 3.21: Components of track structure and substructure for determining in-situ consolidation pressure

$$\sigma'_z = Ip$$

- The slab track comprises two components, the weight of the rail, defined as:

$$W_{rail}(\mathrm{N}) = 2 \times m_{rail}(\mathrm{kg/m}) \times g(\mathrm{m/s^2}) \times 1\mathrm{m} \tag{3.11}$$

The weight of the slab, defined as:

$$W_{slab}(\text{N}) = \rho_{rail}(\text{kg/m}^3) \times l_{slab}(\text{m}) \times h_{slab}(\text{m}) \times g(\text{m/s}^2) \times 1\text{m} \tag{3.12}$$

The total pressure due to the slab structure is therefore expressed as:

$$p_{slab}(\text{kPa}) = \frac{W_{rail}(\text{N}) + W_{slab}(\text{N})}{l_{slab}(\text{m}) \times 1\text{m}} \tag{3.13}$$

- Therefore, the additional vertical stress can be calculated:

$$\sigma'_{z,additional}(\text{kPa}) = \sum I_{SB}\ p_{SB}(\text{kPa}) \tag{3.14}$$

- The influence factors can be calculated as follows:

$$I_{SB} = \frac{1}{\pi}\left\{ f\left[\tan^{-1}\left(\frac{f}{h}\right) - \tan^{-1}\left(\frac{f-1}{h}\right)\right] - \frac{(f-1)h}{(f-1)^2 + (h)^2}\right\}$$

where f and h are functions of the distance along the base of the embankment relative to x and z respectively

- The total vertical stress experienced by soil element A at depth z is therefore:

$$\sigma'_z(\text{kPa}) = \gamma_{subgrade}(\text{kN/m}^3) \times z(\text{m}) \times \sigma'_{z,additional}(\text{kPa}) \tag{3.15}$$

Examining the influence of the individual components contributing to the vertical stress in the subgrade, the effect of varying the inclination δ was minimal. The slab width and upper sub-base width had a small influence over the position of the maximum vertical stress for each contour. Similarly, the degree of compaction of the lower sub-base layer, and subsequently the density ρ_{LSB} had little influence over the maximum vertical stress for the subgrade, shown in Figure 3.22.

The range of densities considered are reflected globally in the rail network. A summary of the range of soil densities for rail tracks are presented in Table 3.9.

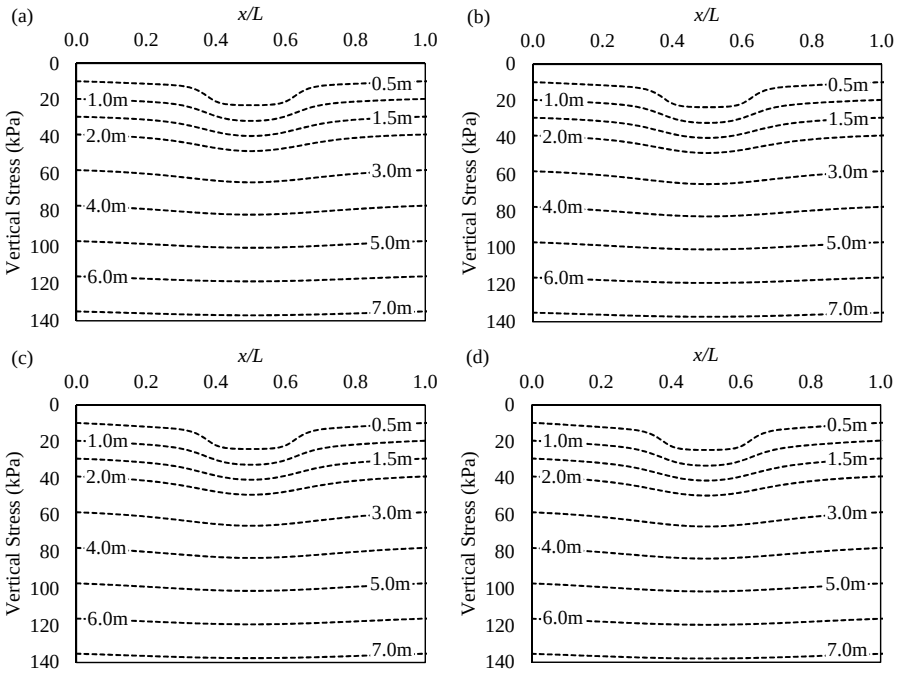

Figure 3.22: The vertical stress distribution beneath the track structure with depth, at 0.5m intervals from 0.5m to 2.0m and from 1.0m intervals to a depth of 6.0m for varying ρ_{LSB}.

l_{slab} = 2.60m ; l_{SB} = 3.40m ; H_{slab} = 0.30m ; H_{USB} = 0.70m ; H_{LSB} = 2.40m ; m_{rail} = 60kg/m ; ρ_{slab} = 3.00Mg/m^3 ; ρ_{USB} = 2.40Mg/m^3 ; $\rho_{subgrade}$ = 1.94Mg/m^3 ; δ = 34 ° (equivalent to 1:1.5 inclination).
For ρ_{LSB} = (a) 1.00Mg/m^3 (b) 1.25Mg/m^3 (c) 1.5Mg/m^3 (d) 1.75Mg/m^3

Table 3.9: Summary of the range of subgrade densities on existing rail and road routes

Route:	Country	Range of Densities (Mg/m^3)	Reference
Shanxi - Hebei	China	1.74 - 2.16	Nie et al. (2016)
Beijing - Shanghai	China	1.87	Bian et al. (2014)
Brussels - Paris	France	1.60 - 2.10	Kouroussis et al. (2011)
SNCF Northern Line	France	1.92 - 2.04	Le Kouby et al. (2010)
Beijing - Kowloon	China	1.75	Liu and Xiao (2010)
Valencia - Barcelona	Spain	1.86	NGI (2005)
Leominster	UK	1.90 - 2.05	Gunn and Nelder (2004)

The greatest change in vertical stress beneath the track structure occurs due to variation in the height of the lower sub-base layer. The vertical stress distribution beneath the track when there is no lower sub-base (h_{LSB}=0.0m) and for increments in height of 0.60m are shown in Figure 3.23.

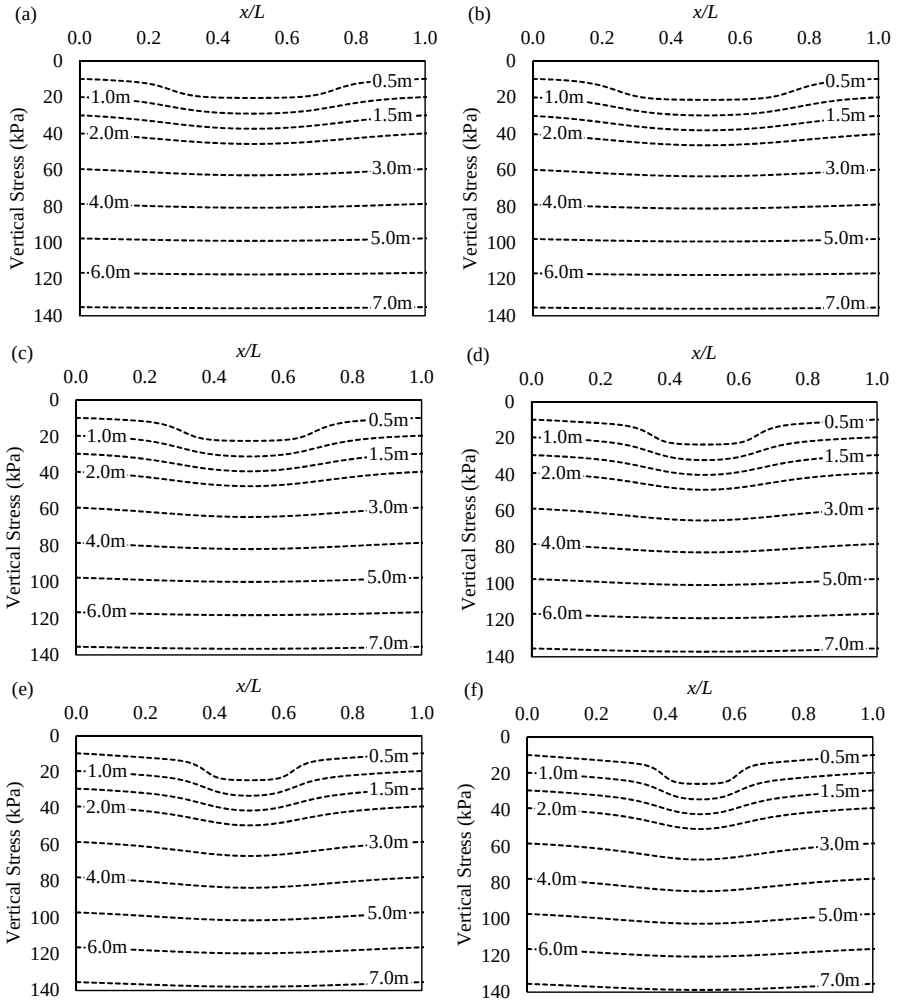

Figure 3.23: The vertical stress distribution beneath the track structure with depth to a depth of 6.0m for varying H_{LSB}.

l_{slab} = 2.60m; l_{SB} = 3.40m; H_{slab} = 0.30m; H_{USB} = 0.70m; m_{rail} = 60kg/m; ρ_{slab} = 3.00Mg/m^3; ρ_{USB} = 2.40Mg/m^3; ρ_{LSB}=1.75Mg/m^3; $\rho_{subgrade}$ = 1.94Mg/m^3; δ=34° (equivalent to 1:1.5 inclination).
For H_{LSB} = (a) 0.0m (b) 0.60m (c)1.20m (d) 1.80m (e) 2.40m (f) 3.00m

The results of Figure 3.23 demonstrate that below 6.0m, the vertical stress in the subgrade strata is not influenced by the track structure. Considering the attenuation of the component of dynamic load with depth, given in Figure 3.24,

for ballastless track the dynamic load reduces by approximately 50% by a depth of 4.0 m. At 6.0m depth below ground level, the influence of dynamic load induced as a result of track or sub-structure irregularities is less than 0.3 in ballast track.

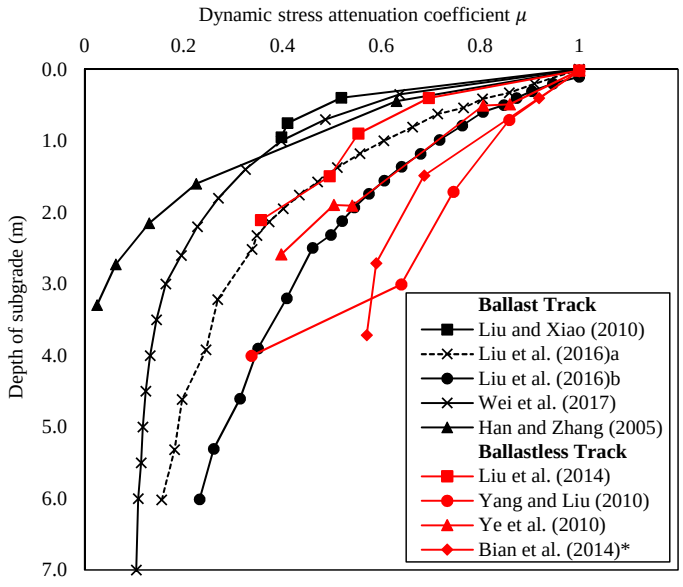

Note: a denotes results for a 23t vehicle; b denotes results for a 30t vehicle.
*(Bian et al. 2014) undertook full scale ballastless experimental tests.

Figure 3.24: Attenuation of dynamic stress with depth of subgrade

For the purpose of laboratory testing of monotonic tests considering strain rate in Section 3.4.4 and cyclic triaxial tests in Section 3.5, the initial confining pressure of the sample has been taken to be 200kPa. This corresponds to a subgrade depth of greater than 6.0m, where there is a low influence as a result of the dynamic load component, in agreement with Xiao et al. (2016) who demonstrated that at a depth of 6m below an embankment, the soil stiffness made a negligible difference to the settlement results compared to those of the static embankment case. It also satisfies the undrained shear strength condition proposed in Section 3.4.2, such that the attained monotonic static strength is sufficient to satisfy both shear wave and undrained shear strength threshold values and the sample is the minimum criteria that would permit in-situ placement without treatment.

3.4.4 Consideration of Strain Rate

Based on the initial confining pressure of 200kPa proposed considering the track subgrade requirements and the effects of slab track and sub-layer loading, undrained monotonic triaxial tests were performed examining the strain rate effects of kaolinite samples on the shear response of the soil. The monotonic triaxial tests considering strain rate are summarised in Table 3.10.

Table 3.10: Summary of undrained monotonic (UM) triaxial tests undertaken on kaolinite samples considering strain rate

Sample ID	Strain rate, $\dot{\epsilon}$	Time to failure (min)
UM_{06}	0.005 %/min	2815
UM_{07}	0.025 %/min	524
UM_{08}	0.05 %/min	260
UM_{09}	0.25 %/min	60

Figure 3.25(a) presents the $q - p'$ space considering the different loading rates applied to the kaolinite samples. The results, supported by the undrained monotonic tests considering initial pre-consolidation pressure, further demonstrate the friction angle of the prepared kaolinite to be 23°. Considering sample UM_{07}, the plot demonstrates the reproducibility of the monotonic tests considering both stress controlled and strain controlled tests for the same initial sample conditions. The results all converge to a similar value of deviatoric stress, q, for a similar mean effective stress at failure. This is demonstrated more clearly in Figure 3.25(b), where the maximum deviatoric strain for samples UM_{06} to UM_{08} converges to approximately 100kPa, irrespective of the applied rate of loading to the sample. The stress at failure for sample UM_{09}, defined as 15% axial strain, is close to 25% higher than those of the other UM samples examined for strain rate, suggesting the kaolinite samples are susceptible to rate effects.

Ladd and DeGroot (2003) demonstrated the strain rate effects experienced by clay soils had two components; effects as a result of partial drainage and those due to viscous effects. For consideration of the tests presented in Table 3.10, the

effect of partial drainage has not been considered due to the control of drainage paths by the GDS triaxial machine. The viscous effects, examined in Section 3.2.1 for one dimensional compression tests, demonstrated that less creep occurred when longer durations of loading were applied to the kaolinite samples.

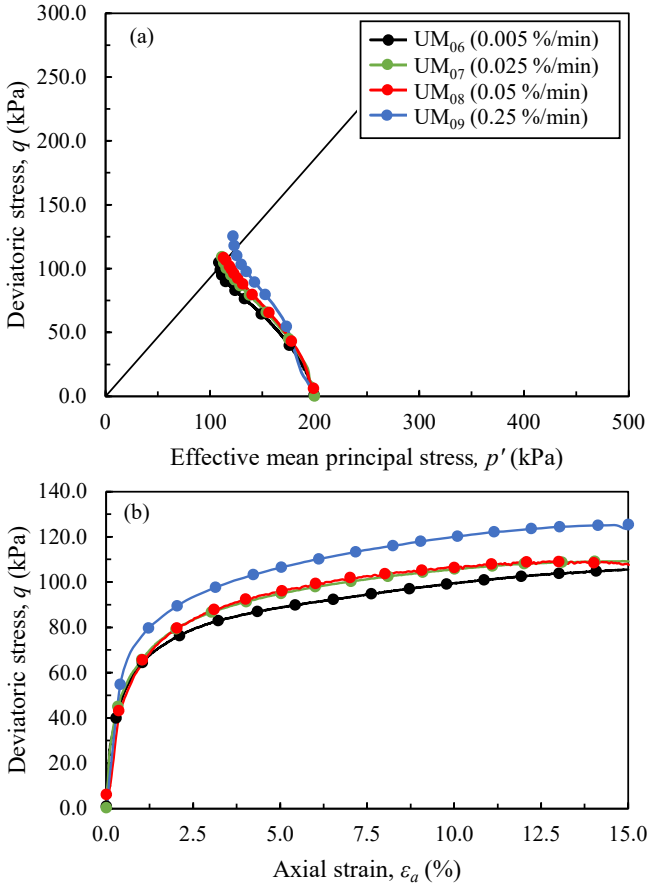

Figure 3.25: (a) p'-q space plot (b) Development of deviatoric stress with respect to axial strain

The authors identified that when samples were sheared quickly, the strength of the soil obtained under varying loading rates, and therefore the rate of strain generated, typically resulted in a higher value of strength than that experienced in the field. As proposed in Section 3.2.1, a slower loading rate permits the excess pore pressures generated in response to applied load to reach an equilibrium. Considering the response of normalised excess pore pressure with respect to the development of axial strain, shown in Figure 3.26, all generated excess pore pressures reached a similar equilibrium, converging to a value of 0.6. There

appears to be negligible difference in the response of the excess pore pressure to the variation in strain rate under consideration. This may be due to the relatively long duration of each test considered in this study, particularly when compared to undrained-unconsolidated (UU) tests which generally reach failure within a 5 minute period, presented in 3.11.

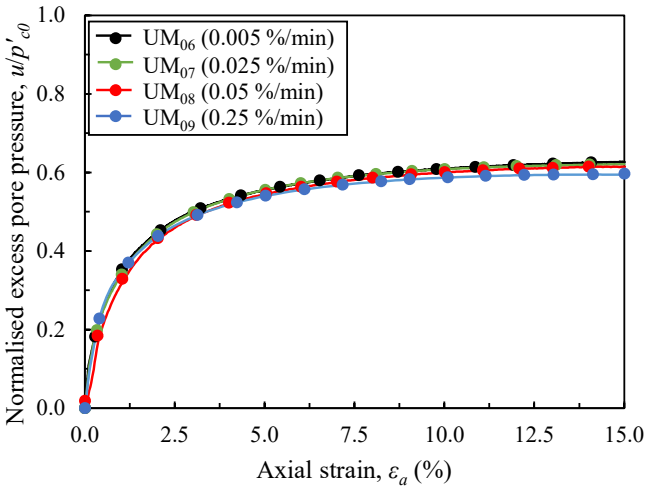

Figure 3.26: Normalised excess pore pressure with respect to axial strain considering variation in strain rate

However, with respect to the duration of the triaxial test, and therefore the time to failure for each sample, shown in Figure 3.27, the results clearly show the variation in deviatoric stress due to strain rate. It is clear the results of UM_{06} to UM_{09} presented in Figure 3.27 support the findings from the one dimensional compression tests undertaken on the kaolin samples and the findings of Ladd and DeGroot (2003) for normally consolidated clays. When considering a higher shear rate, the deviatoric stress of the sample at failure for samples all confined to the same initial pressure is greater. Furthermore, the rate of applied load results in the sample shearing much quicker, failing at 60 minutes in comparison to the failure of 2815 minutes observed for sample UM_{06}.

Table 3.11: Summary of typical time durations to failure for norrmally consolidated clays under different shearing conditions, after Ladd and DeGroot (2003)

Shearing conditions	Time to failure
CPTU, Lab TV, LV	5 seconds
FVT, Lab UUC	5 minutes
Lab CK_0U	5 hours
Field Loading	2 weeks

Duncan and Wright (2005) highlighted the effect of applied rate of loading considering various methods of field and laboratory testing undertaken to determine the undrained shear strength of San Francisco Bay mud. The results for UM_{06} to UM_{09} are presented in Figure 3.28 for the determined undrained shear strength of each sample at failure with respect to the time to failure as a result of different strain rates. For the strain rates considered, there is a decrease in undrained shear strength as a result of slower rates of loading, however the effect over the range of rates considered is small.

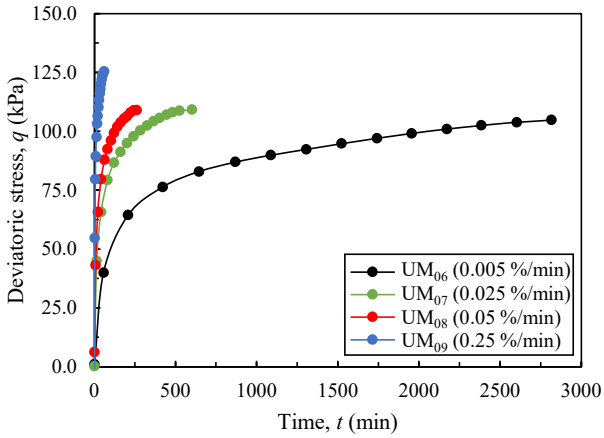

Figure 3.27: Deviatoric stress generation as a result of test duration to failure considering variation in strain rate

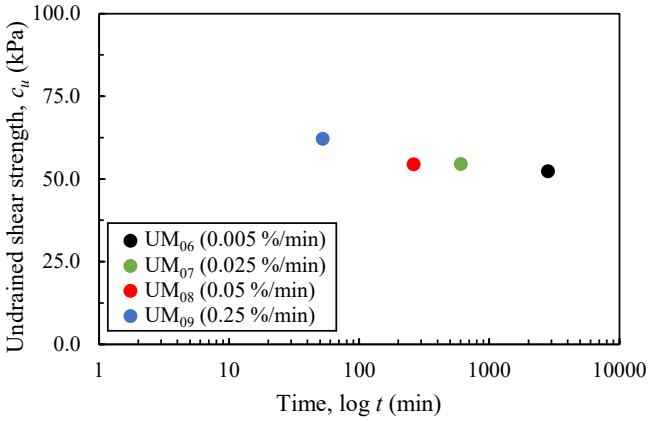

Figure 3.28: Variation in undrained shear strength with respect to the time to failure for samples considering different strain rates

Based on the undrained monotonic load tests presented, there are a number of considerations for implementation with respect to future cyclic triaxial tests to be undertaken;

- From the examination of the normalised excess pore pressure alone, the variation in deviatoric stress at failure, with respect to both initial confining pressure and strain rate, and the difference in undrained shear strength cannot be explained.
- The results also demonstrate that whilst there is some variation in undrained shear strength of the samples considering the different rate of applied loading, whereby higher sample strain rates present a higher undrained shear strength, the results tend to a constant value of undrained shear strength, and over the range of strain rates examined, this influence is limited.
- It is therefore important to consider the development of normalised excess pore water pressure and the generation of axial strain of the triaxial samples under applied loading in conjunction, considering both the rate of loading and the test duration, or time to failure, in order to determine the response of the triaxial samples to cyclic loading.

3.5 Undrained Cyclic Triaxial Tests

Undrained cyclic triaxial tests have been performed on kaolinite samples, consolidated in the triaxial cell to an initial confining pressure of 200kPa, as per the aforementioned monotonic triaxial tests. The undrained cyclic triaxial tests, summarised in 3.12, examine 15 samples considering the variation in the cyclic stress ratio, an assessment of the effect of the magnitude of applied loading on the samples, and the variation in loading frequency.

Table 3.12: Summary of undrained cyclic (UC) triaxial tests undertaken on kaolinite samples

Sample Name:	Frequency (Hz)	CSR	Number of Cycles	Duration (min)	Failure
UC_{01}	0.1	0.4	6000	1000	No
UC_{02}	1.0	0.4	15000	250	No
UC_{03}	2.0	0.4	30000	250	No
UC_{04}	5.0	0.4	34200	114	No
UC_{05}	7.0	0.4	38500	92	No
UC_{06}	0.1	0.6	6000	1000	No
UC_{07}	1.0	0.6	15000	250	No
UC_{08}	2.0	0.6	30000	250	No
UC_{09}	5.0	0.6	34200	114	No
UC_{10}	7.0	0.6	38500	92	No
UC_{11}	0.1	0.8	1726	288	Yes
UC_{12}	1.0	0.8	11736	196	Yes
UC_{13}	2.0	0.8	18256	152	Yes
UC_{14}	5.0	0.8	29565	99	Yes
UC_{15}	7.0	0.8	34624	83	Yes

The magnitude of load applied to the samples was defined in terms of a cyclic stress ratio, previously defined in Chapter 2 and summarised in 3.16 as the ratio between the cyclic deviatoric stress q_{cyc} and the static deviatoric stress at failure q_s;

$$\text{CSR} = \frac{q_{cyc}}{q_s} \tag{3.16}$$

The application of load to the samples, as summarised in Section 3.3, was applied via a load pistol, whereby the PID (proportional integral distance) controller was set to follow a pre-defined sinusoidal wave shape considering one-way loading only, such that extension of the sample during the unload portion of each load cycle was not generated. The range of loading frequencies examined for the UC tests ranged from 0.1Hz through to 7.0Hz and were limited by the capabilities of the triaxial cell loading equipment. However, as presented in the Chapter 2 , the range of frequencies tested target the low range of frequencies, governed by the bogie to bogie spacing of a range of high-speed train specifications reviewed.

Section 3.5.1 examines the undrained sample response under cyclic loading, with respect to the generation of cycles. Section 3.5.2 focuses on the behaviour of kaolinite considering the cyclic stress ratios examined whilst Section 3.5.3 examines the response of the samples considering variation of load frequency. Finally, Section 3.5.4 reviews the post-cyclic behaviour of the undrained cyclic tests and the accumulation of axial strain in stable and failed samples with respect to the monotonic tests undertaken in Section 3.4.4.

3.5.1 Examination of Axial Strain and Pore Pressure Accumulation

The full trace response of the prepared kaolinite samples subject to cyclic load is presented in Figure 3.29 for sample UC_{09}, with a frequency of 5.0Hz and a cyclic stress ratio of 0.6. Following the prescribed number of load cycles, sample UC_{09} remained stable. In contrast, the full cycle trace for sample UC_{14}, considering a CSR of 0.8, is also shown for which the sample failed, attaining an axial strain of 15% and not reaching an equivalent number of load cycles as sample UC_{09}.

Examining sample UC_{09} in detail with respect to the deviatoric stress, q, for the sample, Figure 3.30, shows the stress-strain hysteretic loops of the sample during cyclic loading. The hysteretic response for the stable sample show there is a decreasing accumulation in the axial strain developed for a progressive

number of repeated cycles of load. This is highlighted by the red arrows on Figure 3.30, showing the interval of strain between N_1 and N_{100} for the first 100 cycles of loading and a similar interval of strain between N_{1000} and N_{2000} for 1000 cycles of load. Decreased accumulation with respect to an increased number of cycles can also be observed with respect to the normalised excess pore pressure u/p'_{c0} of the sample.

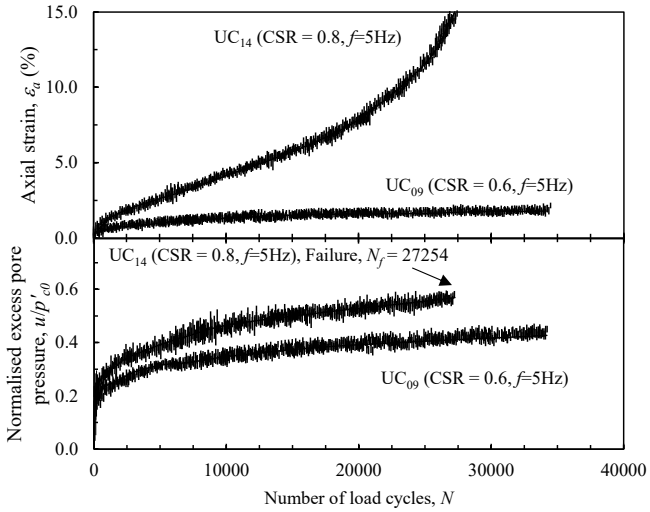

Figure 3.29: Full trace response for axial strain and normalised excess pore pressure generation with respect to load cycles

Making a direct comparison between stable and failed samples with respect to the deviatoric stress alone is difficult to quantify, therefore, as proposed with the use of cyclic stress ratio, Figure 3.32 presents the trend in axial strain for a respective number of cycles given the normalised cyclic stress of each sample.

The strain response of a sample subjected to repeated cyclic loading can be divided into two components; a recoverable, elastic strain presented in Figure 3.31 as ϵ_r and a permanent, plastic strain defined as ϵ_p. This recoverable elastic strain demonstrates the elastic properties of the samples, hence defining the modulus of elasticity or resilient modulus, termed M_r in Figure 3.31. Additionally, as demonstrated from the one-dimensional compression tests, due to the incremental creep strain that occurred under loading, a portion of the stress-strain cycle is an irrecoverable, permanent plastic strain that accumulates with each load cycle. This behaviour shows the soils plastic

properties. Figure 3.29 for sample UC_{09}, with a frequency of 5.0Hz and a cyclic stress ratio of 0.6, shows that the accumulation of plastic strain decreases progressively with consecutive cycles, such that stable samples converge towards a constant value of axial strain. In this case, sample strain stabilises such that the effect of plastic strain at a large number of cycles has a negligible influence on the overall sample response.

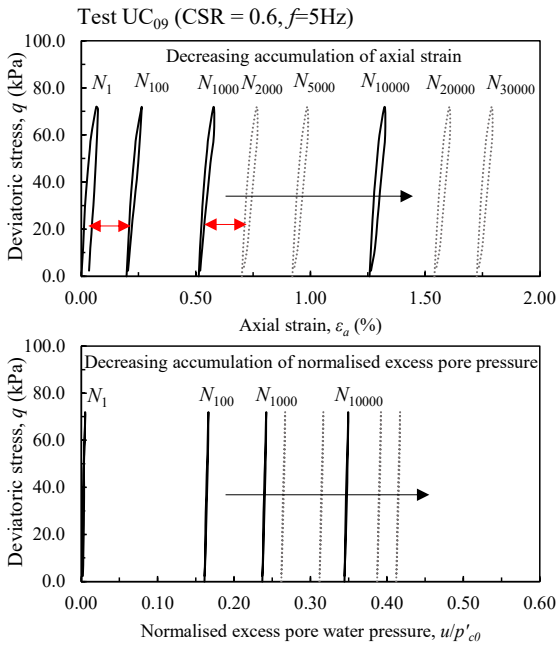

Figure 3.30: Stress hysteretic loops with respect to axial strain and normalised excess pore pressure for sample UC_{09}

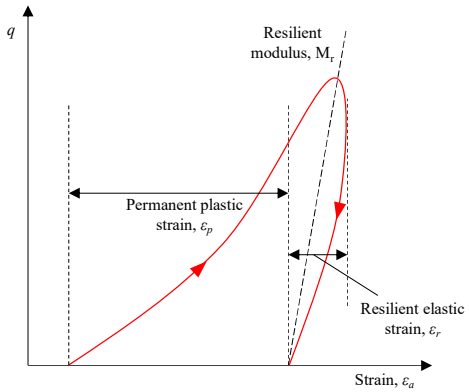

Figure 3.31: Components of non-recoverable plastic and resilient elastic strain for a single load cycle

Tang et al. (2011) concluded that the total cyclic process of Shanghai mucky

clay could be composed of a relatively constant recoverable elastic strain and a progressively attenuating accumulated plastic strain. Figure 3.32 shows the axial strain accumulation for samples UC_{09} and UC_{14}. Reviewing the individual loops in Detail (a), there is a difference in the cycle loop between that of load cycle 1, N_1, and load cycle 100, N_{100}. The loop during the first loading cycle is open, suggesting there is a large accumulation of permanent, irrecoverable, axial strain. By loop 100, the loop is much more closed, suggesting a smaller amount of accumulated plastic axial strain. Whilst the permanent strain development decreases for an increased number of cycles however, the slope of the cyclic loops is still similar, irrespective of the number of load cycles, suggesting similar amounts of elastic strain are developed in the sample regardless of the number of load cycles applied to the specimen.

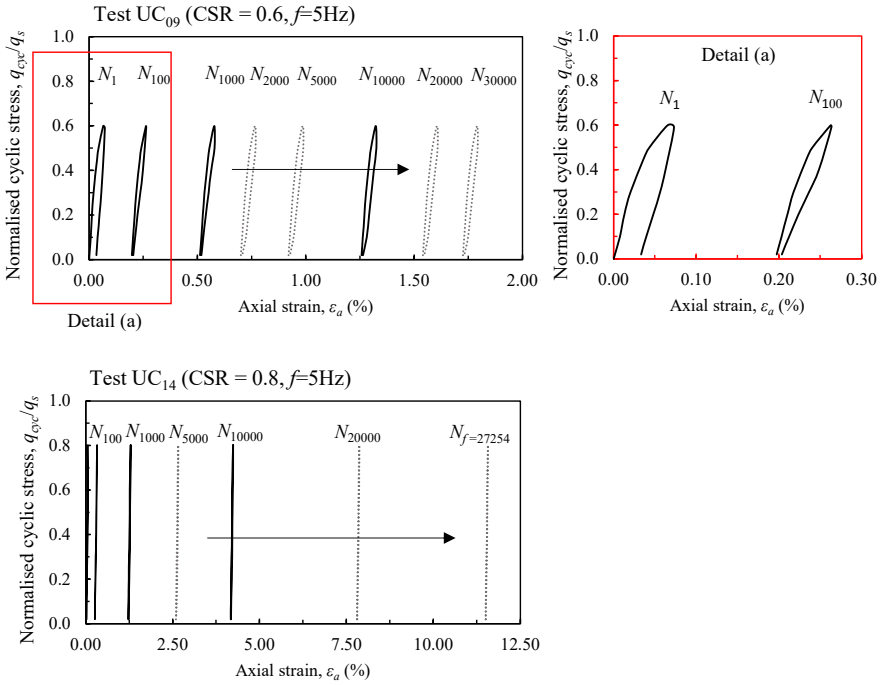

Figure 3.32: Accumulation of axial strain for sample UC_{09} and UC_{14}

Further examination of the accumulation of plastic, non-recoverable, axial strain during the first load cycle is shown in Figure 3.33. Considering sample UC_{07}, for a frequency of 1.0Hz, the strain cycle is larger than the first cycle of UC_{07} considering a frequency of 5.0Hz. This suggests the greatest accumulation of plastic strain occurs for samples at a lower frequency, whereby the load duration

is subsequently greater per cycle. In this case, for frequency of 1.0Hz, where one load cycle occurs every 1 second, results in a greater initial plastic strain accumulation for a single cycle compared to that generated during the first cycle from a load frequency of 5.0Hz, a repeated load every 0.2 seconds. Considering samples at the same stress level, the accumulation of plastic strain in a single cycle appears to be influenced by the load frequency.

Unlike the response in axial strain observed for sample UC_{09}, the axial strain presented in both Figure 3.29 and Figure 3.32 show an increase in axial strain accumulation for sample UC_{15} which reached failure under cyclic loading. Comparing the strain accumulation at different cyclic intervals in Figure 3.32, the strain interval between successive cycles increases as the sample tends to failure. This suggests for failed samples, there is a rapid increase in the plastic strains developed during loading.

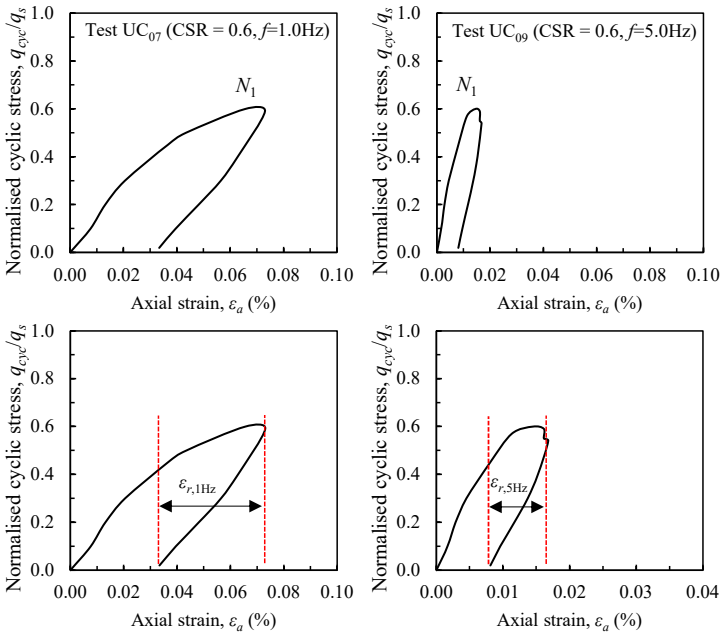

Figure 3.33: Accumulation of non-recoverable plastic strain for the first load cycle

The accumulation in normalised excess pore pressure, presented in Figure 3.34 shows the excess pore pressure accumulation for samples UC_{09} and UC_{14} do not vary regardless of the sample condition at the end of the test. Both samples show a decrease in generation of normalised excess pore pressures with respect

to an increased number of cycles, discussed in further detail in Section 3.5.2. Examining detail (a) and detail (b) for the hysteretic loop of stress with respect to normalised excess pore pressure for CSR of 0.6 and 0,8 respectively, there is little difference between the loops, however the opening of the loop and position of the loop for CSR of 0.8 is greater, suggesting even though both samples generated a similar excess pore pressure, greater accumulation occurs for a sample at failure.

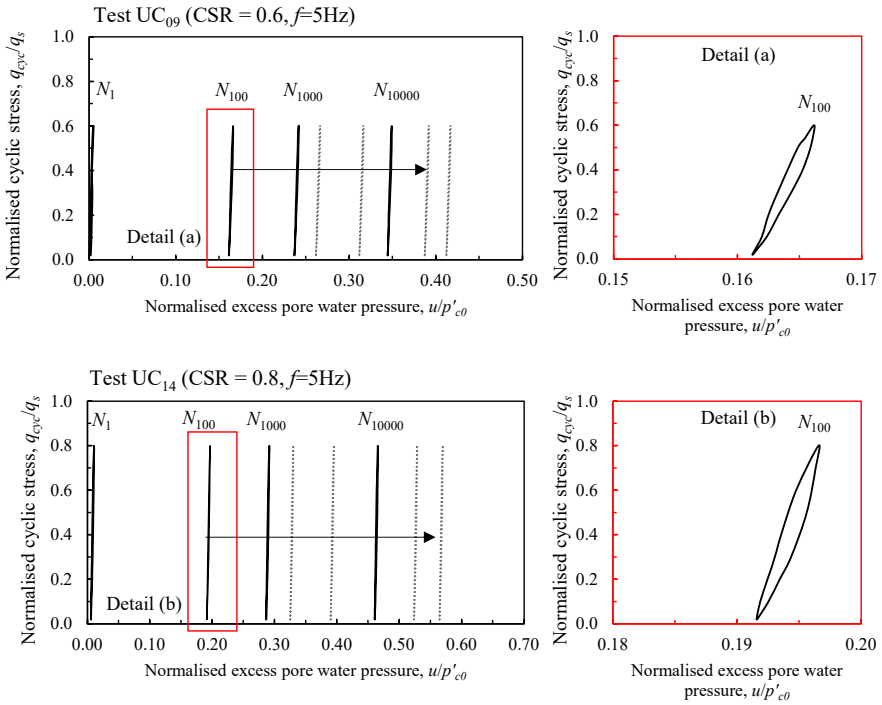

Figure 3.34: Pore water pressure accumulation

3.5.2 Examination of Cyclic Stress Ratio

The results of the cyclic triaxial tests summarised in Table 3.12 considering cyclic stress ratio are presented in Figures 3.35 to 3.39. For each load frequency, the results for the accumulated axial strain and normalised excess pore pressure at each cyclic stress ratio are presented with respect to the number of load cycles applied to the sample.

Examining the axial strain response for each frequency, at low values of CSR

the axial strain generates quickly over a relatively low number of cycles, less than 250, before attaining an "equilibrium" where for each further load cycle, irrespective of the frequency of loading, there is a negligible increase in cumulative axial strain. The results demonstrate, as intuitively would be expected, that for an increase in the applied cyclic load to a sample, there is also an increase the amount of non-recoverable axial strain developed during loading. Unlike samples UC_{01} to UC_{10}, samples considering a cyclic stress ratio of 0.8 did not remain stable during cyclic loading, resulting in failure of the sample at a given number of load cycles. This response is demonstrated by the generation of axial strain shown in Figure 3.42 rapidly increasing toward an axial strain of 15%. Therefore, for kaolinite samples there is a value of cyclic stress, a threshold cyclic stress ratio, between 0.6 and 0.8, below which a sample remains stable and above which a sample undergoes a rapid and continual generation of axial strain. This range of threshold cyclic stress ratio is consistent with that proposed by Pillai et al. (2014), for which a CSR of 0.75 resulted in a similar response in axial strain accumulation and Ansal and Tuncan (1989), noting remoulded samples were more resistant to cyclic loading.

Considering the generation of normalised excess pore pressure, the results of Figures 3.35 to 3.39 also show a similar trend, demonstrating a rapid accumulation over a small number of load cycles during the initial stages of loading and tending towards a constant value. As acknowledged in Chapter 2, the differentiation between a stable and failed sample cannot be made from observation of the normalised excess pore pressure response alone. However, it can be observed from assessing the different cyclic stress ratio trends for individual frequencies, that for an increase in cyclic stress ratio, the normalised excess pore pressure that a sample converges to increases. Hence, considering a greater applied cyclic load, and therefore cyclic stress ratio, a greater initial response in excess pore pressure is generated given the undrained loading conditions of the triaxial test adopted for this assessment. The results demonstrate that following the initial rapid accumulation of excess pore pressure, there is then a stable response that Tang et al. (2011) stated could be defined in terms of a stable excess pore pressure ratio. For a cyclic stress ratio of

0.4, this value of stable excess pore pressure ratio is approximately 0.17, whilst for a CSR of 0.6 the normalised excess pore pressure converges to 0.38. At a cyclic stress ratio of 0.8, the value of stable excess pore pressure ratio is more difficult to determine and is discussed in greater detail in Section 3.5.3, however the results converge to a normalised excess pore pressure value of approximately 0.57.

It should be noted there is a difference in the response observed for sample UC_{12} that occurs after approximately 3000 cycles of loading whereby a jump in the normalised excess pore pressure occurs. A slight change in the axial strain behaviour at the same number of cycles can also be identified, although not as noticeable. It is likely this response is due to sample disturbance such as a seating pressure drop, resulting in a subsequent drop in height of the sample, causing a change in measured axial strain, but causing a new reference point for which the sample must then attain a new equilibrium of excess pore pressure. A similar response, albeit a test criterion for the sample tested due to completing unloading intervals between series of cyclic loads was observed byLiu et al. (2021), as discussed in Chapter 2.

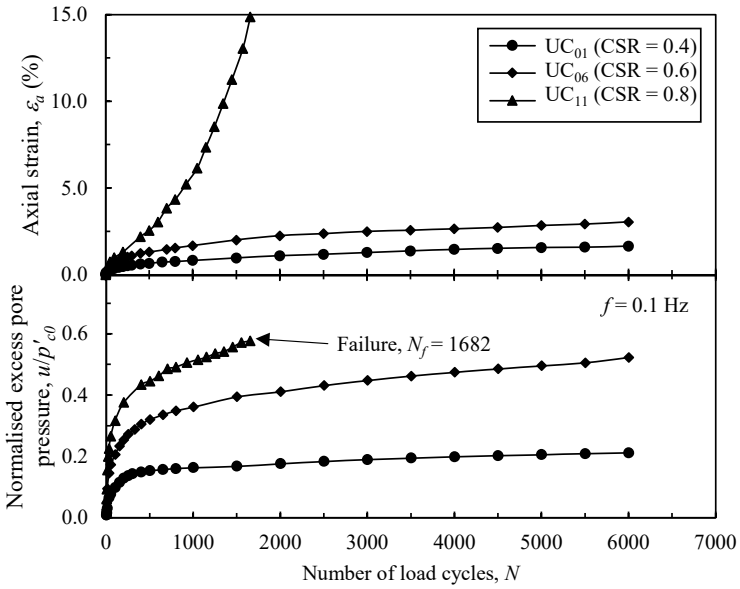

Figure 3.35: Development of axial strain and normalised excess pore pressure considering the number of load cycles for a frequency of 0.1Hz

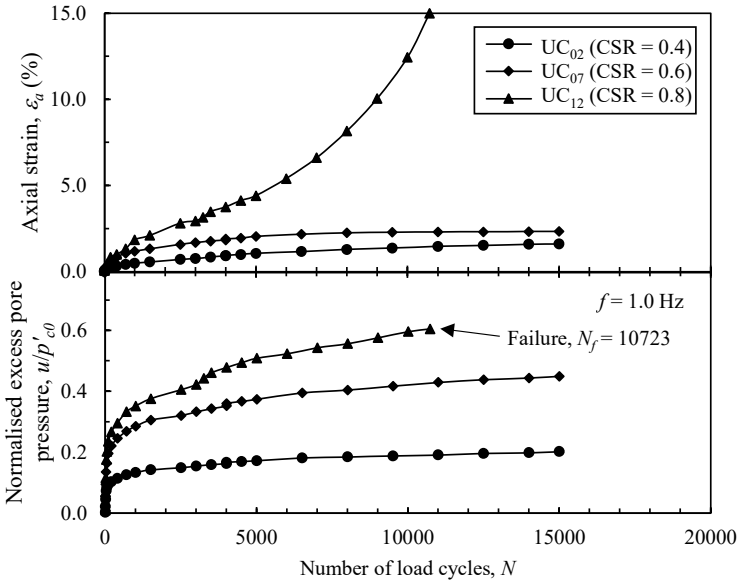

Figure 3.36: Development of axial strain and normalised excess pore pressure considering the number of load cycles for a frequency of 1.0Hz

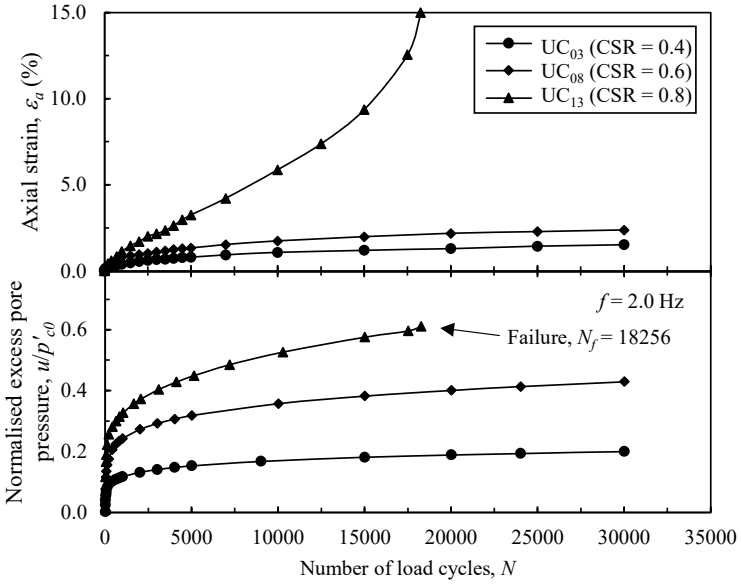

Figure 3.37: Development of axial strain and normalised excess pore pressure considering the number of load cycles for a frequency of 2.0Hz

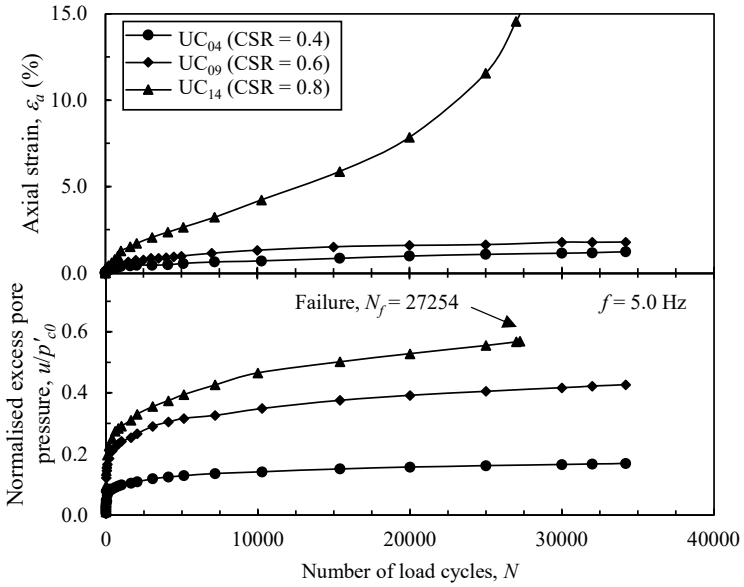

Figure 3.38: Development of axial strain and normalised excess pore pressure considering the number of load cycles for a frequency of 5.0Hz

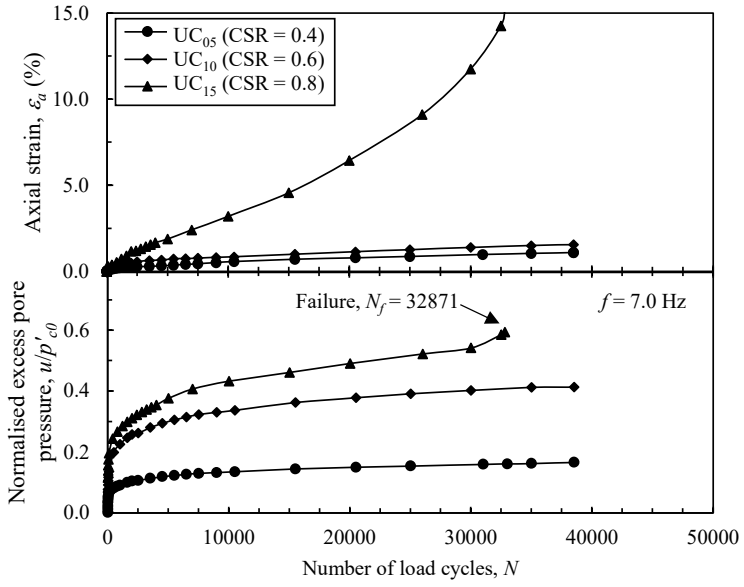

Figure 3.39: Development of axial strain and normalised excess pore pressure considering the number of load cycles for a frequency of 7.0Hz

3.5.3 Examination of Loading Frequency

Considering Samples UC_{01} to UC_{10}, listed in Table 3.12 that remained stable at the end of the duration of cyclic loading, the results presented in Figure 3.40 for a cyclic stress ratio of 0.4 and Figure 3.41 for a cyclic stress ratio of 0.6 respectively show a rapid accumulation in axial strain and pore pressure during the initial stages of loading, irrespective of the load frequency. After the first 1000 cycles of load applied to the samples, both the generated axial strain and normalised excess pore water pressure begin to reach an equilibrium and tend towards a constant value for which there is a negligible effect of repeated load cycles subsequent to this. Under these conditions, the greatest axial strain and normalised excess pore pressure is generated for a frequency of 0.1Hz.

It was demonstrated in Section 3.5.1, that the frequency of cyclic loading influences the accumulation of axial strain whereby a lower loading frequency results in a larger hysteretic stress strain loop with a greater initial plastic strain generation. Considering the results of the undrained cyclic tests with respect to the number of cycles of loading, the greatest axial strain for a CSR of 0.4 in Figure 3.40, CSR of 0.6 in Figure 3.41 and CSR of 0.8 in Figure 3.42 respectively occurs for the sample with the lowest frequency of 0.1Hz, suggesting that per cycle of load, a slightly larger amount of permanent plastic strain is developed. At a high cyclic stress ratio of 0.8, where all samples reached failure, indicated by the rapid accumulation to a trajectory of 15% strain, the lowest frequency of loading resulted in the most rapid accumulation of axial strain with respect to the number of load cycles. Similar response in sample behaviour with respect to load frequency has been observed by Matsui et al. (1980). In this case for the kaolinite samples, sample UC_{11} reached failure after only 1752 load cycles whilst UC_{15}, with a frequency of 7.0Hz, reached 32,809 cycles prior to failure.

With respect to the normalised excess pore pressure, whilst for stable samples at CSR of 0.4 and CSR of 0.6 tended towards a constant value, indicating a negligible increase in accumulated excess pore pressure with respect to the number of cycles, for failed samples, most notably at low frequencies, the

samples did not attain a constant value of excess pore pressure. From the trace of sample UC_{11} for example, the sample only experienced the rapid accumulation of excess pore pressures before failure was reached.

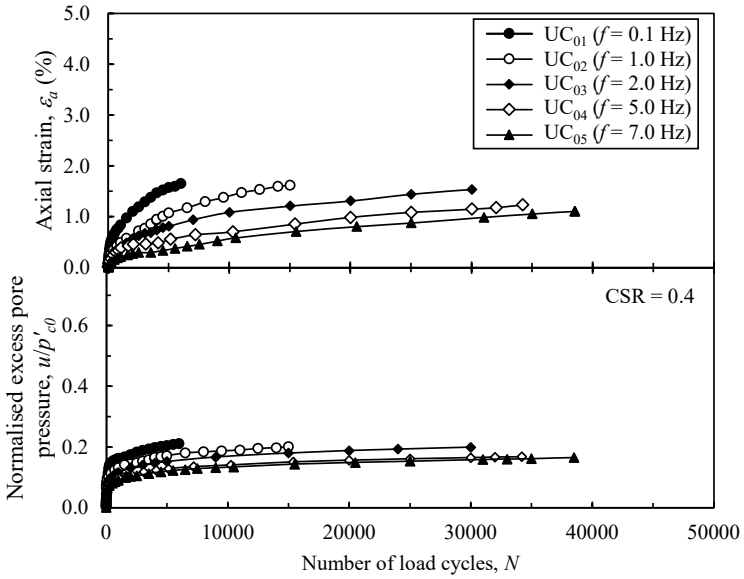

Figure 3.40: Development of axial strain and normalised excess pore pressure considering the number of load cycles for a cyclic stress ratio of 0.4

It was identified in Section 3.5.1, that the response in pore pressure generation under applied loading alone cannot clearly identify if failure of the sample has occurred. Indeed, the failure of the sample is clearly demonstrated from the axial strain trace measured during the triaxial test. The accumulation of normalised excess pore pressure with respect to the generation of axial strain is presented in Figure 3.43, considering the results for both undrained monotonic and cyclic loaded samples that underwent failure in accordance with an exceedance of the 15% axial strain limit. Figure 3.43 demonstrates that given the same drainage conditions, the pore pressure response of the sample under both monotonic and cyclic loading when normalised with respect to the initial confining pressure for failed samples is unaffected, converging to the same value of approximately 0.57. It could be argued that for the undrained monotonic tests, the accumulation of normalised excess pore pressure occurs at slightly lower levels of axial strain when compared to cyclic tests, likely due to the application of a constant shearing load unlike the cyclical load application.

This suggests that under the application of cyclic load, for an equivalent axial strain, the generation of excess pore pressure occurs at a slower rate to that in monotonic tests whilst attaining the same final accumulated pore pressure value.

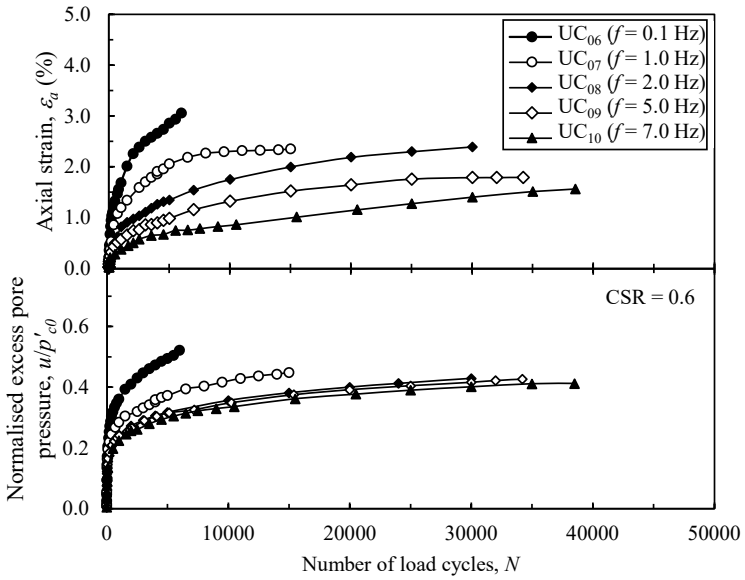

Figure 3.41: Development of axial strain and normalised excess pore pressure considering the number of load cycles for a cyclic stress ratio of 0.6

Due to the viscosity of clay soils, consideration of the cyclic response with respect to time, rather than number of cycles has been recommended by a number of authors including Yang et al. (2019). Figures 3.44, 3.45, and 3.46 show the development and axial strain and normalised excess pore pressure for a cyclic stress ratio of 0.4, 0.6 and 0.8 respectively. Examining the normalised excess pore pressure response with respect to the test duration rather than load cycles, the convergent response is observed much clearer, showing the excess pore pressures attain a stable value for a given cyclic stress ratio, irrespective of the sample frequency. In this way, samples UC_{01}, UC_{06} and UC_{11} for a frequency of 0.1Hz, all show a lower generation normalised excess pore pressure compared to samples at greater frequencies. This is likely to be due to the load duration being longer, permitting quicker equilibration of excess pore pressures between subsequent cycles and resulting in less initial rapid accumulation. It should be noted that for the frequencies and samples examined, pore pressure

equalisation does not appear to be an issue as all trace responses converge. This issue had been previously identified by Sangrey et al. (1978) who suggested that at high frequencies, the measured pore pressures may not reflect the actual measured values during initial load cycles, since sufficient time is not allowed for equalisation. However Hyde and Ward (1985) noted the importance of the early accumulation of pore pressure and the risk of neglecting this in the consideration of overall soil response with respect to the underestimation of final converged pore pressure.

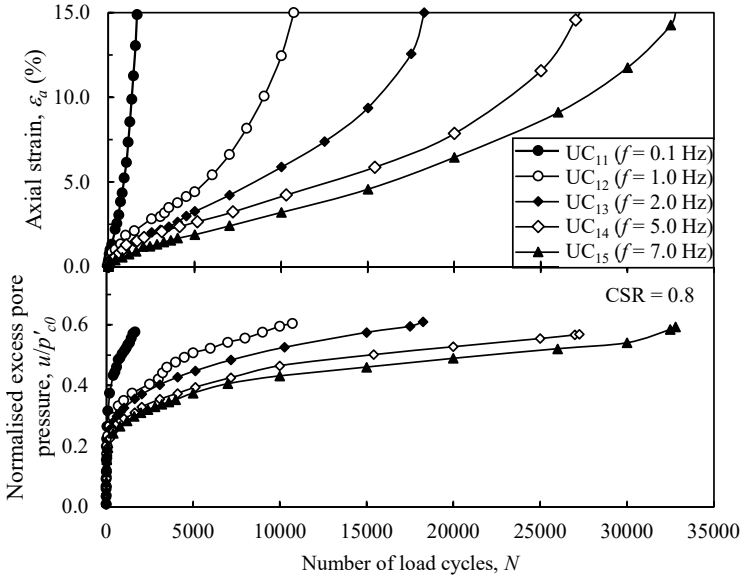

Figure 3.42: Development of axial strain and normalised excess pore pressure considering the number of load cycles for a cyclic stress ratio of 0.8

The accumulation of axial strain with respect to the frequency of loading illustrates the trend identified from assessing individual numbers of cycle hysteretic loops in Section 3.5.1. For samples loaded at a lower frequency, whereby the load cycle duration is therefore longer, the accumulation of axial strain for an individual cycle is greater, however with respect to the load duration this strain response is less than for other frequencies, and therefore less incremental plastic strain is generated in the initial stage during which the rapid strain accumulation occurs. As noted by Ansal and Tuncan (1989) and discussed in earlier sections, the effect of the rate of loading is more dominant during the initial cycles. Therefore as the number of cycles increases, the effect

of variation in loading rate diminishes progressively and the samples converge asymptotically to an axial strain for a given cyclic stress ratio.

As highlighted in Section 3.5.2, the failure of the samples at a cyclic stress ratio of 0.8 was identified by the rapid accumulation of axial strain to a trajectory of 15%, whereby unlike the decreased progressive accumulation of axial strain observed for stable samples, tests UC_{11} to UC_{15} indicate softening of the sample. For a CSR of 0.8, it was shown considering the response with respect to the number of cycles that an increase in the frequency of applied loading to the samples meant the number of load cycles a sample could withstand prior to failure increased. However, considering this trend with respect to time rather than number of cycles, shown in Figure 3.46, the results demonstrate that the greater the frequency of applied loading, and subsequently the smaller the interval between consecutive loading cycles, the shorter the duration of loading the sample withstands prior to failure. In contrast to the assessment with respect to the number of load cycles, Sample UC_{11} reached failure after 192 minutes (1752 load cycles) whilst UC_{15}, with a frequency of 7.0Hz, reached 78 minutes duration (32,809 cycles) prior to failure.

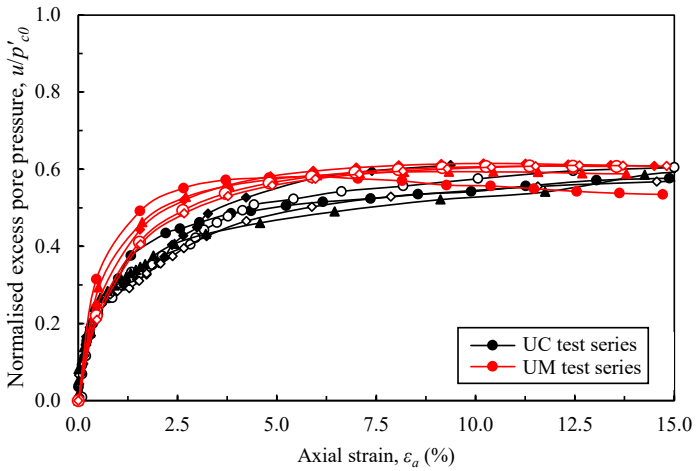

Figure 3.43: Accumulation of normalised excess pore pressure with respect to axial strain for monotonic and cyclic undrained triaxial tests

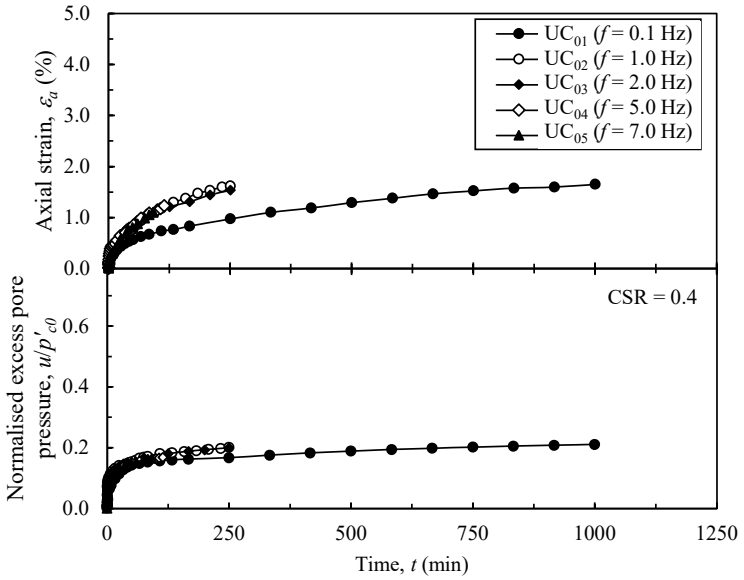

Figure 3.44: Development of axial strain and normalised excess pore pressure considering test duration for a cyclic stress ratio of 0.4

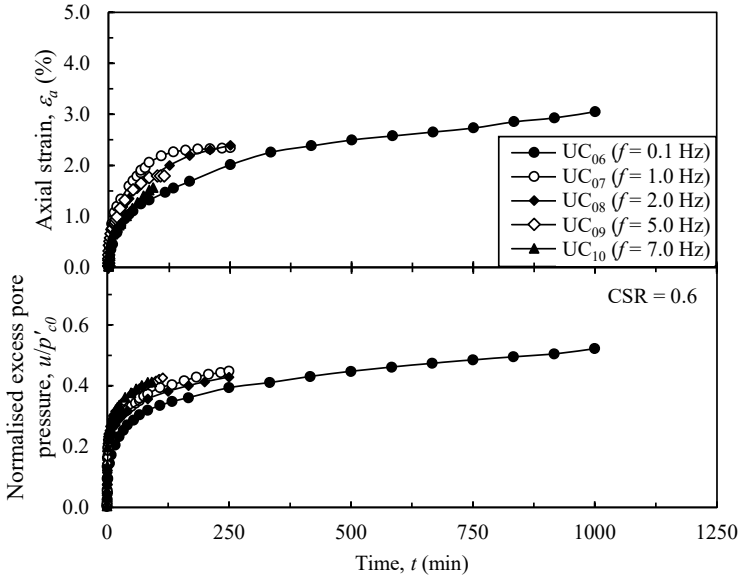

Figure 3.45: Development of axial strain and normalised excess pore pressure considering test duration for a cyclic stress ratio of 0.6

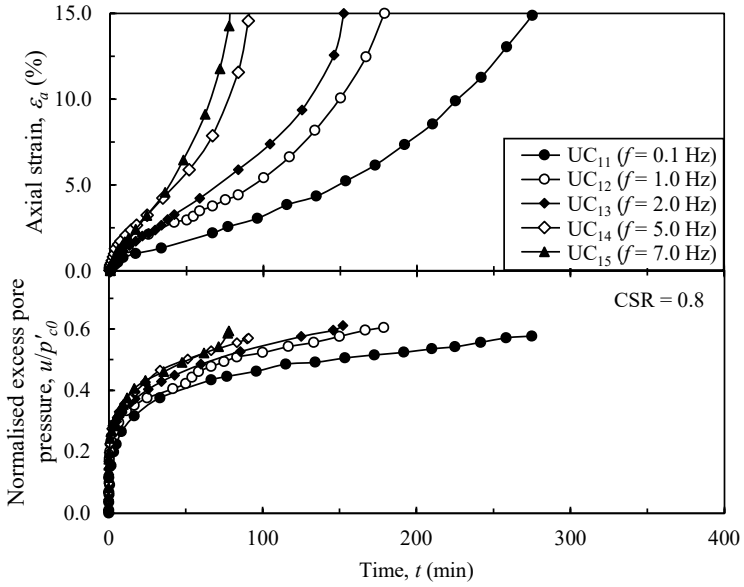

Figure 3.46: Development of axial strain and normalised excess pore pressure considering test duration for a cyclic stress ratio of 0.8

Hyde and Ward (1985) proposed the stress state of the sample under cyclic loading had an influence over the pore pressure generated, as presented in the above plots, acknowledging the importance of the initial pore pressure generation stage in estimating the overall excess pore pressures. The pore pressure rate for the first cycle of load, a_1 was shown to be related to the peak deviatoric stress under repeated cyclic loading normalised with respect to equivalent pressure, in this case defined as the cyclic stress ratio. This relationship presented in Equation 3.17 uses coefficients A and B based on the sample stress history.

$$\log_{10} a = A + B\,CSR \tag{3.17}$$

Subsequently the rate of normalised pore pressure accumulation, $\dot{u}$, with respect to the number of cycles, N, can be defined;

$$\frac{\dot{u}}{p'_{c0}} = aN^{\beta} \tag{3.18}$$

where β is the pore pressure decay constant. The normalised excess pore

pressure developed over N cycles therefore becomes;

$$\frac{u}{p'_{c0}} = \frac{a}{\beta+1}(N^{\beta+1}-1)+\beta \tag{3.19}$$

Considering the pore pressure results with respect to both load cycles and test duration, shown in Figure 3.47, the results show close agreement with the test data given A of -2.254 and B of 1.528. Conversely, if the converged normalised excess pore pressure value is known, the number of cycles of load to attain failure for a sample can be determined.

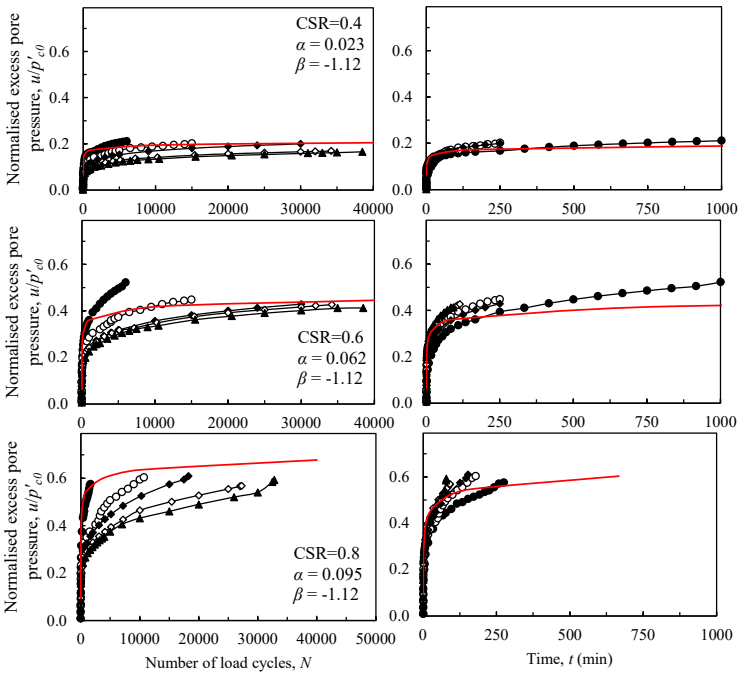

Figure 3.47: Development excess pore pressure for all frequencies, compared to the pore pressure generation determined using Equation 3.19 from Hyde and Ward (1985)

It has been demonstrated from the cyclic triaxial tests undertaken that following an initial number of load cycles, the overall response of the sample is unaffected by frequency of loading, moreso the response is dependent on the test duration, and for equivalent durations the accumulation of axial strain is similar for all samples examined. The axial strain response is dependent on the magnitude of applied load and therefore cyclic stress ratio for the sample. The accumulation of axial strain with respect to cyclic stress ratio is presented in Figure 3.48 at

a different number of load cycles. As presented in Section 3.5.2, the threshold value of cyclic stress ratio, CSR* in Figure 3.48, was found to exist between 0.6 and 0.8. Considering the response of soils to traffic loading, a significant number of load cycles are performed on the sample over the design life of transportation infrastructure. Figure 3.48 presents the accumulation of axial strain following 1,000 cycles of load for a frequency of 1.0Hz, alongside the equivalent load durations for samples at higher frequencies. The shakedown concept has been adopted by a number of authors to determine two threshold values of cyclic stress ratio. The low threshold of cyclic stress ratio, CSR** that defines the limit between plastic shakedown and plastic creep shakedown is shown in Figure 3.48 to exist at approximately 0.37, defined at the cyclic stress ratio for which strain greater than 1% is attained. The higher threshold presented throughout this study is refined from the range of between 0.6 and 0.8 previously described, to a value of 0.71 using Mitchell and Soga (2005), whereby the tangent lines for initial accumulation and rapid accumulation of strain intersect. Sun et al. (2017) proposed the range between these two threshold values represented an important zone with respect to subgrade performance for traffic loading.

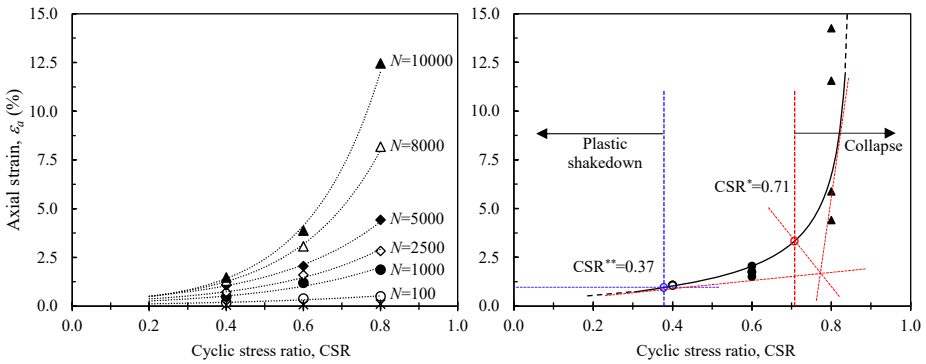

Figure 3.48: Determination of threshold cyclic stress ratio for kaolin samples

Considering this range of cyclic stress ratio, where samples remained stable, the accumulation of axial strain with respect to the load duration of samples at different frequencies is presented in Figure 3.49 on a logarithmic scale. Examination of this response clearly demonstrates the independence of the strain response with variation of frequency. The same response can be seen in Figure 3.50 for a cyclic stress ratio of 0.6. This function has been converted to

consider load cycles, shown in Figure 3.51 and demonstrates a distinct relationship with respect to cycles of load. The initial non-linear component of the strain accumulation path has been neglected, such that the horizontal scale extends from 10 load cycles.

Examining the linear relationship between axial strain and the number of load cycles, the following functions were determined;

For CSR=0.4 $\epsilon_a = 0.051N^{0.503}$ (3.20)

For CSR=0.6 $\epsilon_a = 0.076N^{0.500}$ (3.21)

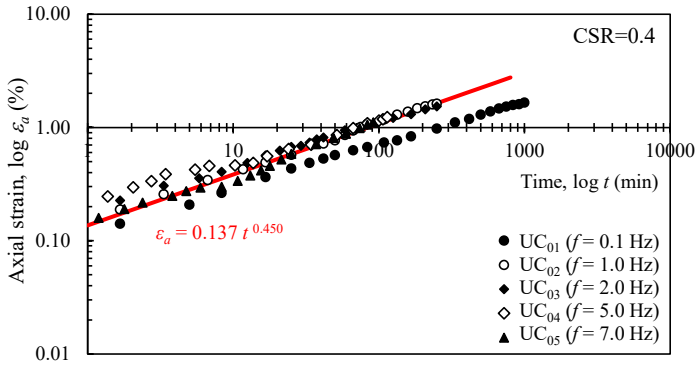

Figure 3.49: Development of axial strain after 10 cycles for a cyclic stress ratio of 0.4

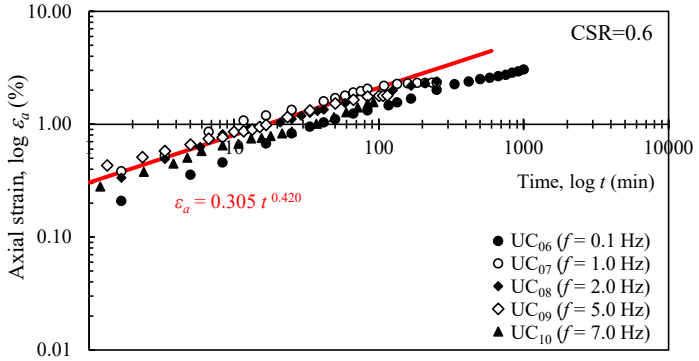

Figure 3.50: Development of axial strain after 10 cycles for a cyclic stress ratio of 0.6

In this way, the linear relationship demonstrates that irrespective of the cyclic stress ratio of the sample, the gradient of the strain-cycle relationship is approximately constant. For the kaolinite samples examined, this slope equates to a value of 0.5. The factor applied to the number of cycles in the above equations varies. This corresponds to the intercept and therefore the initial accumulation of axial strain at load cycle number 10, and varies dependent on the cyclic stress ratio applied to the sample such that the greater the applied load, the larger the initial strain response of the sample during the first 10 load cycles.

Noting that the initial strain response of a sample for the first ten load cycles is dependent on the cyclic stress ratio of the sample, it is important to consider what happens during the cyclic triaxial tests. Considering the response of axial strain with a progressive number of cycles, Figure 3.52 demonstrates for a given number of load cycles the relationship between axial strain and applied cyclic stress ratio is exponential. In this way, the strain developed in the first ten load cycles can be estimated by;

$$\Delta\epsilon_{a,\mathrm{N=10}} = 0.0284\exp^{1.564\mathrm{CSR}} \tag{3.22}$$

In this case, based on Equation 3.22, for a CSR of 0.4 this equates to an intersect of 0.053% strain at cycle 10, whilst for a CSR of 0.6, a strain value of 0.073%.

The equation provides a good estimate of the accumulated strain for a given number of load cycles fitted to Figure 3.51, however it is only applicable for cyclic stress ratios below the threshold value and is incapable of predicting sample failure. The function above demonstrates that for samples that remained stable, and therefore those under consideration with respect to prolonged cyclic loading for the assessment of traffic loading response, the accumulation of axial strain has a dependency on the cyclic stress ratio of the sample. In order to determine if this relationship can be extended for clays other than kaolinite, Wenzhou clay cyclic undrained triaxial tests presented by Li et al. (2011) for a frequency of 0.1Hz have been considered. The cyclic stress ratio of the samples was recalculated to reflect the same derivation as adopted

in this study (considering q_{cyc}/q_s) such that the CSR was 0.36. Adopting a value of κ/V of 0.034 based on assessment of Wenzhou clay by Guo et al. (2020), the results presented in Figure 3.52 show close agreement between the undrained cyclic triaxial test strain accumulation path and that predicted by Equation 3.22.

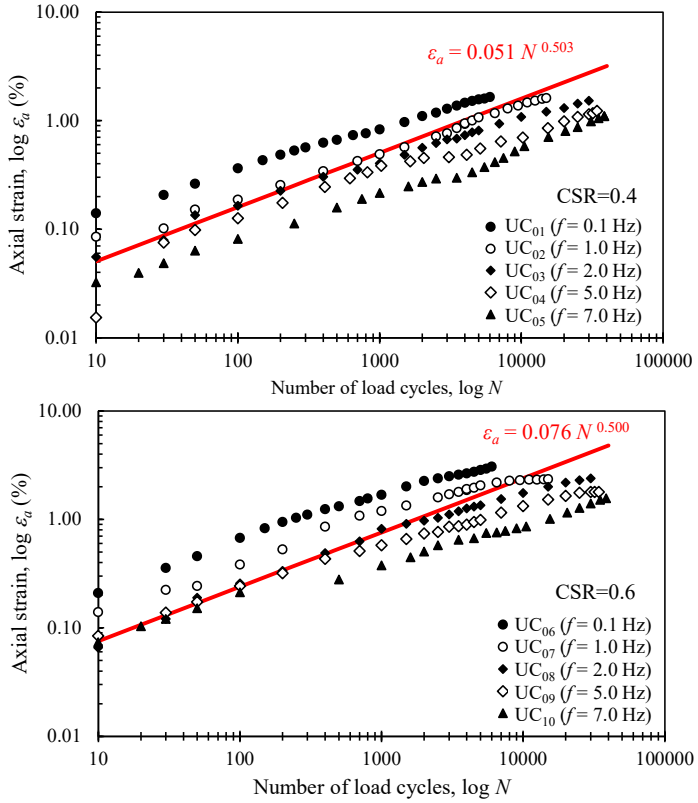

Figure 3.51: A relationship for axial strain accumulation under undrained cyclic loading

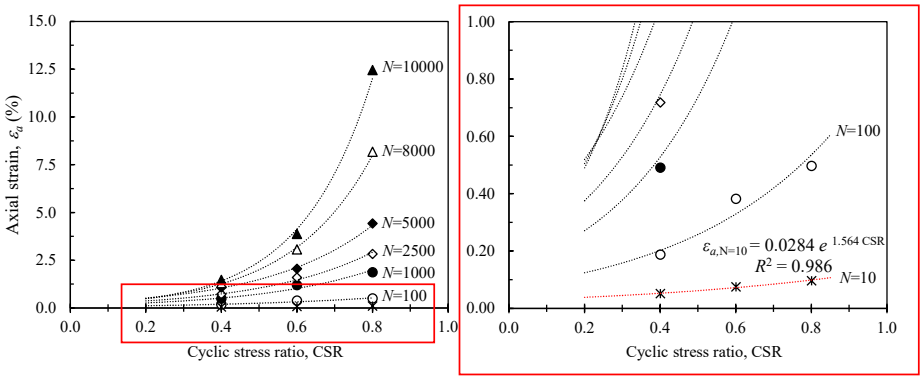

Figure 3.52: Development of axial strain at 10 cycles with respect to cyclic stress ratio

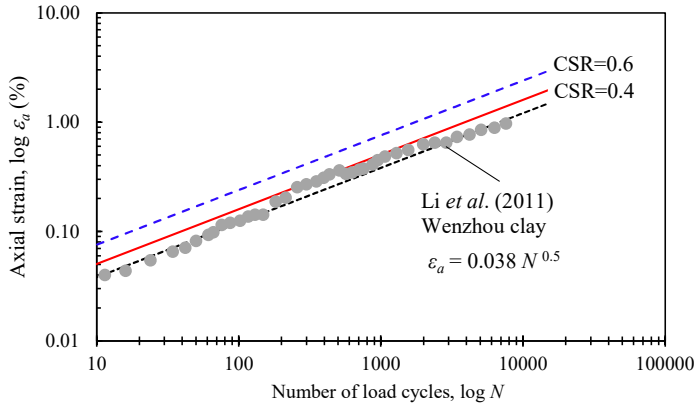

Figure 3.53: Prediction of axial strain on Wenzhou clay using the results of Li et al. (2011)

3.5.4 Effect of Post-Cyclic Recompression

The results of the UC undrained cyclic triaxial tests suggest the critical cyclic stress ratio of kaolinite exists between 0.6 and 0.8, thus as the ratio of load magnitude with respect to undrained strength of the soil at failure tends towards 1, the sample attains a failed state. For samples where the end state after a series of load cycles remained stable, with both a decrease in the accumulation of excess pore water pressure generation and axial strain, it is also important to consider the stability of these samples compared to equivalent samples presented in Section 3.4 for monotonic loading. Post-cyclic undrained static shearing was undertaken on samples with a cyclic stress ratio of 0.4 and 0.6. Figure 3.54 (a) and (b) present the stress-strain response for undrained monotonic test UM_{03}, considering an initial p'_{c0} of 200kPa, as per the initial mean effective stress of the cyclic load tests examined, against the results for a CSR of 0.4 and 0.6 at a frequency of 0.1Hz and 1.0Hz respectively. The results presented only describe the monotonic shearing response subsequent to the cyclic loading portion of the test.

Examining the accumulation of deviatoric stress, the strength of post-cyclic tests decreases due to the undrained cyclic loading that the sample has experienced prior to shearing. This response demonstrates the stress loading history of the sample, in this case the cyclic loading, has an effect on the overall response of the sample. It is also demonstrated that for an increase in cyclic stress ratio,

and thus greater cyclic loading, there is a greater degradation in the post-cyclic undrained shear strength of the sample. Furthermore, comparing Figure 3.54 (a) for a frequency of 0.1Hz against (b) for a higher frequency of 1.0Hz, the results also show the the influence of the number of cycles loading prior to shearing, demonstrating a greater number of load cycles results in a greater reduction in the undrained shear strength of the samples. Considering the stress path of the two tests at a frequency of 1.0Hz compared to the monotonic stress path for the portion of monotonic shear only, the results in Figure 3.55 show that the initial confining pressure of the monotonic shear test has reduced as a result of cyclic loading. As such, under undrained shearing, the sample reaches the failure line quicker than for the UM test. The summary of results for the post-cyclic strength of samples at a frequency of 0.1Hz and 1.0Hz are presented in Table 3.13.

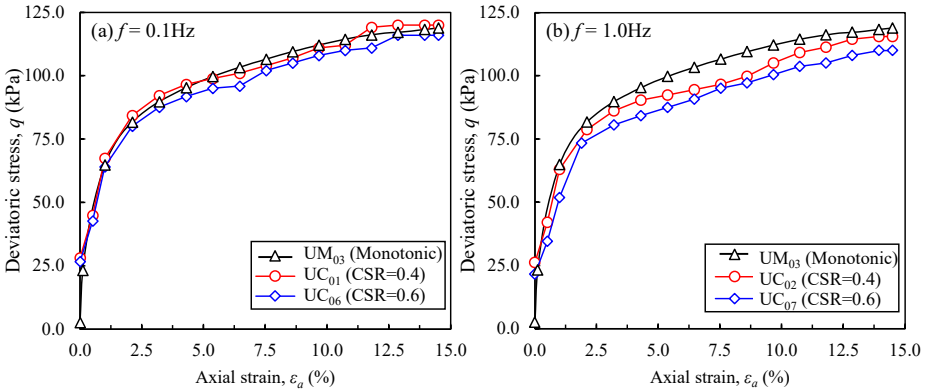

Figure 3.54: The stress strain response of undrained post-cyclic monotonic shear tests

The curvature of the stress paths after cyclic loading suggest some overconsolidation of the sample has occurred. Some authors have previously suggested this 'apparent' overconsolidation is related to the destruction of bonds within the clay structure leading to a reduction in shear strength. This will be described in greater detail in Section 4.2 where the effects of preloading and their influence on cyclic load response of soft soils are considered. This behaviour is explained graphically in Figure 3.56, whereby the cyclic load and therefore excess pore pressure response results in a stress condition, p'_{c1} at the end of cyclic loading that subsequently becomes the starting value of initial confining pressure for post-cyclic monotonic shearing. With respect to a larger

degradation in undrained shear strength observed for a greater cyclic stress ratio, the results presented in Section 3.5.2 and Section 3.5.3 showed a larger accumulation of excess pore pressure was observed at a cyclic stress ratio of 0.6 compared to 0.4, and hence in Figure 3.56 a larger Δu_{cyc} is developed.

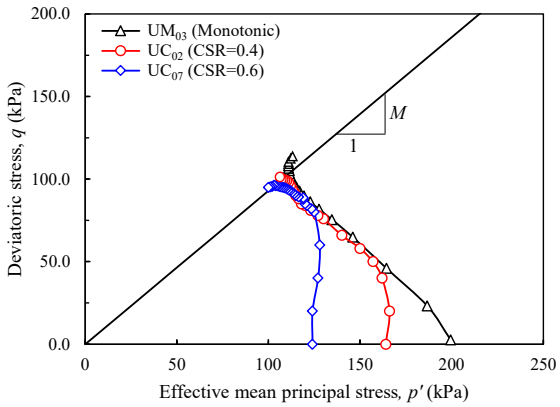

Figure 3.55: The stress path of undrained post-cyclic monotonic shear tests

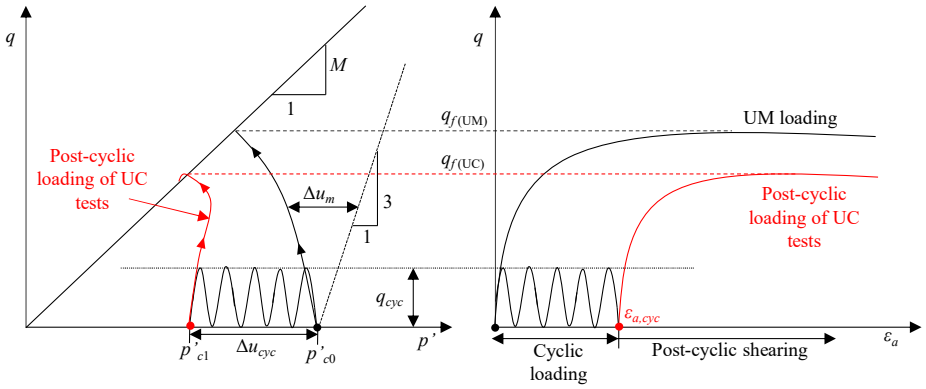

Figure 3.56: A graphical representation of the post-cyclic shear behaviour observed in triaxial tests

Table 3.13: Summary of post-cyclic undrained shear triaxial tests undertaken on kaolinite samples

Sample Name:	Frequency (Hz)	CSR	Number of Cycles	Post-cyclic loading c_u (kPa)	Degradation of c_u
UC_{01}	0.1	0.4	15000	60.7	9.09%
UC_{02}	1.0	0.4	30000	57.8	12.50%
UC_{06}	0.1	0.6	15000	58.4	12.12%
UC_{07}	1.0	0.6	30000	55.4	16.67%

The response of post-cyclic normalised pore pressure is presented in Figure 3.57. As for the stress-strain diagrams, the results are presented for the post-cyclic component of the test only, demonstrated by the intercept of the normalised excess pore pressure with the y axis. Both the results for a cyclic stress ratio of 0.4 and 0.6 converge to a similar normalised excess pore pressure value of approximately 0.77. Considering the post-cyclic response, the excess pore pressure behaviour is independent of the frequency of loading however it is observed a greater excess pore pressure accumulation occurs at a lower cyclic stress ratio. Examining the stress path shown in Figure 3.55, and presented in greater detail in 3.58, this is again demonstrated, whereby the greatest increment in excess pore pressure will occur for a lower cyclic stress ratio, demonstrated by p'_{c1} and the corresponding magnitude of Δu_{c1} when compared to that of Δu_{c2}. Subsequently therefore, an increase in the overconsolidation of the sample results in a reduction in the normalised excess pore pressure response.

Yasuhara et al. (1982) reported there was no significant effect on the post-cyclic undrained shear strength of a material with a variation in frequency of loading whilst Ansal and Tuncan (1989) reported a reduction in shear strength up to 65% could be observed during cyclic simple shear tests. However, the results all support the conclusion that after a significant number of cycles of load, the effect of frequency on the overall response can be neglected, both during cyclic loading presented in Section 3.5.3 and during post-cyclic shearing presented in this section. This consideration is purely applicable to traffic loading whereby the number of cycles over the design life of an asset is significantly large and therefore not applicable to consideration of seismic events.

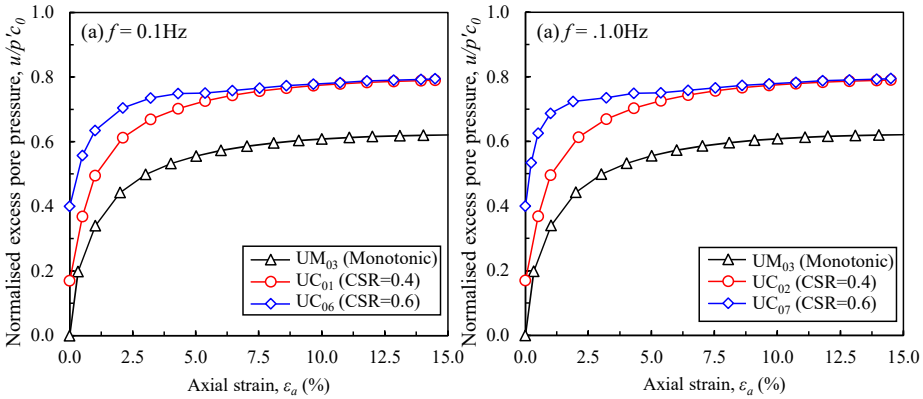

Figure 3.57: The normalised excess pore pressure response of undrained post-cyclic monotonic shear tests

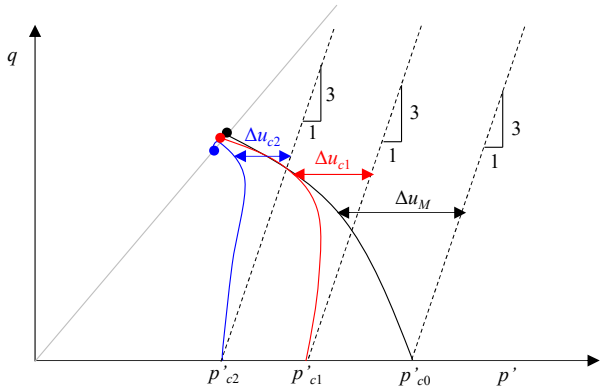

Figure 3.58: Pore pressure response during post-cyclic monotonic shearing

3.6 Conclusions

Undrained monotonic and cyclic tests have been undertaken on soft kaolinite samples, representative of in-situ conditions beneath slab track.

- One dimensional compression tests provided a baseline for considering the long term settlement effects of loaded the prepared kaolinite samples. Considering the period of loading and load intervals, a greater load duration resulted in the determination of less overall sample strain.
- Based on the criteria for Rayleigh wave speed required to ensure the safe passage of high speed trains over soils, such that dynamic amplification of track displacements is minimised, there exists a limit of undrained shear

strength such that the majority of soils with a strength greater than this would satisfy dynamic considerations of high-speed rail. Furthermore, this undrained shear strength satisfies static settlement criteria such that typically these soils would remain in place without treatment. This undrained shear strength value has been established as approximately 66kPa.

- The results of undrained monotonic tests completed on kaolinite samples examined the initial confining pressures of the sample and confirmed the properties determined from one dimensional compression tests. The confining stress corresponding to an undrained shear strength of 66kPa were subsequently applied to the cyclic triaxial tests.
- As demonstrated for the one dimensional compression tests, considering the strain rate of undrained monotonic triaxial tests, the greater the rate of shearing applied to the sample, the greater the determined undrained shear strength of a sample. Over the rates considered for examination, this influence was negligible and converged to an undrained shear strength of approximately 68kPa.
- The undrained cyclic loading tests were performed on kaolinite samples for a range of frequencies and cyclic stress ratios. The samples demonstrated a clear response with respect to the applied cyclic load magnitude, where samples with a CSR of 0.8 failed whilst samples with a CSR of 0.4 and 0.6 remained stable. This response was noted for samples tested at all load frequencies and demonstrated a threshold cyclic stress ratio exists between 0.6 and 0.8, supporting the findings of Pillai et al. (2014).
- At a lower frequency of loading, per cycle of load a greater accumulation of strain for an individual hysteretic loop was identified. Considering the number of cycles of loading, an increase in load frequency from 0.1Hz up to 7.0Hz resulted in a greater number of load cycles the sample could withstand prior to failure. With respect to the duration of the test, samples loaded at higher frequencies, and therefore more rapidly, tended to failure quicker. This failure was identified from the response of axial strain, where failure of a sample was determined from the accumulation of axial strain that continued to a rapid trajectory of 15% axial strain, defined as failure by ASTM guidance.

- The response of the normalised excess pore pressure for the undrained cyclic loaded samples showed a response dependent on the cyclic stress ratio, where for a greater applied load, the response in the generation of excess pore pressure was greater. The samples, irrespective of condition at the end of the test, demonstrated an initial rapid accumulation of excess pore pressures. In the first 1000 cycles of loading, the effect of the rate of loading is dominant, however in the latter part of the test, the accumulation of excess pore pressure diminishes progressively and the influence of loading frequency can be neglected. From the examination of excess pore pressure alone, it is not possible to determine if a sample has failed or remains stable at the end of testing. Furthermore, in consideration with the monotonic tests undertaken, there is little difference in the accumulated excess pore pressure response with respect to time with both UC and UM samples attaining a similar value of normalised excess pore pressure at failure. During the initial portion of the tests where accumulation occurs, the generation appears to be quicker for monotonic loading, where the load is applied constantly, compared to during cyclic loading. The response in excess pore pressure observed in the undrained cyclic triaxial tests agrees well with the accumulation equation proposed by Hyde and Ward (1985).

- Post-monotonic cyclic strength was examined for samples with a cyclic stress ratio of 0.4 and 0.6, where the accumulation of strain with respect to load cycles and test duration had gradually become asymptotic with a negligible increase in strain accumulation with test progression. Samples were subsequently sheared under undrained conditions and showed a reduction in post-cyclic strength of the sample dependent on the cyclic stress ratio that had previously been applied to the sample. The stress-strain response of samples suggested both the duration, and therefore number of cycles of load, had an influence over the post-cyclic undrained shear strength as well as the magnitude of cyclic load such that the cyclic loaded samples attained a lightly over-consolidated state when subject to shearing. Irrespective of the cyclic stress ratio, cyclic samples converged to a similar magnitude of excess pore pressure, however the greatest accumulation in excess pore pressure during shearing occurred for samples with a lower cyclic stress ratio.

Chapter 4

Impact of In-Situ Conditions on the Loading Behaviour of Soils

4.1 Introduction

Chapter 3 introduced the response of kaolinite samples subject to monotonic and cyclic loading under conditions representative of the confinement of subgrade layers underlying slab track formation, for which the sample soil strength would be sufficient for the layer to remain in-situ. However, the consideration of a constant cyclic load applied with undrained triaxial conditions is an idealised consideration with respect to the loading conditions experienced by a soil element in the field. This Chapter examines separate conditions that could be seen as a more refined representation of the in-situ condition, for which due consideration has been given to determine the effect and influence of cyclic loading, namely;

- Preloading, since ground strength improvement techniques can be used to reduce the settlement experienced subsequent to track construction and application of cyclic load, discussed in Section 4.2, and
- Partial drainage, since the in-situ conditions in the field typically would not remain as undrained over the lifetime of the structure, discussed in

Section 4.3,

4.2 Soil Response due to Preloading

As presented in Chapter 3 Section 3.4.2, it was identified that an undrained shear strength of approximately 66kPa represented a potential practical limit of which a cohesive soil could remain in-situ without requiring the aforementioned ground improvement techniques.

There are a number of ground stabilisation methods that are commonly adopted in order to improve the condition of the ground and enable safe construction of rail infrastructure. One method other than excavate and replace of problematic soils for satisfying the static and dynamic subgrade performance requirements of soft cohesive deposits is to introduce a surcharge and hold period into the construction sequence. Preloading is a cost-effective method adopted in construction intended to accelerate the primary consolidation of a soil as a result of an applied distributed surface load to the zone of subgrade under consideration. This can further be enhanced by coupling the defined preloading method with the introduction of prefabricated vertical drains to promote dissipation of excess pore water pressures via facilitating a horizontal drainage path. The introduction of vertical drains and their performance under cyclic load has previously been examined by Ni (2012). Adopting only a preload solution, the application of load typically remains for a duration of between 6 months to 1 year in order to allow the generated excess pore water pressure response to dissipate effectively. In some cases, it may be more efficient to introduce a higher preload for a shorter duration of loading as a more cost effective solution considering construction durations of assets.

4.2.1 Principles of Preloading

Whilst some authors, discussed in Chapter 2.3.2.2, have examined the response of overconsolidated samples subjected to cyclic loading, most have examined

naturally overconsolidated samples, for instance those that have been overconsolidated as a result of periods of glaciation, or samples that have been overconsolidated in order to replicate this in-situ condition. As such, these studies have focussed on samples whereby the maximum pre-consolidation pressure, (p'_{OC}) in Figure 4.1, has been constant and the overconsolidation ratio has been achieved by unloading and swelling of the sample to various different pressures. This response is different to that achieved by preloading of the soil, whereby p'_{c0} remains constant and the magnitude of pressure applied to the sample increases to achieve an overconsolidated sample. Presented in Chapter 2, many studies on overconsolidated cyclic tests have therefore shown than an increase in OCR leads to a negative effect on the sample, resulting in greater strain accumulation and less cycles to failure for these samples. This Chapter therefore focusses on determining the cyclic response of overconsolidated samples where the applied pressure, and subsequent overconsolidation ratio, has been used to improve the strength of a sample.

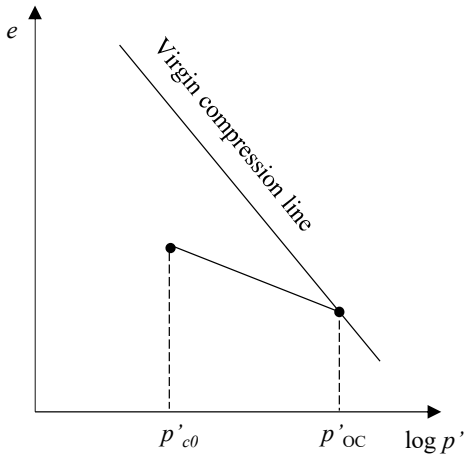

Figure 4.1: Principle of preloading and overconsolidation

The principle of preloading is presented in Figure 4.1 whereby a soil element is loaded with an applied magnitude of surcharge. Under this condition, the vertical effective stress of the sample, σ will increase as excess pore pressures generated in response reach an equilibrium and dissipate. Once the temporary surcharge, resulting in a vertical effective stress of p'_{OC} is removed, the soil will undergo unloading and return to an effective stress of p'_{c0} in Figure 4.1 such

that this vertical stress will be the initial stress state of the soil prior to any future load events as a result of construction and train loading. As a result, the application of a preload therefore imposes an over-consolidated state on the soil element under consideration, defined as the ratio between the maximum stress caused by the preload to the unloaded stress of the sample.

For consistency, p'_{c0} represents the initial confining pressure at the *start* of the monotonic or cyclic load portion of the triaxial test, such that as defined in Figure 4.1, the samples all return to the same value of p'_{c0} as adopted in triaxial tests presented in Chapter 3. In this case, for an OCR of 2.0 the sample was isotropically consolidated to $p'_{OC} = p'_{c0}$ x OCR, before the effective confining pressure was reduced back to p'_{c0}. During this consolidation stage, the deviator stress was maintained at close to zero to ensure samples were isotropically consolidated.

In conclusion with respect to the one dimensional consolidation tests presented in Section 3.2.1, it was clear that in order to maintain small vertical displacements subsequent to unloading and removal of a load, a sample should not be reloaded to a stress level greater than that to which it had previously been exposed to. This principle is applied with respect to preloading, such that the magnitude of surcharge selected for the ground improvement method should be greater than the load to be experienced during subsequent construction and in-service loading conditions. As such, the stress state of the soil under consideration should remain traversing the unload/reload portion of the curve presented in Figure 4.1.

Four undrained monotonic overconsolidated tests, UOM tests, were completed on the kaolinite samples in order to determine the response to load and undrained shear strength of the samples at various overconsolidation ratios, OCR. OCR values of 1.0, 2.0, 4.0 and 8.0 were selected to capture a range of consolidation behaviours, from lightly overconsolidated (LOC) to more heavily overconsolidated (HOC) samples at an OCR of 8.0. The UOM tests undertaken are presented in Table 4.1. Whilst in practise achieving a high OCR can have limitations with respect to the significant overburden that would be required in

some cases, a high value has been tested as part of this study in order to determine if the improvement in the number of cycles attained prior to failure is continual.

Table 4.1: Summary of undrained overconsolidated monotonic (UOM) triaxial tests undertaken on kaolinite samples

Sample Name:	OCR	Undrained shear strength, c_u (kPa)
UOM_{01}	1.0	66.4
UOM_{02}	2.0	109.2
UOM_{03}	4.0	135.1
UOM_{04}	8.0	163.4

Figure 4.2 presents the relationship between deviatoric stress with respect to the development of axial strain. The results show the trend is similar for all samples, however as summarised in Table 4.1 the overconsolidation ratio affects the maximum deviatoric stress of the sample, and as such the undrained shear strength. As the starting effective stress for all samples irrespective of historic loading is the sample, p'_{c0}, the greater the magnitude of applied historic pressure, and therefore overconsolidation of the sample, the greater the undrained shear strength of the sample. As noted in Chapter {2, had the samples been unloaded from the same pre-consolidation pressure, p_{OC}, the opposite effect in undrained shear strength would be observed. Examining the response in terms of normalised excess pore pressure with respect to axial strain of the UOM samples, negative excess pore pressure is observed for the sample with the higher OCR examined, an OCR of 8. This demonstrates the dilative response of clays that are overconsolidated, whereby due to the undrained nature of the triaxial tests adopted in this study, volume expansion is reflected by the generation of negative excess pore water pressure. This concept has been studied by a number of authors, whereby at low values of OCR, the response of a sample is to contract, whilst for a clay at high OCR values, on the dry side of critical (Schofield (1993)) it will dilate.

This behaviour can be seen in Figure 4.3 for the effective stress paths of samples UOM_{01} to UOM_{04}. The results normalised with respect to the maximum

pressure applied to the sample p'_{OC} are presented in Figure 4.4. The stress paths for samples at different overconsolidation ratios vary dependent on the generation of excess pore pressure for each sample. Indeed, as the overconsolidation ratio of the sample increases, there is a reduction in the excess pore pressure generated and gradually this excess pore pressure becomes negative.

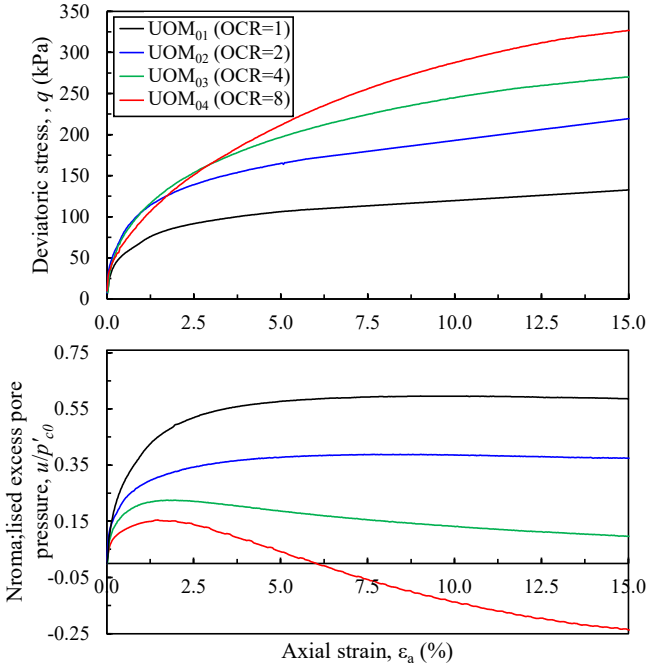

Figure 4.2: Deviatoric stress and normalised excess pore pressure against axial strain

As presented in Chapter 2, the overconsolidation ratio has an effect on the undrained shear strength of a sample. For the monotonic tests undertaken, the proposed ratio between normally and overconsolidated undrained shear strength values presented by Mayne and Kulhawy (1982) after Ladd et al. (1977) is adopted in equation 4.1, where Λ is the strength rebound parameter;

$$\frac{\left(\frac{c_u}{p'_{c0}}\right)_{OC}}{\left(\frac{c_u}{p'_{c0}}\right)_{NC}} = OCR^{\Lambda} \tag{4.1}$$

The ratio of normalised undrained shear strength is presented in Figure 4.5, where the initial confining pressure of the sample p'_{c0} is 200kPa and Λ is 0.473.

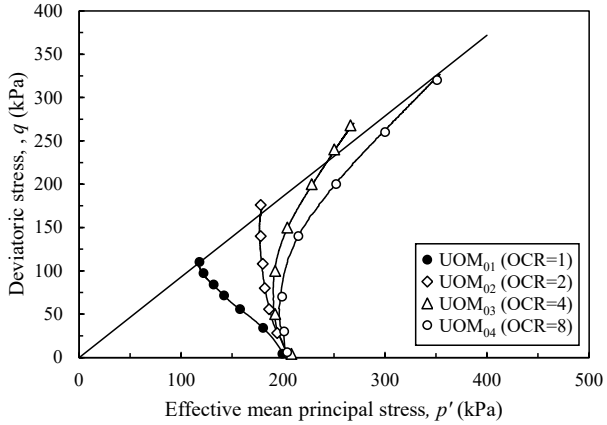

Figure 4.3: Effective stress path, q-p′ for monotonic overconsolidated triaxial tests

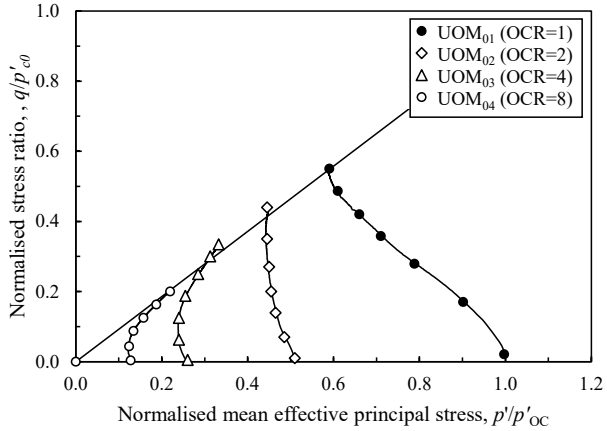

Figure 4.4: Normalised effective stress path, q-p′ for monotonic overconsolidated triaxial tests

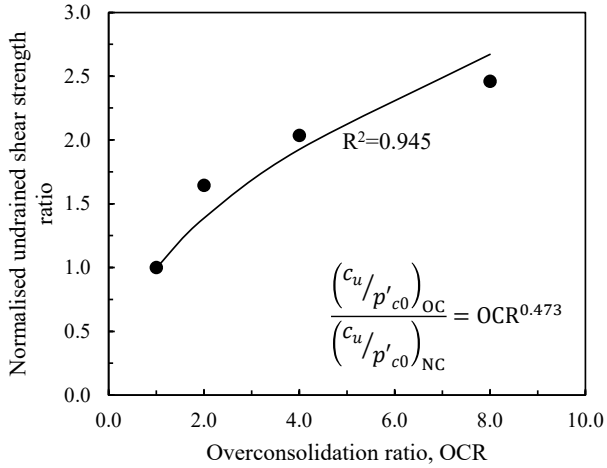

Figure 4.5: Relationship between normalised undrained shear strength ratio and OCR

4.2.2 Preloaded Cyclic Triaxial Tests

The undrained cyclic loaded triaxial tests, UOC, undertaken in this Section are summarised in Table 4.2, considering the effect of over-consolidation and therefore the degree of improvement in monotonic soil response with respect to cyclic loading. As discussed in Chapter 2, a number of authors have previously considered the response of clay soils subject to cyclic loading considering various values of overconsolidation ratio, OCR, however the overconsolidation ratios considered did not generally adopt the same initial stress, p'_{c0} from which cyclic loading was subsequently undertaken and as such cyclic loading has a detrimental effect on the soil response.

The UOC tests presented examine a range of overconsolidation ratios, considering a high frequency of 5.0Hz and low frequency of 1.0Hz within the range previously examined for UC triaxial tests in Chapter 3. Furthermore, cyclic stress ratios of 0.6 and 0.8 were examined, that had previously demonstrated a threshold cyclic stress ratio for normally overconsolidated clays existed within this range.

The results presented in Figure 4.6 demonstrate the cyclic response of samples UOC_{01} to UOC_{05}, considering a cyclic stress ratio of 0.6 and a frequency of 1.0Hz for variation in the overconsolidation ratio of the samples. The result for UOC_{01}, an OCR of 1.0, show the result of test UC_{07} for Section 3.5. A similar trend in development of axial strain with respect to load cycles is shown for all samples irrespective of the overconsolidation ratio. All samples loaded with a cyclic stress ratio of 0.6 remained stable following a period of cyclic load and in agreement with the monotonic overconsolidated tests, the greater the magnitude of historic applied pressure to the sample, the smaller the generation of axial strain for the same number of load cycles.

Table 4.2: Summary of undrained overconsolidated cyclic (UOC) triaxial tests undertaken on kaolinite samples

Sample Name:	CSR	OCR	Frequency (Hz)	Number of Cycles	Failure
UOC_{01}	0.6	1.0	1	15000	No
UOC_{02}	0.6	2.0	1	15000	No
UOC_{03}	0.6	4.0	1	15000	No
UOC_{04}	0.6	6.0	1	15000	No
UOC_{05}	0.6	8.0	1	15000	No
UOC_{06}	0.6	1.0	5	32400	No
UOC_{07}	0.6	2.0	5	32400	No
UOC_{08}	0.6	4.0	5	32400	No
UOC_{09}	0.6	6.0	5	32400	No
UOC_{10}	0.6	8.0	5	32400	No
UOC_{11}	0.8	1.0	1	10723	Yes
UOC_{12}	0.8	2.0	1	12293	Yes
UOC_{13}	0.8	4.0	1	15482	Yes
UOC_{14}	0.8	6.0	1	16243	Yes
UOC_{15}	0.8	8.0	1	16934	Yes
UOC_{16}	0.8	1.0	5	28093	Yes
UOC_{17}	0.8	2.0	5	29782	Yes
UOC_{18}	0.8	4.0	5	35001	Yes
UOC_{19}	0.8	6.0	5	30457	Yes
UOC_{20}	0.8	8.0	5	26085	Yes

Considering the normalised excess pore pressure response for the stable samples, the accumulation for samples with an OCR $\leq$ 4.0 showed a response similar to previous undrained cyclic load tests undertaken. However, for UC samples, the normalised excess pore pressure converged to a constant value irrespective of frequency. In the case of the overconsolidated samples, the accumulation of excess pore pressure decreases with an increase in OCR, suggesting a resistance to excess pore pressure generation with cyclic loading, as suggested by Hyodo et al. (1999). At high OCRs, a similar response to that observed in UOM tests is shown whereby the excess pore pressure with continual cycles of load converges to a negative value, suggesting dilation of the sample. This response explains

why the improvement in axial strain accumulation at high OCRs is incrementally less than for lightly over consolidated samples, whereby the position of the stress path relative to the critical state line of the soil lies on the dry side.

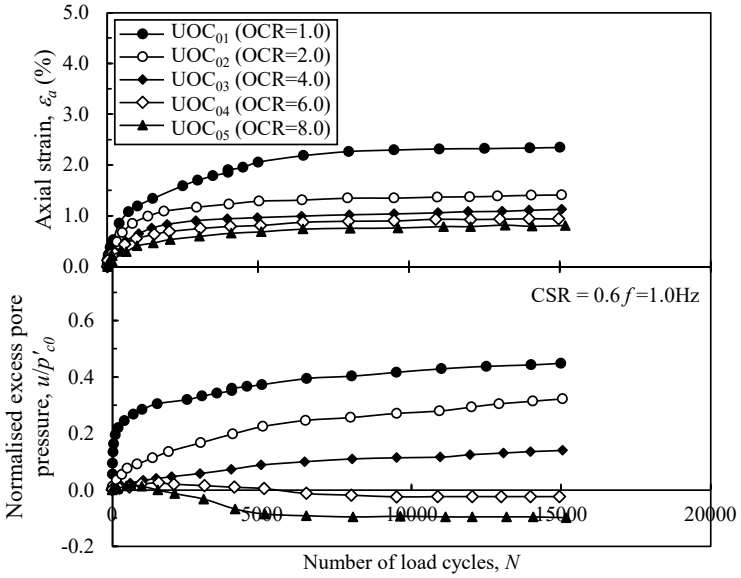

Figure 4.6: Development of axial strain and normalised excess pore pressure considering the number of load cycles for a cyclic stress ratio of 0.6 at various OCR values

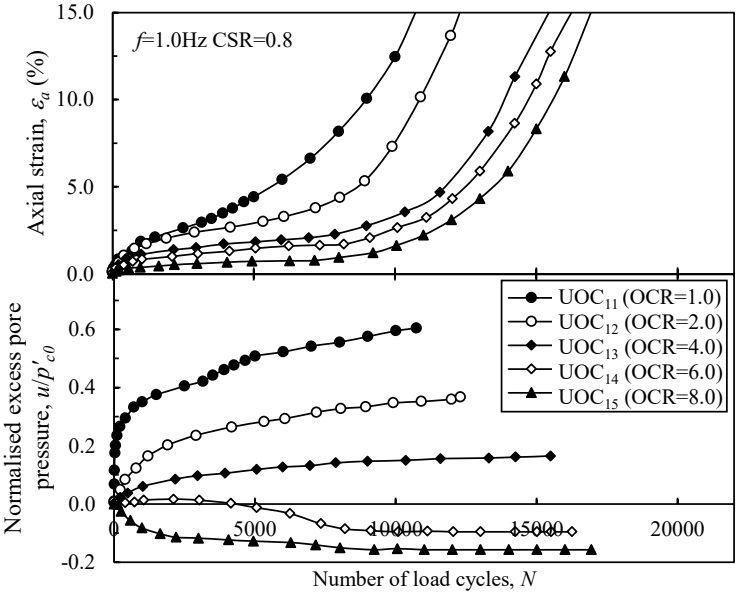

Figure 4.7: Development of axial strain and normalised excess pore pressure considering the number of load cycles for a cyclic stress ratio of 0.8 at various OCR values

Considering the response of samples at a cyclic stress ratio of 0.8, the samples

all still failed irrespective of overconsolidation ratio. In comparison to sample UOC_{11} for a frequency of 1.0Hz, the results show a similar trend with respect to overconsolidation ratio whereby for an increase in OCR, the number of load cycles a sample withstands prior to failure increases. As per Figure 4.6 the response of axial strain accumulation with respect to number of cycles shows the increase in axial strain between subsequent increments in OCR decreases. Meimon and Hicher (1980) demonstrated that for cohesive soils with the same initial state of effective stress, in this case p'_{c0}, but with different overconsolidation ratios, and therefore loaded to different p'_{OC}, the value of threshold stress increases with overconsolidation ratio. In the case of the samples examined in this study, this behaviour was not observed suggesting the critical cyclic stress ratio still exists between 0.6 and 0.8. Further examination within this range would be required in order to determine if, although the threshold stress still exists between 0.6 and 0.8, it would be higher than for that of the UC tests presented in Chapter 3.

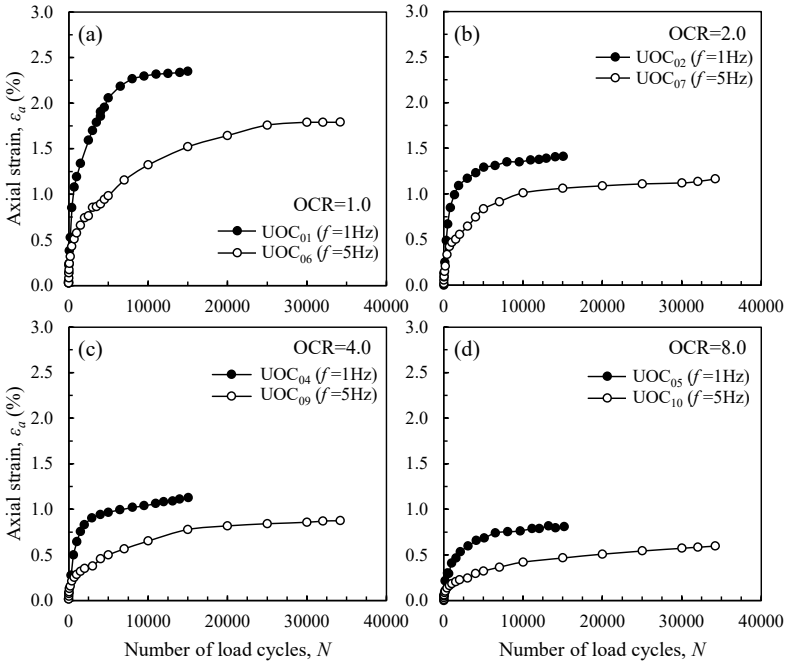

Figure 4.8: Development of axial strain at f=1.0Hz and f=5.0Hz considering the number of load cycles for a cyclic stress ratio of 0.6 at various OCR values

Examining the undrained overconsolidated cyclic test normalised excess pore

pressure response, the results show a higher degree of excess pore pressure was attained for failed samples, in agreement with previous UC tests completed on the kaolinite. Furthermore, from the response of excess pore pressure alone, the stability of the sample at the end of the test and therefore failure could not be identified. Again, the convergence of normalised excess pore pressure for failed UOM samples is close to that observed from the UOM tests presented in Section 4.2, similar to the trend observed in normally consolidated cyclic and monotonic tests. At high overconsolidation ratios, the response of excess pore pressure is similar to that observed by Hyde and Brown (1976) under repeated loading.

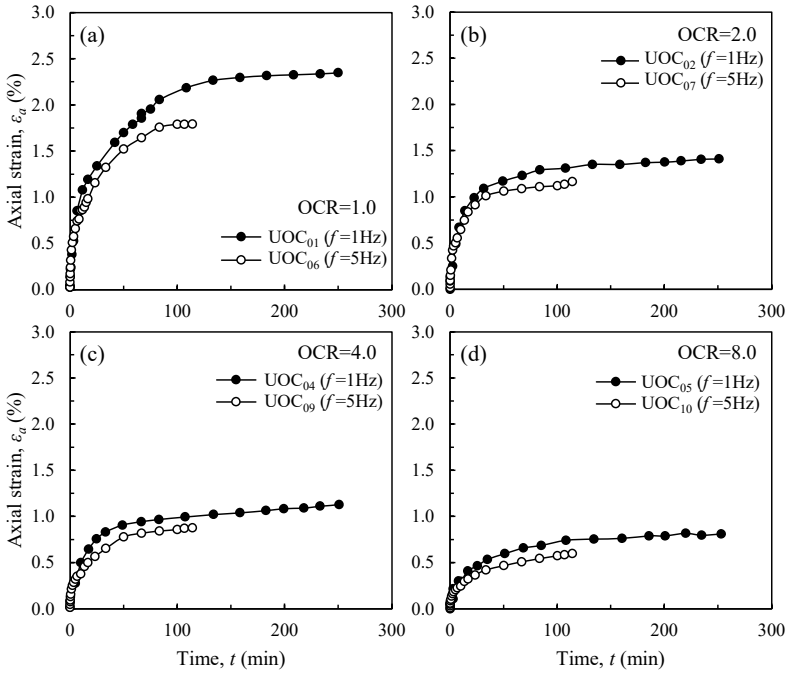

Figure 4.9: Development of axial strain at f=1.0Hz and f=5.0Hz considering test duration for a cyclic stress ratio of 0.6 at various OCR values

Considering the effects of loading frequency, two frequencies were considered for the examination of overconsolidated samples, 1.0Hz and 5.0Hz. Figure 4.8 presents the results for samples that remained stable with a cyclic stress ratio of 0.6 at a frequency of 1.0Hz and 5.0Hz. With respect to the number of load cycles, the results show the higher the frequency of load applied to the sample, the less axial strain accumulation the sample experiences. Conversely, supporting

the conclusions with respect to normally consolidated samples presented in Chapter 3, when examining the results of the cyclic loaded overconsolidated samples with respect to test duration, the results show that whilst the higher frequency samples typically generate greater magnitudes of axial strain, the frequency of load had a negligible effect on the overall strain response within the frequency range considered.

4.2.3 Consideration of Energy Effects

For undrained cyclic UC triaxial tests, it has been demonstrated that greater axial strain development occurs for samples at higher cyclic stress ratios, such that the applied cyclic stress tends towards the static strength of the sample. At cyclic stress ratios above the threshold value that exists for the kaolinite samples between 0.6 and 0.8, the sample undergoes failure. However, in the case of the overconsolidated UOC tests undertaken, for the same cyclic stress ratio as normally consolidated samples, less axial strain accumulates for the same number of cycles of load. As such, as well as the cyclic stress ratio adopted for cyclic loading of the sample, there is another element that controls strain accumulation in stress-controlled cyclic triaxial tests.

Singh and Mitchell (1968) proposed a general function for soils that expressed the strain rate of a soil under a sustained deviator stress to consider creep loading effects, presented in Equation 4.2. The strain rate, $\dot{\epsilon}_a$ was expressed as a function of time, t where ζ is the decay constant and coefficient A was subsequently defined by Li and Selig (1996) for the consideration of traffic loading.

$$\dot{\epsilon}_a = At^{-\zeta} \tag{4.2}$$

A was defined based on the ratio of stress with respect to the static strength of the soil, in this case the cyclic stress ratio;

$$A = \alpha \left(\frac{\sigma_d}{\sigma_s}\right)^m = \alpha CSR^m \tag{4.3}$$

where α and m are material parameters. The results of Brown et al. (1975) have suggested for some, more granular soils, the value of m is 1.0, where a value greater than 1.0 signifies softening of a soil. Li and Selig (1996) proposed a range for α between 0.3 and 3.5.

Ni (2012) previously demonstrated for undrained cyclic triaxial tests, step loading intervals could be considered based on the integrated strain rate equation by Singh and Mitchell (1968) to analyse the response of a soil with respect to cyclic stress ratio for normally consolidated samples. As originally presented by Hyde (1974), the applied cyclic load during a half cycle can be divided into equal time intervals, such that the approximate sine curve can be represented by a step function. In each step interval, the portion of the curve can be defined as a straight line where the horizontal step is the mean value of q_{cyc} over the interval, Δt_i. As such, for a given number of intervals, n, the total axial strain based in Singh and Mitchell (1968) can be written;

$$\epsilon_a = \sum_{i=1}^{n} \int_0^{t_i} \alpha \left(CSR_i\right)^m {t_i}^{-\zeta} \, dt \tag{4.4}$$

For a load step, the time interval Δt_i is;

$$\Delta t_i = \frac{\left[\sin^{-1}\left(i\frac{2}{n} - 1\right) - \sin^{-1}\left((i-1)\frac{2}{n} - 1\right)\right]}{2\pi} \frac{1}{f} \qquad \text{for } i = 1, 2....n \tag{4.5}$$

Subsequently, the axial strain can be written;

$$\epsilon_a = \sum_{i=1}^{n} \alpha \left(CSR_i\right)^m \frac{\left(t_i\right)^{1-\zeta}}{1-\zeta} \tag{4.6}$$

where t_i is defined with respect to the total duration examined, t_{total};

$$t_i = 2t_{total} \frac{\left[\sin^{-1}\left(i\frac{2}{n} - 1\right) - \sin^{-1}\left((i-1)\frac{2}{n} - 1\right)\right]}{2\pi} \qquad \text{for } i = 1, 2....n \tag{4.7}$$

Extending the analysis of Ni (2012) to consider overconsolidated samples, the response of samples to loading, irrespective of consolidation, has been shown to

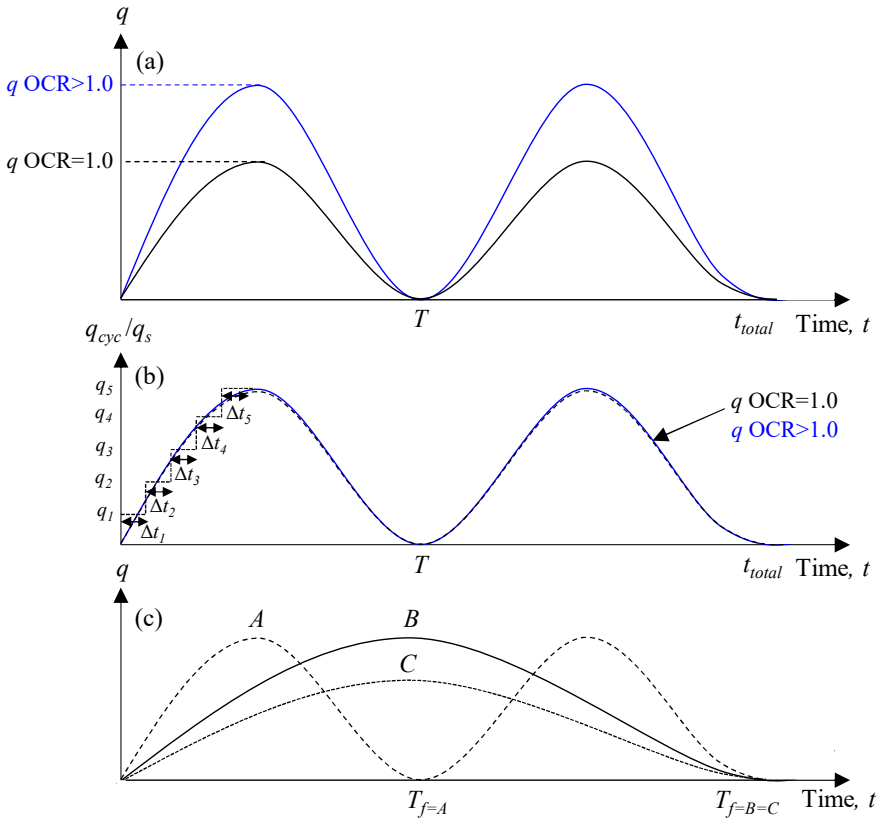

Figure 4.10: The influence of q on cyclic loading

be significantly influence with respect to cyclic stress ratio rather than frequency. For B and C traces in Figure 4.10 (c) with the same frequency, and therefore value of T_f this influence of cyclic stress ratio, represented by a difference in q, is demonstrated. Conversely for samples with different load frequencies, considering the duration for one cycle only, ie the same value of N, less strain is developed for the sample at the higher frequency, A compared to the sample of the same CSR at a lower frequency, B. Considering the same duration for different load frequencies, the accumulation of axial strain is similar irrespective of the frequency.

Considering the overconsolidated samples, the magnitude of q applied to a sample is greater than that of a normally consolidated sample, an OCR of 1.0 demonstrated in Figure 4.10 (a). However, consideration in this format implies a greater accumulation of axial strain as a result of increased area beneath the

sinusoidal curve for samples with an OCR > 1.0, shown by the blue line. This is incorrect from the response observed in the UOC tests that have been performed. However, it is important to note that samples were loaded with a magnitude of q_{cyc}, determined based on the undrained static strength of a sample for the same stress history. Considering this in Figure 4.10 (b), it is demonstrated that the cyclic stress ratio for all samples was the same, thus demonstrating the applicability of Equation 4.6.

Considering the cyclic stress ratio of the samples is the same, regardless of overconsolidation, this also means the value of p' is the same, as samples were all unloaded to the same value of p'. This is demonstrated in Figure4.11 (a). Again, as examination with respect to only p' does not acknowledge the stress history of the sample, normalising this value with respect to the magnitude of pressure applied to the sample in order to create an overconsolidated state, p'_{OC}, Figure 4.11 (b) shows the area beneath the curve, and therefore the amount of axial strain, decreases as the normalised pressure p'/p'_{OC} decreases. As the samples have the same value of p', a decrease in p'/p'_{OC} signifies a greater degree of overconsolidation. Therefore another function is needed to define the reduction in axial strain that occurs for overconsolidated samples.

Hyde (1974) considered the relationship between strain and time as per Singh and Mitchell (1968), noting the function for defining strain accumulation was constant for creep and repeated load tests given the same stress history, and therefore consolidated state of the sample. With respect to a variation in stress history, a function based on the repeated loading of a sample, dependent on the deviatoric stress was proposed. This function was defined for various overconsolidation ratios. The results of repeated load tests undertaken by Hyde (1974) for an OCR of 4.0 and 10.0 are presented in Figure 4.12 (a) and (b) respectively. As such the results demonstrated a decrease in strain rate with increased overconsolidation of the sample.

In this way, the strain rate defined by Singh and Mitchell (1968) became the

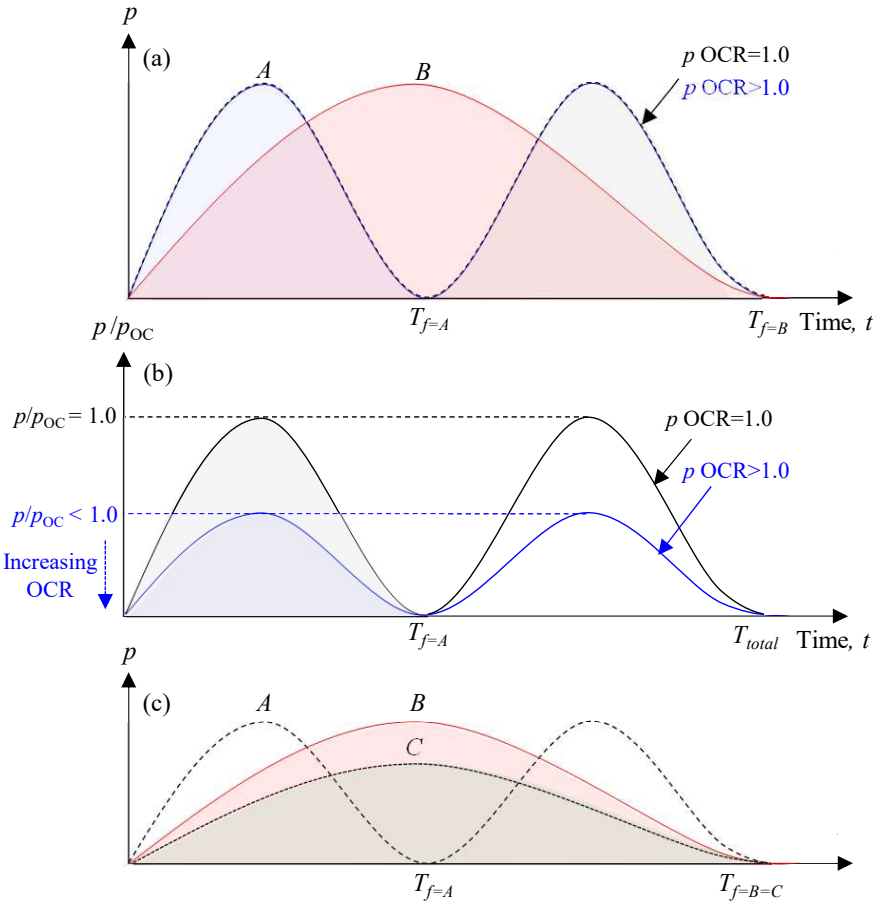

Figure 4.11: The area method

following;

$$\dot{\epsilon}_a = e^b t^{-\zeta} \tag{4.8}$$

where b is defined based on Figure 4.12. The corresponding functions for repeated load are defined in Equations 4.9 and 4.10 for Ariake Clay, where q_r represents the magnitude of repeated deviatoric stress applied to the sample;

$$b = \ln \dot{\epsilon}_a = 0.036 q_r - 9.5 \tag{4.9}$$

$$b = \ln \dot{\epsilon}_a = 0.029 q_r - 9.2 \tag{4.10}$$

However the functions in Equations 4.9 and 4.10 need to be investigated and

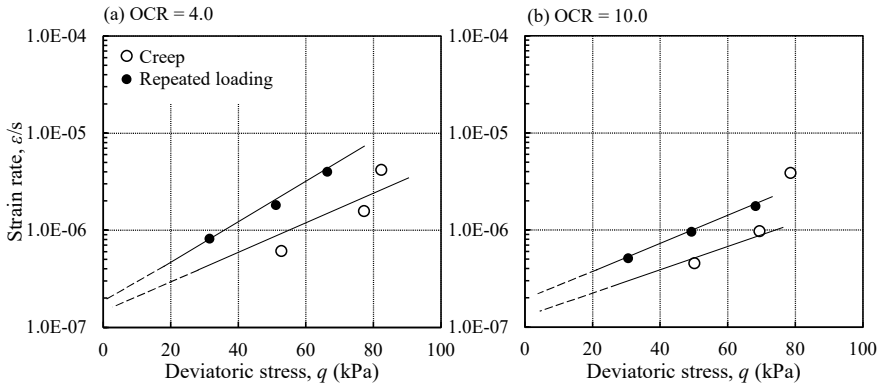

Figure 4.12: Strain rate for creep loading and repeated loading with respect to OCR, after Hyde and Brown (1976)

defined for each overconsolidation ratio under consideration in order for this relationship to be considered. The function itself does not relate specifically to the overconsolidation ratio, rather it is still based on the deviator stress. In the case of the UOC tests, the cyclic stress ratio for samples, irrespective of OCR is the same, however it is clear that there is a reduction in axial strain given by the reduced area, shaded blue in Figure 4.11 independent of the stress ratio.

Idriss et al. (1978) proposed that under load repetitions, a soil would degrade. The amount of degradation a soil experiences is dependent on a number of factors, as presented in Chapter 2 where one significant influence was the overconsolidation ratio of the soil. It was proposed for stress controlled triaxial tests, the degradation factor δ could be defined;

$$\delta = \frac{\frac{\sigma_r}{\epsilon_{a,N}}}{\frac{\sigma_r}{\epsilon_{a,1}}} = \frac{\epsilon_{a,1}}{\epsilon_{a,N}} \tag{4.11}$$

Zhou and Gong (2001) defined a degradation factor in terms of overconsolidation ratio. Subsequently for each increment of axial strain, the factor can be incorporated such that the axial strain is appropriately factored to account for degradation. The degradation model with respect to time, t_i is proposed;

$$\delta = \left[X + Y\right] Z \ln\left(t_i f\right) + 1.00 \tag{4.12}$$

where $X = \left(a_1 OCR^2 + a_2 OCR + a_3\right) \ln OCR$

$$Y = b_1\left(CSR - CSR^*\right) + b_2$$

$$Z = \left(\frac{1}{f}\right)^{c_1} \tag{4.13}$$

where CSR^* defines the threshold cyclic stress ratio for the development of pore pressure and a, b and c are test parameters. The equation above demonstrates that for an increase in overconsolidation ratio, the degradation ratio increases. Subsequently when applied to Equation 4.6, the strain therefore reduces as overconsolidation increases, in line with the proposed blue trace in Figure 4.11(a).

The area method was proposed such that the red shaded area of a low frequency sample, B, has an equivalent area to the shaded areas of a higher frequency sample, A for the same duration of testing in Figure 4.11. As all tests are undrained, and therefore equilibrium of the system is conserved, ie. no energy losses can be attributed to drainage of the system, it would appear that irrespective of the frequency of loading, the same energy dissipation occurs. Examining the response of a sample with respect to energy has been completed for cohesionless soil, particularly for consideration of liquefaction, Voznesensky and Nordal (1999) summarised the energy approach stating;

- With respect to energy, there is a direct influence as a result of the magnitude or intensity of loading, thus supporting the graphics in Figure 4.10(c) and Figure 4.11(c) where the red zone represents a higher cyclic stress ratio, and thus a greater area and absorbed energy than that of the green shaded area.
- The absorption of energy is independent of waveform, in the case of seismic studies meaning stress histories were not required, whilst in the case of the UC and UOC tests presented in Figure 4.10(c) and Figure 4.11(c) supporting the conclusion that for the same cyclic stress ratio, considering the same duration of test the energy absorption is independent of frequency.

Considering the principles of energy absorption with respect to soil fabric, the accumulation of axial strain occurs as the bonding or attraction between clay particles within the soil structure is broken. Therefore, there is an amount of accumulated energy required within the test duration considered that must apply for the sample to settle. This energy can be determined from the stress-strain hysteretic loop of a sample, where the area of the loop represents the absorbed energy in that load cycle (Azeiteiro et al. (2015)). It is important to note that not all energy absorbed during a load cycle is used with respect to particle rearrangement, and therefore strain, and some energy will be converted to heat or kinetic energy. Voznesensky and Nordal (1999) stated this component of energy was included in the subsequent load cycle.

In terms of the area method when considering the overconsolidated sample, for the same cyclic stress ratio the shaded blue area is less than that of the grey area for a normally consolidated sample in Figure 4.11(b), demonstrating less axial strain is developed. As the absorbed energy of the sample is related to the clay particle structure, it is therefore important to consider what happens during preloading with respect to this. Figure 4.13 demonstrates for the UOC samples considered, with an increase in overconsolidation ratio, the initial voids ratio of the sample decreases. As such, the resistance to deformation increases for overconsolidated samples under the same loading conditions, and the absorbed energy to achieve the same amount of strain as NC samples increases. This conclusion supports the findings of Azeiteiro et al. (2015) who concluded that looser samples would require less energy to achieve the same deformation of denser samples with a lower void ratio.

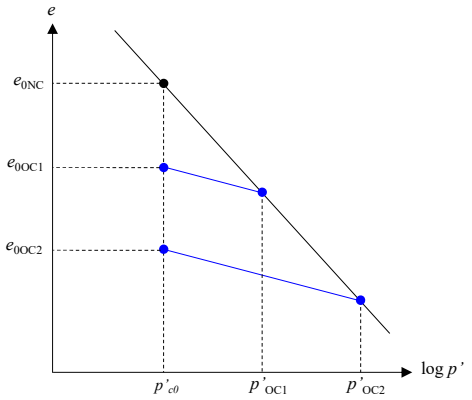

Figure 4.13: Relationship between void ratio and mean effective stress for overconsolidated samples

4.2.4 Consideration of Post-Cyclic Recompression

Examining the post-cyclic undrained monotonic response of the overconsolidated UOC triaxial tests, the critical state of the samples are presented in Figure 4.14 considering the frequencies of 1.0Hz and 5.0Hz examined. In agreement with the post-cyclic undrained shearing presented for UC samples, there is a small difference between the strength reduction dependent on the frequency of the sample, where the higher frequency sample attains a lower strength upon shearing. For all overconsolidation ratios examined, the post-cyclic strength reduction did not reduce by more than approximately 22% (for a normally consolidated sample under a cyclic load frequency of 5.0Hz, the post-cyclic undrained shear strength reduction was 21.5%). This supports the conclusions of Yasuhara et al. (1982) who acknowledged for an overconsolidation ratio of less than 10, the post-cyclic undrained shear strength did not reduce by more than 20% of monotonic undrained shear strength value. The reduction in post-cyclic shear strength is more marked for low OCR values and as the overconsolidation ratio of the sample increases, the reduction in undrained shear strength with respect to the equivalent monotonic test is less. Furthermore, the critical state of all samples suggest that the effective stress parameters of the kaolinite are not influenced by cyclic loading.

As discussed in Chapter 3 considering the post-cyclic behaviour of UC samples at a cyclic stress ratio of 0.4 and 0.6, when post-cyclic monotonic undrained shearing of the samples is undertaken, there is a reduction in the undrained shear strength of cyclic loading samples compared to monotonic samples. One explanation for this is the 'apparent' overconsolidation of samples, presented in Figure 3.56 in Section 3.5.4, whereby due to the accumulation of pore pressure that occurs during cyclic loading, the sample attains an overconsolidated state prior to shearing. Azzouz et al. (1989) made a clear distinction with respect to this process, acknowledging that unlike typical overconsolidation whereby the water content of the sample varies as a result, the response under cyclic loading occurs under a constant volume. Guo et al. (2020) defined this post-cyclic overconsolidation, POCR, as;

$$\text{POCR} = \frac{p'_{c0}}{p'_{c1}} = \frac{p'_{c0}}{p'_{c0} - \Delta u_{cyc}} \tag{4.14}$$

where p'_{c0} and p'_{c1} correspond to the mean effective stress of the sample at the start and end of cyclic loading respectively.

Noting the post-cyclic response of samples is similar to that of overconsolidated samples, the behaviour presented in Figure 4.15 can be considered, where C1 is produced under cyclic loading, from C0 with a difference of Δu_{cyc}. Guo et al. (2020) proposed that this point was the same as that produced from a typical unload-reload response, unloading the sample from point Cx. As such, the post cyclic overconsolidation ratio POCR can be rewritten in terms of the swelling and compression indexes obtained from standard one dimensional compression tests.

$$\log \text{POCR} = \left(1 - \frac{C_s}{C_c}\right) \log \text{OCR} \tag{4.15}$$

As such, the original equation presented by Mayne and Kulhawy (1982) in Equation 4.1, can be rewritten;

$$\frac{\left(\frac{c_u}{p'_{c1}}\right)_{\text{POC}}}{\left(\frac{c_u}{p'_{c0}}\right)_{\text{NC}}} = \left[\text{POCR}^{\frac{C_c}{C_c - C_s}}\right]^{\Lambda} \tag{4.16}$$

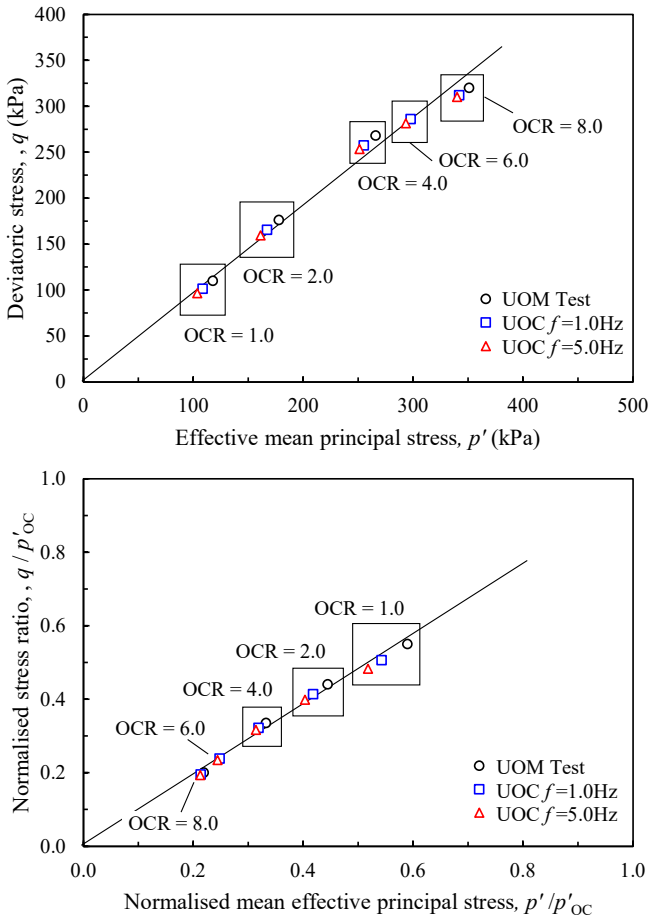

Figure 4.14: q-p' plot of monotonic post-cyclic shear tests on UOC samples

Considering the UC samples presented in Section 3.5.4 and adopting the values of C_c and C_s proposed from the one dimensional compression tests in Section 3.2.1 alongside the value of Λ of 0.473 determined from UOM tests, Figure 4.16 presents the corresponding curve, whereby the cyclic triaxial tests have been corrected for their apparent overconsolidation, POCR, due to cyclic loading. Whilst the trendline follows the data as a lower bound, as only two cyclic stress ratios were considered in this study it is difficult to draw conclusions from this data alone. However, considering the overconsolidated cyclic triaxial tests, as discussed above the post-cyclic overconsolidation decreases as the initial overconsolidation of the sample prior to cyclic loading increases. As such, the framework presented above is extended to consider the UOC tests discussed in Section 4.2.2. Figure 4.17 extends the trendline, showing close agreement between the post-cyclic undrained shear strength ratio from monotonic

undrained triaxial tests and the modified equation of Equation 4.16.

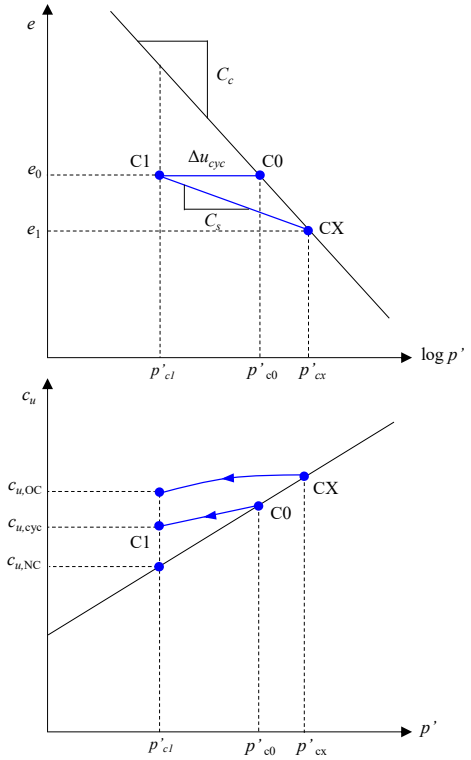

Figure 4.15: Critical state of monotonic post-cyclic shear tests on UOC samples

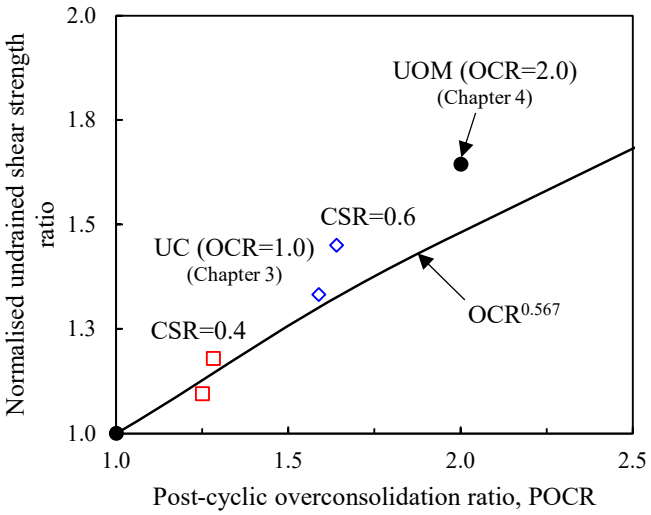

Figure 4.16: Effect of overconsolidation on normalised shear strength for UC tests

Based on Figure 4.17, it is therefore possible to determine the post-cyclic undrained shear strength of a sample knowing only the undrained monotonic

shear strength response, and therefore Λ, and the swelling and compression properties of a sample obtained from one dimensionally compression tests. In this case, a Λ value of 0.473 from overconsolidated monotonic undrained triaxial tests and a C_c of 0.40 and C_s of 0.07 such that the ratio between swelling and compression is 1.20 result in a relationship of $OCR^{0.567}$. Using this relationship requires no knowledge of the response of pore pressure during cyclic triaxial test itself in order to provide an estimation of the undrained shear strength.

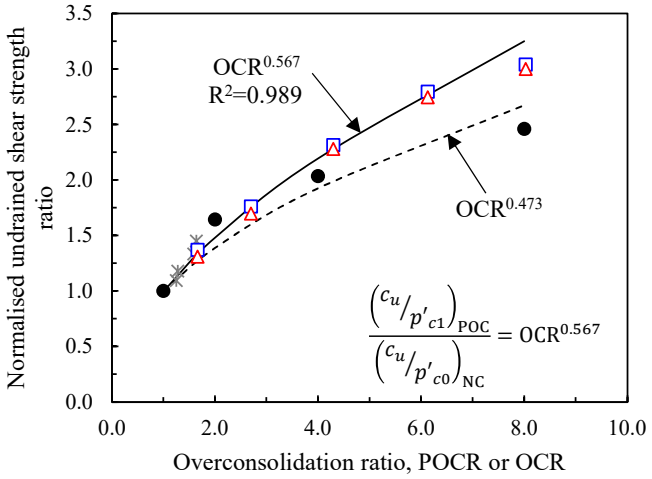

Figure 4.17: Effect of overconsolidation on normalised shear strength for UOC tests (UC tests shown in grey)

4.2.5 Economical Considerations of Preloading

In agreement with the monotonic overconsolidated tests, the greater the magnitude of historic pressure or surcharge pressure applied to the sample, the smaller the generation of axial strain for the same number of load cycles. The results of axial strain of UOC samples also demonstrate that the reduction in axial strain is greatest for low overconsonsolidation ratios. Considering stable samples with a cyclic stress ratio of 0.6 or less, the results of UOC tests show that for an incremental increase in overconsolidation, the corresponding reduction in axial strain between OCR value diminishes, therefore it is important to consider the economical effects of preloading as applying a significant surcharge load may not be optimum solution for reducing axial

strain.

The principle of surcharge applied to the samples within this study has been discussed in Section 4.2, however in practise there are two aspects to be considered when specifying a preload solution for track earthworks. In addition to the magnitude of the pressure applied to the sample, there is also an influence with respect to the duration that the preload is in place prior to removal, demonstrated in Figure 4.18. In the case of this study, $h_{surcharge}$ has effectively been varied, corresponding to p_{OC} in Figure 4.1, however in practise the aim is to apply a preload for a duration of time such that an amount of settlement, s_{target} has been reached. On the subsequent removal of this surcharge, the amount of settlement during the in service duration of an earthwork is then expected to remain within permissible design limits at $\Delta s_{inservice}$.

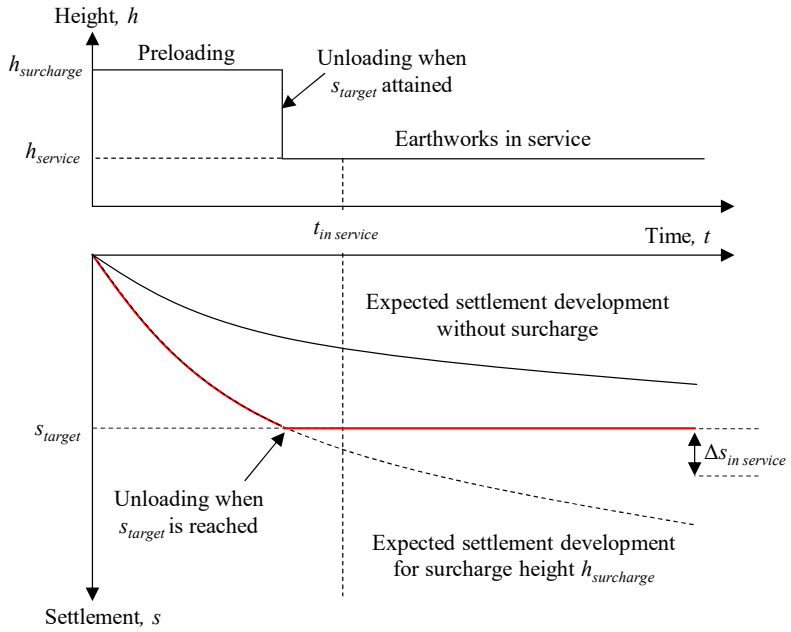

Figure 4.18: Conceptual principle of the design procedure for surcharging soft soils, reproduced after Spross and Larsson (2021)

There are therefore two commercial considerations, one of expense as a result of load magnitude and one as a result of load duration. Few studies have presented the costs associated with surcharge of soft soils, perhaps as this can

depend on a number of external factors such as transportation costs as well as being contractor dependant. However, Liu et al. (2018) presented a cost comparison between ground improvement methods considering vacuum preloading with and without surcharging for the case of dredger fill foundations. It was reported that surcharging cost 12533 yuan per 100m^2, approximately £14 per m^2 however it was unclear what height of surcharge this value corresponded to. Kim et al. (2014) undertook Monte Carlo simulation under ideal considerations of installation for both pre-fabricated vertical drain treatment and preloading. Within this stochastic analysis, the unit cost incorporated materials, labour and equipment required to undertake ground improvement. The costs, replotted to consider £ per m^2, are presented in Figure 4.19 based on treatment of coastal land reclamation in Malaysia after Chen (2004).

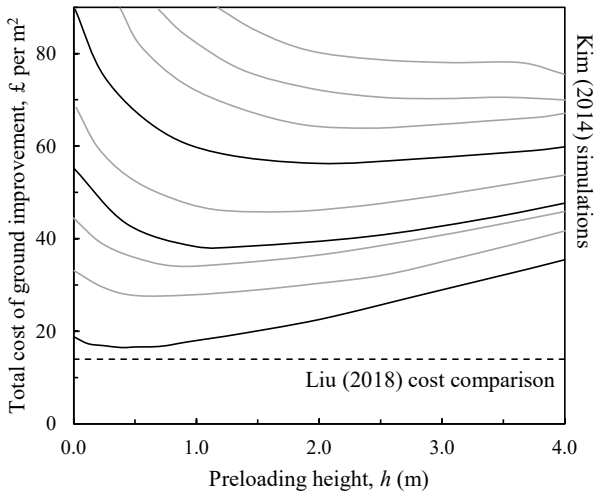

Figure 4.19: Variation of ground improvement cost (£ per m^2) with height of preloading, modified from Kim et al. (2014)

For all curves presented, the minimum cost in ground improvement is associated with a preload height of between 0.7m and 1.0m. Below this value, the cost per metre of preload is higher, most probably due to the economies involved in transportation and labour for a small preload. Beyond 1m of preload this cost increases. In the case of the overconsolidation ratios examined, the preload to achieve an OCR of 8.0 and the associated costs based on the trajectory presented in Figure 4.19 would be significant.

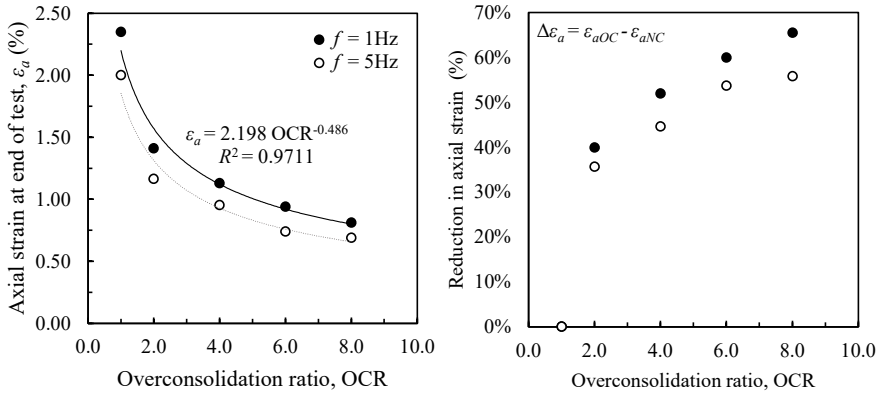

Figure 4.20: Final axial strain and percentage reduction in axial strain for variation in overconsolidation ratio

Figure 4.20 presents the reduction in axial strain achieved with respect to the progressive increase in overconsolidation ratio. The results show the greatest reduction in axial strain with respect to the axial strain that accumulates as a result of normally consolidated samples, an OCR of 1.0, is greatest for low overconsolidation ratios. As such, the cost increase associated with achieving a high OCR may not be justified for the resulting low level of additional improvement in the strain response of the kaolinite samples with a cyclic stress ratio of 0.6. Whilst in practise, significant overconsolidation at the higher end of the presented scale will generally not be achieved, the cost benefits with respect to achieving less settlement for different degrees of OCR is important to consider. Based on the results presented, preloading samples is advantageous for samples where the resulting overconsolidation ratio would be less than 2 due to the significant reduction in axial strain achieved; a reduction of 40% when compared to the strain for an OCR of 1.0.

4.2.6 Conclusions

Undrained monotonic and cyclic tests have been undertaken on overconsolidated kaolinite samples, examining the effect of preloading.

- Undrained monotonic triaxial tests were performed at a range of overconsolidation ratios. With an increase in OCR, the strength attained at

failure increased. Considering the generation of excess pore pressure, with an increase in OCR the sample begins to exhibit a dilative response, existing to the "dry" side of critical state. For the kaolinite samples, the strength rebound parameter, describing the relationship between OCR and the normalised undrained shear strength response, was shown to be 0.475.

- Cyclic undrained triaxial tests were performed demonstrating the threshold cyclic stress ratio still existed between 0.6 and 0.8 for samples with an overconsolidation ratio of upto 8.0.
- For an OCR of less than 4.0, the response of cyclic overconsolidated tests was similar to previous tests performed in Chapter 3. As the degree of overconsolidation of the sample increases, the axial strain of the sample decreases. However, as has been demonstrated for monotonic tests, negative pore pressures developed.
- The reduced axial strain developed in the sample under cyclic loading with respect to an increase in overconsolidation ratio can be explained considering the energy effects during the cyclic testing whereby the degradation index of a sample with respect to time increases.
- Considering the soil fabric, a greater reduction in voids ratio occurs when a sample attains a higher degree of overconsolidation, such that the resistance to deformation increases and the absorbed energy to achieve the same amount of strain as a normally consolidated sample increases.
- Extending the relationship between OCR and the normalised undrained shear strength response for cyclic loading, the results suggest that accounting for the unload-reload response via the coefficients determined from one-dimensional compression tests in Chapter 3.2.1, the estimation of post-cyclic strength of preloaded samples can be determined from monotonic tests alone.
- The adoption of preloading is a commercial decision whereby the benefit, or degree of improvement in subgrade performance, should be considered against the cost of achieving it. Whilst the greater the overconsolidation ratio, the greater the reduction in axial strain, an OCR of 2 provided the greatest

incremental reduction in axial strain; 40% compared to normally consolidated samples.

4.3 Soil Response due to Partial Drainage

4.3.1 Principles of Partial Drainage

The response of soils under cyclic loading conditions has been investigated by a number of authors. Sangrey et al. (1969) undertook low frequency undrained cyclic triaxial tests. More recently, Guo et al. (2013) examined the long term response of soft clays to cyclic loading. The analytical work of Hu (2010) suggested that the long term settlement of a clay subsoil subject to cyclic loading could consider the drained condition such that the soil settlement was governed by the deformation behaviour of the soil neglecting the pore pressure response. However, acknowledging the low permeability of clay soils, a number of authors have examined the long term response of cohesive soils considering partially drained conditions, whereby pore pressures are simultaneously generated and dissipated. Sakai et al. (2003)) stated this response was more representative of in situ soil behaviour, previously acknowledged by Hyodo and Yasuhara (1988) stating drainage conditions had a significant impact on the settlement response, as summarised in Section 4.3.

The response of soils under partial drainage could be considered akin to the response observed by undrained loading followed by a drainage period, presented in Figure 4.21. Yasuhara et al. (1988) proposed the change in void ratio under reconsolidation due to drainage after undrained cyclic loading, Δe_r would be equivalent to that experienced under partially drained conditions.

Sakai et al. (2003) further demonstrated that the accumulation of excess pore pressure under undrained conditions, route AB in Figure 4.22 would also be accumulated in partially drained tests, A'B', whilst also undergoing a change, Δu_c, such that the partially drained response of excess pore pressure follows

A'C and partial dissipation of total excess pore pressure Δu_d occurs. As this dissipation of Δu_d occurs over the time period Δt, volumetric strain on path DE develops, $\Delta \epsilon_v$ which is governed by the coefficient of volume compressibility of the sample.

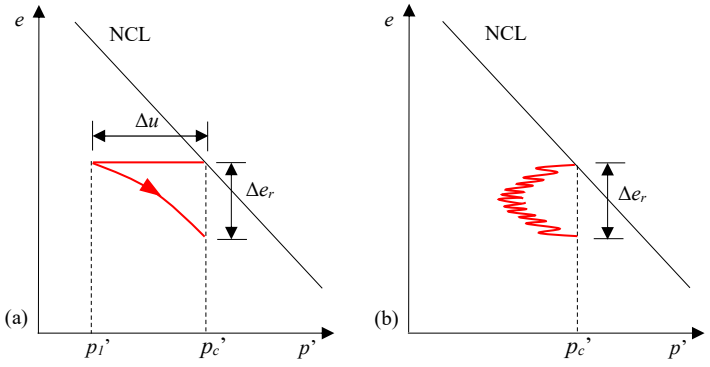

Figure 4.21: e - log p' for (a) cyclic loading followed by drainage and (b) partially drained cyclic loading, reproduced from Hyodo et al. (1992), after Yasuhara et al. (1988)

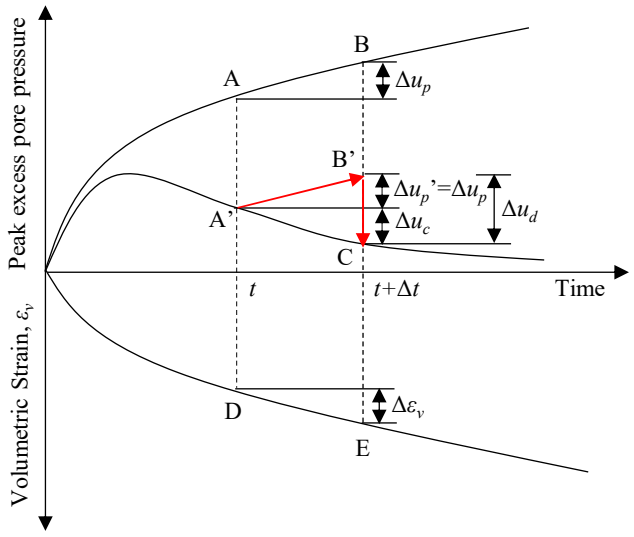

Figure 4.22: Procedure for evaluating the behaviour of soil under partially drained conditions of cyclic loading, reproduced from Sakai et al. (2003)

4.3.2 Recommendations for Partially Drained Triaxial Tests

In order to assess the partially drained response of cyclic loaded clays using the standard cyclic triaxial equipment, modifications to the standard procedure

typically adopted for undrained cyclic triaxial tests are required. Therefore, a series of recommendations are presented based on the partially drained triaxial tests that have been undertaken herein to facilitate the use of standard cyclic triaxial machines for the determination of partially drained cyclic response:

- Samples should be consolidated under the same conditions as for undrained tests, whereby the samples in the case of this study were isotropically consolidated over a period of greater than 24 hours under a load increment upto 200kPa.
- The saturation of the sample should still be checked to ensure a B check value of greater than 0.97, subsequent consolidation and the application of cyclic load, combined with the opening of the drainage lines should only be performed once the value of B has been confirmed.
- For partially drained cyclic triaxial tests, the drainage line remains open. Whilst this is a drained condition for the sample, due to the low permeability of the kaolinite samples, this generates a partially drained response under loading. When drainage is permitted vertically through the sample in this way, the boundary for drainage is horizontal. To facilitate drainage along this boundary, filter drains were applied to the circumference of the sample.
- Porous stones were soaked in de-aired water prior to commencing test assembly. The stones had an equivalent cross-section to that of the sample to facilitate drainage at the top and bottom of the sample whilst maintaining a solid support. Aluminium oxide stones were used, with a smooth surface to reduce friction at the boundary.
- Whilst pore pressure is measured during these samples, it is important to note that it is measured via the drainage lines at the base of the sample. Under partially drained conditions, the pore pressure generation throughout the sample will be uneven and as such may not be representative of the overall response of the sample. From sensitivity studies completed, filter paper drains applied to the sides of the samples improved the pore pressure response obtained for the samples, however

at high frequencies, care should be taken examining the pore pressure response due to the rapid accumulation of pore pressures in cohesive low permeability samples.

- One-way undrained stress controlled cyclic loading was studied as per the UC and UOC tests summarised in previous sections in accordance with ASTM D5311 (American Society for Testing and Materials (2004)). In the case of the tests completed, the intention is not necessarily destruction, such that the accumulation of axial strain and determination of a failed state or threshold value can be identified in accordance with determination of cyclic stability in ASTM guidelines. The same threshold limiting strain of 15% was adopted to determine failure of a sample. It should be noted had the tests been completed on sand samples, a 5% strain limit may be more applicable for consideration of liquefaction.

4.3.3 Partially Drained Cyclic Triaxial Tests

Partially drained cyclic triaxial tests have been performed on kaolinite samples, consolidated in the triaxial cell to an initial confining pressure of 200kPa, summarised in Table 4.3. The 12 samples consider the variation in cyclic stress ratio and the variation in loading frequency in order to compare the response of soil samples under different drainage conditions.

Examining the response of the partially drained tests with respect to the number of load cycles, the response of axial strain is similar to that observed during undrained loading, whereby for a sample loaded at a lower frequency, the axial strain accumulated per load cycle increases as the load frequency decreases. After the first 1000 load cycles, for cyclic stress ratios of 0.4, shown in Figure 4.23, and for 0.6, shown in Figure 4.24, the axial strain again begins to tend towards an equilibrium such that the increment in strain accumulation in subsequent cycles decreases. Similarly, there is a clear distinction in the axial strain response of samples tested with a cyclic stress ration of 0.6, samples PC_{09} to PC_{12}, where rapid accumulation to 15% strain in an upwards trajectory occurs. The results

suggest that the threshold or critical cyclic stress ratio still exists between 0.6 and 0.8.

Table 4.3: Summary of partially drained cyclic (PC) triaxial tests undertaken on kaolinite samples

Sample Name:	Frequency (Hz)	CSR	Number of Cycles	Duration (min)	Failure
PC_{01}	0.1	0.4	6000	1000	No
PC_{02}	1.0	0.4	15000	250	No
PC_{03}	2.0	0.4	30000	250	No
PC_{04}	5.0	0.4	34200	114	No
PC_{05}	0.1	0.6	6000	1000	No
PC_{06}	1.0	0.6	15000	250	No
PC_{07}	2.0	0.6	30000	250	No
PC_{08}	5.0	0.6	34200	114	No
PC_{09}	0.1	0.8	1831	305	Yes
PC_{10}	1.0	0.8	12675	211	Yes
PC_{11}	2.0	0.8	20876	174	Yes
PC_{12}	5.0	0.8	29565	99	Yes

However, the excess pore pressure response observed for tests PC_{01} to PC_{12} such that drainage is permitted during cyclic loading demonstrates an initial rapid accumulation before attaining a lower value of normalised excess pore pressure with subsequent load cycles. There is therefore a peak in excess pore pressure which defines the point at which the accumulation subsequently becomes dissipation. Whilst the drainage lines are open, it should be noted the excess pore pressure in this case does not fully dissipate. This response in normalised excess pore pressure shows a similar trend to that observed by Sakai et al. (2003) when performing tests on Ariake clay.

Subsequently, Chen et al. (2020) has schematically demonstrated this principal of excess pore pressure accumulation and dissipation with respect to partially drained conditions considering granular fill material, shown in Figure 4.26. The authors suggested, in agreement with the findings of Hyodo et al. (1992), that excess pore pressure rose until the peak value was attained and then continued,

as demonstrated by the response of the undrained tests observed so far in the analysis presented, whilst also dissipating via a parabolic response.

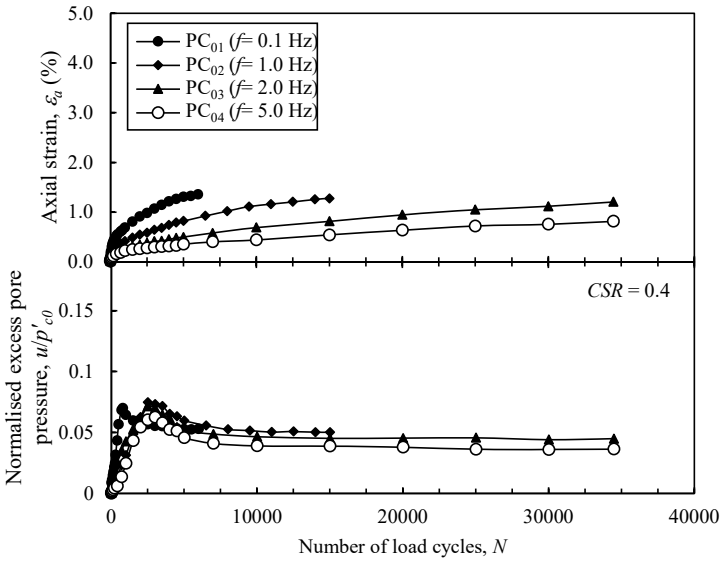

Figure 4.23: Development of axial strain and normalised excess pore pressure for partially drained tests considering the number of load cycles for a cyclic stress ratio of 0.4

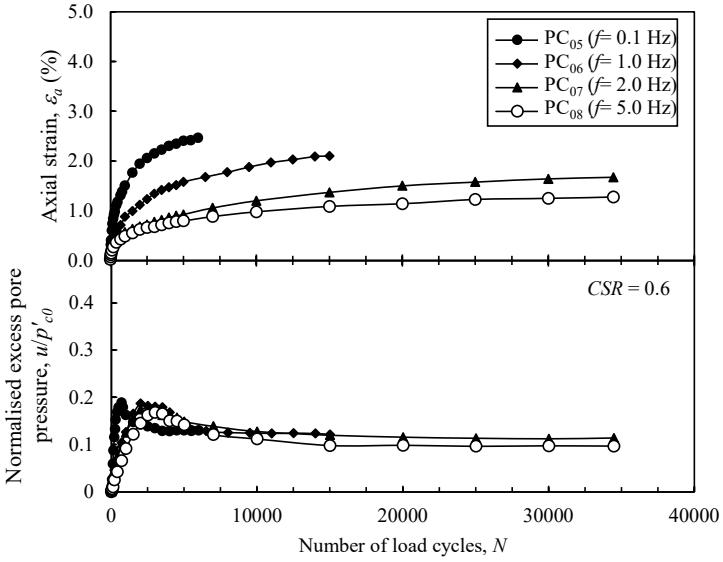

Figure 4.24: Development of axial strain and normalised excess pore pressure for partially drained tests considering the number of load cycles for a cyclic stress ratio of 0.6

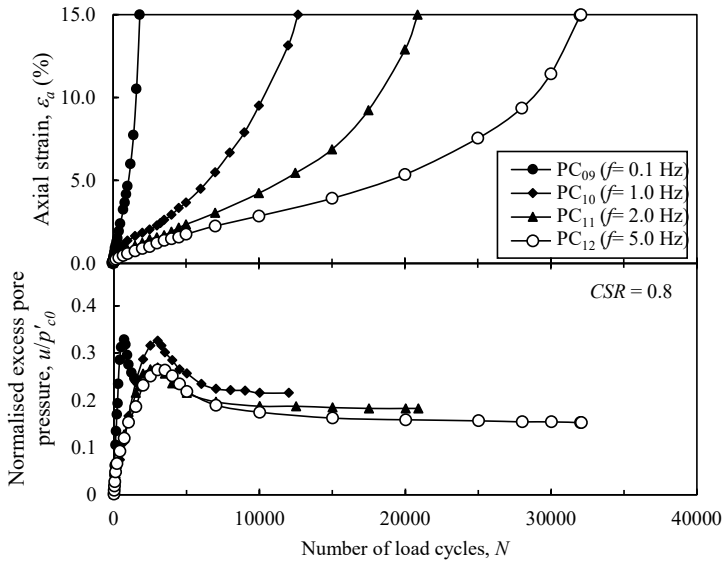

Figure 4.25: Development of axial strain and normalised excess pore pressure for partially drained tests considering the number of load cycles for a cyclic stress ratio of 0.8

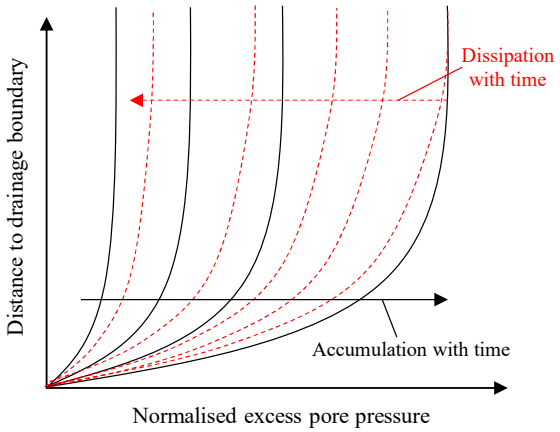

Figure 4.26: Schematic of simulataneous accumulation and dissipation of excess pore pressure under partially drained loading, after Chen et al. (2020)

4.3.3.1 Comparison with Undrained Cyclic Triaxial Tests

Whilst the response of axial strain developed in partially drained tests is similar to that observed in undrained triaxial tests, it is important to contrast the two responses given the difference in drainage conditions. The results for frequencies of 0.1Hz to 5.0Hz comparing the axial strain accumulation and normalised excess pore pressure are shown in Figure 4.27 through to Figure 4.30.

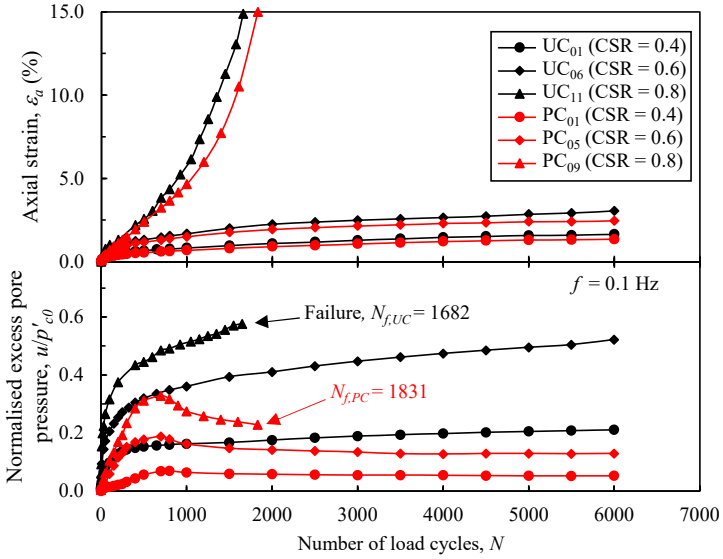

Figure 4.27: Comparing the development of axial strain and normalised excess pore pressure for undrained and partially drained tests for a frequency of 0.1Hz

Examining the accumulation of axial strain in partially drained and undrained tests, the axial strain accumulated with drainage is less than for the equivalent undrained test, irrespective of the cyclic stress ratio adopted. Furthermore, considering samples with a cyclic stress of 0.8 where failure is attained, a greater number of load cycles are achieved for partially drained tests, summarised in Table 4.4.

Examining the pore pressure response, the response with respect to partially drained tests is evident. Whilst for the first few cycles of loading, the excess pore pressure accumulation in both undrained and partially drained tests follows the same trend. Gradually, as the number of load cycles increases, the excess pore

pressure in partially drained tests begins to dissipate such that the peak attained is less than the equivalent test under undrained conditions. As established by Sakai et al. (2003) and presented in Figure 4.22, this pore pressure dissipation response is related to the developed volumetric strain, reviewed in Section 4.3.4.

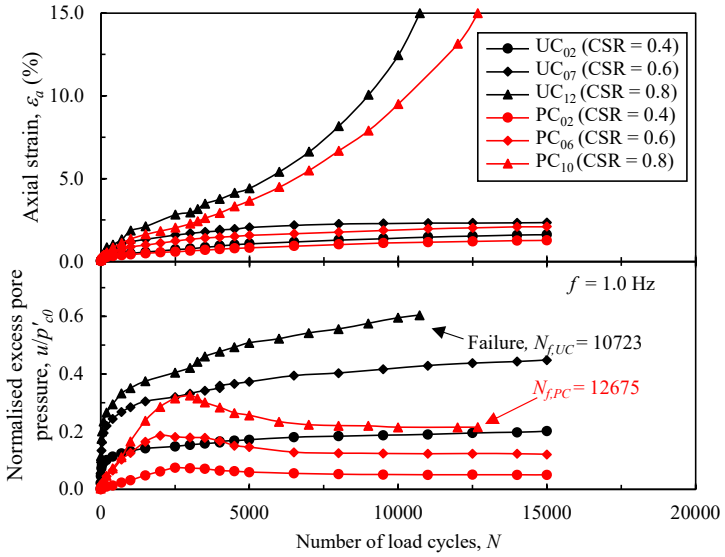

Figure 4.28: Comparing the development of axial strain and normalised excess pore pressure for undrained and partially drained tests for a frequency of 1.0Hz

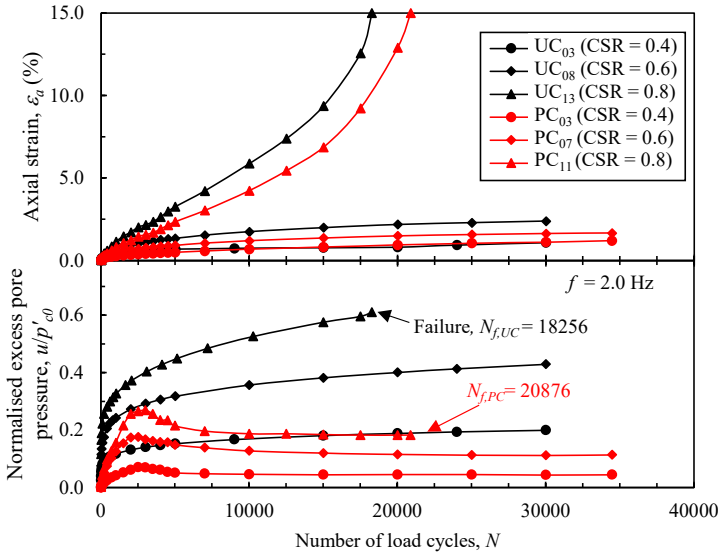

Figure 4.29: Comparing the development of axial strain and normalised excess pore pressure for undrained and partially drained tests for a frequency of 2.0Hz

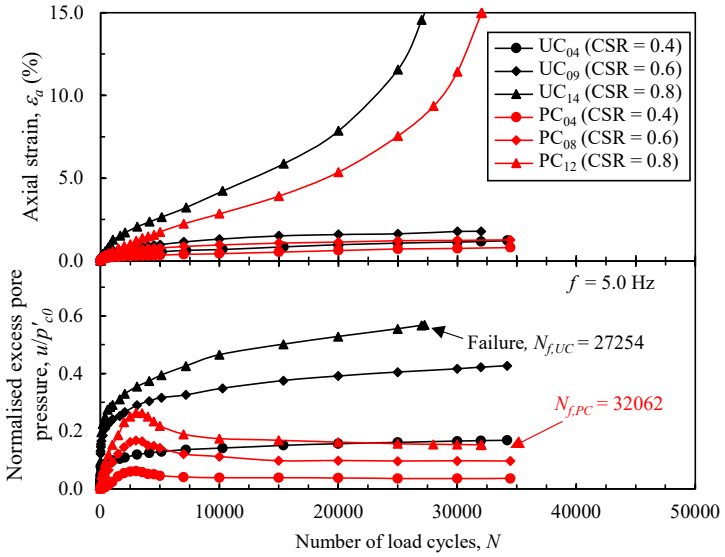

Figure 4.30: Comparing the development of axial strain and normalised excess pore pressure for undrained and partially drained tests for a frequency of 5.0Hz

Table 4.4: Summary of undrained (UC) and partially drained cyclic (PC) triaxial test, number of cycles at failure, N_f

Sample Name:	N_f	$N_{f,PC}/N_{f,UC}$
UC$_{11}$	1682	
PC$_{09}$	1831	1.11
UC$_{12}$	10723	
PC$_{10}$	12675	1.18
UC$_{13}$	18256	
PC$_{11}$	20876	1.14
UC$_{14}$	27254	
PC$_{12}$	32062	1.18

4.3.4 Examination of Pore Pressure and Volumetric Strain Accumulation

So far the examination of partially drained tests has focussed on the axial strain and normalised excess pore pressure. However, in the case of partially drained tests whereby the drainage is permitted vertically through the sample, the excess pore pressure response is coupled with the development of volumetric

strain in the sample. The response of pore pressure and volumetric strain are presented in Figures 4.31 through to 4.33 for cyclic stress ratios of 0.4 to 0.8 respectively. As the volumetric strain accumulation is related to the normalised excess pore pressure, failure in the sample with a cyclic stress ratio of 0.8 could not be determined from the volumetric strain response of the sample alone.

Sakai et al. (2003) considered the excess pore pressure dissipated in a partially drained triaxial test, u_d to comprise of two parts; the excess pore pressure generated in the equivalent undrained cyclic triaxial test u_p and the change in excess pore pressure that is observed in a partially drained test u_c, assuming that the pore pressure accumulation in undrained and partially drained tests could be considered to be equivalent, after Hyodo and Yasuhara (1988). Considering the peak normalised excess pore pressure in partially drained tests, shown in Figure 4.34 with respect to the cyclic stress ratio of the sample, similarly to the undrained tests, the increment of excess pore pressure generated in response to the load cycle, of which the cyclic stress ratio is a function, increases with increasing stress ratio. As a result therefore, shown in Figure 4.34, the volumetric strain response also increases, presented alongside the results of Sakai et al. (2003). It should be noted the cyclic stress ratio adopted in these studies was equivalent to the cyclic deviatoric strain normalised with respect to the mean effective stress of the sample, p'_{c0}, therefore the results from the partially drained tests performed in Section 4.3.3 have been corrected for this definition.

Whilst the results from Sakai et al. (2003) are for a value of K_0 of 0.5, it should be noted Thammathiwat and Chim-oye (2004) observed no influence of K_0 on the normalised excess pore pressure response.

Considering the components of normalised excess pore pressure, Table 4.5 demonstrates the response of the pore pressure, u_p, determined to be equivalent for partially drained and undrained tests, to increase with cyclic stress ratio, irrespective of the frequency of loading. A similar response can be observed with respect to u_c, showing the change in excess pore pressure is also dependent on the cyclic stress ratio applied during loading.

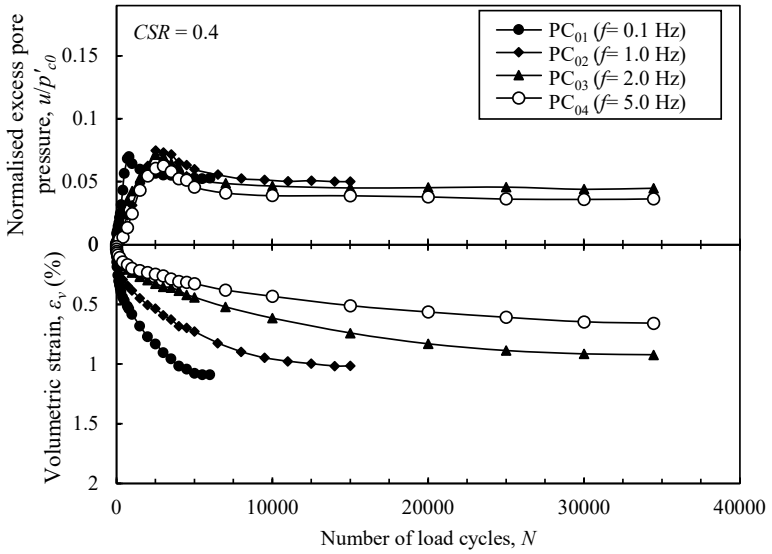

Figure 4.31: The development of normalised excess pore pressure and volumetric strain with number of cycles for a cyclic stress ratio of 0.4

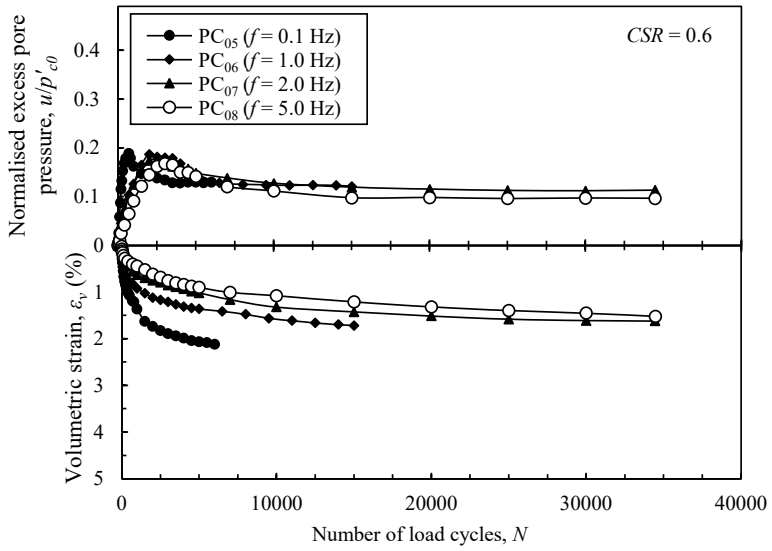

Figure 4.32: The development of normalised excess pore pressure and volumetric strain with number of cycles for a cyclic stress ratio of 0.6

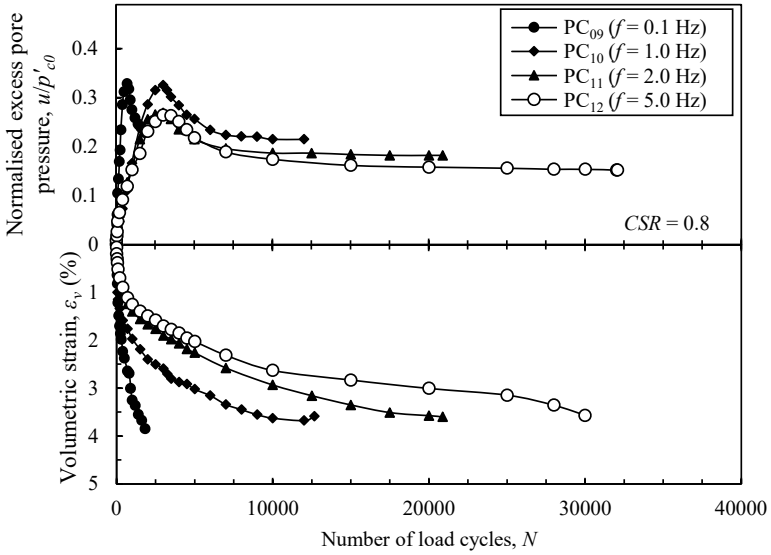

Figure 4.33: The development of normalised excess pore pressure and volumetric strain with number of cycles for a cyclic stress ratio of 0.8

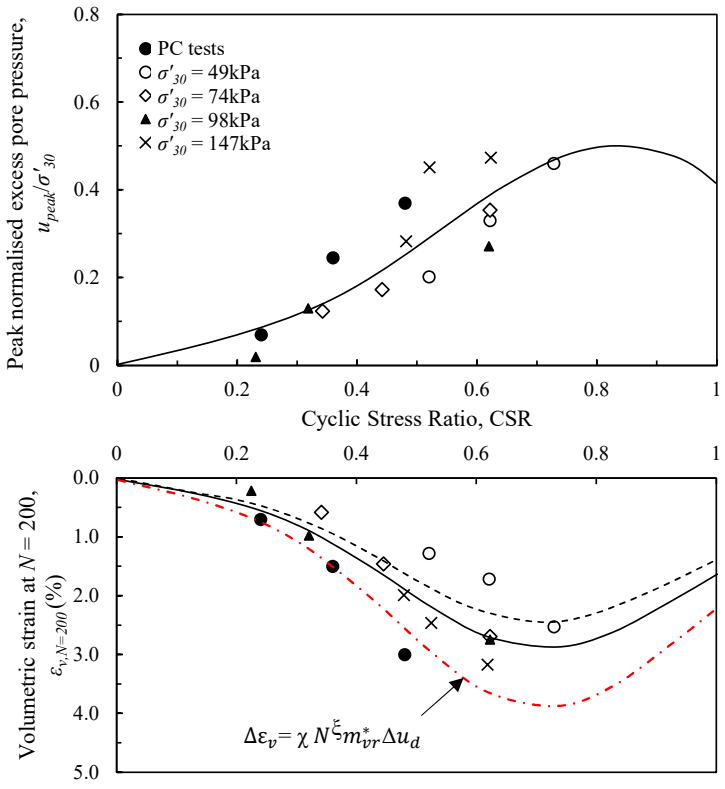

Figure 4.34: The development of normalised excess pore pressure and volumetric strain with cyclic stress ratio

Therefore, the greater the cyclic stress ratio, the greater the total excess pore pressure partially dissipated over consideration of the given interval. As identified when considering the response of undrained triaxial tests, considering the partially drained response of the sample with respect to time, the results, shown in Figure 4.35 for a CSR of 0.4 and Figure 4.36 for a CSR of 0.6 are similar.

Table 4.5: Summary of partially drained cyclic (PC) triaxial tests undertaken on kaolinite samples

f = 0.1Hz	CSR= 0.4	CSR= 0.6	CSR= 0.8	f = 1.0Hz	CSR= 0.4	CSR= 0.6	CSR= 0.8
$\Delta u_p / p'_{c0}$	0.055	0.123	0.131	$\Delta u_p / p'_{c0}$	0.053	0.128	0.183
$\Delta u_c / p'_{c0}$	0.017	0.059	0.100	$\Delta u_c / p'_{c0}$	0.025	0.065	0.110
$\Delta u_d / p'_{c0}$	0.072	0.182	0.231	$\Delta u_d / p'_{c0}$	0.078	0.194	0.292

f = 2.0Hz	CSR= 0.4	CSR= 0.6	CSR= 0.8	f = 5.0Hz	CSR= 0.4	CSR= 0.6	CSR= 0.8
$\Delta u_p / p'_{c0}$	0.068	0.137	0.207	$\Delta u_p / p'_{c0}$	0.050	0.137	0.214
$\Delta u_c / p'_{c0}$	0.027	0.062	0.087	$\Delta u_c / p'_{c0}$	0.026	0.071	0.112
$\Delta u_d / p'_{c0}$	0.095	0.199	0.294	$\Delta u_d / p'_{c0}$	0.076	0.208	0.326

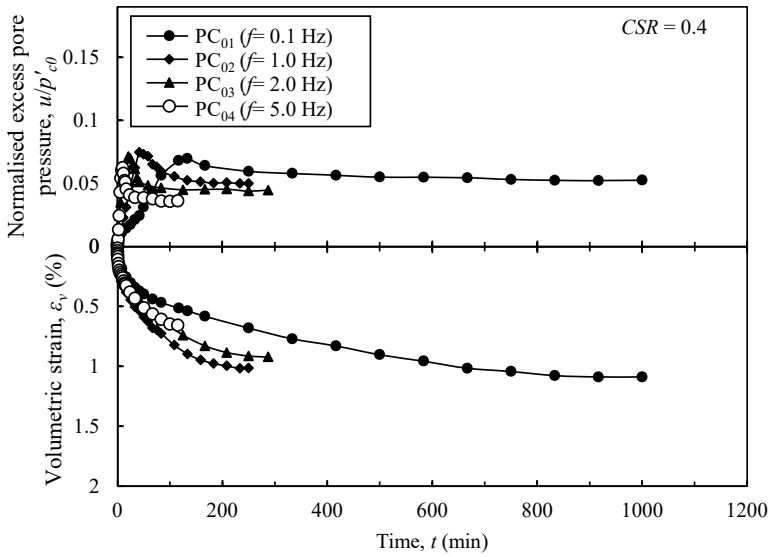

Figure 4.35: The development of normalised excess pore pressure and volumetric strain with time for a cyclic stress ratio of 0.4

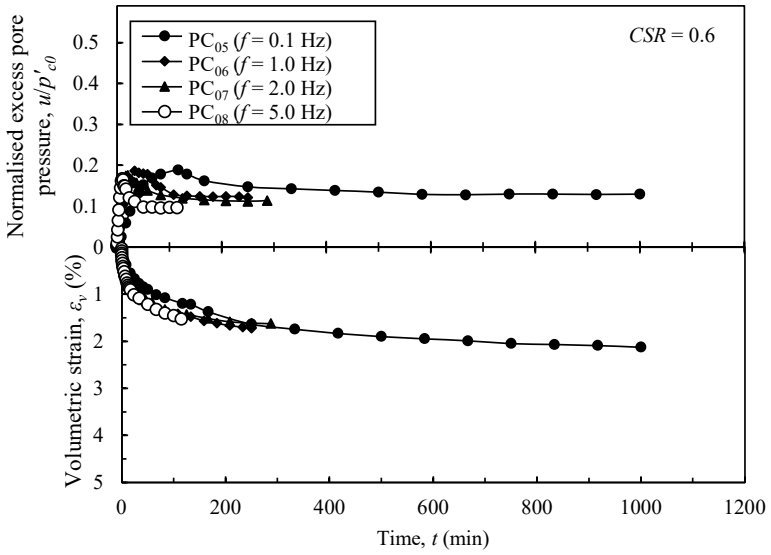

Figure 4.36: The development of normalised excess pore pressure and volumetric strain with time for a cyclic stress ratio of 0.6

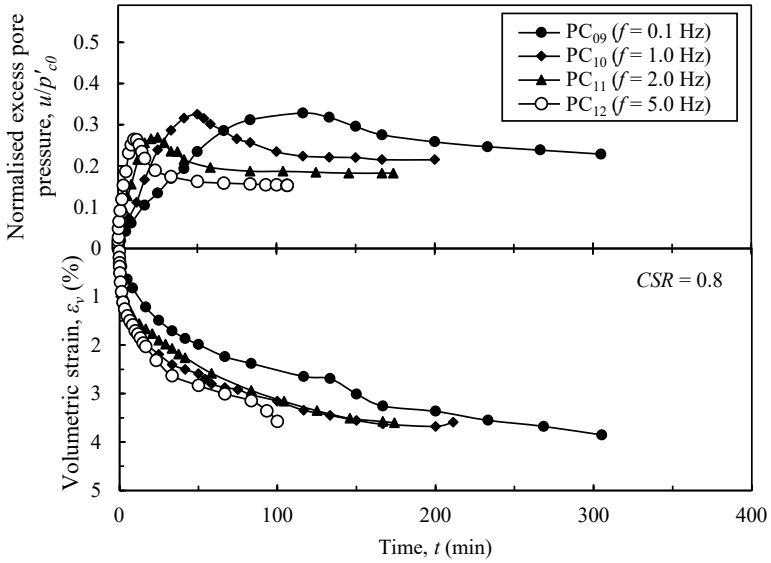

Figure 4.37: The development of normalised excess pore pressure and volumetric strain with time for a cyclic stress ratio of 0.8

It has been proposed that the change in volumetric strain accumulated under partial strain, $\Delta\epsilon_v$ can be determined as a function of the dissipated excess pore pressure, Δu_d over a given time period, Δt;

$$\Delta\epsilon_v = m_{vr}\Delta u_d = \chi N^{\xi} m^*_{vr}\Delta u_d \tag{4.17}$$

such that

$$m^*_{vr} = \frac{0.434\alpha_c c_s}{(1+e_c)\left(1-\frac{u_p}{p'_{c0}}\right)p'_{c0}} \tag{4.18}$$

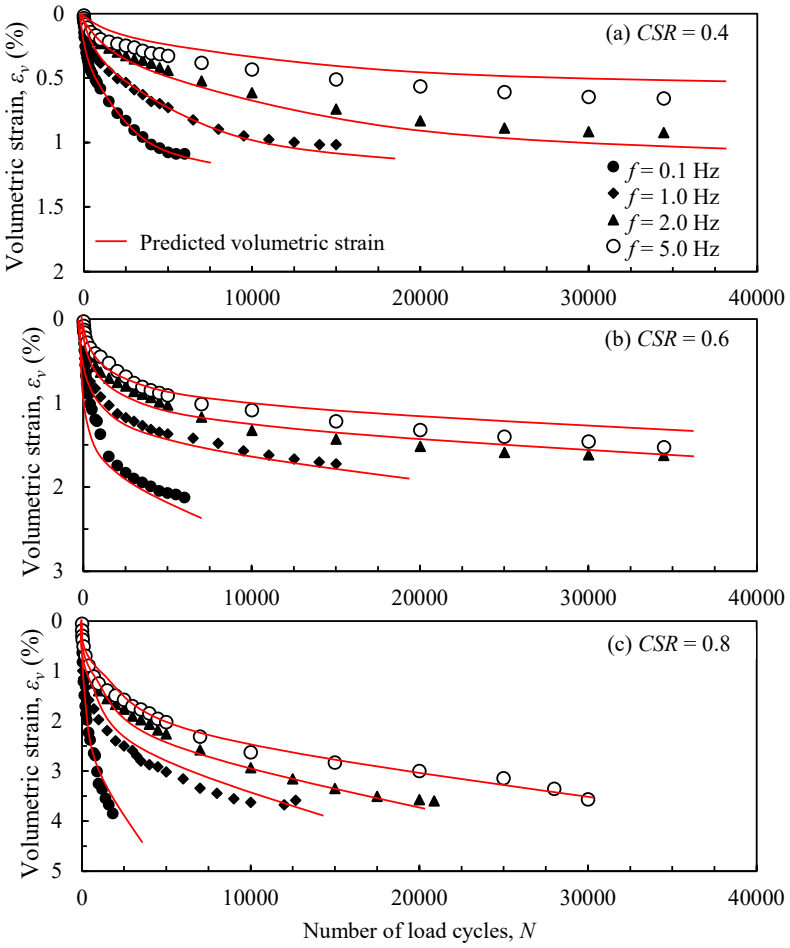

Figure 4.38: Prediction of volumetric strain accumulation using Sakai et al. (2003)

In this manner, the coefficient of compressibility can be determined for the samples, considering the swelling index obtained from the oedometer tests

presented in Section 3.2.1, C_s, the void ratio, e_c and experimental parameter, α_c. Subsequently, given χ>1.0 and ξ<0, the volumetric strain accumulation can be determined using Equation 4.17. The proposed equation shows close agreement with the results of the partially drained triaxial tests performed in this Chapter. For samples that remained stable at the end of the test duration, this response is a better prediction as due to the volumetric strain dependence on excess pore pressure response, failure of a sample cannot be determined using the equations above.

4.3.5 Consideration of Post-Cyclic Consolidation

Whilst the coefficient of volume compressibility was defined by Sakai et al. (2003) with respect to the peak excess pore pressure, u_p, it is the result of the change in volumetric strain with respect to post-cyclic pore pressures that occurs during reconsolidation. Unlike in Chapter 3, where the examination of post-cyclic recompression was performed in undrained conditions, resulting in a post-cyclic strength reduction, considering reconsolidation, drainage is permitted prior to shearing. As partially drained triaxial tests for cohesive soils are not covered within the existing commercial laboratory test framework, in this Section the results of partially drained triaxial tests are contrasted with those of undrained cyclic triaxial tests where a drainage period has been permitted prior to facilitate sample reconsolidation. The two tests were undertaken for samples with a cyclic stress ratio of 0.4 and 0.6 and a frequency of 1.0Hz.

Examining the response of undrained cyclically loaded samples, followed by reconsolidation, the change in void ratio during this recompression with respect to mean effective principal stress of the sample is presented in the semi natural logarithmic plot in Figure 4.39. Reframing this with respect to an equivalent one dimensional consolidation tests, as performed on the samples in Section 3.2.1, demonstrate the response alongside the consolidation and swelling lines previously determined.

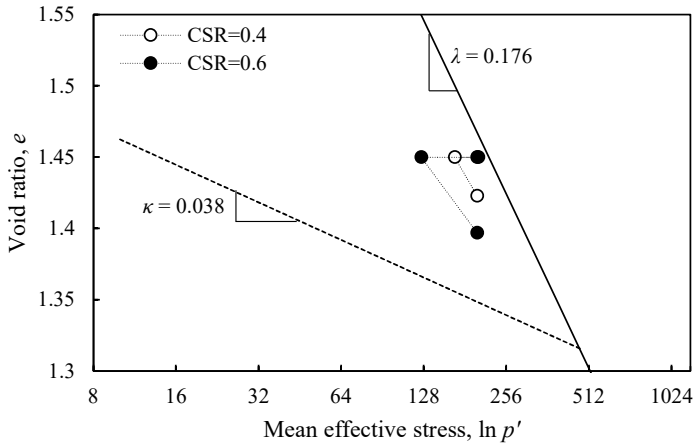

Figure 4.39: e- ln p' plot for UCR_{01} (CSR=0.4) and UCR_{02} (CSR=0.6)

The volumetric strain development with respect to post-cyclic reconsolidation that is permitted due to drainage can subsequently be determined. For a cyclic stress ratio of 0.4, the volumetric strain developed during reconsolidation can be calculated as 1.10% from Figure 4.39. Reconsolidation of the sample with a cyclic stress ratio of 0.6 resulted in a volumetric strain of 2.16%.

Extending Figure 4.39 further, Figure 4.40 presents the results of the undrained cyclic load-reconsolidation stage against those calculated from the equivalent partially drained test, with the same frequency of 1.0Hz and cyclic stress ratio of 0.4 and 0.6. The response observed is similar to that theoretically proposed by Yasuhara et al. (1982). As such, considering the partially drained response of a soil in practical terms for universal application, the test could be replicated by an undrained cyclic load test for the same duration, followed by reconsolidation of the sample.

To calculate the development of volumetric strain, the response can be determined considering $\Delta p'$ to be equivalent to Δu. This has determined for undrained cyclic triaxial tests presented in Chapter 3 using Equation 3.19, repeated below for convenience, where a and b are presented in Figure 3.47 for a cyclic stress ratio of 0.4 and 0.6. Adopting $\lambda = 0.176$ and $\kappa = 0.038$, Equation 4.20 presented the theoretical determination of volumetric strain. Table 4.6 summarises the volumetric strain determined from both undrained and partially drained triaxial tests alongside the empirical prediction based on

equations 4.19 and 4.19.

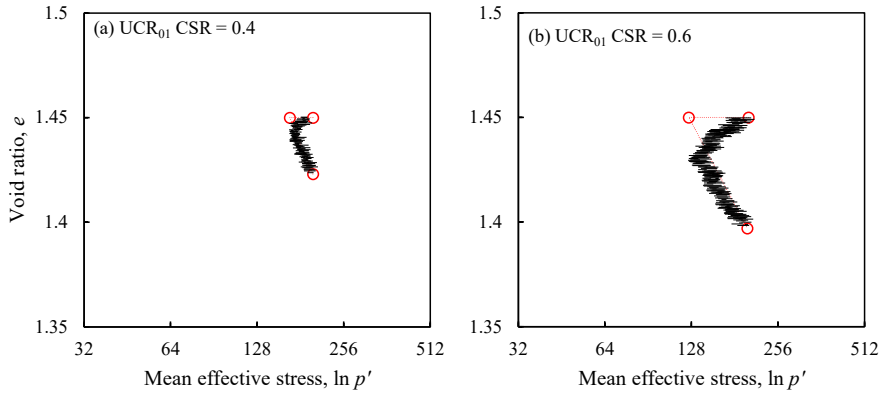

Figure 4.40: Comparison between post-cyclic reconsolidation of undrained tests and partially drained triaxial results

$$\frac{u}{p'_{c0}} = \frac{a}{\beta+1}(N^{\beta+1}-1)+a \tag{4.19}$$

$$\Delta\epsilon_v = \frac{\lambda-\kappa}{1+e}\frac{\Delta p'}{p'_0} \tag{4.20}$$

Table 4.6: Summary of post-cyclic undrained shear triaxial tests undertaken on kaolinite samples

Sample	CSR	Volumetric strain, ϵ_v		
		Partially Drained Test	Undrained Test	Empirical Equation
UCR_{01}	0.4	1.08%	1.10%	0.96%
UCR_{02}	0.6	2.12%	2.16%	2.14%
-	0.8	3.81%	-	3.78%

Determination of the volumetric strain developed in a partially drained test is shown to be comparable to both that obtained via post-cyclic reconsolidation of an undrained cyclic test, permitting drainage. This only applies therefore for a cyclic test with a cyclic stress ratio less than the critical cyclic stress ratio. However, considering the empirical relationship with respect to the normalised excess pore pressure developed in an undrained cyclic triaxial test, the volumetric strain developed in a test with a cyclic stress ratio of 0.8 can also be determined showing good agreement with the partially drained equivalent test.

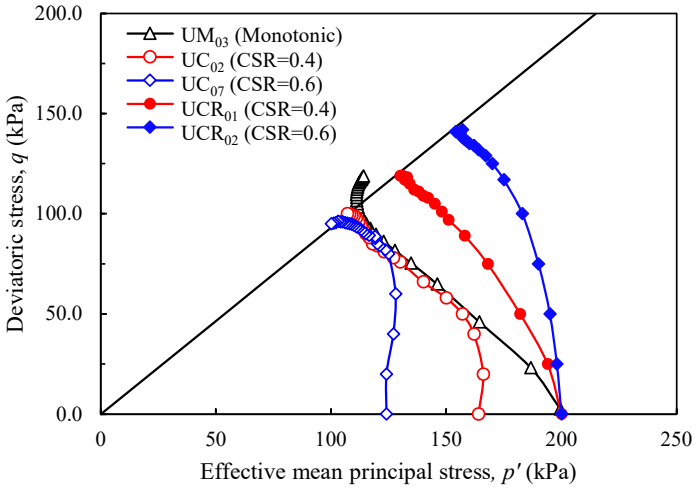

Figure 4.41: Post-cyclic undrained shear strength of kaolin samples, with and without reconsolidation due to drainage

Subsequently shearing the reconsolidated samples, the post-cyclic strength of UCR samples has been compared against the monotonic test and the equivalent undrained cyclic tests followed by undrained shearing. Samples for which drained reconsolidation was permitted prior to shearing attained a greater undrained shear strength compared to the cyclic and static tests presented in Chapter 3, predominately due to the change in void ratio that occurs in the sample during drainage. For a cyclic stress ratio of 0.4, the undrained shear strength attained was approximately 68kPa, whilst for a ratio of 0.6, this strength rose to 71kPa. As a result, it can be considered that where drainage is permitted over the lifetime of a traffic system, cyclic loading could be beneficial to the overall strength of the subgrade system, provided the reconsolidation period is great enough for the sample to stabilise in this stage.

4.3.6 Conclusions

Partially drained cyclic triaxial tests, examining the simultaneous accumulation and dissipation of excess pore pressures, have been examined. These tests are considered to be representative of in-situ conditions beneath slab track.

- Partially drained conditions have been shown to be representative of the in-situ conditions for a soil element under traffic loading by a number of

authors. A series of recommendations for performing partially drained triaxial tests have been presented.

- Whilst the response in axial strain is similar to that observed in undrained cyclic tests, the excess pore pressure response showed an initial rapid accumulation to a peak value before some dissipation occurred. Partially drained samples also demonstrated a threshold cyclic stress ratio between 0.6 and 0.8, although a greater number of cycles were attained prior to failure when compared to undrained cyclic tests.

- The volumetric strain response for partially drained tests was examined, showing the result was independent of frequency and increased with respect to cyclic stress ratio due to the greater response of excess pore pressure under applied load.

- Considering the model for the accumulation of volumetric strain proposed by Sakai et al. (2003), the results of the partially drained tests performed on kaolinite samples demonstrated a good fit with the prediction.

- The response of partially drained tests observed in this Chapter can instead be demonstrated by an undrained cyclic triaxial test followed by a period of reconsolidation of the sample, permitting drainage. The results of these tests demonstrated close agreement with respect to the volumetric strain developed. Similarly, the response of volumetric strain can be determined empirically considering the swelling and compression indices obtained from one-dimensional compression tests and the excess pore pressure response of undrained cyclic tests.

- The post-cyclic strength of the samples, whereby undrained cyclic loading was performed followed by a period of reconsolidation, was greater than the equivalent static triaxial test and post-cyclic test response without drainage. This strength increase can be attributed to the decrease in void ratio permitted during reconsolidation of the sample.

- In practical terms therefore, for application in industry, the consideration of partially drained tests could instead be achieved by adopting a period of

undrained cyclic loading followed by a period of drainage which exhibited similar results.

Chapter 5

A Proposed Model for Cyclic Traffic Loading of Clay Soils

5.1 Introduction

Chapters 3 and 4 presented the long-term cyclic response of kaolinite soil under confinement conditions representative of subgrade slab track formation. The results of partially drained triaxial tests, and undrained triaxial tests with a drainage period, demonstrated that when considering traffic loading, the accumulation of axial strain determined from assessing a purely undrained loading response may be overestimated. This could result in over-conservative design solutions and expensive settlement mitigation methods proposed on regions that, upon consideration of partial drained conditions, satisfy settlement requirements. Chapter 5 presents a proposed model for analysing the respond of cyclic loading, specifically in the case of traffic loading where the consideration of partially drained conditions can be applied.

As demonstrated in Chapter 2, a number of authors have considered the numerical implementation of cyclic loading of soils examining both stress and strain controlled behaviour. Typically, the number of parameters that are required for such models are significant and require complex derivations that

cannot be done using standard laboratory tests. This makes their application to industry practise and the subsequent consideration for rail track performance limited. It is therefore advantageous to consider a cyclic loading model for which the number of additional parameters to describe the cyclic loading and drainage condition of the soil is low and where these can be determined from typical soil characterisation and compression tests. Ni (2012) considered the model originally developed by Carter et al. (1982) that considered cyclic loading of soft clay soils within the framework of the modified Cam-Clay model. The inclusion of two additional parameters to describe the cyclic degradation of the soil integrated the frequency of loading into the Cam-Clay framework and provided a good agreement with isotropic and anisotropic cyclic undrained triaxial tests that had been undertaken.

A proposed cyclic model based on the framework developed by Carter et al. (1982) and expanded by Ni (2012) is presented, incorporating the analysis of preloaded soils and introducing the development of volumetric strain and pore pressure development under partially drained conditions.

5.2 The Modified Cam-Clay Cyclic Framework

5.2.1 A Summary of Modified Cam-Clay (MCC)

In the framework of the Modified Cam-Clay model under monotonic loading, as presented for the consideration of one-dimensional compression tests and monotonic triaxial tests in Chapter 3, at the application of load initially, the sample will compress along the virgin consolidation line. Under drained conditions, when the sample is subsequently unloaded, the soil will follow the unload-reload line, characterised by the gradient defined with a rebound parameter, κ. As discussed in Section 3.2.1, when the sample is subsequently reloaded, the soil will follow the unload reload path back to point B, presented below in Figure 5.1, whereby provided the stress applied to the sample remains less than p'_B the sample will continue to move along this path of gradient κ. If

the load applied to the sample exceeds p'_B, the soil will move back along the virgin compression line to point E, where should unloading subsequently occur, it will follow a new path of the same unload-reload gradient as the original path, however with a different specific-volume response to mean stress.

Again, as presented in Section 4.2, considering samples that have been preloaded, this response is also captured in this framework, whereby if during ground load improvement the application of load, p'_E, is considered, upon removal of surcharge the soil sample then commences its response to subsequent load application from point p'_F and has a smaller change in specific volume from change in mean stress provided the applied load remains less than p'_E. In this way, the volume change resulting from an increment of mean stress for a normally consolidated soil (Equation 5.1) and for an overconsolidated, or reloaded soil (Equation 5.2) can be defined;

$$v = N - \lambda \ln p' \tag{5.1}$$

$$v = v_C - \kappa \ln p' \tag{5.2}$$

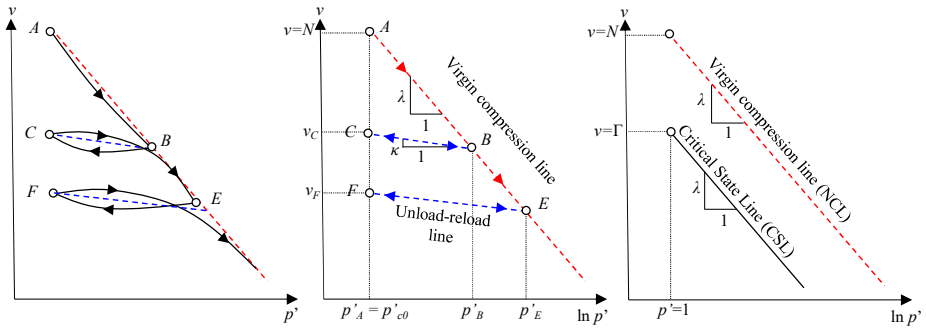

Figure 5.1: Presentation of critical state concept

As demonstrated by the UM and UOM tests undertaken, the samples eventually attain a stress level for which strain progressively continues to develop with no further change in stress, or volume of the sample. The progressive shearing of the sample is characterised by the critical state line, CSL, of a sample that has the same gradient as that of the normal consolidation line, NCL, shown in

Figure 5.1. The critical state line can be defined by;

$$v_f = \Gamma - \lambda \ln p' \tag{5.3}$$

where the specific volume at unit pressure, Γ, can be used to determine the specific volume at failure v_f. The relationship with respect to the deviatoric, or shear, stress at failure for a mean effective stress p', can therefore be described as per Equation 5.4 defined as the yield function;

$$f(q, p') = q^2 + M^2 p'(p' - p'_c) \tag{5.4}$$

The yield surface exists whereby f=0 to produce an ellipse in q-p' space. At this state, plastic deformation governed by the associated flow rule above takes place. p'_c is defined as the consolidation stress, also demonstrated by the intersection between the mean effective stress, p' and the elliptical cap, shown in Figure 5.2 such that it acts as a hardening parameter. M for triaxial compression tests can be written;

$$M = \frac{6 \sin \phi}{(3 - \sin \phi)} \tag{5.5}$$

In this way, the yield function parameter is defined as a function of p'_c, defined as a in Figure 5.2, whereby in the case of the modified Cam-Clay model, the cap shape factor, α=1;

$$a = \frac{\alpha}{1 + \alpha} p'_c = \frac{1}{2} p'_c \tag{5.6}$$

Further to the critical state yield surface, an infinite number of surfaces exist defined by a value of p'_y, representing loading surfaces and intermediate stress states throughout the loading process. Each loading surface presented in Figure 5.2 can therefore be defined;

$$p'_y = p' + \left(\frac{q}{M}\right)^2 \frac{1}{p'} \tag{5.7}$$

When the soil is loaded, based on the reference to the initial yield surface in Figure 5.2, the following conditions therefore apply;

- When $dp'_y = dp'_c > 0$, hardening occurs (on the "wet side" of critical or sub-critical behaviour)
- When $dp'_y = dp'_c < 0$, softening occurs (on the "dry side" of critical or super-critical behaviour)

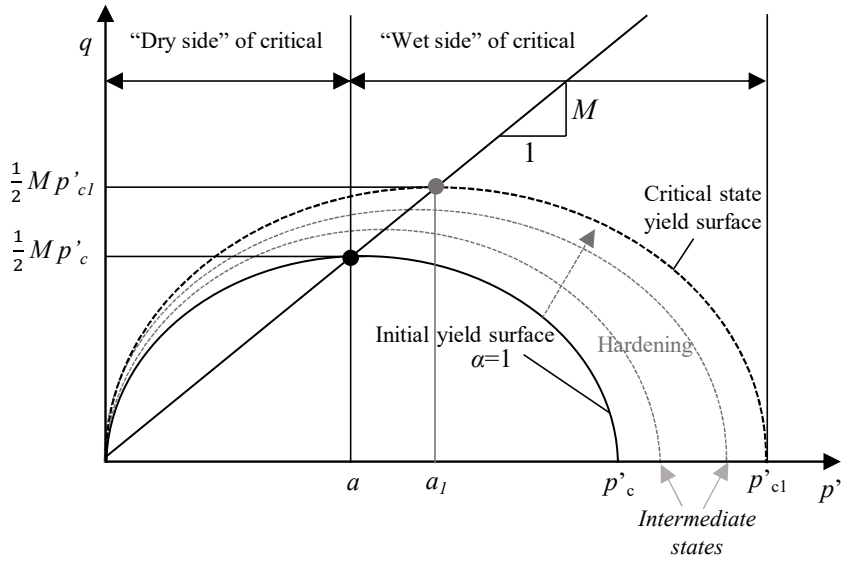

Figure 5.2: Determination of super and sub-critical soil response

And the yield locus during plastic deformation varies in accordance with;

$$\frac{dp'_c}{p'_c} = \frac{dp'_y}{p'_y} \tag{5.8}$$

Elastic Stress-Strain Relationship

When the stress state is elastic within this range, the following incremental relationship applies considering the elastic volumetric and shear strains, ϵ^e_v and ϵ^e_s respectively;

$$\begin{Bmatrix} dp' \\ dq \end{Bmatrix} = \begin{Bmatrix} K & 0 \\ 0 & 3G \end{Bmatrix} \begin{Bmatrix} d\epsilon^e_v \\ d\epsilon^e_s \end{Bmatrix} \tag{5.9}$$

G defines the shear modulus of the soil, provided as an input to the solution

whilst K defines the bulk modulus of the soil;

$$K = \frac{(1+e)\,p'}{\kappa} \tag{5.10}$$

Plastic Stress-Strain Relationship

When the stress state is plastic, as identified in Equation 5.8, the yield position changes. The permanent incremental volumetric strain, ϵ_v^p can be written;

$$d\epsilon_v^p = \left(\frac{\lambda-\kappa}{1+e}\right)\frac{dp'_c}{p'_c} \tag{5.11}$$

whilst the incremental permanent stress strain response is defined;

$$\begin{Bmatrix} d\epsilon_v^p \\ d\epsilon_s^p \end{Bmatrix} = \begin{Bmatrix} C_{11} & C_{12} \\ C_{21} & C_{22} \end{Bmatrix} \begin{Bmatrix} dp' \\ dq \end{Bmatrix} \tag{5.12}$$

$$C_{11} = \left(\frac{\lambda-\kappa}{1+e}\right)\frac{a}{p'} + \left(\frac{\kappa}{1+e}\right)\frac{1}{p'} \tag{5.13}$$

$$C_{12} = C_{21} = \left(\frac{\lambda-\kappa}{1+e}\right)\left(\frac{1-a}{p'}\right) \tag{5.14}$$

$$C_{22} = \left(\frac{\lambda-\kappa}{1+e}\right)\frac{b}{p'} + \frac{1}{3G} \tag{5.15}$$

And a, b can be written in terms of the frictional value of stress ratio at critical state M and stress ratio η;

$$a = \frac{M^2-\eta^2}{M^4+\eta^4} \tag{5.16}$$

$$b = \frac{4\eta^4}{M^4-\eta^4} \tag{5.17}$$

$$\eta = \frac{q}{p'} \tag{5.18}$$

5.2.2 Extension to Cyclic Loading

As demonstrated from Chapter 3 considering the comparison between monotonic and cyclic triaxial tests under the same initial conditions, the accumulation of axial strain occurs over the whole loading process, but with initial development being greater for a smaller number of cycles. The form of Equation 5.8 in its' current form would mean only permanent strain and pore pressures are determined during the initial load cycle, such that subsequent cycles would not be able to a generate permanent excess pore pressure and strain response as observed in the triaxial tests. For the consideration of cyclic loading, Equation 5.8 is modified such that for elastic unloading, ϑ is introduced after Carter et al. (1982). This inclusion modifies the function of the yield surface, maintaining the same elliptical shape whilst reducing the size of the ellipse in response to elastic unloading, such that the loading surface, p'_y is within p'_c and reducing.

$$\frac{dp'_c}{p'_c} = \vartheta \frac{dp'_y}{p'_y} \tag{5.19}$$

When cyclic degradation parameter $\vartheta = 0$, this therefore reverts back to the original Modified Cam-clay model. At a value of 1.0, the yield surface would contract. Typically, the value of ϑ is small such that only a small contraction in yield surface occurs, whereby Ni (2012) proposed ϑ decreases with an increased number of load cycles, defined as;

$$\vartheta = \frac{1}{\xi_1 N + \xi_2} \tag{5.20}$$

where ξ_1 and ξ_2 are experimental constants.

The introduction of the cyclic degradation parameter bu Ni (2012) results in a changing yield surface whereby during each load cycle, the stress path follows the pattern shown in Figure 5.3, exhibiting an increase in excess pore pressure accumulation and decrease in effective stress of the sample that reaches load surface at point A, at a value of q equivalent to q_{cyc} in the cyclic triaxial tests performed in Chapters 3 and 4. Upon unloading of the sample during the load

cycle, the effective mean stress attained during the load stage, $A*$, subsequently remains constant with the removal of $q_c yc$, resulting in a new value of p', $p'_{y,A}$ from which the next load cycle commences. This results in a change to the yield surface, defined as per Equation 5.19, rewritten in Equation 5.21

$$p'_{cU,A} = p'_{cL,A} \frac{p'_{y,A}}{p'_{cL,A}}^{\vartheta} \tag{5.21}$$

Upon reloading, the stress state follows the same original path of unload-reload, behaving elastically for a value of q less than the yield surface intersection to point B' for $p'_{cU,A}$. At a value of deviator stress greater than this, the stress state is plastic and the effective stress of the soil again decreases, to point B on yield surface $p'_{cL,B}$. This value of deviator stress is defined;

$$q_{B'} = \sqrt{(p'_{cU,A} - p'_{y,A}) M^2 p'_{y,A}} \tag{5.22}$$

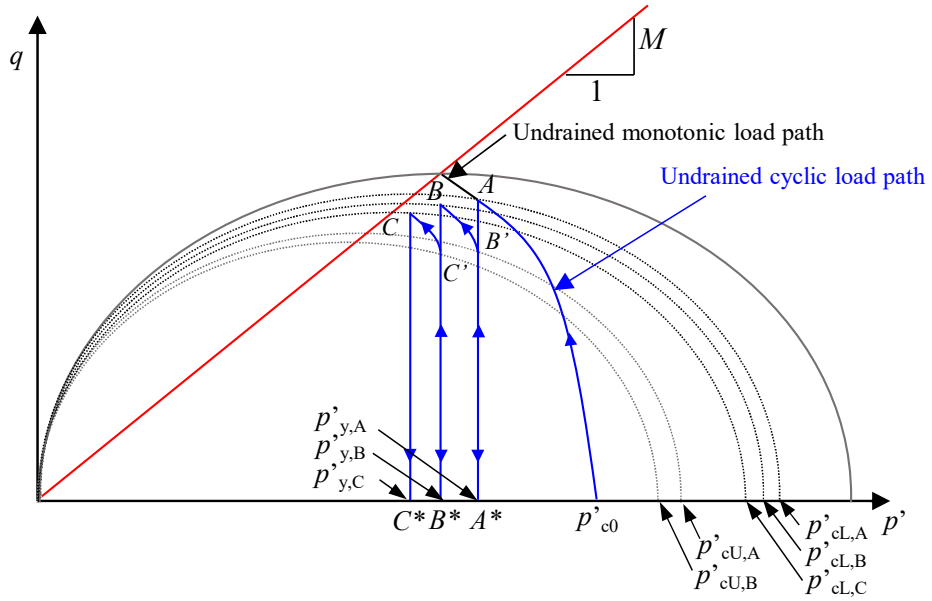

Figure 5.3: Framework of undrained cyclic load model, after Ni (2012)

5.3 Application to Cyclic Triaxial Tests

Reviewing the cyclic model with respect to the undrained cyclic triaxial tests performed in Chapter 3.5, the following input parameters for the soil properties and initial states are proposed.

Table 5.1: Summary of UC test parameters for undrained cyclic model

p'_0	p'_{c0}	q'_0	e_0	λ	κ	M
200kPa	200kPa	0kPa	1.434	0.174	0.030	0.93

Table 5.2: Summary of UC test parameters for undrained cyclic model

Frequency, f	Samples	ξ_1	ξ_2
0.1Hz	UC_{01}, UC_{06}, UC_{11}	2.7	75
1.0Hz	UC_{02}, UC_{07}, UC_{12}	2.8	275
2.0Hz	UC_{03}, UC_{08}, UC_{13}	2.7	385
5.0Hz	UC_{04}, UC_{09}, UC_{14}	2.9	540
7.0Hz	UC_{05}, UC_{10}, UC_{15}	2.8	630

The results presented in Figures 5.4 to 5.8 show the response of the existing undrained cyclic model developed by Ni (2012). The prediction captures the undrained response of cyclic loaded samples with a cyclic stress ratio less than the critical value well. In terms of failed samples, the number of cycles of load prior to failure is predicted however the trend in accumulation given by the model is much more abrupt than observed in the laboratory tests.

With respect to degradation parameter ξ_1, the value is related to the soil properties. As such, these kaolin samples have a similar value of approximately 2.9 to those tests performed by Ni (2012). The degradation parameter ξ_2 is instead dependent on the cyclic stress ratio and frequency during cyclic triaxial testing, such that for a given cyclic stress ratio, as $1/\xi_2$ increases the number of cycles to failure increases. For a constant value of $1/\xi_2$ presented in the model developed by Ni (2012), the number of cycles to failure decreases as the cyclic stress ratio increases.

As such, the difference in response observed between the tests performed in this study to those analysed previously is a result of the confining pressure and therefore the stress state at commencement of cyclic loading.

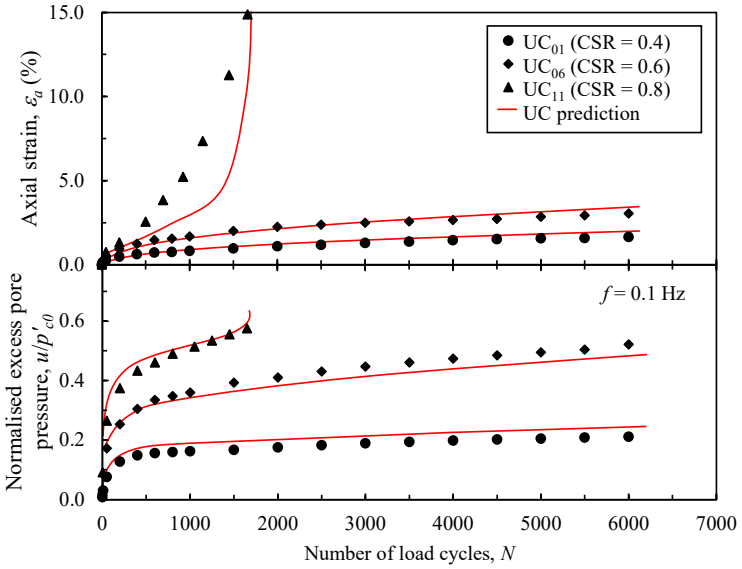

Figure 5.4: Undrained cyclic model prediction for f=0.1Hz

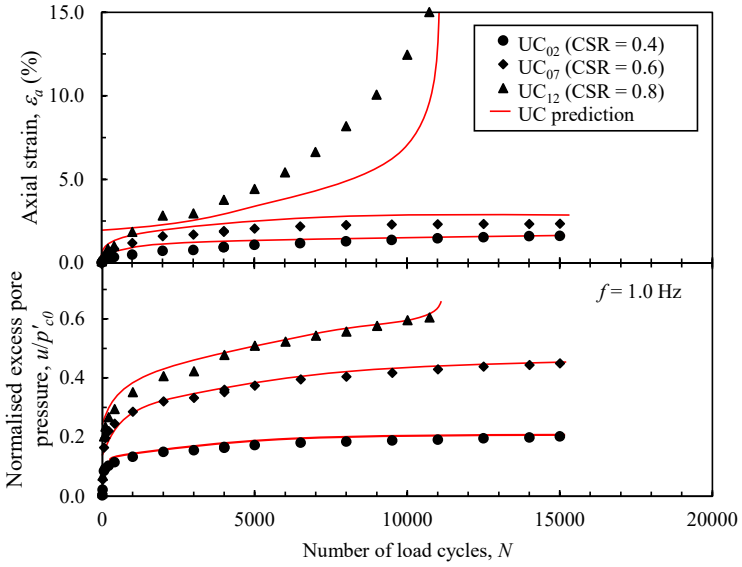

Figure 5.5: Undrained cyclic model prediction for f=1.0Hz

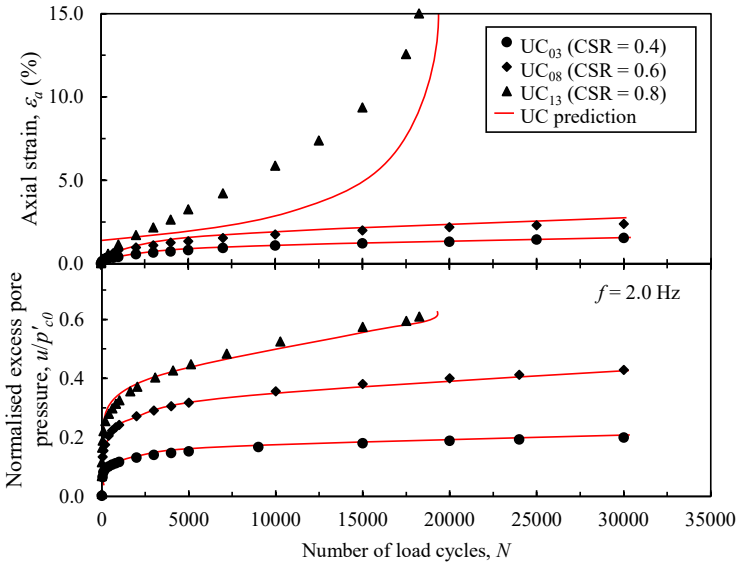

Figure 5.6: Undrained cyclic model prediction for f=2.0Hz

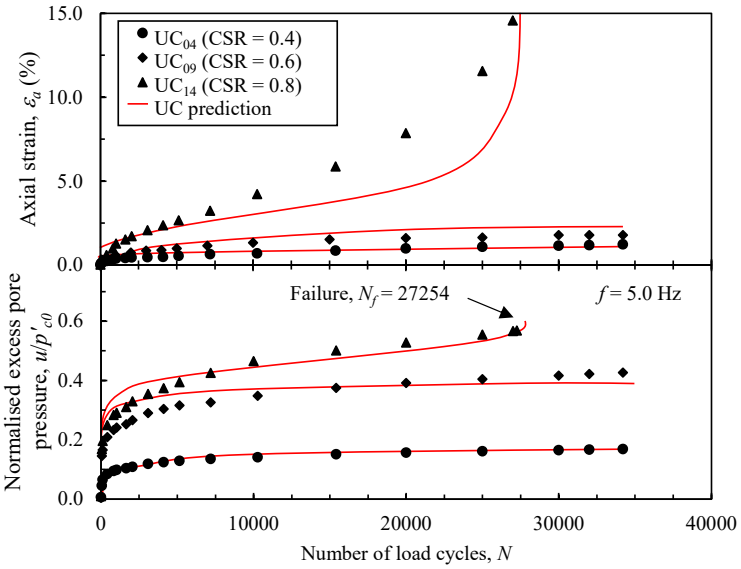

Figure 5.7: Undrained cyclic model prediction for f=5.0Hz

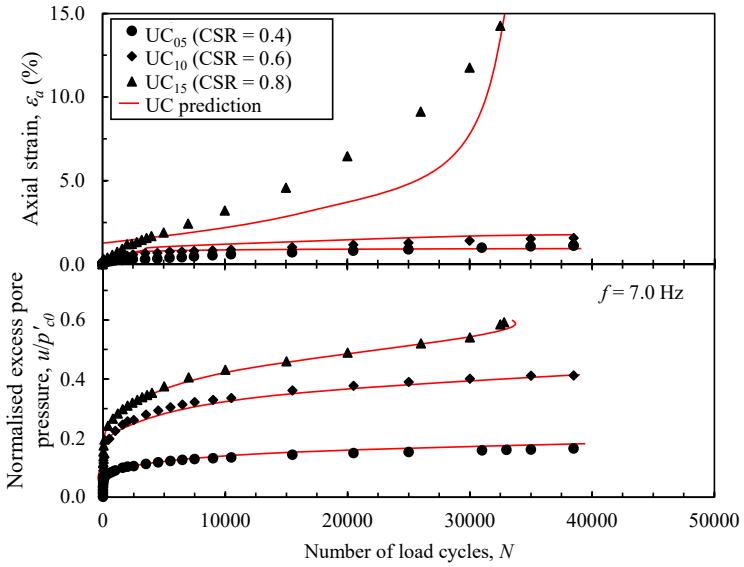

Figure 5.8: Undrained cyclic model prediction for f=7.0Hz

Several authors including Guo et al. (2013) have demonstrated a greater accumulation of axial strain and increase in excess pore pressure in response to cyclic loading as a result of increased confining pressure in the tests. This influence can further be examined, extending the undrained cyclic predictions to consider the preloaded samples that were subject to undrained cyclic loading in Chapter 4.2.2. The results of the model prediction are presented in Figure 5.9 and Figure 5.10. The model predicts lightly overconsolidated to moderately consolidated samples well. Beyond an OCR of 6, the prediction deviates from the results of the laboratory testing.

Considering the Modified Cam-Clay yield function, when the stress ratio q/p is less than M, the plastic strain response described by the model will be contractive. At high values of OCR, this is not the response observed in the laboratory tests where dilation instead begins to occur. This response is coupled with the generation of negative excess pore water pressures. As a result the model underpredicts this response. However, given the likely range of overconsolidation that would be achieved with preloading, as discussed in Chapter 4.2, the model characterises well the response of treated formations.

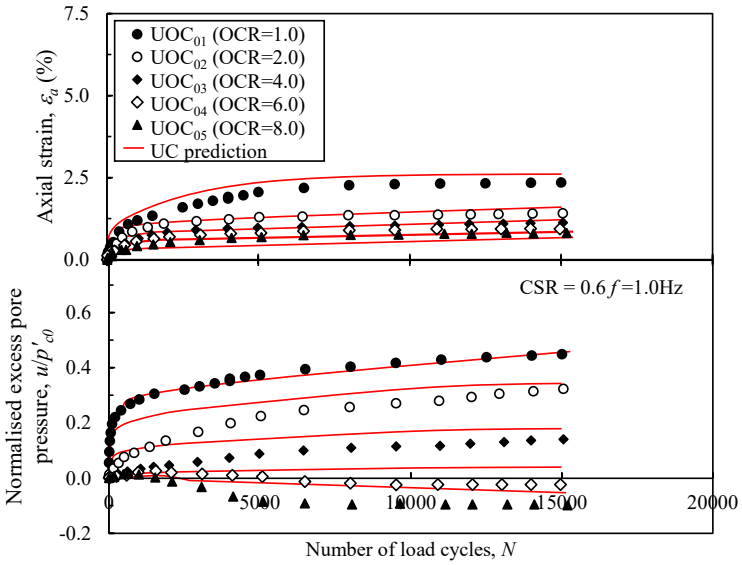

Figure 5.9: Undrained cyclic model prediction for overconsolidated samples, f=1Hz, CSR=0.6

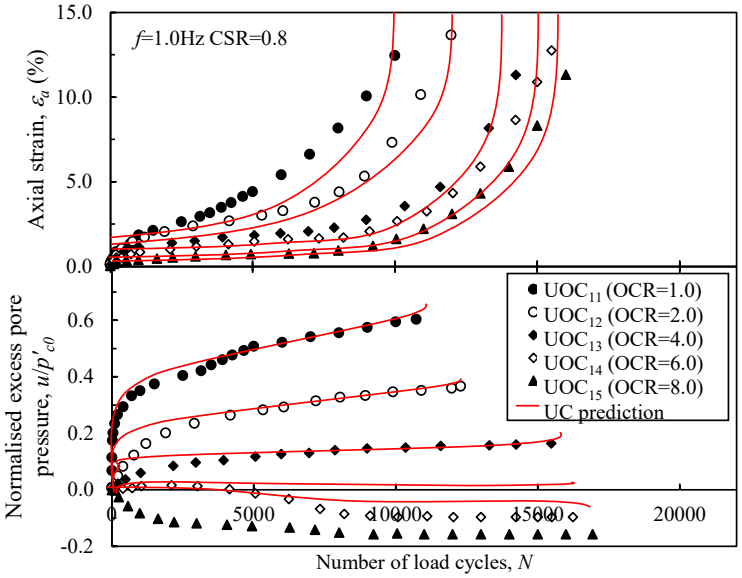

Figure 5.10: Undrained cyclic model prediction for overconsolidated samples, f=1Hz, CSR=0.8

5.3.1 Assessment of Confining Pressure

To further assess the performance of the existing model for future predictions following the model modification presented in future sections of this chapter, the performance of the original undrained cyclic model has further been assessed against the laboratory tests performed by Moses et al. (2003).

High plasticity marine clay samples with a plasticity index of 60% were analysed by the authors considering a range of frequencies, cyclic stress ratios and confining pressures. The initial properties adopted in the model prediction are summarised in Table 5.3

Table 5.3: Summary of input test parameters for undrained cyclic model, after Moses et al. (2003)

p'_0	p'_{c0}	q'_0	e_0	λ	κ	M
varies	75kPa	0kPa (assumed)	2.13	0.674	0.823	1.86

The model prediction demonstrates close agreement with the laboratory results of Moses et al. (2003). Furthermore, considering the variation of the vertical confining pressure of the sample, the greater the confining pressure, the greater the response of excess pore water pressure.

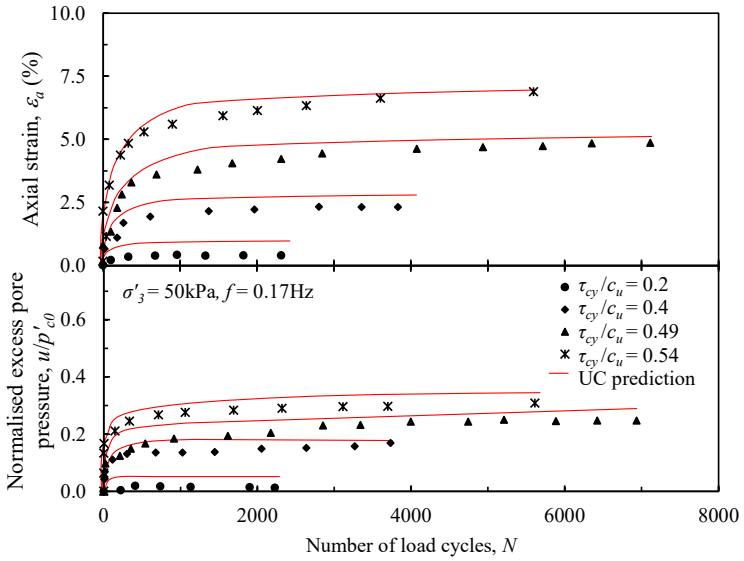

Figure 5.11: Undrained cyclic model prediction for samples with a confining stress, σ'_3 = 50kPa

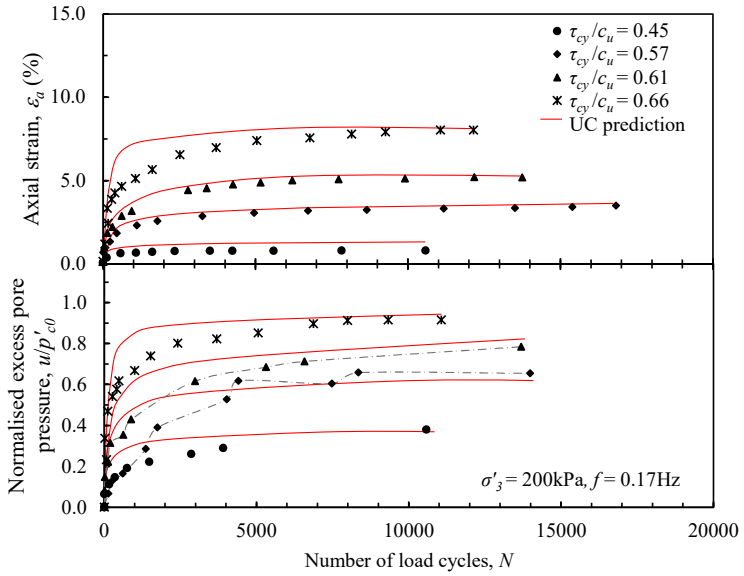

Figure 5.12: Undrained cyclic model prediction for samples with a confining stress, σ'_3 = 200kPa

The authors proposed the cyclic threshold for an confining pressure was dependent on the stress history of the sample and the frequency applied as well as the cementation of the marine samples tested. The results demonstrated a threshold cyclic stress ratio of greater than 0.54 for samples with a pressure of 50kPa and greater than 0.66 for samples at 200kPa. The prediction of the undrained cyclic model resulted in threshold cyclic stress ratios of 0.62 and 0.75 respectively however this could not be calibrated against the laboratory test data.

5.4 Introduction of Partial Drainage

Section 5.2.2 presents an introduction to the undrained cyclic model proposed by Ni (2012) that overcame the shortcomings of the original cyclic model developed by Carter et al. (1982) as described in Chapter 2, to better determine the accumulation of excess pore pressure. Section 5.3 demonstrates the applicability of the existing cyclic framework to the undrained kaolinite triaxial tests undertaken in Chapter 3. However, considering in-situ drainage conditions under cyclic traffic loading explored in Chapter 4, the condition of partial drainage has been demonstrated to be more applicable to traffic loading scenarios. Therefore, the model proposed above has been modified to incorporate the simultaneous generation and dissipation of excess pore pressures that occurs under partial drainage.

As presented in Chapter 4, the simultaneous generation and dissipation of excess pore pressures can be represented as per Figure 5.13 based on the work developed by Hyodo and Yasuhara (1988). The model assumes the generation of excess pore pressure that occurs under partially drained conditions is equivalent to that determined from an undrained cyclic test, such that $\Delta u_p = \Delta u'_p$ for the same number of cycles, whilst undergoing a change of Δu_c over a time interval of Δt. As a result, the excess pore pressure Δu_d is partly dissipated over time interval, Δt. The incremental volumetric strain, due to the generation and subsequent partial dissipation of excess pore pressure, Δu_d for a given time

interval can therefore be written;

$$\Delta\epsilon_v = m_v \Delta u_d \tag{5.23}$$

where Sakai et al. (2003) extended the relationship, presented in Chapter 4 to consider post-cyclic recompression such that,

$$\Delta\epsilon_v = \chi N^{\zeta} m^*_{vr} \Delta u_d \tag{5.24}$$

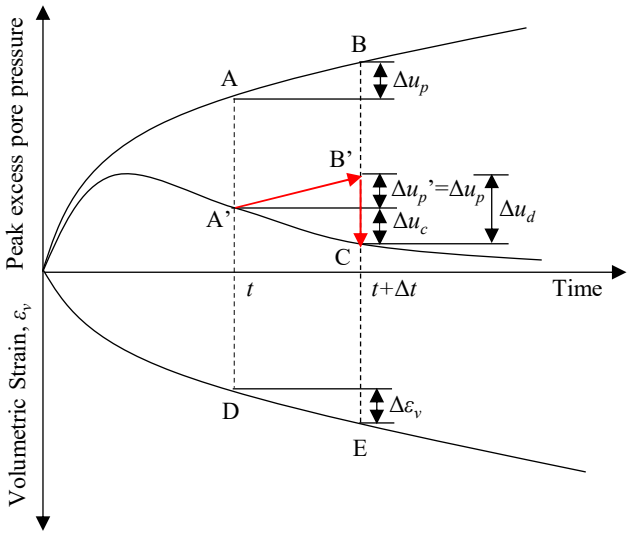

Figure 5.13: Procedure for evaluating the behaviour of soil under partially drained conditions of cyclic loading, reproduced from Sakai et al. (2003)

5.4.1 Stress Path for Partial Drainage

The stress path of the proposed model is characterised as per Ni (2012) and summarised in this Section for completeness. Based on the determined pore pressure Δu_p, the excess pore pressure response under partial drainage, in this case due to vertical drainage, can be considered. Under the same framework set out in Figure 5.3;

- A soil element, isotropically consolidated, commences its' stress path at p'_{c0}. Upon the loading portion of the cycle, it reaches the yield stress at point A, $p'_{cL,A}$. This causes a reduction in the mean effective stress of the

sample

- Subsequently, during the unloading portion of the cycle, the element reaches reference point $A*$ resulting in an increase in the mean effective stress, characterised by $p'_{y,A}$
- The yield stress is therefore $p'_{cU,A}$ previously described in Section 5.2.2.

The stress path can therefore be described in Figure 5.14.

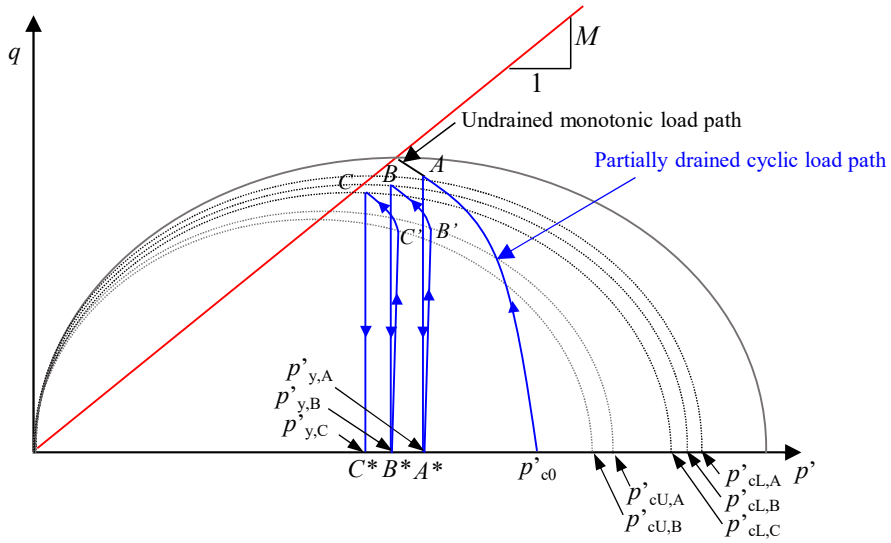

Figure 5.14: Stress paths for the behaviour of soil under partially drained conditions of cyclic loading, after Ni (2012)

5.4.2 Accumulation of Deviatoric Stress

The framework of the model is adapted from that proposed by Ni (2012) considering horizontal partial drainage due to the inclusion of vertical drains, whilst the drainage condition has been modified, the foundation for the determination of cyclic stress response is similar to that previously presented. The development of cyclic deviatoric stress within the model framework is summarised in this section. For the first cycle of loading, the following calculation step is applied for the time dt of step dq, where initial anisotropy can be accounted.

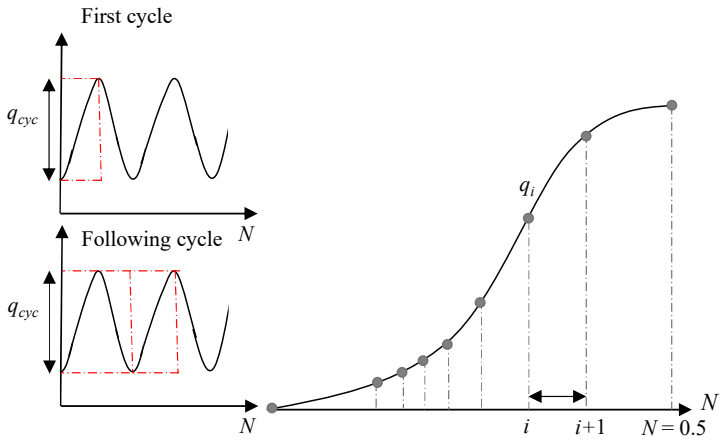

Figure 5.15: Determination of dt and dq

Considering a semi-sinusoidal waveform, the first half of the cycle can be written in terms of period, T, the inverse of the load frequency, f and the velocity, $2\pi f$;

$$q_i = q_0 + \frac{q_{cyc}}{2}\left(1 + sin\left(\frac{2\pi t_i}{T} - \frac{\pi}{2}\right)\right) \tag{5.25}$$

As such, dividing the waveform into equal intervals, n, the deviatoric stress, shown in Figure 5.15, can be written;

$$q_i = q_0 + i\frac{q_{cyc}}{n} \tag{5.26}$$

such that;

$$i = \frac{n}{2}\left[\frac{q_{cyc}}{2}\left(1 + sin\left(\frac{2\pi t_i}{T} - \frac{\pi}{2}\right)\right)\right] \tag{5.27}$$

Therefore, the time interval can be described;

$$t_i = T\left[\frac{\sin^{-1}\left(\frac{2i}{n} - 1\right) + \frac{\pi}{2}}{2\pi}\right] \tag{5.28}$$

The accumulation over a time interval, presented in Figure 5.15, can be

determined from;

$$dt_{i+1} = t_{i+1} - t_i = T\left[\frac{\sin^{-1}\left(\frac{2(i+1)}{n} - 1\right) - \sin^{-1}\left(\frac{2i}{n} - 1\right)}{2\pi}\right] \qquad 1 < i \leq n \tag{5.29}$$

In the subsequent cycles, the following routine applies based on whether the soil behaviour is elastic or plastic.

- When soil behaviour is elastic, such that $q \leq q_y$, the magnitude of q is proportional to q_y - q_0, t_i then becomes;

$$t_i = T\left[\frac{\sin^{-1}\left(\frac{2\ i\ q_y - q_0}{n_1 q_{cyc}} - 1\right) + \frac{\pi}{2}}{2\pi}\right] \qquad 1 < i \leq n_1 \tag{5.30}$$

  The incremental deviatoric stress at time, dt_{i+1} is dq_{i+1}, such that $q_{i+1} = q_i + dq_{i+1}$. Therefore, when the soil is elastic, the mean effective stress p_{i+1} can be determined;

$$p'_{i+1} = p'_i \tag{5.31}$$

  and pore pressure, $du_{p_{i+1}}$ can be calculated;

$$du_{p_{i+1}} = p'_i - p'_{i+1} + \frac{dq_{i+1}}{3} \tag{5.32}$$

- When soil behaviour is plastic, such that $q_{i+n_1} \geq q_y$, the magnitude of q is proportional to q_{cyc} -(q_y - q_0), t_{i+n_1} then becomes;

$$t_{i+n_1} = T\left[\frac{\sin^{-1}\left(\frac{2\ (n_2 - 1)()q_y - q_0)}{n_2 q_{cyc}} + \frac{2i}{n_2} - 1\right) + \frac{\pi}{2}}{2\pi}\right] \qquad 1 < i \leq n_2 \tag{5.33}$$

  The incremental deviatoric stress at time, dt_{i+1} is dq_{i+1}, such that $q_{i+1} =$

$q_i + dq_{i+1}$. Therefore, when the soil is plastic, the mean effective stress p_{i+1} can be determined;

$$\frac{p'_i}{p'_{i+1}} = \left[\frac{M^2 + \left(\frac{q_{i+1}}{p_{i+1}}\right)^2}{M^2 + \left(\frac{q_i}{p_i}\right)^2}\right]^{\frac{\lambda-\kappa}{\lambda}} \tag{5.34}$$

and pore pressure, $du_{p_{i+1}}$ can be calculated;

$$du_{p_{i+1}} = p'_i - p'_{i+1} + \frac{dq_{i+1}}{3} \tag{5.35}$$

This section has summarised the initial calculation steps for calculating the excess pore pressure and subsequently the strain response under cyclic loading considering partial drainage. The following section presents the determination of dissipation of excess pore pressure, considering u_p determined above for elastic and plastic stages of applied stress.

5.4.3 Pore Pressure Generation

Previously the application of partially drained conditions has been examined in the context of installation of vertical drains providing a horizontal drainage pathway for the dissipation of excess pore pressures. As such the finite difference method was used to solve the equation for partially drained excess pore pressure response in the horizontal direction. In the case of the samples examined in this study, the drainage lines of the triaxial cell have been opened such that the drainage pathway is vertical. Based on Darcy's Law, the following equations are proposed for the case outlined in Figure 5.16.

Darcy's law can be written, such that the flow, Q in the vertical direction, z of a soil block of dimensions dx and dy is;

$$\frac{dQ}{dt} = kiA = kidxdy \tag{5.36}$$

where i_z is the hydraulic gradient of the material in the vertical direction. The

flow into the element under consideration, Q_{in} can be summarised;

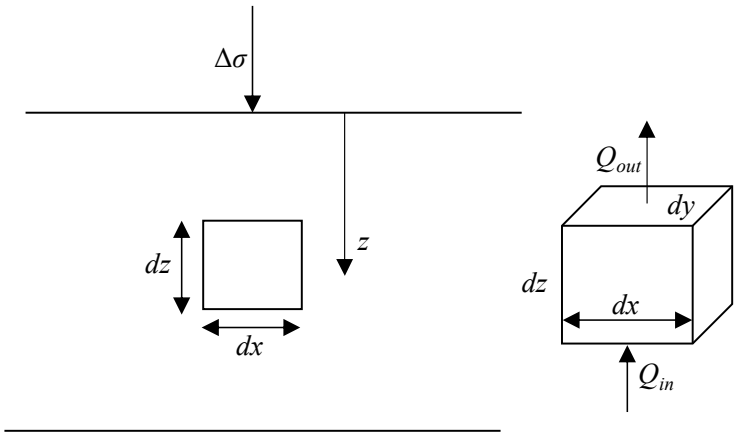

Figure 5.16: The theory of 1 dimensional vertical consolidation

$$dQ_{in} = ki_z dxdydt \tag{5.37}$$

$$i_z = \frac{1}{\gamma_w}\frac{\delta u}{\delta z} \tag{5.38}$$

The flow out of the element under consideration, Q_{in} can be summarised;

$$dQ_{out} = ki_{z+dz} dxdydt \tag{5.39}$$

$$i_{z+dz} = i_z + \frac{\delta i_z}{\delta z}dz = \frac{1}{\gamma_w}\frac{\delta u}{\delta z} + \frac{1}{\gamma_w}\frac{\delta^2 u}{\delta z^2}dz \tag{5.40}$$

The change in flow dQ can therefore be determined;

$$dQ = dQ_{in} - dQ_{out} \tag{5.41}$$

$$dQ = \Big[\frac{k}{\gamma_w}\frac{\delta u}{\delta z} - \Big(\frac{k}{\gamma_w}\frac{\delta u}{\delta z} + \frac{k}{\gamma_w}\frac{\delta^2 u}{\delta z^2}dz\Big)\Big]dxdydt = -\frac{k}{\gamma_w}\Big(\frac{\delta^2 u}{\delta z^2}dz\Big)dxdydt \tag{5.42}$$

Therefore;

$$dQ = dV \tag{5.43}$$

$$dV = -\frac{k}{\gamma_w}\Big(\frac{\delta^2 u}{\delta z^2}dz\Big)dxdydt \tag{5.44}$$

$$dV = \epsilon_v dxdydz \tag{5.45}$$

$$\epsilon_v = -\frac{k}{\gamma_w}\Big(\frac{\delta^2 u}{\delta z^2}\Big)dt \tag{5.46}$$

The volumetric strain can also be written;

$$\epsilon_v = -m_v\Big(\frac{\delta u}{\delta t}dt\Big) \tag{5.47}$$

such that by equating terms;

$$\frac{k}{\gamma_w}\Big(\frac{\delta^2 u}{\delta z^2}\Big)dt = m_v\Big(\frac{\delta u}{\delta t}\Big)dt \tag{5.48}$$

$$c_v = \frac{k}{\gamma_w m_v} \tag{5.49}$$

$$c_v\Big(\frac{\delta^2 u}{\delta z^2}\Big) = \frac{\delta u}{\delta t} \tag{5.50}$$

Based on the drainage of liquefied sands, presented by **?**, this can be written in terms of the excess pore pressure dissipation;

$$c_v\Big(\frac{\delta^2 u}{\delta z^2}\Big) = \frac{\delta u}{\delta t} - \frac{\delta u_p}{\delta t} = \frac{\delta u_c}{\delta t} + \frac{\delta u_p}{\delta t} \tag{5.51}$$

On this basis, adopting the finite difference approach presented by Ni (2012), considering vertical consolidation for the time interval dt presented in Section 5.4.2, the average rate of change in excess pore pressure can be described by;

$$\frac{u_{i,j}(t+dt) - u_{i,j}(t)}{dt} = c_v\Bigg[\frac{1}{2}\Big(\frac{u_{i,j-1}(t+dt) - 2u_{i,j}(t+dt) + u_{i,j+1}(t+dt)}{dz^2}\Big) + \frac{1}{2}\Big(\frac{u_{i,j-1}(t) - 2u_{i,j}(t)u_{i,j+1}(t)}{dz^2}\Big)\Bigg] + \frac{u(t+dt) - u(t)}{dt} \tag{5.52}$$

And at time, $t + dt$;

$$u_{i,j}(t+dt) = -u_{i,j}(t) + dtc_v\Bigg[\frac{1}{2}\Big(\frac{u_{i,j-1}(t+dt) - 2u_{i,j}(t+dt) + u_{i,j+1}(t+dt)}{dz^2}\Big) + \frac{1}{2}\Big(\frac{u_{i,j-1}(t) - 2u_{i,j}(t)u_{i,j+1}(t)}{dz^2}\Big)\Bigg] + u(t+dt) - u(t)$$

(5.53)

This is summarised in Figure 5.17, reproduced from Ni (2012)

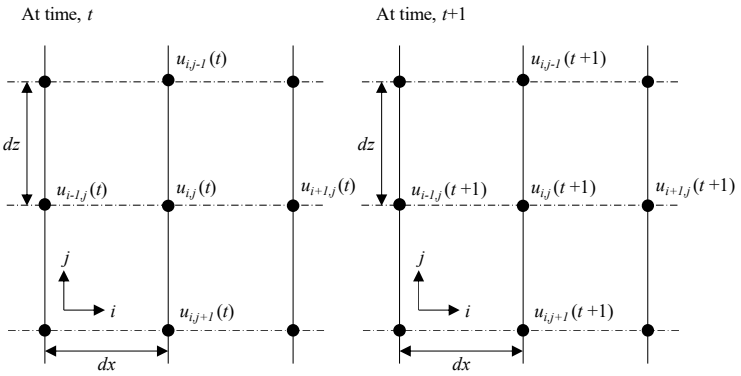

Figure 5.17: The finite difference method, after Ni (2012)

This is a consideration of the existing model for vertical drainage such that when $f_z = c_v dt/dz^2$;

$$u_{i,j}(t+dt) = \frac{1-f_z}{1+f_z}u_j(t) + \frac{f_z}{2(1+f_z)}\Big[u_{j-1}(t) + u_{j-1}(t+dt) + u_{j+1}(t)u_{j+1}(t+dt)\Big] + \frac{1}{1+f_z}\big[u(t+dt) - u(t)\big] \tag{5.54}$$

At the end of the time interval, the excess pore pressure can be written;

$$u_j(t+dt) = \frac{1-f_z}{1+f_z}u_j(t) + \frac{f_z}{2(1+f_z)}\Big[u_{j-1}(t) + u_{j-1}(t+dt) + u_{j+1}(t)u_{j+1}(t+dt)\Big] + \frac{1}{1+f_z}\big[u(t+dt) - u(t)\big] \tag{5.55}$$

In this manner, the vertical drainage of the solution can be considered.

5.4.4 Volume Change due to Vertical Flow

Subsequently, from determination of the excess pore pressure, the mean effective stress, p_{i+1} can be recalculated and the volumetric strain, ϵ_v can be determined;

$$\epsilon_{v_{i+1}} = \frac{e_{i+1} - e_0}{1+e_0} \tag{5.56}$$

Considering the elastic portion of the response;

$$\int dp'_{i+1} = \int K_{i+1}\Big(\frac{-de_{i+1}}{1+e_{i+1}}\Big) \tag{5.57}$$

where

$$e_{i+1} = (1+e_i)exp\Big(-\frac{-p'_2-p'_1}{K_{i+1}}\Big) \tag{5.58}$$

Considering the plastic portion of the response;

$$\int \frac{-de_{i+1}}{1+e_{i+1}} = \int C_{11}dp' + \int C_{12}dq \tag{5.59}$$

where

$$e_{i+1} = (1+e_i)exp\Big(-C_{11}(p'_2-p'_1) - C_{12}(q_2-q_1)\Big) - 1 \tag{5.60}$$

The settlement of a soil layer can be expressed;

$$S(t) = \frac{e_0 - e(t)}{1+e_0}H \tag{5.61}$$

such that the degree of consolidation in terms of settlement is;

$$U(z,t) = \frac{\Delta u}{u} = 1 - \frac{u_d}{u} \tag{5.62}$$

5.5 Verification of the Proposed Model

The model presented in Section 5.4 has been examined with respect to the cyclic partially drained triaxial tests performed on kaolinite in Chapter 4.3. The soil properties adopted in the model analysis are summarised in Table 5.4. The results of the model comparison are presented in Figures 5.18, 5.19 and 5.20.

Table 5.4: Summary of PC parameters for partially drained model prediction

p'_0	p'_{c0}	q'_0	c_v	e_0	λ	κ	M
200kPa	200kPa	0kPa	0.01m^2/day	1.450	0.170	0.040	0.93

The model prediction presented considers a frequency of 1.0Hz for each of the cyclic stress ratios analysed. Examining first the excess pore water pressure accumulation, the model prediction is acceptable, considering the long duration of cyclic loading that is applicable in the case of traffic loading. The model results presented consider a node at the centre of the sample, considering drainage at both the top and bottom of the sample. The excess pore pressure peak attained in the model agrees with that of the cyclic triaxial tests, however the dissipation curve is more gradual than in the laboratory assessment. For an increased cyclic stress ratio, the peak of excess pore pressure increases, and the dissipation steepens. Similarly, for each of the cyclic stress ratios examined, the volumetric strain response is in close agreement with the laboratory tests.

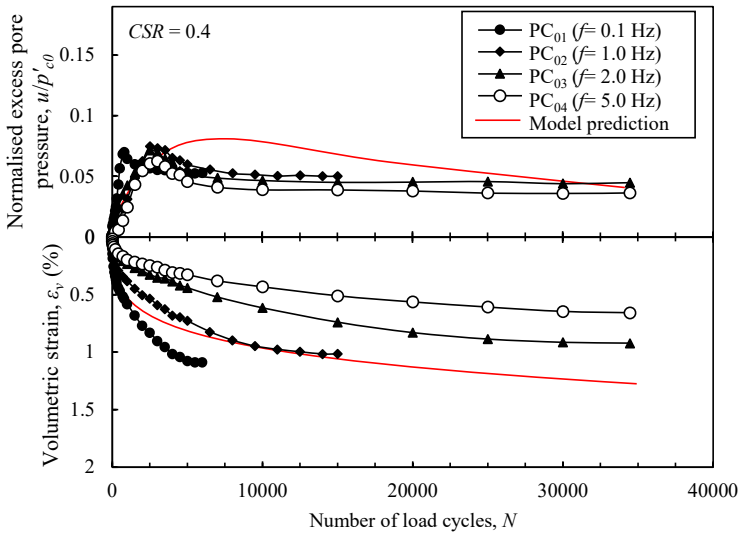

Figure 5.18: Partially drained cyclic model prediction for a frequency f = 1 Hz at a cyclic stress ratio of 0.4

Further to the review of the proposed model with respect to the laboratory tests undertaken in this study, the performance of the model has been assessed against the results of Hyodo et al. (1992) where drained cyclic triaxial tests were performed on reconstituted Ariake Clay with the following properties;

Table 5.5: Summary of test parameters for partially drained cyclic model, after Hyodo et al. (1992)

p'_0	p'_{c0}	c_v	λ	κ	M	f
198kPa	198kPa	0.01m^2/day	0.304	0.071	1.60	0.1Hz

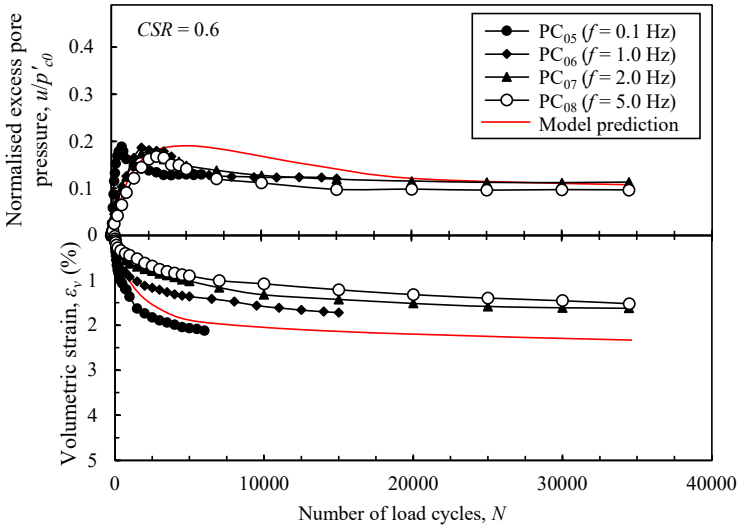

Figure 5.19: Partially drained cyclic model prediction for a frequency f = 1 Hz at a cyclic stress ratio of 0.6

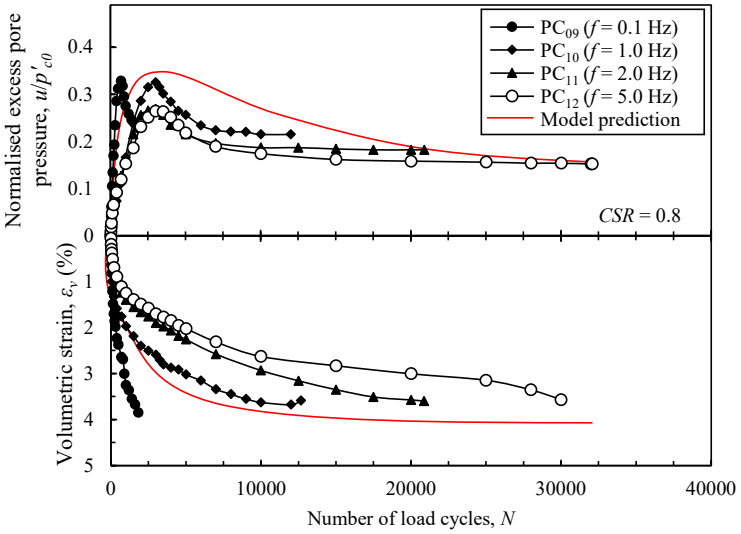

Figure 5.20: Partially drained cyclic model prediction for a frequency f = 1 Hz at a cyclic stress ratio of 0.8

The results of normalised excess pore pressure, both the undrained generated excess pore pressure and the dissipated pore pressure are presented alongside the measured excess pore pressure for the clay samples under undrained cyclic loading of 0.1Hz. As observed from the consideration of the partially drained tests examined, the dissipated excess pore pressure is an under-prediction due to the model only considering consolidation and drainage effects in the vertical direction.

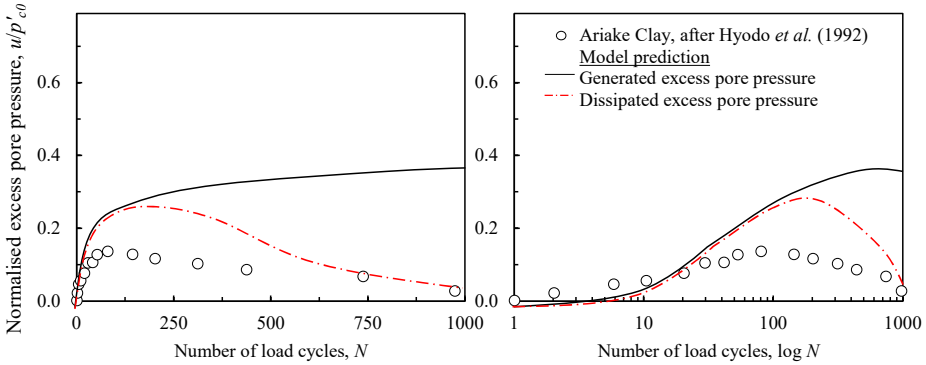

Figure 5.21: Partially drained model prediction of excess pore pressures determined by Hyodo et al. (1992)

5.5.1 Effect of Cyclic Stress Ratio

The partially drained response has been examined in terms of varying the cyclic stress ratio for a given set of input parameters, presented in Figure 5.22. An increase in cyclic stress ratio results in an increase in the excess pore pressure response peak. At low cyclic stress ratios, lines (a) and (b) the accumulation in excess pore pressure under drainage is negligible. At greater cyclic stress ratios, following the initial response, a greater amount of dissipation occurs. Figure 5.22 also presents the influence of frequency, however, for a stable sample the effect of frequency with respect to time has been shown to be negligible. It is shown that considering the same number of load cycles, whilst for the same cyclic stress ratio, the peak excess pore pressure attained is similar (under a lower frequency it is slightly greater), for a lower frequency where the period of cyclic loading is therefore greater, the excess pore pressure dissipates faster, as a greater duration of consolidation is permitted. As such this explains why

for an equivalent number of cycles, the volumetric strain is greater for a lower frequency.

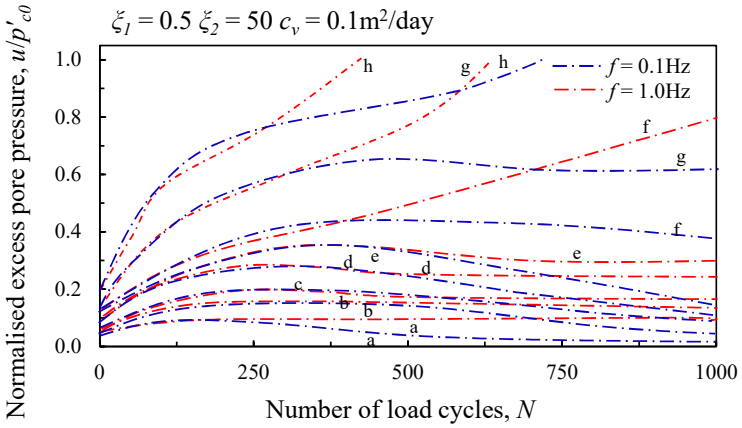

Figure 5.22: Partially drained cyclic model prediction examining the influence of cyclic stress ratio at a frequency of 0.1Hz and 1.0Hz

Further considering the effect of cyclic stress ratio, the prediction of normalised excess pore pressure response under partial drainage has been examined considering the cyclic triaxial tests performed by Moses et al. (2003).

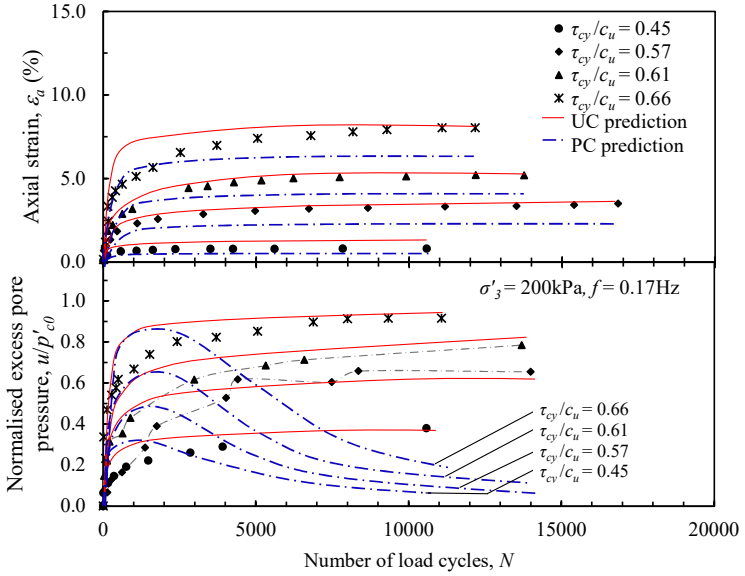

Figure 5.23: Partially drained cyclic model prediction for case study on marine clay presented by Moses et al. (2003)

The results presented in Figure 5.23 show the undrained model provides an close agreement to the authors experimental data. The dissipation of excess pore pressures is predicted using the model, demonstrating the influence of cyclic stress ratio on the pore pressure under partial drainage. Under the initial accumulation the response is greater for a greater CSR, the rate of excess pore pressure dissipation increases for an increase in CSR before beginning to converge. This demonstrates a similar response to the partially drained triaxial tests performed, in agreement with the conclusions of O'Reilly et al. (1991), Hyde et al. (2007) and Paul et al. (2015).

5.5.2 Effect of Degradation Parameters

As had originally been proposed in the model by Carter et al. (1980), when degradation parameter ξ_1=0, the determination of the critical cyclic stress ratio was not possible. Figure 5.24 demonstrates the influence of the degradation parameter ξ_2 considering vertical consolidation.

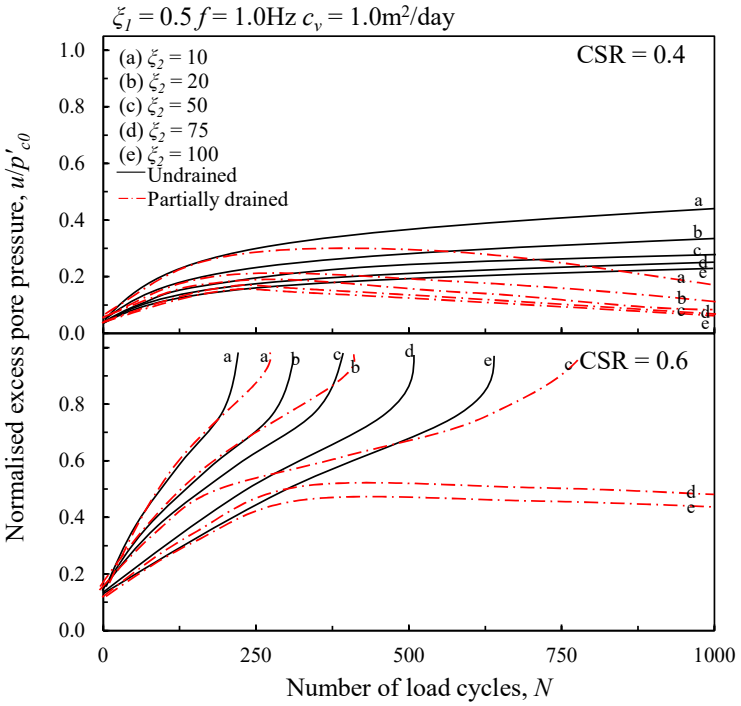

Figure 5.24: Influence of degradation parameters on the partially drained cyclic model prediction

The inclusion of drainage results in a reduced accumulation of normalised excess pore pressure. Supporting the laboratory studies undertaken, as the cyclic stress ratio increases the excess pore pressure increases. With low values of ξ_2 this will result in failure. As ξ_2 increases, the analyses tend towards a stable state. Even for analyses that attain failure, under partial drainage, the number of cycles attained prior to failure increases such that the sample has a greater resistance to cyclic load.

5.5.3 Effect of Vertical Coefficient of Consolidation

The response of partial drainage is as a result of the vertical dissipation, as such the coefficient of vertical consolidation is an important consideration within the model framework presented. Figure 5.25 presents the sensitivity of the model to the coefficient of consolidation. For the input degradation parameters presented, the black lines represent the undrained model prediction whilst the red dashed line presents the partially drained prediction. The model predictions demonstrate the greater the consolidation coefficient, the greater the dissipation of excess pore pressure, as would be expected. As such, as the coefficient of consolidation decreases, such that dissipation is inhibited, the greater the accumulation of excess pore pressures and the greater the potential for the sample to attain a failed state. Whilst the sensitivity of the laboratory tests did not demonstrate the threshold cyclic stress ratio changed, with a greater analysis of cyclic stress ratio it is suggested the threshold value would increase with the coefficient of consolidation.

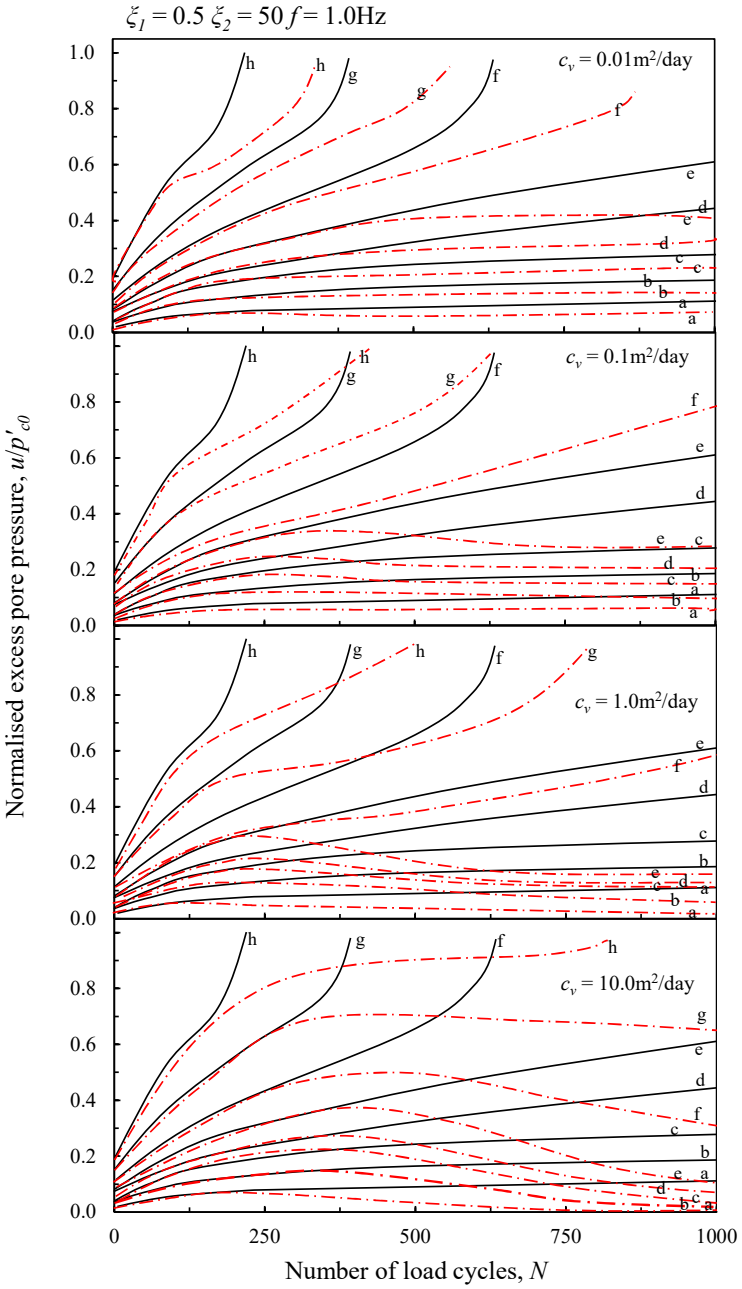

Figure 5.25: Partially drained cyclic model prediction for varying coefficients of vertical consolidation, c_v

5.6 Application to Saga Airport

One well known case study examining the effects of cyclic loading on subgrade performance is the Saga Airport road, referenced in Chapter 2. The performance of the partially drained cyclic model presented in this chapter has been examined with respect to the measured field settlements below the road subgrade. The proposed case study soil profile is presented in Figure 5.26 alongside the geological properties previously presented by Sakai et al. (2003). The upper Ariake clay layer had a plasticity index of 55%, shown in Figure 5.26, whilst the lower layer had an index of approximately 40%.

Considering the top Ariake Clay layer to be influenced by traffic loading, the following input parameters for this layer have been proposed;

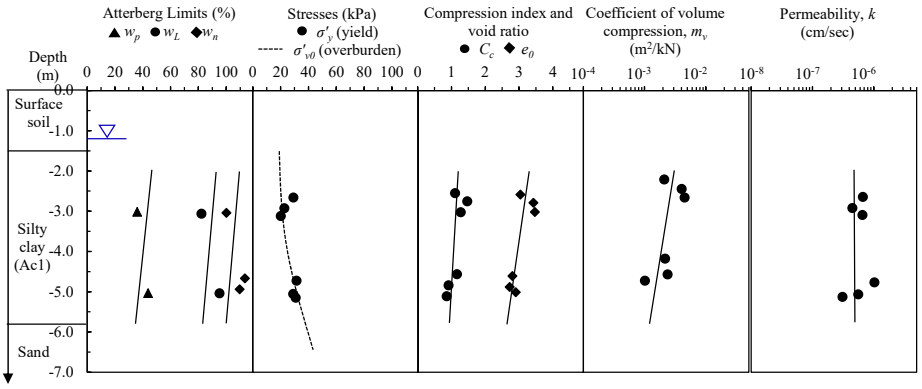

Figure 5.26: Summary of ground model and soil properties, after Sakai et al. (2003)

Table 5.6: Summary of Sakai airport road model parameters

p'_0	p'_{c0}	q'_0	c_v	e_0	C_c	C_s	M
varies	75kPa	25kPa[a]	0.07m^2/day	1.49[b]	0.89	0.076	1.75[c]

(a) Assuming K_0 = 0.5 (b) Taken as the average void ratio of cyclic loading tests performed by Sakai et al. (2003) (c) Obtained from undrained triaxial tests by Sakai et al. (2003)

Sakai et al. (2003) reported around 800 vehicles per day used the road during the time frame over which settlements were measured. As a result, the frequency for partially drained test simulation has been taken to be 0.01Hz (800 cycles ÷ 60 x 60 x 24 = 0.00925Hz). The authors proposed a cyclic applied vertical

stress of 35kPa. The results of the accumulated settlement under cyclic loading considering vertical drainage are presented in Figure 5.27. Under this case the settlements are an over-prediction to the measured settlements however fair agreement is obtained. Two influences on the prediction of settlement that may account for this small overestimate are the magnitude of load considered with respect to traffic loading and the coefficient of compression adopted in the analysis. Given the low frequency of load adopted, the amount of settlement attained increases due to the greater duration of load and subsequent dissipation of excess pore pressure.

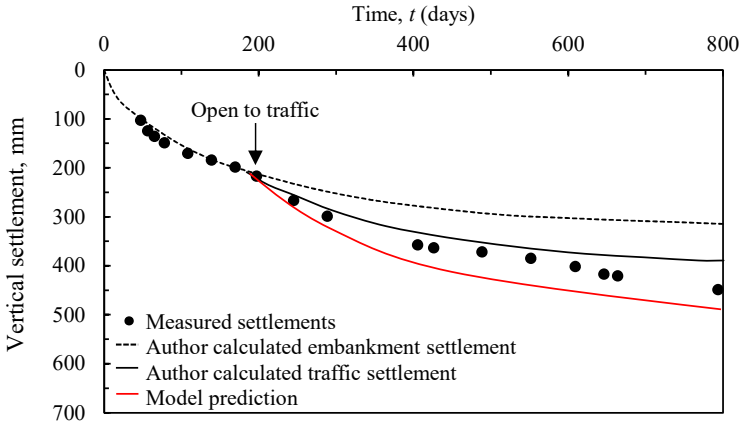

Figure 5.27: Partially drained cyclic model prediction for the settlement of the Saga Airport road

5.7 Conclusions

The cyclic undrained model of Ni (2012) has been examined, considering the case of vertical drainage such that a partially drained response can be predicted. This model is capable of predicting the response of cyclic triaxial tests in which drainage lines remained open, permitting vertical flow through the sample and therefore considering the vertical consolidation of a sample under cyclic loading. In turn, this can be considered to be representative of the case of an in-situ soil element subjected to traffic loading. The initial model of Ni (2012) has been summarised, including the determination of computational steps over a given time interval, where each load cycle can be subdivided. The determination of

the mean effective principal stress in response to a given cyclic load has been presented, such that the excess pore pressure change is calculated. Based on the finite difference method using Terzaghi's theory of vertical consolidation, the change in pore pressure has been determined such that the mean effective stress position in partially drained conditions can be recalculated. Subsequently, the strain accumulation can be derived.

Examining the response of cyclic loading under partially drained conditions, the model prediction is shown to be in close agreement with the results of the laboratory tests in Chapter 4.3;

- Considering the response of the excess pore pressure for varying cyclic stress ratio, the greater the cyclic stress ratio the greater the magnitude of excess pore pressure generated and therefore peak response. Subsequently, this excess pore pressure dissipates, with a difference in excess pore pressure from the peak increasing with CSR. This has been further illustrated by considering the cyclic triaxial response of marine clay performed by Moses et al. (2003). This subsequently explains the increase in strain accumulation with cyclic stress ratio.
- Similarly, with respect to the number of cycles of load, as the frequency of loading decreases such that the load period increases, the greater the strain accumulation and the greater the dissipation of excess pore pressure. Over a significant load duration, such as that anticipated for traffic loading with a long service life for the infrastructure under consideration, this effect decreases and eventually the strain accumulation will converge to a similar value, irrespective of frequency.
- The degradation parameters initially proposed by Carter et al. (1980) and Ni (2012) govern the excess pore pressure response. As the degradation parameters increase, the excess pore pressure accumulation decreases, such that the sample can withstand a greater cyclic stress ratio, and therefore cyclic load application, without failure.
- The influence of vertical coefficient of consolidation has also been studied. As the coefficient increases, the rate at which excess pore pressure can

dissipate under a given load increases such that the sample can withstand greater cyclic loading.

The performance of the model considering the well known case study of the Saga Airport road has been examined. The model prediction considering settlement accumulation as a result of partial drainage of the Ariake clay layer provides a close agreement with the measured data at the site. The prediction is an over estimation of the settlement response, attributed to the simplified characterisation of the cyclic loading as a result of traffic passage, and due to uncertainty or variability in the field of the coefficient of vertical consolidation.

Chapter 6

The Cyclic Performance of Gault Clay

The previous chapters have presented the performance of laboratory prepared kaolin samples subject to cyclic loading under the consideration of a range of in-situ conditions. Both an empirical solution and finite difference solution for the cyclic load response have been presented that have been shown to perform well against previously published case histories of the Saga Airport Road and Ledsgård Rail link.

This chapter considers the response of clay samples from the Gault Formation, using material prepared from bulk samples obtained during site investigation for the new High-Speed Two rail link in the United Kingdom. Classification of the index properties of the Gault clay is presented in order to contrast the response against that of previous kaolin samples. Undrained cyclic triaxial tests have similarly been performed considering a range of frequencies and cyclic stress ratios, determining the threshold cyclic stress ratio of the Gault Formation. The influence of the index properties of the Gault Clay on the cyclic undrained response have been examined, and a model prediction has been provided considering the change in performance of partially drained samples. Furthermore, the influence of the index properties on the post-cyclic strength and stiffness of the samples has been examined, considering the influence

this has on the cyclic degradation of the samples in relation to energy effects previously discussed in Chapter 4. Subsequently, stop-start triaxial tests have been performed, as suggested in conclusion to examination of partially drained conditions in Chapter 4.3.

6.1 Introduction to the Gault Formation

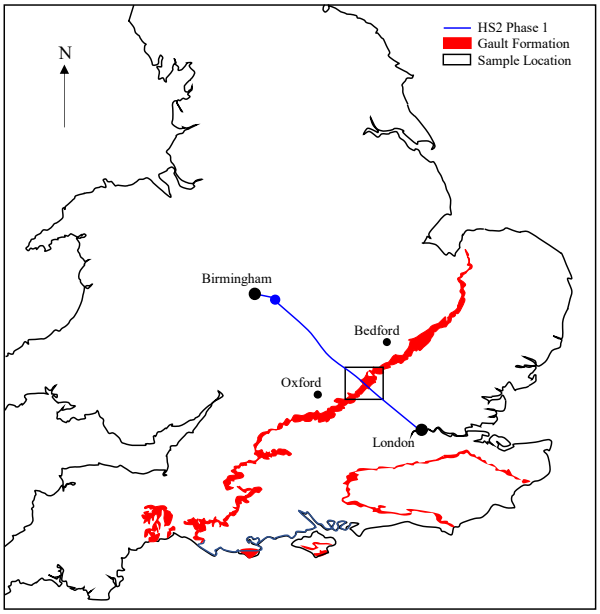

Figure 6.1: Gault Formation in the UK

Bulk samples of the Gault Formation were obtained from site investigation undertaken for the new proposed high speed rail link between London and Birmingham. The Gault Formation can be found to outcrop in the East Midlands, extending south towards Bedford and to the South West of the UK, shown in Figure 6.1. Samples considered in this study were obtained from between Bedford and Oxford, marked on Figure 6.1, in proximity to the proposed High-Speed Two route. This formation is a Cretaceous formation of clays, siltstones and mudstones and due to the high smectite content can be prone to shrink-swell processes. The location of the samples suggests the presence of smectite in accordance with the regional distribution presented by Forster et al. (1994). The bulk clay samples were obtained from trial pits.

6.1.1 Index Properties

The Gault clay considered for this study had the following properties, performed using the testing methods previously summarised in Chapter 3.1.1.

- A specific gravity of G_s= 2.69
- A plastic limit of w_p = 30%
- A liquid limit of w_L = 76%
- Therefore, a plasticity index of I_p = 46%.

The liquid limit and therefore plasticity index of the samples is greater than Loach (1987) determined, summarised in Table 6.1, however the moisture content of samples in this study was selected to reduce the influence of the plasticity index when comparing the results to Keuper Marl. However the results are in agreement with the index properties by other authors including those presented in the comprehensive study undertaken by Hosseini Kamal (2012).

Table 6.1: Summary of index properties for Gault clay from literature

Authors	Plastic Limit, w_p	Liquid Limit, w_L	Clay Fraction	Sample Type
Garrett and Barnes (1984)	28%	75%	-	U100 sample
Loach (1987)	25%	61%	39%	Reconstituted sample
Parry (1988)	30%	76%	-	Hollow Stem Auger sample
Hosseini Kamal (2012)	28%	74%	46%	Block sample, Rotary Core sample, Reconstituted sample

Particle size distribution tests were performed in accordance with ASTM D6913. The results of the test, are presented in Figure 6.2, demonstrating the samples to be a silty clay with a clay fraction of approximately 53% clay. The median particle diameter, D_{50}, is approximately 2.3μm.

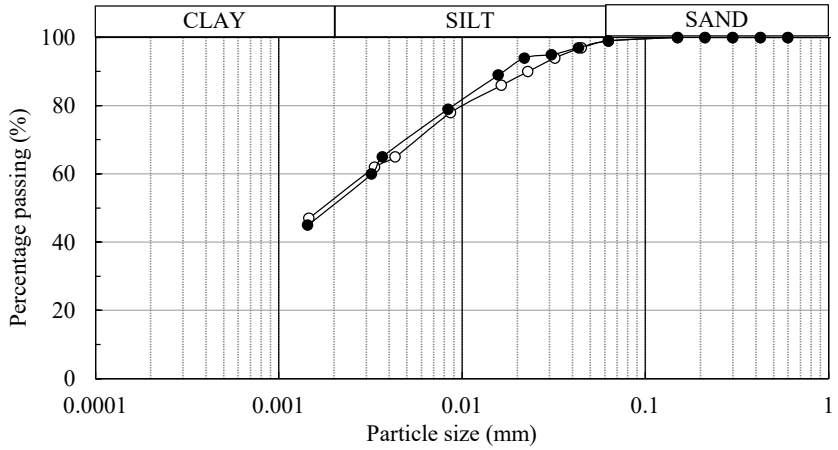

Figure 6.2: Particle size distribution tests for Gault clay

As such, the activity of the sample, ie. the ratio of plasticity index to the clay fraction of the material can be determined. For the Gault clay, the activity is 0.86, plotting as a high plasticity clay "CH" shown in Figure 6.3. In the same plot, the kaolinite samples presented in Chapter 3 plot slightly lower, indicating the kaolinite to be an intermediate clay "CI" of medium plasticity.

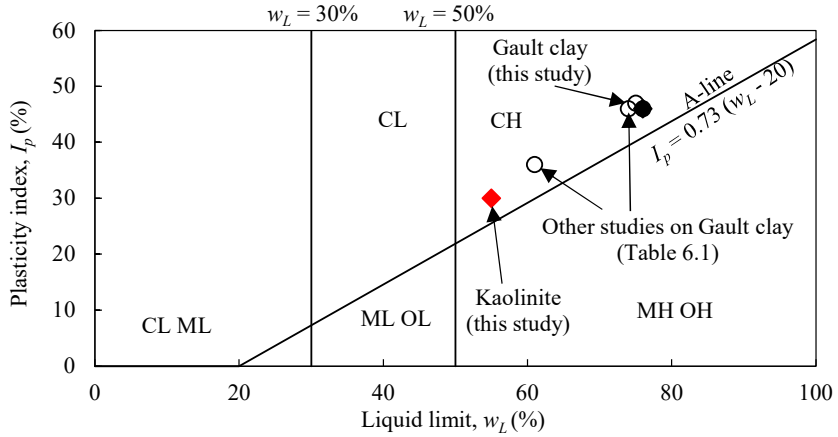

Figure 6.3: Soil activity for the Kaolinite and Gault clay samples in this study

6.1.2 Compression and Strength Properties

One-dimensional compression tests were performed to characterise the load-unload response of the reconstituted Gault clay samples, presented in

Figure 6.4. The compression and rebound indices are shown in Table 6.2, suggesting in comparison to the kaolinite samples previously examined, the deformation response of the samples under an equivalent load would be greater. The values for compression and rebound indices are comparable to samples presented by Hosseini Kamal (2012), with $\lambda = 0.06$ and $\kappa = 0.034$, and those of Nash et al. (1996). Whilst the clay fraction of the Gault clay is less than that of the kaolinite samples studied in Chapter 3 and 4, the compression index and swelling index are both influenced by the smectite content, demonstrated by Lodahl (2017) to increase linearly with respect this.

Table 6.2: Summary of compression properties for the Gault clay

C_c	λ	C_s	κ
0.468	0.204	0.115	0.050

Undrained monotonic triaxial tests were performed to determine the undrained shear strength of the samples to be adopted for the cyclic stress ratio applied in the cyclic tests. In comparison with the kaolinite samples previously examined, a series of tests were performed such that the undrained shear strength of the sample at a given confining pressure was close to 60kPa, previously demonstrated to be the criteria for a soil that did not achieve the range of G_0 based on the analyses by Vardanega et al. (2013). The results of the undrained triaxial tests demonstrated that a lower confining pressure was required to achieve an equivalent undrained shear strength to that obtained for the kaolinite samples. In this case, an initial mean effective stress, p'_{c0} of 150kPa resulted in an undrained shear strength of 60kPa, presented in Figure 6.5. This confining pressure is slightly higher for a similar undrained shear strength when compared to the findings of undrained monotonic triaxial tests performed by Hosseini Kamal (2012). These samples were cut and prepared from block samples such that the effect of weathering on the in-situ structure of the Gault clay can be observed in the mechanical response. In the case of the reconstituted samples in this study prepared from bulk samples, whilst the index properties can be accounted for, the initial sample structure will not be influenced by the pressure of fissures. This has been reported by several authors whom acknowledged that the natural structure of the sample resulted

in an increase in the slope M in q-p space when compared to reconstituted samples.

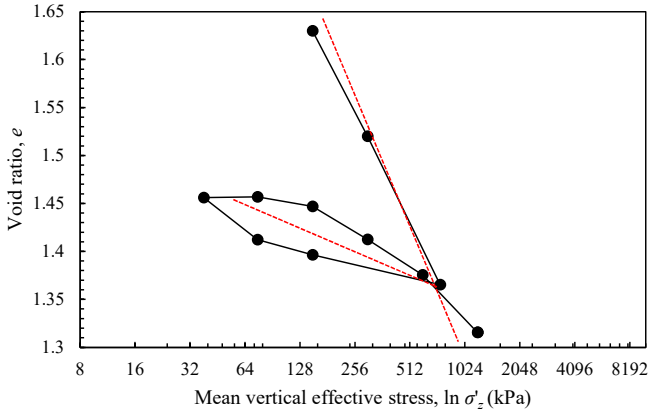

Figure 6.4: One dimensional compression test for Gault clay

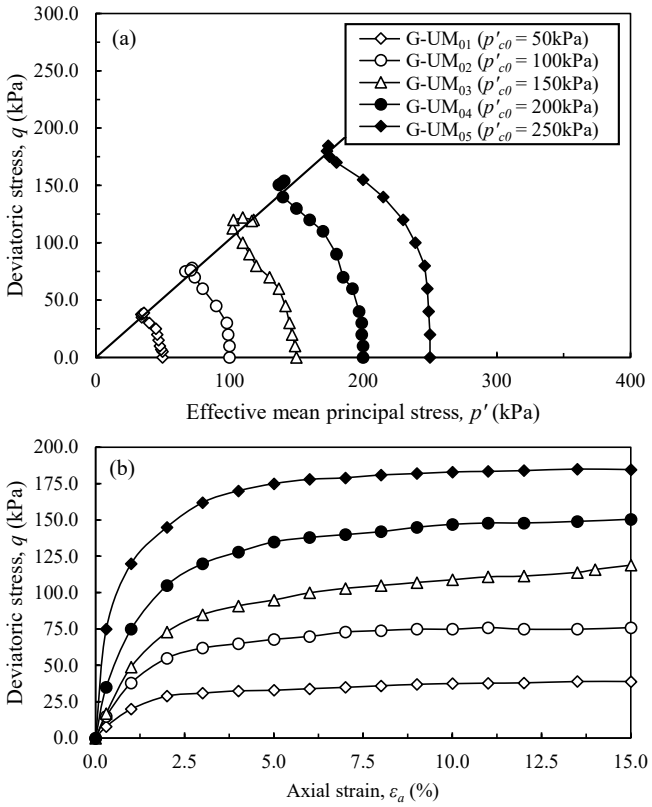

Figure 6.5: Undrained monotonic triaxial tests for Gault clay (a) q-p' space and (b) stress-strain response

Given the cyclic stress ratio adopted is a function on undrained shear strength,

this has been selected to be the consistent property for comparison against previous laboratory testing undertaken on kaolin. Subsequent tests on the cyclic performance of Gault clay samples were isotropically consolidated to a confining pressure of 150kPa.

6.1.3 Undrained Cyclic Triaxial Tests

Cyclic undrained triaxial tests were performed on the reconstituted Gault clay samples considering cyclic stress ratios of 0.4, 0.6, 0.8 and 0.9 with a test frequency of up to 5Hz, summarised in Table 6.3. A cyclic stress ratio of 0.9 was selected as the threshold cyclic stress ratio was found to be greater than 0.8. The results examining the cyclic stress ratio with respect to the number of cycles are presented in Figures 6.6 through to 6.9.

The results demonstrate a similar strain accumulation response to the previous studies presented so far for kaolinite. The equivalent kaolinite profile for a frequency of 1.0Hz at each cyclic stress ratio are shown by the grey dashed line on each figure for comparison. In comparison to the kaolinite samples, the axial strain response for the Gault clay samples is less than the equivalent kaolin sample. In conjunction with this, the normalised excess pore pressure response of the Gault clay samples is less. For instance, considering a cyclic stress ratio of 0.6, the normalised excess pore pressure generated during the cyclic loading of kaolinite was determined to be 0.43. For the Gault clay samples under the equivalent cyclic stress ratio, G-UM_{02} to G-UM_{04} for a frequency of 0.1Hz to 5.0Hz respectively, the normalised excess pore pressure response is 0.37.

Table 6.3: Summary of undrained cyclic (UC) triaxial tests undertaken on Gault clay samples

Sample Name:	Frequency (Hz)	CSR	Number of Cycles	Duration (min)	Failure
GUC_{01}	0.1	0.4	6000	1000	No
GUC_{02}	1.0	0.4	15000	250	No
GUC_{03}	5.0	0.4	30000	100	No
GUC_{04}	0.1	0.6	6000	1000	No
GUC_{05}	1.0	0.6	15000	250	No
GUC_{06}	5.0	0.6	30000	100	No
GUC_{07}	0.1	0.8	6000	1000	No
GUC_{08}	1.0	0.8	15000	250	No
GUC_{09}	5.0	0.8	30000	100	No
GUC_{10}	0.1	0.9	1800	289	Yes
GUC_{11}	1.0	0.9	11736	196	Yes
GUC_{12}	5.0	0.9	22400	75	Yes

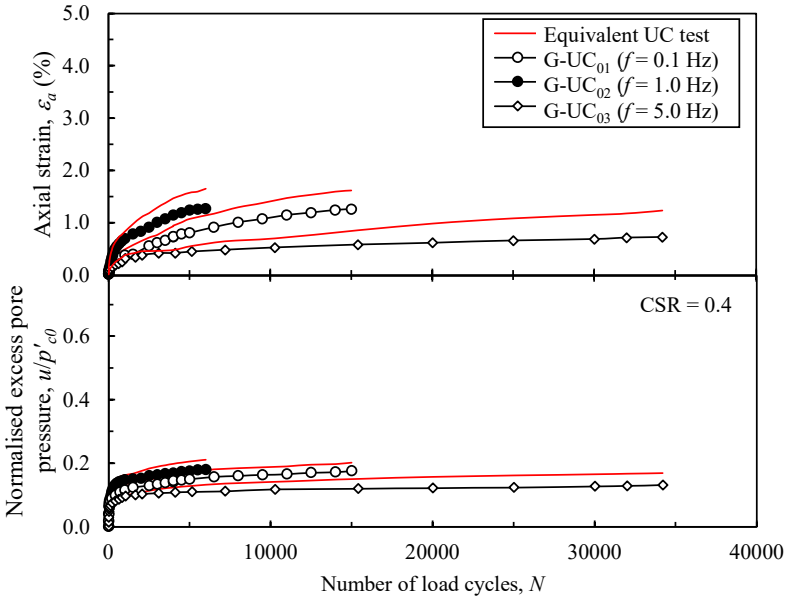

Figure 6.6: Development of axial strain and normalised excess pore pressure considering the number of load cycles for a cyclic stress ratio of 0.4

Figure 6.8 and 6.9 demonstrate the threshold cyclic stress ratio is greater than for that determined in Chapters 3 and 4 for the kaolinite samples. The threshold cyclic stress ratio for Gault Clay is determined to be between 0.8 and 0.9. This

conclusion supports the critical cyclic stress ratio determined by Pan et al. (2021) who determined a value of between 0.6 and 0.8 for samples with significant accumulation of axial strain and an unstable state. Recalculating the cyclic stress ratio from ($\Delta\sigma'_{cyc}/2p_0$) where $\Delta\sigma_{cyc}$ is defined as the vertical increment of cyclic stress applied to the sample, the cyclic stress as defined in the studies examined in Chapters 3 and 4 is between 0.7 and 0.9. Given the samples in this study were block samples, it is likely the higher cyclic threshold stress determined is given due to the uniformity of the reconstituted sample.

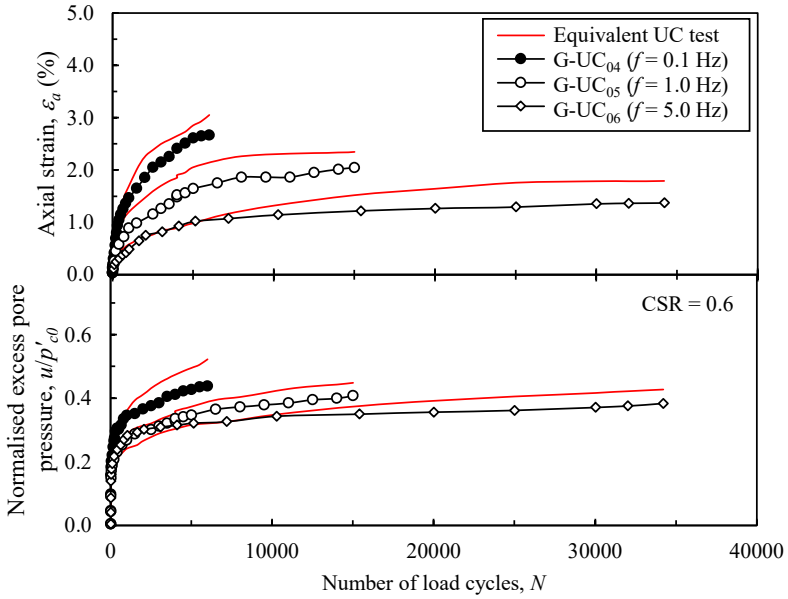

Figure 6.7: Development of axial strain and normalised excess pore pressure for Gault clay considering the number of load cycles for a cyclic stress ratio of 0.6

As such, the response of the Gault clay samples, with respect to the reduced accumulation of axial strain at a lower confining pressure to those of the kaolinite samples, whilst at the same cyclic stress ratio, given the same undrained shear strength of samples should be examined. It is important to note the Gault clay samples have a higher plasticity index. In the following sections within this Chapter, the influence of the plasticity index with respect to the soil response, degradation of the samples and resilient modulus will be presented alongside the practical implications for consideration in the field.

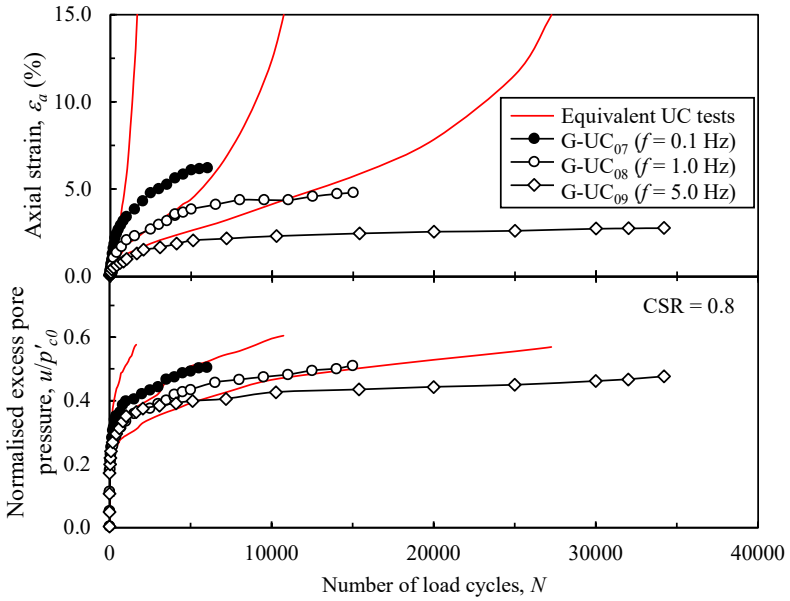

Figure 6.8: Development of axial strain and normalised excess pore pressure for Gault clay considering the number of load cycles for a cyclic stress ratio of 0.8

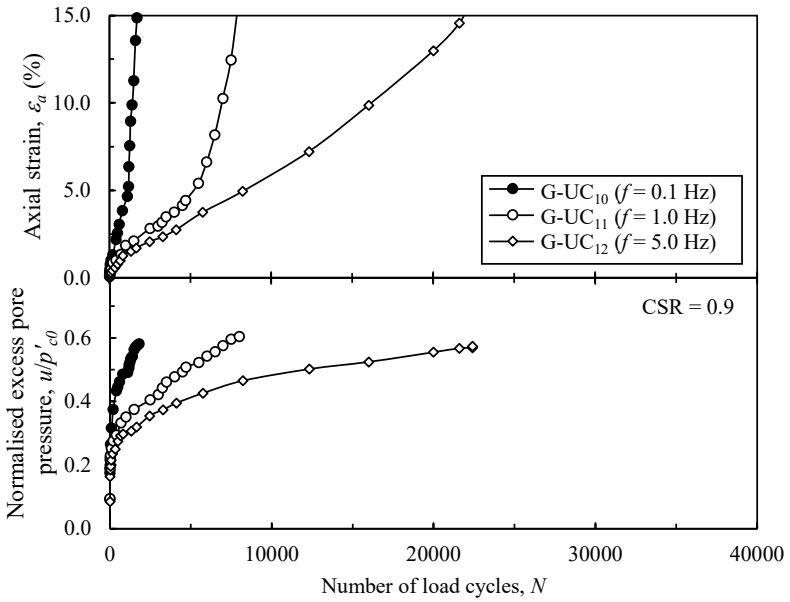

Figure 6.9: Development of axial strain and normalised excess pore pressure for Gault clay considering the number of load cycles for a cyclic stress ratio of 0.9

6.1.4 Examination of Sample Degradation

The response of the Gault clay samples illustrated in Section 6.1.3 shows for an equivalent cyclic stress ratio to that applied in kaolinite samples previously

examined, the generation of axial strain and excess pore pressure over the same number of load cycles is less. As such, the cyclic stiffness of the material is proposed to increase. This response has previously been acknowledged by Hyodo et al. (1999) whom demonstrated the cyclic stiffness of a clay increased with an increase in the plasticity index of the soil. Plasticity index has been shown by several authors (Vucetic and Dobry (1991), Hsu and Vucetic (2006) and Erken and Can Ulker (2007)) to be a key factor in the degradation of a sample under cyclic loading. Okur and Ansal (2007) examined a range of fine-grained soils ranging from a plasticity index of 9% to 40% under two-way cyclic loading. The authors concluded the damping ratio and subsequently the dynamic shear modulus of the soil were influenced by the plasticity index. The authors showed for stress-controlled tests, the elastic threshold for strain accumulation, and therefore cyclic degradation, was governed by the pore pressure response of the sample. A sample therefore degrades more with increased strain accumulation, resulting in particle breakdown and sample softening (Idriss et al. (1978)).

Idriss et al. (1978) originally proposed the concept of a degradation index, δ, whereby the change in shear modulus as a result of cyclic loading can be presented in terms of shear stresses. Subsequently, Mortezaie and Vucetic (2013) proposed for stress-controlled cyclic tests the degradation index could be rewritten, later proposed by Zhou and Gong (2001) as;

$$\delta = \frac{\frac{\sigma_r}{\epsilon_{a,N}}}{\frac{\sigma_r}{\epsilon_{a,1}}} = \frac{\epsilon_{a,1}}{\epsilon_{a,N}} \tag{6.1}$$

where $\epsilon_{a,1}$ is the cyclic strain in the first cycle of cyclic loading, remaining constant, whilst $\epsilon_{a,N}$ increases in the case of undrained cyclic tests. Therefore, as the number of cycles increases, the degradation index for stress-controlled tests, δ will decrease. Subsequently, the degradation parameter, t can be presented;

$$t = \frac{\log \delta}{\log N} \text{ or } \delta = N^{-t} \tag{6.2}$$

Authors have reported that for one way tests, such as those presented in this study, the degradation of samples is less than for two way tests where strain

reversal is permitted. Considering the above framework, the results for the kaolinite and Gault clay samples are presented with respect to the degradation index, δ determined considering the strain response from cyclic undrained triaxial tests.

Considering the degradation response with respect to the number of cycles of load, as the number of cycles increases, the degradation increases, shown in Figure 6.10. Similarly, as the cyclic stress ratio increases, the number of cycles to attain a degree of degradation decreases. As such, as the excess pore pressure generated in response to the applied the value of δ decreases, leading to greater degradation of the sample. Comparing the results of the Gault clay with respect to the kaolinite samples, the degradation of the Gault clay samples is less than for an equivalent kaolinite sample. Due to the higher plasticity of the Gault clay, the generation of excess pore pressure during cyclic loading is less, resulting in a decreased reduction in effective stress and greater resistance to cyclic loading. With respect to the plasticity of the samples, as the plasticity increases, the sample better attracts neighbouring particles forming clusters capable of withstanding greater magnitudes of cyclic loading. As such, a higher plasticity index, where the sample has a greater specific surface and generally a lower permeability, means the cyclic loads can be partially distributed to the water held within the soil skeleton resulting in reduced response to cyclic load. Similar conclusions were proposed by Soralump and Prasomsri (2016) whom suggested that for compacted clays, lower pore pressure generation occurred as a result of the soil structure having less capacity for converting volume reduction into a pore pressure response.

It was demonstrated in Chapter 4.2.3 that the response of a soil subjected to cyclic loading could be explained in terms of energy conservation. Considering the influence of plasticity on a sample and as identified above, the effect of plasticity on the inter particle forces responsible for the undrained cyclic response of the soil with respect to excess pore pressure accumulation and strain development, damping of the system must be considered in order conserve the energy of the system presented previously. As a result, the magnitude of plasticity index therefore governs the damping of the system,

previously identified by Okur and Ansal (2007), whereby as the plasticity index increases, the damping ratio of the system decreases.

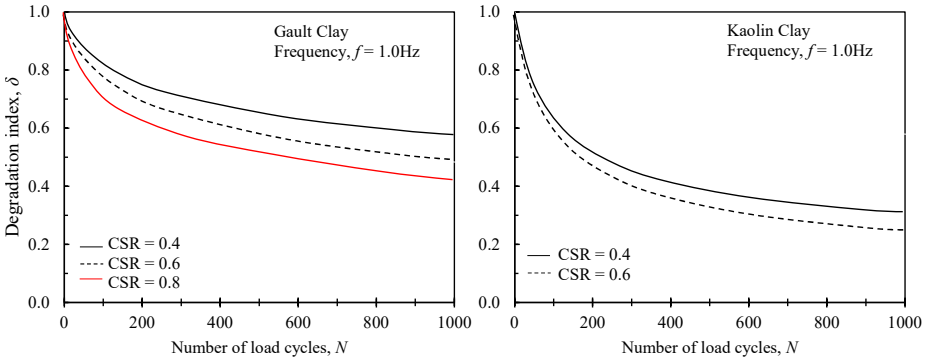

Figure 6.10: Degradation of Gault clay and kaolinite samples under cyclic loading for varying cyclic stress ratios

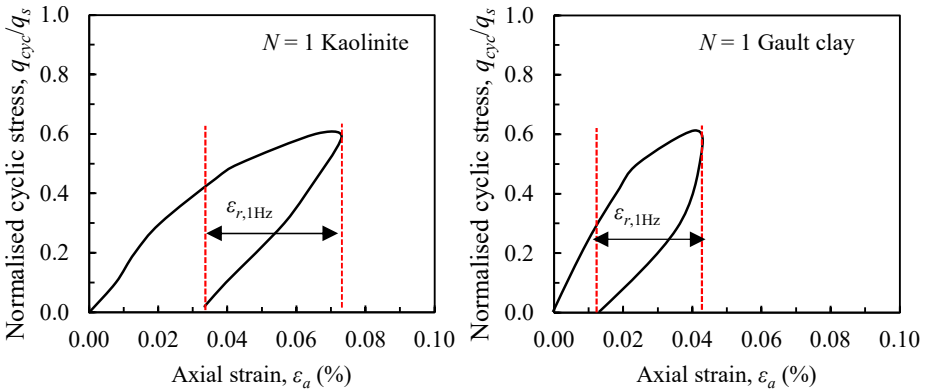

Figure 6.11: Components of non-recoverable plastic and resilient elastic strain for a single load cycle for Gault clay and kaolin samples

The damping ratio is defined as the ratio between the dissipated strain energy and elastic strain energy in a cyclic of loading. In accordance with ASTM standards, the damping ratio can be calculated from the area of the stress strain hysteresis loop, A_{loop}, representing the dissipated energy, and a triangular portion of the hysteresis loop, A_{Δ}, shown in Figure 6.12, representing the peak energy attained in one load cycle and calculated via;

$$D = \frac{A_{loop}}{\pi A_{\Delta}} \tag{6.3}$$

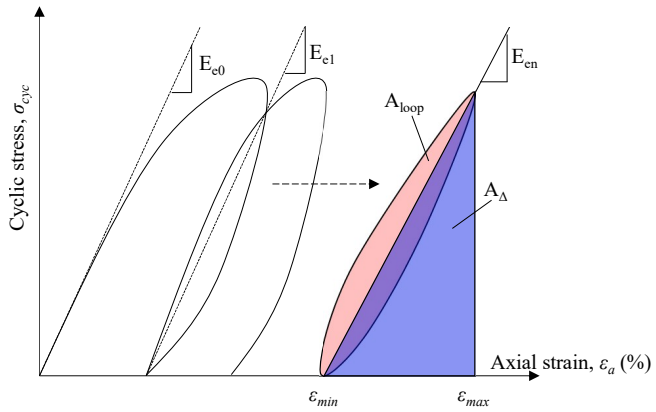

Figure 6.12: Determination of elastic modulus, dynamic shear modulus and damping ratio

Examining the response of the first load cycle for Gault clay against that of the previous kaolinite samples, there are two considerations. The first is the shape of the cycle, where the lower plasticity kaolin sample cycle is flatter and more extended than that of the Gault clay sample, suggesting the high plasticity sample has a greater resilient or recoverable strain. Although the Gault clay has less resilient strain development during one cycle in terms of magnitude, as a total of the cycle strain, a greater proportion of the strain is recoverable compared to the lower plasticity sample. Tafili et al. (2021) concluded a similar response for undrained cyclic strain controlled triaxial tests, demonstrating greater pore pressure accumulation occurred for kaolinite samples over Lower Rhine clay samples of high plasticity. The hysteretic loops examined by the authors showed the lower plasticity samples of kaolin were flatter when compared to the high plasticity clay, suggesting the high plasticity samples had a greater recoverable strain portion.

This is further demonstrated considering the damping of the system with respect to Equation 6.3. For the kaolinite sample, the damping ratio is determined to be 6.14% whilst for the Gault clay sample, the ratio is 5.94%, supporting the conclusion of Okur and Ansal (2007). As such, under the same applied load, and therefore energy applied to the sample, for a low plasticity clay, greater damping occurs such that the soil skeleton deforms in response to the load and greater degradation occurs. For the Gault clay, instead due to the higher

plasticity, a greater proportion of the load is taken by the water within the soil skeleton, inhibiting axial strain and excess pore pressure generation.

6.1.5 Examination of Post-Cyclic Response

Chapter 4 demonstrated the post-cyclic response of the sample when considered with drainage and full reconsolidation, was akin to the response of a partially drained soil. When drainage was not permitted and the sample sheared following undrained cyclic loading, the strength of the sample decreased. Figure 6.14 shows the results of Gault clay samples sheared without reconsolidation considering a frequency of 1.0Hz. These samples are initially sheared from a higher confining pressure compared to the kaolinite samples previously examined, given the increased resistance to cyclic loading when compared to the lower plasticity samples. The decrease in post-cyclic strength of the Gault clay is summarised in Table 6.4 for the samples for comparison against the equivalent CSR for kaolinite samples.

Table 6.4: Summary of strength reduction in undrained post-cyclic tests of Gault clay and kaolinite samples

Sample Name:	CSR	Strength reduction	Sample Name:	CSR	Strength reduction
GUC_{02}	0.4	6.35%	UC_{02}	0.4	12.50%
GUC_{05}	0.6	16.31%	UC_{07}	0.6	16.67%
GUC_{08}	0.8	21.61%			

For samples where drainage was permitted, considering full reconsolidation, the results of post-cyclic undrained shear strength are presented in Figure 6.14. For an increase in cyclic stress ratio, and therefore cyclic deviator stress applied to the sample, the post-cyclic strength increases as previously demonstrated for the kaolinite samples. However, for a given cyclic stress ratio, the increase in the post-cyclic strength attainment of the Gault clay, summarised in Table 6.5, appears to be less than for the kaolinite samples. This could be considered to be in contrast to expected due to the gault samples exhibiting less degradation when compared to the kaolinite clay samples, however given under cyclic loading the initial structure degrades and the subsequent drainage permits

particle rearrangement, it is proposed that less degradation, and less generation of excess pore pressure, results in less dissipation during reconsolidation and therefore the resulting strength attained following a drainage period is less. The two different responses considering drainage and no drainage are shown in Figure 6.15.

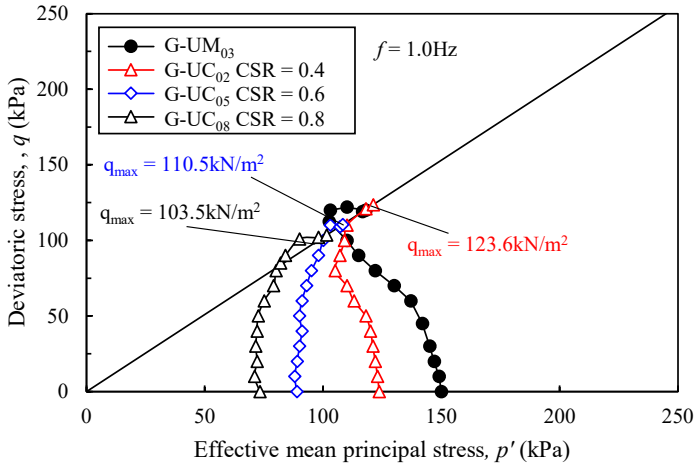

Figure 6.13: Post-cyclic monotonic triaxial test $q - p'$ plot for Gault clay without drainage

Table 6.5: Summary of strength increase in post-cyclic tests of Gault clay and kaolinite samples where recompression is permitted prior to shearing

Sample Name:	CSR	Strength increase	Sample Name:	CSR	Strength increase
GUC_{02}	0.4	3.33%	UC_{02}	0.4	7.00%
GUC_{05}	0.6	9.50%	UC_{07}	0.6	18.3 %
GUC_{07}	0.8	13.7%			

Yasuhara et al. (1988) proposed the following equation considering the strength change as a ratio to the monotonic undrained shear strength of the material, rewritten to consider the undrained strength following post-cyclic drainage in proportion to the amount of excess pore pressure developed during cyclic loading;

$$\frac{c_{ud,cyc}}{c_u} = \left[\frac{1}{1 - \frac{\Delta u}{p'_{c0}}}\right]^{\frac{\Lambda_0 \frac{C_s}{C_c}}{1 - \frac{C_s}{C_c}}} \tag{6.4}$$

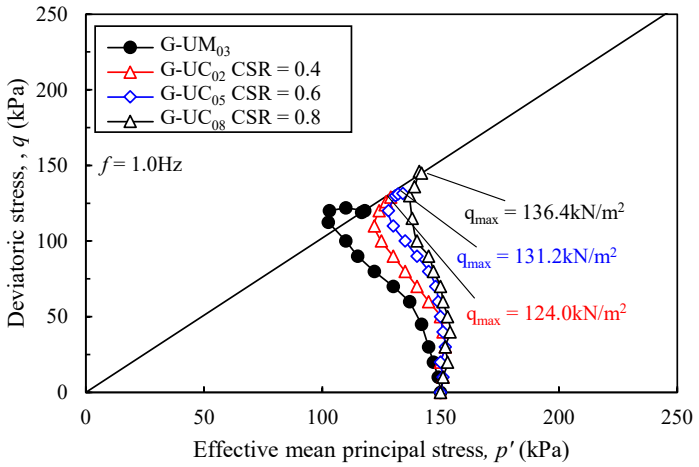

Figure 6.14: Post-cyclic monotonic triaxial test $q - p'$ plot for Gault clay with drainage

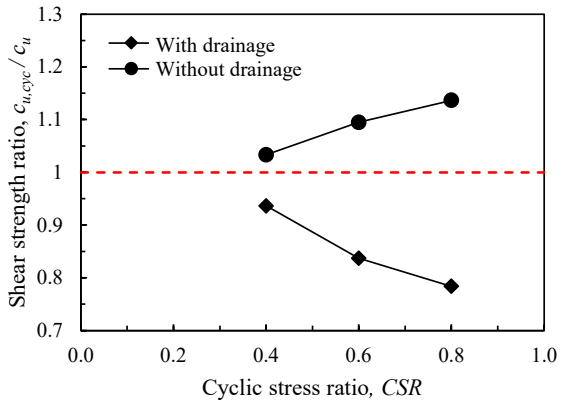

Figure 6.15: Influence of CSR on shear strength ratio for both samples sheared with and without drainage

Considering the undrained strength of the post-cyclic kaolinite samples following drainage, the value of Λ was determined in Chapter 4.2.4 for these samples. Considering the same relationship for the Gault Clay, the value of Λ_0 shown to best fit the undrained shear strength, shown in Figure 6.16, is between 0.5 and 0.6.

This is an important note for practical construction considerations, whilst when exposed to undrained cyclic loading high plasticity clays appear more resistant to axial strain accumulation. Subsequent to a drainage period that would be expected to occur in the field, the strength attained is less than for low plasticity samples, resulting in a softer material in comparison.

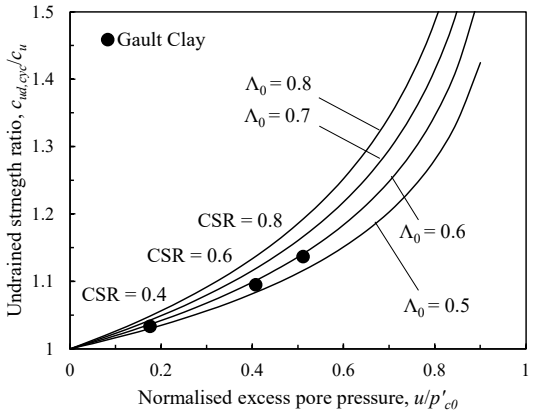

Figure 6.16: Relationship between undrained strength ratio and the normalised excess pore pressure accumulation for Gault clay considering drainage

6.2 Cyclic Model Prediction

The model presented in Chapter 5 has been used to predict the response of the high plasticity Gault clay, as well as contrasting the response of both a high and low plasticity clay.

The results predicting the partially drained response of the Gault clay samples are presented in Figure 6.18, contrasted against the response of volumetric strain and pore pressure development obtained from the previous undrained cyclic loading followed by drained reconsolidation. In practice, due to the low permeability of the sample and high plasticity, performing partially drained triaxial tests was not feasible and samples attained a liquified state due to test limitations. Considering the model prediction therefore, the model shows good agreement with the excess pore pressure generated during undrained cyclic loading. The partially drained excess pore pressure response determined from the model is also presented and the corresponding volumetric strain determined. The volumetric strain at low values of cyclic stress ratio shows close agreement to that determined from the equivalent post-cyclic drained recompression, presented in in Figure 6.17. However, as the cyclic stress ratio increases, the prediction of volumetric strain from the model is less than that

determined from drained recompression.

A consideration with respect to the model, is the coefficient of volume compressibility and the permeability of the soil. The values adopted in the prediction of the Gault clay are shown in Table 6.6. As c_v, and therefore permeability, inhibit the dissipation with respect to time, the volumetric strain determined from the model diverges from the equivalent static recompression strain as the magnitude of initial excess pore pressure increases. It should be noted the prediction is given at 30,000 cycles, which is approximately 8.0 hours of loading, whilst the recompression was permitted over 24 hours. This explains why for low cyclic stress ratio, with therefore less dissipation required in recompression, the predictions are comparable whilst at the reference number of cycles given in the prediction for higher cyclic stress ratios, total recompression and therefore dissipation of pore pressure has not occurred.

Table 6.6: Summary of UC test parameters for undrained cyclic model

p'_0	p'_{c0}	c_v	λ	κ	M	f
150kPa	150kPa	0.01m^2/day	0.204	0.050	0.98	0.1Hz

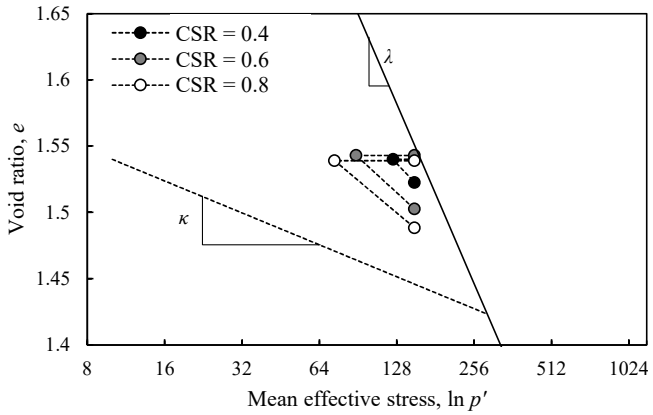

Figure 6.17: Change in void ratio during reconsolidation for Gault Clay samples

This also explains the findings presented in Section 4.3.5 with respect to the undrained strength of the material following reconsolidation. Whilst less excess pore pressure is dissipated when compared to the kaolinite samples, the samples undergo a greater decrease in void ratio due to the higher coefficient of compression. However, samples reconsolidate from a greater void ratio such

that the reconsolidated sample is less dense than the samples examined in Chapters 3 and 4. As such, it is less resistant to the load subsequently applied and attains a lower degree of undrained shear strength improvement.

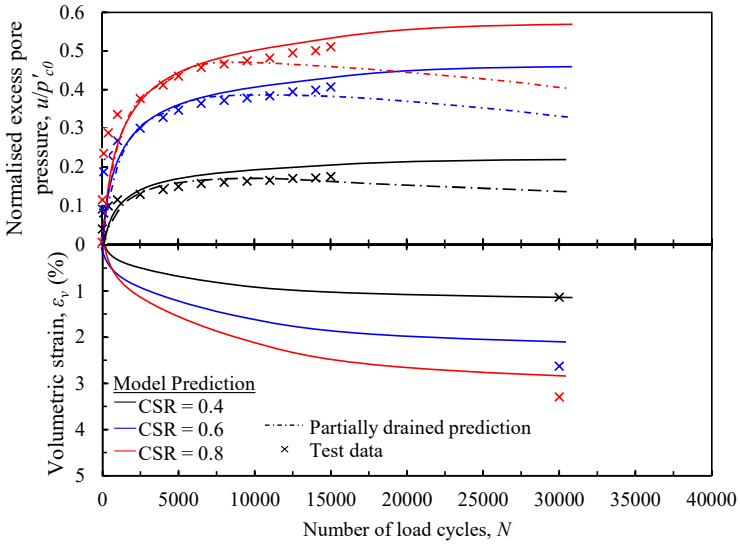

Figure 6.18: Results of the undrained and partially drained model prediction for cyclic loading of the Gault clay samples

Table 6.7: Summary of post-cyclic undrained shear triaxial tests undertaken on Gault clay samples

Sample	CSR	Volumetric strain, ϵ_v	
		Undrained Drained Test	Empirical Calculation
G-UCR$_{01}$	0.4	1.13%	1.11%
G-UCR$_{02}$	0.6	2.62%	2.58%
G-UCR$_{04}$	0.8	3.29%	3.24%

As presented in Equation 4.20, the volumetric strain could be determined from only the excess pore pressure response of a sample in undrained cyclic loading. From assessment against the model prediction, it is proposed this should be the limit to which the volumetric strain tends to. The calculated volumetric strain is presented in Table 6.7, showing close agreement with the recompression tests for total excess pore pressure dissipation.

6.2.1 Influence of Plasticity Index

As presented by Vucetic and Dobry (1988), the plasticity index of a soil defines the amount of water required to transform a soil from semi-solid to liquid state. The authors demonstrated the plasticity index played an important role on the cyclic response of marine clays, dependent on the soil composition. A high plasticity clay is typically characterised by an high void ratio and a greater coefficient of compression. Several empirical correlations to describe the relationship between the coefficient of compression and the plasticity index and liquid limit of a soil are presented in Table 6.8 and the relationships demonstrated in Figure 6.19, where I_p = 0.73(w_L - 0.2).

Table 6.8: Summary of correlations between compression index and plasticity index

Reference	Correlation	Applicability
Skempton and Jones (1944)	$C_c = 0.007(w_L - 10)$	Remoulded clays
Hough (1957)	$C_c = 0.29(e_0 - 0.27)$	Inorganic cohesive silts and clays
Terzaghi and Peck (1967)	$C_c = 0.009(w_L - 10)$	All clays
Azzouz et al. (1976)	$C_c = 0.37(e_0 + 0.003w_L - 0.34)$	All clays
Mayne (1980)	$C_c = 0.0072(I_p + 26)$	All clays
Koppula (1981)	$C_c = 1.325I_p$	Remoulded clays
Jain and Dixit	$C_c = 0.0082I_p + 0.0475$	River deposits

In this study, the performance of the model with respect to input parameters that are influenced by the plasticity index, are presented based on an existing case study, and subsequently extended to examine the partially drained response prediction.

Further extending the analysis to consider a high plasticity and low plasticity sample, the higher plasticity sample transfers a greater proportion of the cyclic load to the water trapped within the soil volume, as demonstrated by the Gault clay samples. These cohesive forces are a function of the plasticity, and subsequently therefore governed in the model by the coefficient of volume compressibility, initial void ratio of the sample and importantly the permeability.

Considering the studies undertaken by Prakasha and Chandrasekaran (2005), various sand mixes were analysed under cyclic triaxial testing, the inclusion of a clay fraction resulted in an increase in plasticity index and an increase in the compression index properties for the marine soils examined. A summary of the index properties determined by the authors for the various mixtures are summarised in Table 6.9.

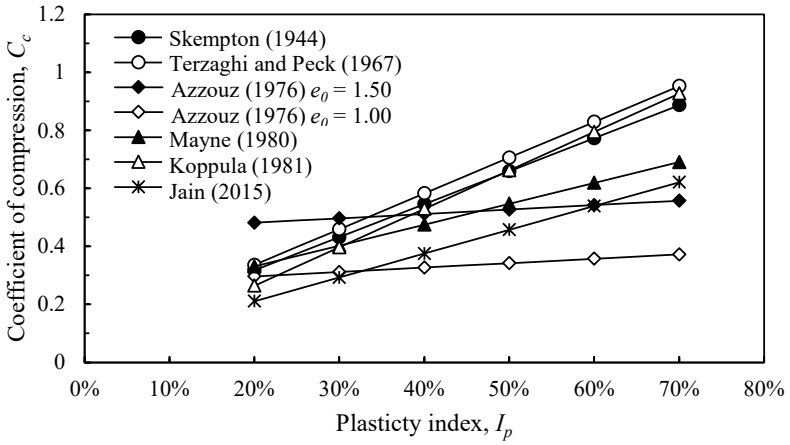

Figure 6.19: Summary of correlations between compression index and plasticity index

Table 6.9: Summary of marine clay index properties, after Prakasha and Chandrasekaran (2005)

Sand / Clay	I_p	c_v	λ	κ
50% / 50%	30	0.026 m^2/day	0.207	0.013
30% / 70%	38	0.007 m^2/day	0.255	0.022
10% / 90%	50	0.006 m^2/day	0.345	0.030
0% / 100%	57	0.002 m^2/day	0.376	0.038

The response of the normalised excess pore pressure and axial strain generated under undrained conditions for varying plasticity indices is presented in Figure 6.20, against the response of the undrained cyclic model. The prediction shows good agreement with the axial strain accumulation of the marine clay tests performed by the authors. For the sample with only 50% clay content, the results show the prediction of failure is achieved however the number of cycles prior to failure is greater than observed in the test. The excess pore pressure response is typically lower than from the triaxial tests, however as demonstrated in Figure 6.21 the excess pore pressure response of the model prediction takes

longer than the initial 160 cycles in Figure 6.20 to converge.

Figure 6.21 presented the prediction of excess pore pressure, both considering the undrained model and partially drained extension. The response is compared to a similar prediction for the partially drained model presented by Paul et al. (2020). Examined in greater detail, and normalised with respect to σ_c as presented in the study under consideration, the partially drained model predicts a similar response to the Paul model with respect to trend for increasing plasticity index. As the index increases, the initial accumulation of excess pore pressure decreases. Subsequently the dissipation of excess pore pressure is also inhibited and in comparison to the peak value of excess pore pressure generated, less dissipation occurs.

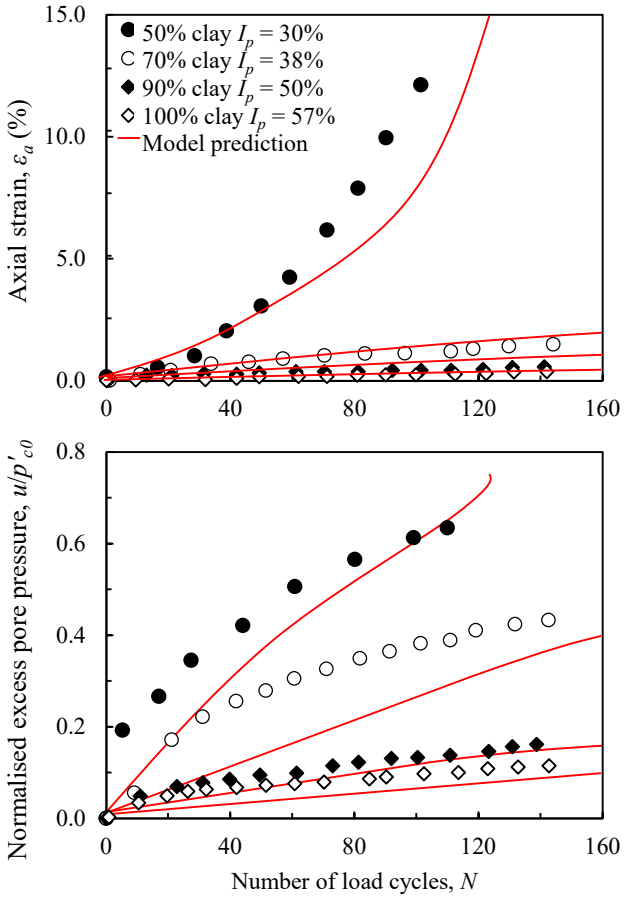

Figure 6.20: Undrained cyclic model prediction for axial strain accumulation and normalised excess pore pressure response for marine clay samples, f = 1.0Hz, CSR (τ/σ_c) = 0.147, after Prakasha and Chandrasekaran (2005), for varying plasticity indices

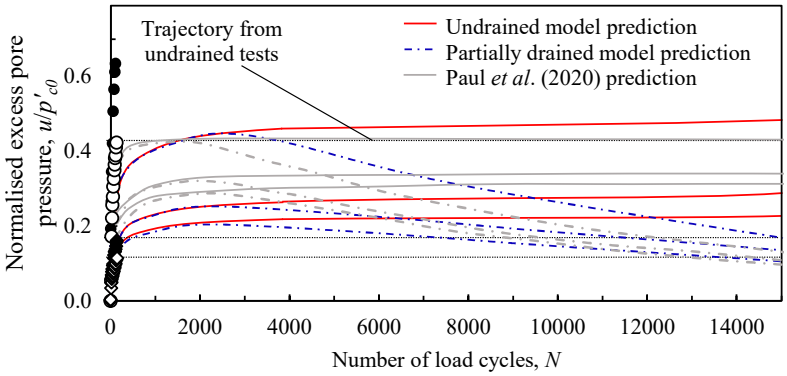

Figure 6.21: Undrained and partially drained excess pore pressure prediction for varying plasticity indices based on initial properties of Prakasha and Chandrasekaran (2005)

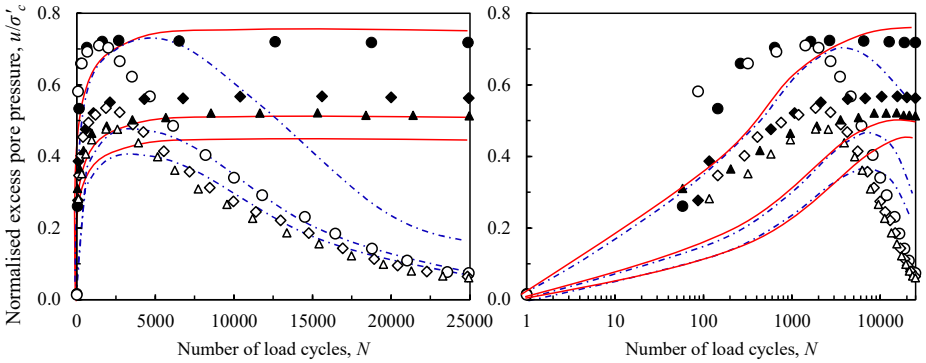

Figure 6.22: Undrained and partially drained excess pore pressure prediction, normalised with respect to σ_c for varying plasticity indices, compared to the pore pressure predictions of Paul et al. (2020)

6.3 Consideration of Degree of Reconsolidation

So far, the analysis presented with respect to partially drained conditions and post-cyclic attainment of strength has considered full reconsolidation prior to shearing or no reconsolidation. However, in the field, and particularly considering the clay samples under consideration whereby recompression to dissipate the total excess pore pressures that accumulate during undrained cyclic loading can be long, this is not a practical consideration. As demonstrated in the analysis of the Gault clay samples, the results for the prediction of volumetric strain considering full reconsolidation were greater than from the model prediction where at 30,000 cycles, less dissipation had occurred. As a result, a series of post-cyclic undrained shear strength tests have

been performed for a range of degrees of reconsolidation, at 25%, 50% and 75%. The tests are summarised in Table 6.10, with the corresponding undrained shear strength determined. All results were performed on the Gault Clay samples with a cyclic stress ratio of 0.6 and a frequency of 1.0Hz.

In order to achieve the degree of reconsolidation, U, adopted in the triaxial tests, a back pressure was subsequently applied following undrained loading such that;

$$U = 1 - \frac{p_{back}}{\Delta u_{cyc}} \tag{6.5}$$

Table 6.10: Summary of strength reduction in undrained post-cyclic tests of Gault clay and kaolinite samples

Sample Name:	CSR	Degree of reconsolidation, U	Undrained shear strength, c_u
G-UCR$_{01}$	0.6	0%	55.2kPa
G-UCR$_{02}$	0.6	25%	56.2kPa
G-UCR$_{03}$	0.6	50%	58.4kPa
G-UCR$_{04}$	0.6	75%	60.2kPa
G-UCR$_{05}$	0.6	100%	65.6kPa

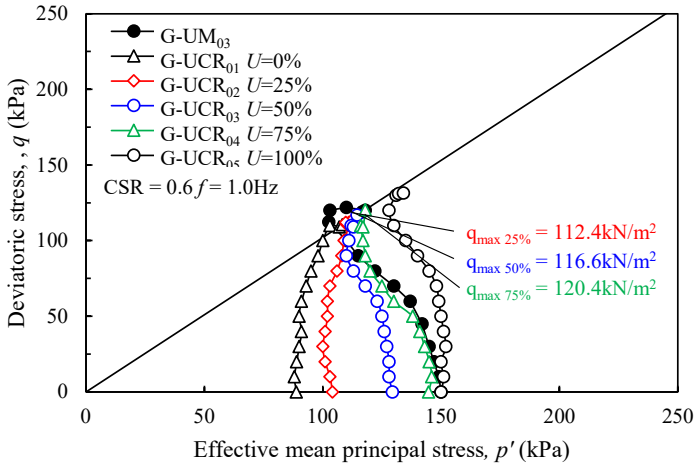

Figure 6.23: Stress path plots for Gault clay considering degree of reconsolidation for post-cyclic shearing

The results of the post-cyclic shear tests performed following cyclic loading and

reconsolidation to a specified degree are presented in Figure 6.23. The results demonstrate that as the degree of reconsolidation increases, the undrained shear strength of the Gault clay increases. This is further demonstrated in Figure 6.24, where roughly 75% reconsolidation would need to be achieved prior to shearing to attain the sample undrained shear strength prior to cyclic loading such that the cyclic loading has a negligible impact on the strength of the sample.

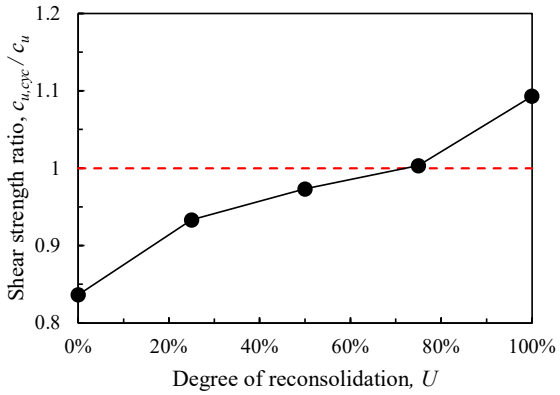

Figure 6.24: Influence of degree of reconsolidation on the shear strength ratio

6.4 Consideration of Loading Intervals

The studies so far have considered a constant duration of cyclic load followed by post-cyclic monotonic shearing. In reality, a period of cyclic load followed by a period of rest is more characteristic of traffic loading. Given the strength response of the Gault clay samples following various degrees of reconsolidation, this is therefore an important consideration. A series of stop-start triaxial tests have been performed for the Gault clay samples, summarised in Table 6.11.

Samples SS_{01} through to SS_{03} examine the influence of duration of load and rest considering a constant total time period and a constant cyclic stress ratio of 0.6 at a frequency of 1.0Hz, whilst SS_{04} and SS_{05} consider the response of stop-start loading varying the cyclic stress ratio between consecutive load intervals. A total load period of 1 hour was chosen in order to determine any distinct effect due to a drainage period duration.

Table 6.11: Summary of stop-start triaxial tests

Sample Name:	Load Duration	CSR
SS_{01}	10 min / 50 min	0.6
SS_{02}	30 min / 30 min	0.6
SS_{03}	50 min / 10 min	0.6
SS_{04}	30 min / 30 min	0.6 / 0.8
SS_{05}	30 min / 30 min	0.6 / 0.4

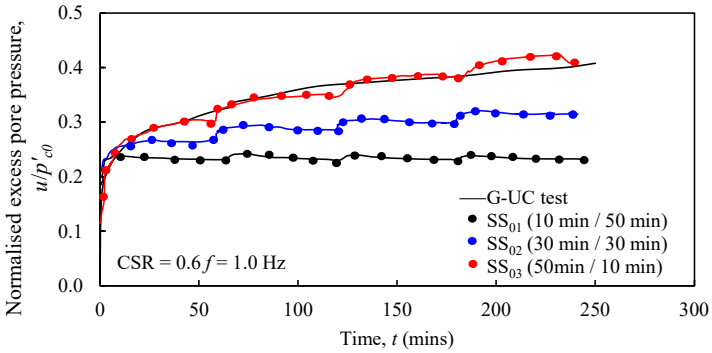

Figure 6.25: Influence of variation in drainage period for intermittent cyclic loading

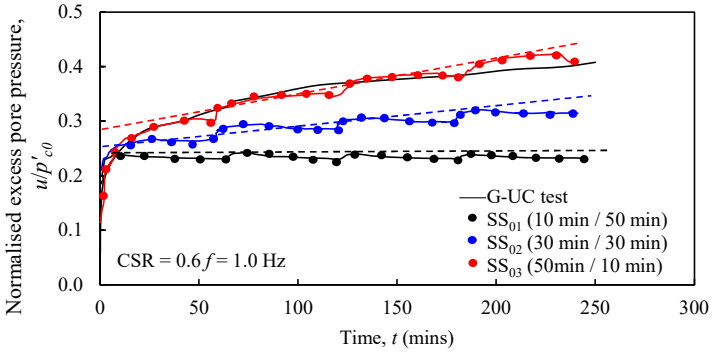

Figure 6.26: Influence of variation in drainage period for stop-start cyclic loading, considering gradients

The response of the normalised excess pore pressure for samples SS_{01} to SS_{03} is presented in Figure 6.25. The initial increase in load response is similar to that of the undrained cyclic test performed on the Gault clay. For sample SS_{01} with the shortest load duration compared to drainage period, the increase in excess pore pressure gradually tends away from the undrained response, due to there being greater time for dissipation of excess pore pressure. Subsequently, as greater reconsolidation has occurred in comparison to the other samples,

the sample is much denser and more resistant to subsequent pore pressure accumulation. This is further demonstrated by the dashed gradient of peak pore pressure response presented in Figure 6.26. All samples undergo an increase in axial strain as the strength attainment during drainage is less than the 75% previously identified as the threshold for cyclic strength increase in Figure 6.24. As the period of load, relative to the period of drainage, increases, the peak in pore pressure generated in response to subsequent loading becomes more distinct and the decrease due to dissipation during drainage is less.

Considering the pore pressure dissipation response, the seepage velocity i of the Gault clay samples after Darcy can be examined. Equation 6.6 presents the time for a water particle to pass through the drainage path, after Tafili et al. (2021);

$$v = ki = k\frac{H}{D_{50}} \tag{6.6}$$

$$t_{min} = \frac{D_{50}}{v} \tag{6.7}$$

where D_{50} is the average grain size, such that 50% of particles pass, in this case 0.0018mm. k is the permeability of the Gault clay, proposed to range between 2.60 x 10^{-11}m/s to 12.70 x 10^{-11}m/s at a confining pressure of 100 - 150kPa in accordance with Forster et al. (1994). For 6.8m depth, the permeability was given as 12.70 x 10^{-11}m/s such that the velocity can be determined between 2.5 x 10^{-6}m/s and therefore t_{min} is 12.2 minutes. Considering this as the minimum time required for a water particle to drain, this helps to explain the gradient change between profiles in Figure 6.26, such that when the drainage is 50 minutes, (SS_{01}) the pore water has started to drain whilst as the time decreases, greater accumulation occurs in subsequent cycles.

The results of the three tests suggest that considering the load-no load duration influences the excess pore pressure accumulation, however these responses are such that the undrained test, and prediction, would generally represent an upper bound case whilst the partially drained model prediction would, following a number of load cycles be a lower bound solution.

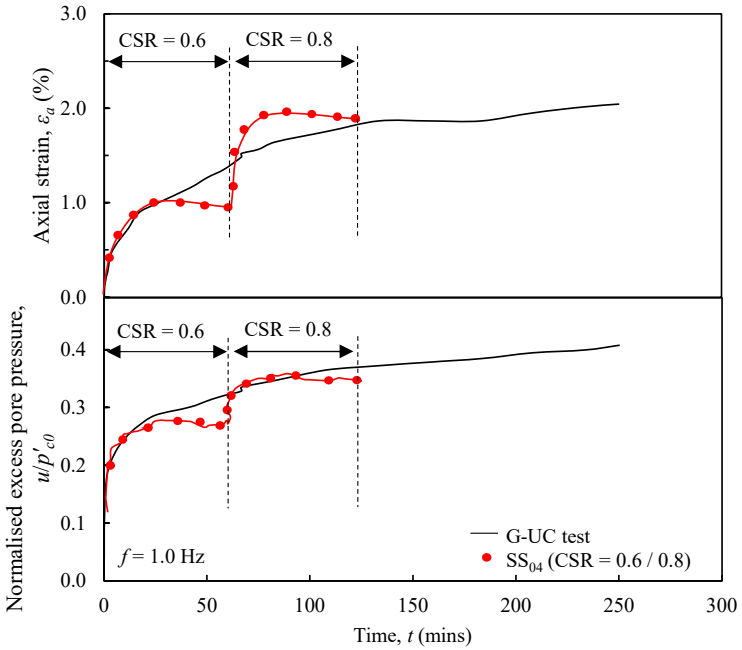

Figure 6.27: Influence of increasing cyclic stress ratio for stop-start loading

Considering the response of SS_{04} and SS_{05}, where a period of cyclic load with a cyclic stress ratio of 0.6 was followed by a period with a cyclic stress ratio of 0.8 and 0.4 respectively, the change in excess pore pressure response and axial strain are presented in Figures 6.27 and 6.28. For sample SS_{04}, where the subsequent load period had a cyclic stress ratio of 0.8, the axial strain and excess pore pressure both increase by an amount greater than observed for sample SS_{02} considering a constant cyclic stress ratio of 0.6. Although compared to the undrained test the samples have a greater strength, a greater cyclic stress ratio results in a greater excess pore pressure generation. However, in comparison to the equivalent strain for a cyclic stress ratio of 0.8, the accumulation is less. As such, incrementally increasing the cyclic stress ratio reduces the anticipated axial strain compared to a direct application of a high CSR. For Figure 6.28 where the CSR of 0.4 was applied during the second period, the excess pore pressure response is reduced, and the axial strain less than the equivalent undrained sample. During the second stage, less loading is applied compared to the first period. Therefore there is better performance with respect to excess pore pressure dissipation during drainage.

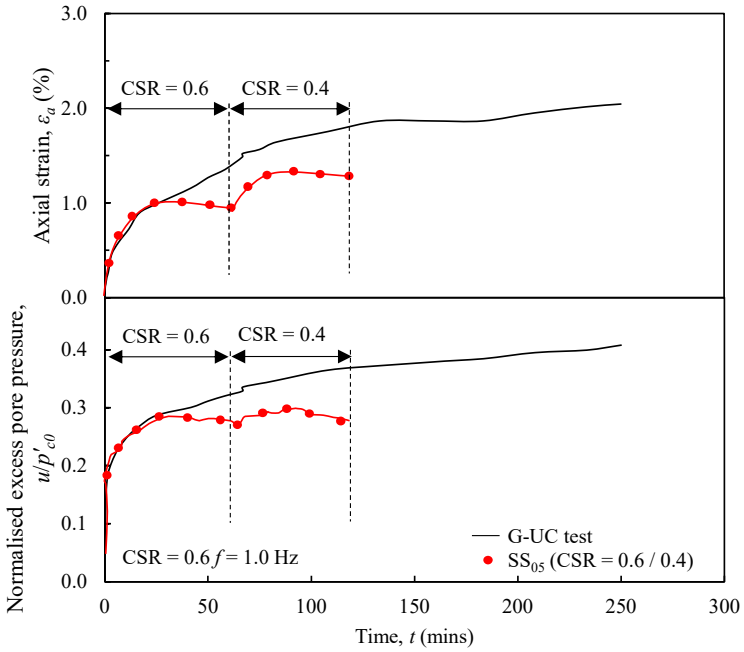

Figure 6.28: Influence of decreasing cyclic stress ratio for stop-start loading

6.4.1 Examination of Resilient Modulus

The cyclic triaxial tests performed on the kaolinite and Gault clay samples have demonstrated that the application of a cyclic load leads to softening of the sample. Several authors (Drumm et al. (1997), Gu et al. (2016)) have demonstrated that rather than considering the strength attainment of the sample post cyclic load, in fact the soil modulus decrease is greater. The inclusion of a drainage period however results in a strengthening effect for the normally consolidated Gault clay samples such that there is greater resistance to subsequent undrained cyclic loading. Examining samples SS_{04} and SS_{05} the response can be discussed in terms of the stiffness of the samples.

Figure 6.29 presents the first cycle of load for the first load interval of 1 Hz with a cyclic stress ratio of 0.6. The results present the three cases considered for 30 minutes loading followed by 30 minutes of drainage. As drainage is permitted, a degree of reconsolidation occurs prior to the second hysteretic loop shown in each plot in red. As such the stiffness of the sample at start of the second period of load is greater than at the end of the first period of loading.

Table 6.12 summarises the stiffnesses of the three cases presented. For SS_{03}, applying the same magnitude of load, the loop is more closed showing less plastic strain and greater stiffness and resistance to load in the second period. Considering SS_{04} there is a stiffness decrease, as the load applied is greater than previously experienced. However, the increases stiffness at the end of the first load period reduces the effect of this applied load increase. For a reduced load in the final period, the stiffness is greatly improved and the axial strain accumulation significantly less, reflecting the response observed in Figure 6.28.

Table 6.12: Summary of resilient modulus for samples considering loading intervals of varying cyclic stress ratio

Sample Name:	CSR	Stiffness	% Original Stiffness
SS_{03}	0.6 / 0.6	277MPa	11% increase
SS_{04}	0.6 / 0.8	223MPa	10% decrease
SS_{05}	0.6 / 0.4	369MPa	48% increase

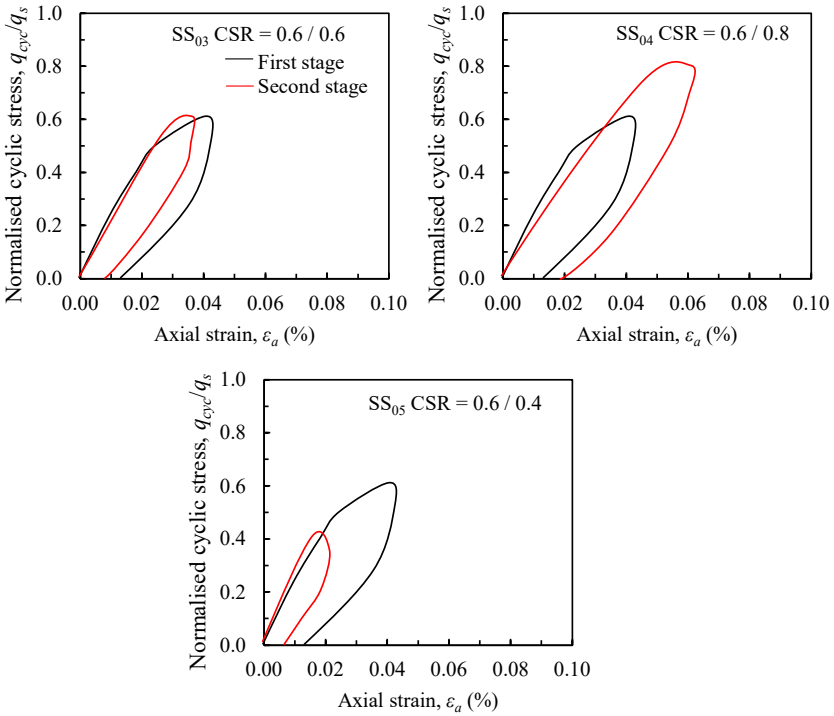

Figure 6.29: Influence of stop start loading with varying cyclic stress ratio

6.5 Conclusions

The response of the Gault clay has been examined, based on reconstituted samples prepared from site excavated bulk samples provided by HS2 Ltd. Considering the response determined from cyclic loading performed on kaolin samples, the response has been compared and the difference in response examined.

- The Gault clay is characterised as a high plasticity silty clay. Undrained monotonic tests demonstrated the samples attained a greater strength under the same confining pressure as the kaolin samples. The cyclic stress ratio adopted in the cyclic triaxial tests considered in this Chapter has been applied to samples confined to a stress such that the same deviatoric stress at static failure is achieved.
- Cyclic undrained triaxial tests performed on the Gault clay demonstrated less axial strain and excess pore pressure response compared to the kaolin samples. As a result, a greater cyclic stress ratio could be applied to the samples prior to failure. The critical cyclic stress ratio for the Gault clay exists between 0.8 and 0.9.
- The degradation of both kaolin and Gault samples has been examined. The degradation of a sample has been demonstrated by several authors (Idriss et al. (1978) and Vucetic (1984)) to be influenced by the plasticity index of the soil. As the cyclic stress ratio applied to a sample increases, the degradation index at a given number of cycles increases. Due to the higher plasticity of the Gault clay, the excess pore pressure generated under cyclic loading is less, resulting in greater resistance to load. As the plasticity of a sample increases, greater attraction between neighbouring particles occurs, distributing the load rather than accumulation excess pore pressures.
- Further assessment of the hysteretic loops demonstrate greater damping occurs in kaolin samples, whilst for the Gault clay a greater proportion of the total strain generation for one cycle is elastic and therefore recoverable.

- Two series of post-cyclic monotonic undrained triaxial tests have been performed. Considering undrained tests with no drainage period, a decrease in the post-cyclic strength is attained following cyclic loading. As the sample is loaded following cyclic loading, the Gault clay samples are loaded from a greater initial pressure, due to less excess pore pressure accumulation during cyclic load, such that less strength reduction occurs compared to the kaolin samples. As the cyclic stress ratio applied to a sample increases, the cyclic strength ratio decreases.

- However, when drainage is permitted, the strength increase due to permitting reconsolidation is also less than that determined for kaolin samples. As less degradation occurs during cyclic loading, less reconsolidation also happens, such that the sample is less dense and the strength attainment is therefore reduced. As the cyclic stress ratio applied to a sample increases, the cyclic strength ratio increases.

- The cyclic model presented in Chapter 5 shows good agreement with the results of the Gault clay samples. The partially drained response shows less volumetric strain accumulation than that determined from recompression tests where drainage was permitted. It is likely therefore that the duration for 100% reconsolidation was greater than the duration presented in the cyclic model. Further analyses studying case studies for varying plasticity demonstrated agreement with the model prediction under partially drained conditions.

- The degree of reconsolidation has also been examined. Approximately 75% reconsolidation would be required in order for a cyclically loaded sample to attain the equivalent strength as a monotonic test. This is an important consideration for clay soils such that the partially drained model could be considered a lower bound solution and in fact the response under cyclic loading for clay exists somewhere between undrained and partially drained given the duration for reconsolidation.

- Further considering stop-start loading, where durations of no-load were permitted, a series of undrained cyclic triaxial tests were performed, demonstrating the increase in the period of drainage that occurs, the

shallower the gradient of increase in excess pore pressure. Permitting a period of drainage prior to a second stage of loading, improves the strength of the soil relative to the undrained cyclic load tests previously performed. As such, a greater cyclic stress ratio can subsequently be applied resulting in reduced axial strain response. Whilst there is a decrease in the stiffness of a sample for this case, this is less than for a sample loading from the initial state with this magnitude, demonstrating a strengthening effect.

Chapter 7

Analysis of Cyclic Loading of Clay Soils

7.1 Introduction

The analysis presented has provided a database of cyclic triaxial testing on kaolinite samples, considering undrained triaxial tests and the post-cyclic strenght attainment, the application in the field with respect to preloading and partially drained loading and the influence on the strength of the sample. This has further been expanded considering site won Gault clay samples, identifying the importance of plasticity of the soil with respect to the cyclic load response and post-cyclic strength. The undrained model, and extension to partially drained conditions, has demonstrated good agreement with the cyclic triaxial tests performed in this study, and extended to case studies undertaken by other authors. However, the use of the model, whilst requiring a small number of additional input parameters from standard laboratory tests, is limited by the availability of software. This Chapter presents a comparative study with respect to the high speed train line at Ledsgård and subsequently, a series of design charts based on model simulations are presented that could be used for industry application.

7.2 Cyclic Model Performance

Chapter 2 summarised a series of case studies where significant track or road settlements had occurred since being open to traffic. One notable case study was Ledsgård where the organic, soft, highly compressible gyttja formation experienced significant settlements under the passage of X2000 trains. In order to examine the performance of the model with respect to this case history, there are a number of considerations;

- Determination of model parameters for soft soil subgrade
- Characterisation of train load due to ballast track at subgrade level in Chapter 2.1.1
- Determination of train passage, discussed in Chapter 2.1.2.2

7.2.1 Model Parameters for Ledsgård Site

The site at Ledsgård was characterised by 3.5m of organic clay soils overlying clay subsoil of the gyttja formation. Holm et al. (2002) proposed the undrained shear strength of this material to be approximately 15kPa. The water content of the layer varied between 40% and 150% across the site. The void ratio based on Das (2007) for a "soft organic clay" ranges between 2.3 and 3.2. A lower bound void ratio of 2.3 was selected, in agreement with the void ratio determined for Finnish clays by Löfman et al. (2021) considering 856 tests. The swelling and compression indices of the material were defined as the mean values determined from the samples examined by the authors, summarised in Table7.1 below. Whilst not explicit to the Ledsgård site, the database of Finnish clays presented by Löfman et al. (2021) were classified as Organic clays, Organic silts and Gyttja, representing CH and OH clays.

Table 7.1: Statistical summary of Finnish clay database, after Löfman et al. (2021)

Parameter	Number	Minimum Value	Median Value	Maximum Value	Mean Value
e_0	856	0.520	2.302	5.200	2.309
c_u	413	5.20	22.50	240.0	30.2
C_c	856	0.026	1.287	9.284	1.417
C_s	500	0.052	0.260	0.495	0.254

The small strain shear modulus of the organic clay was determined using, based on the measurements from Alves Costa et al. (2010) presented in Table 7.2;

$$G_0 = \rho V_s^2 \tag{7.1}$$

Table 7.2: Summary of the properties determined by Alves Costa et al. (2010) for Ledsgård site

Strata / Layer	Thickness (m)	Density, ρ (kg/m^3)	Shear wave velocity, V_s (m/s)
Embankment	1.50	1800	250
Dry crust	1.10	1500	60
Organic clay	3.50	1250	42
Clay	To depth	1470	50 - 122.9

As a result, the proposed parameters for the soft clay subgrade under consideration are presented in Table 7.3.

Table 7.3: Summary of model parameters for the organic clay subgrade at Ledsgård

e_0	c_v	λ	κ	M	G	K_0
2.50	0.00035m^2/day*	0.615	0.110	1.34	2.2MPa	0.6

* Based on Larsson and Mulabdic (1991), note the authors identified organic clay and gytjja c_v was 5 - 10 times less than for inorganic clays

7.2.2 Dynamic Load Characterisation

A number of load models have been presented in Chapter 2.1.2.2. These load models typically consider train speed, wheel dimensions and characteristic such that the static load is factored by a dynamic load factor. The trains at Ledsgård

were 32 tonne X2000 trains. Considering each carriage in accordance with Figure 2.10, the axle load under static conditions is 156.9kN. A speed of 55m/s, approximately 200km/h, was proposed, such that the dynamic amplification factor applied to the static load, based on Figure 2.13 ranges between 1.3 and 2.4. Considering an average value of 1.85 and given the undrained strength of the organic clay, this would result in a cyclic stress ratio of 5.8 under each wheel load. It is therefore important to consider the distribution of this load with respect to the overlying embankment and ballast track to determine the stress increase as a result of train passage at the level of the organic clay layer. This study examines the performance of a 3D ABAQUS model, developed to determine the dynamic induced stress response of the subsoil.

7.2.2.1 Calibration

The 3D FE model implemented in this study adopts a semi-infinite space such that the boundary effects of the model can be eliminated, shown in Figure7.1. To ensure the model can capture the static response, upon which the analysis of dynamic influence is examined, the settlement induced as the result of a $1m^2$ loaded area has been compared to the response determined using the analytical model of Boussinesq for settlement of a semi-infinite, homogenous, isotripic elastic half-space, defined in Equation 7.3.

$$s = \frac{qBI_p(1-\nu^2)}{E} \tag{7.2}$$

where B in this case is 1m, the width of the load area, E is the Young's Modulus and q is the applied stress. I_p is the influence factor accounting for the shape of the foundation and thickness of underlying soil zone, in this case 0.88. The model, shown in Figure 7.1, summarised in Table 7.4, demonstrates that the model is capable of predicting the static displacement of undrained material and can be considered for determining the stress influence beneath the track at subgrade level.

Table 7.4: Calculation of static displacement, comparison between analytical method and ABAQUS 3D model

Model	Load	ABAQUS Analysis (mm)	Boussinesq Calculation (mm)
E = 10MPa	200kN	13.8	13.4
E = 20MPa	200kN	7.23	6.69
E = 10MPa	400kN	27.1	26.6
E = 20MPa	400kN	14.2	13.8

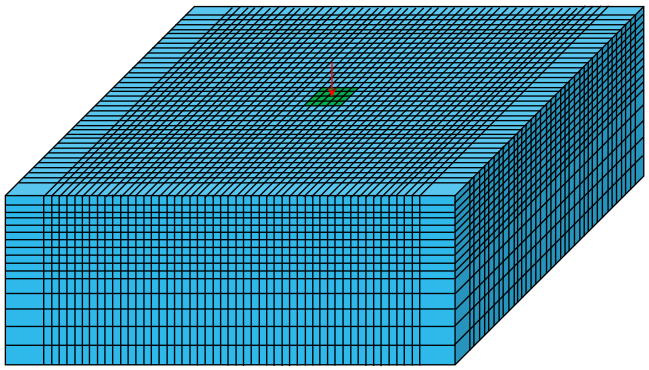

Figure 7.1: ABAQUS moodel for consideration of static displacement of 1m^2 area

Subsequently, this model has been extended to consider the passage of a train and to determine the dynamic stress induced at subgrade level. The schematic of this system is presented in Figure 7.2.

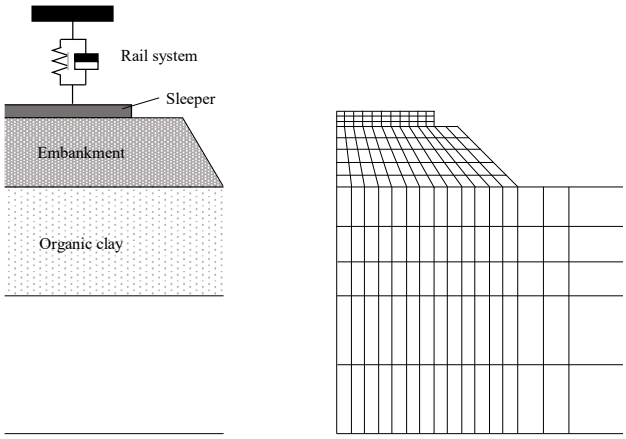

Figure 7.2: Track arrangement and ABAQUS 2D section model schematic

Table 7.5: Summary of model parameters at Ledsgård

Model Component	Parameter	Value
UIC 60 rail	Density (kg/m^3)	7800
	Elastic modulus (MPa)	2.10x10^5
	Poisson's ratio (-)	0.30
	Damping ratio (-)	0.03
Sleeper	Density (kg/m^3)	2500
	Elastic modulus (MPa)	3.50x10^4
	Poisson's ratio (-)	0.20
	Damping ratio (-)	0.01
Ballast	Density (kg/m^3)	1590
	Elastic modulus (MPa)	97.0
	Poisson's ratio (-)	0.12
	Damping ratio (-)	0.06
Embankment Foundation	Density (kg/m^3)	2000
	Elastic modulus (MPa)	60
	Poisson's ratio (-)	0.35
	Damping ratio (-)	0.03

Table 7.5 summarises the properties of the rail, modelled in accordance with UIC60 design, sleeper, ballast and embankment material, where the top 0.75m of embankment was assumed to be ballast. The difference in soil stress in response to the dynamic amplified load at the top of the clay layer was determined, such that the applied cyclic deviatoric stress for the model input could be calculated. The difference in stress is such that the dynamic stress attenuation at a depth of 1.5m below ground level is 0.32. This is in agreement with the stress attenuation coefficient determined by Liu et al. (2018) for a 32 tonne train on ballast track, presented in Figure 3.24, determined to be 0.28. As a result, the cyclic stress ratio to be adopted in the model comparison is 0.86 at a frequency of 6.0Hz.

7.2.3 Model Comparison against Ledsgård Case History

The predicted settlements are compared against the settlements measured by Alves Costa et al. (2010), presented in Figure 7.3. These settlements have had the initial settlement response at load cycle 1 removed. Under partially drained conditions, it is assumed drainage is akin to that of post-cyclic recompression tests performed on the sample and similar to one dimensional compression.

The partially drained model under predicts the settlements experienced at Ledsgård considering the proposed input parameters. With respect to the partially drained model, where the prediction could be considered more representative of in-situ conditions, one potential reason for this under estimation is the values considered for the permeability and coefficient of consolidation adopted in the model prediction. The smaller the value of c_v adopted, the longer reconsolidation will take and the less dissipation of excess pore pressure accumulated through cyclic loading. Thian and Lee (2017) remarked with respect to high plasticity offshore clays, the in-situ permeability of the soil was greater than for laboratory samples, such that the permeability of laboratory samples was underestimated due to it's deformation resistance. A better agreement in terms of total settlement in response to train loading beyond load cycle 1 is therefore determined considering an increased permeability and therefore c_v, where an increase of an order of magnitude was adopted.

The case of Ledsgård is typically used as a case for dynamic amplification whereby the velocity of the train and generated shear waves in the soil attenuate and subsequently reinforce each other rather than dissipate, resulting in significant displacements, demonstrated by the blue line for static settlements from Carchiolo et al. (2017). Another source of under prediction in terms of settlements is therefore likely to be due to the dynamic displacement amplification. Whilst this cannot be captured with the model proposed, the prediction shows the determination of an initial stress distribution to determine the cyclic deviatoric stress as an input to the model, based on an empirical load

correlation, provides a fair result when compared to the measured data and an improvement compared to static settlement calculation.

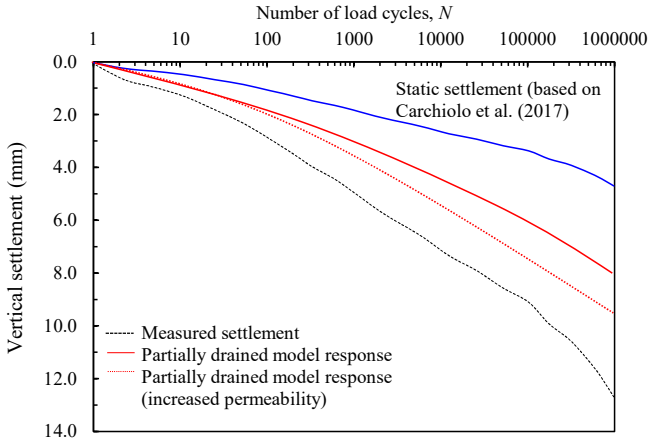

Figure 7.3: Partially drained model prediction for Ledsgård

As such, this identifies a limitation of the analyses presented, where the model applicability is more suited to low to moderate train or vehicle speeds. For higher train speeds, such as those associated with high-speed rail, the model is still suitable, provided the shear velocity of the underlying subgrade is sufficient such that dynamic amplification of displacements is limited.

7.3 Development of Design Charts

The model has demonstrated good agreement with case studies and the laboratory tests presented, whilst also demonstrating limitations with respect to the settlement accumulation of significantly soft layer subject to high speed loading where displacement amplification has been reported to occur (Alves Costa et al. (2010), Connolly et al. (2012)). Whilst the partially drained model includes few additional cyclic parameters, it's application is limited to the existing computational framework of development. A series of design charts have therefore been developed, in the first instance to present the influence of applied dynamic stress with depth and subsequently the degree of consolidation under partially drained loading and influence of different clay

types on the cyclic response.

A series of analyses have been performed using the load model developed in ABAQUS to determine an initial influence of dynamic stress with respect to depth for the track structure outlined below in Figure 7.4, considering track slab formation. For the different layers presented in Figure 7.4 alongside the determined stress distribution under X2000 rail loading, the properties outlined in Table 7.6 were adopted.

Table 7.6: Summary of model parameters for the organic clay subgrade at Ledsgård

Model Component	Parameter	Value
UIC 60 rail	Density (kg/m^3)	7800
	Elastic modulus (MPa)	2.10x10^5
	Poisson's ratio (-)	0.30
	Damping ratio (-)	0.03
Track Slab	Density (kg/m^3)	2700
	Elastic modulus (MPa)	3.50x10^4
	Poisson's ratio (-)	0.17
	Damping ratio (-)	0.05
Mortar	Density (kg/m^3)	1800
	Elastic modulus (MPa)	1.00x10^4
	Poisson's ratio (-)	0.3
	Damping ratio (-)	0.2
Concrete base	Density (kg/m^3)	2700
	Elastic modulus (MPa)	2.40x10^4
	Poisson's ratio (-)	0.20
	Damping ratio (-)	0.05
Foundation	Density (kg/m^3)	1820
	Elastic modulus (MPa)	143
	Poisson's ratio (-)	0.35
	Damping ratio (-)	0.05

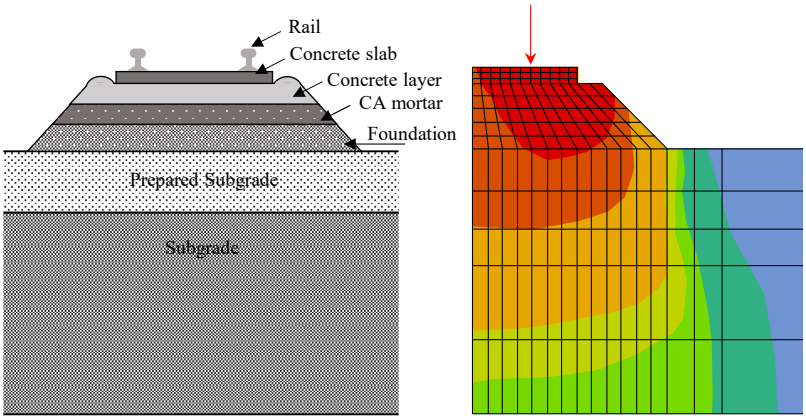

Figure 7.4: Slab track construction and ABAQUS model showing displacements under train load

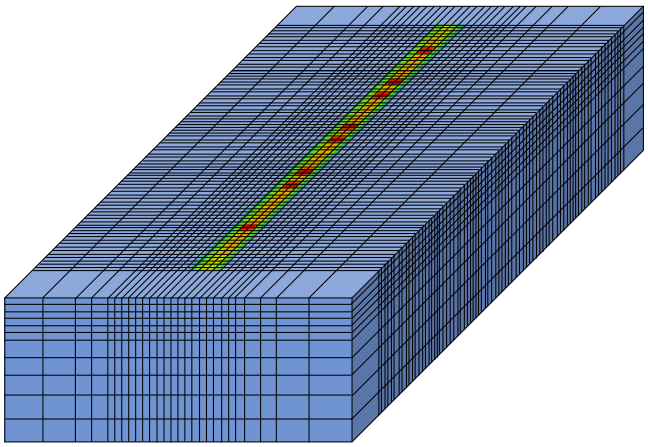

Figure 7.5: 3D ABAQUS model, excluding track structure

7.3.1 Influence of Train Load

One factor for determining the dynamic stress that should be considered in the model, is the magnitude of load applied at rail level. Three train loads were examined; 26 tonnes, 30 tonnes and 34 tonnes. Examining a cross-section along the centre of the embankment, Figure 7.7, the results demonstrate under the passage of a train with the same speed, the zone of additional stress induced as a result of the train passage beneath the rail is greater as the load increases. Considering this in Figure 7.6, the results show there is a stress increase as a result of greater load from track level down. However, most of the change in dynamic stress for increasing load is concentrated to the track structure layers.

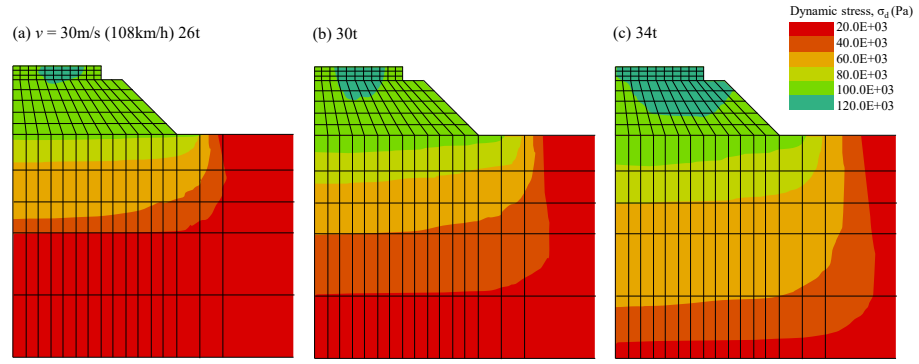

Figure 7.6: Dynamic stress distribution for varying train loads

(a) v = 30m/s (108km/h) 26t

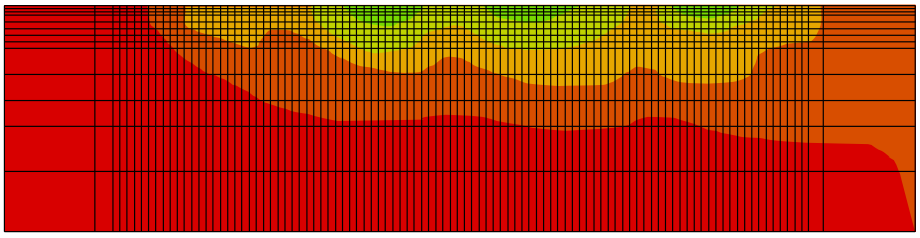

(b) v = 30m/s (108km/h) 30t

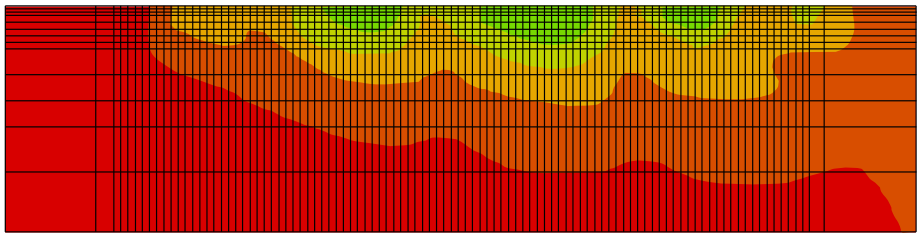

(c) v = 30m/s (108km/h) 34t

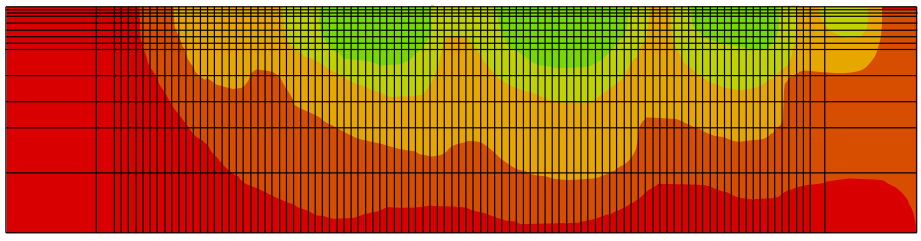

Figure 7.7: Stress distribution under a passing train of 30m/s (108km/h) considering different train loads

Below this track formation and foundation layer, the dynamic stress gradually increases as a result of train speed, presented in Figure 7.8, however this result suggests that rather than the load itself, it is the dynamic load factor influence

that influences the dynamic stress.

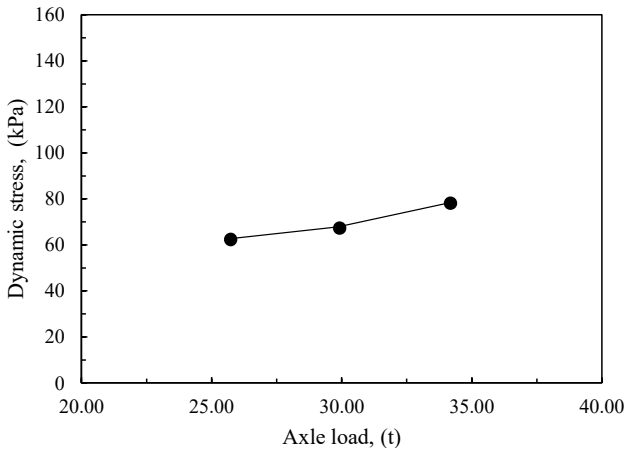

Figure 7.8: Dynamic stress distribution for varying train speeds

7.3.2 Influence of Train Speed

A series of analyses were performed considering train speeds ranging from approximately 100 to just under 300km/h. In these studies, an axle load of 24 tonnes was adopted for consistency. The response for the same cross-section presented for Section 7.3.1, is shown in Figure 7.9. The results demonstrate as the velocity increases, there is a more significant change in the dynamic stress than when considering the static load of the train.

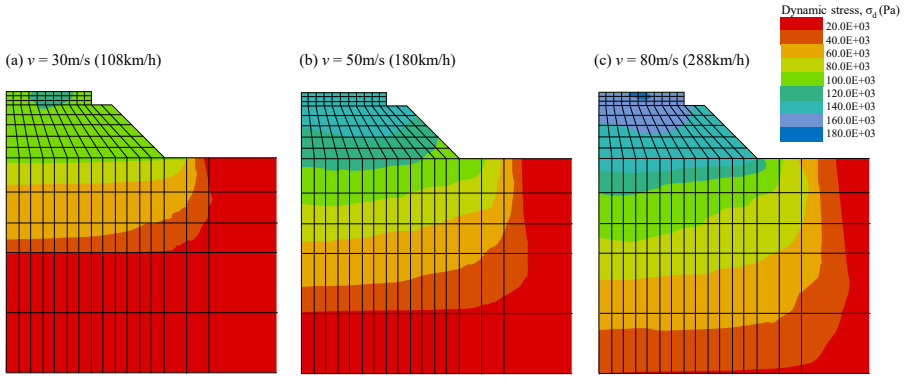

Figure 7.9: Dynamic stress distribution for varying train speeds at top of subgrade level

Figure 7.10 shows the response of dynamic stress with respect to the distance

from the centreline of the track formation at the top of the subgrade. The dynamic stress increases as the vehicle speed increases, however, with respect to the maximum stress at top of slab, transmitted from the rail, the decrease in dynamic stress is a consistent ratio, decreasing from the maximum value by approximately 20%.

The analysis supports the development of a dynamic load factor, such as those presented in Chapter 2, where several authors and regulatory bodies present the factor as a function of the train's dimensions and speed. Considering the wheel diameter remains constant in the study, D, Table 7.7 presents a summary of the dynamic stress increase induced at slab track level, in order to determine a dynamic load factor, Φ, on the basis the contact area is constant such that the factor can be considered in terms of stress. Based on the analysis in the format;

$$P_{design} = \Phi P = 1 + \left(a_1 \frac{v}{D}\right) P \tag{7.3}$$

A value of a_1 = 2.8 agrees with the analyses in ABAQUS 3D presented. As such, knowing the static train load and the speed of the train, the stress at slab track can be determined. Subsequently, this stress can be translated down to subgrade level.

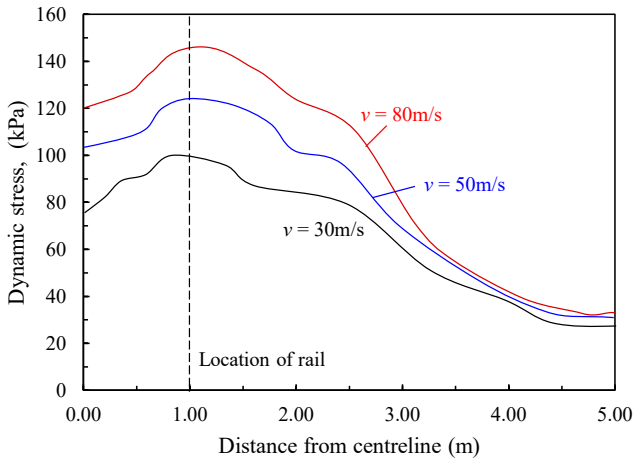

Figure 7.10: Dynamic stress distribution for varying train speeds

Table 7.7: Calculation of static displacement, comparison between analytical method and ABAQUS 3D model

Speed	Slab stress	Ratio to static stress	Φ
108km/h	200kN	1.14	1.19
180km/h	200kN	1.35	1.33
288km/h	400kN	1.54	1.52

It has been demonstrated that at subgrade level, beneath a slab track there is a reduction in the dynamic stress due to the slab track layers and damping, irrespective of vehicle speed and low. At the top of subgrade level, this reduction is between 15 and 25%. Therefore, the design charts have been characterised for two considerations; the influence of the prepared subgrade and the influence of the performance of the underlying clay subgrade.

7.3.3 Influence of Prepared Subgrade

The influence of the prepared subgrade has been examined considering a total thickness underlying the slab track of 10.0m. As typically excavation and replace methods for providing a prepared subgrade layer are limited by the depth of treatment, such that a significant excavation depth would be prohibitive with respect to mass haul and material costs, the influence has been examined considering increasing thicknesses of prepared subgrade to a maximum depth of 2.0m.

Figure 7.11 presents the proposed chart for the determination of a dynamic stress coefficient. The coefficient is within the range of values observed for slab track systems presented in literature in Figure 3.24. This can be applied as a factor to the determined in-situ stress to determine the cyclic deviatoric stress to be adopted in the analysis such that the load distribution through the slab system can be accounted for. With an increasing depth of prepared subgrade, that has an improved stiffness in comparison with underlying subgrade layer, the applied dynamic rail load influence on the subgrade soil stress decreases. This would result in a lower cyclic stress ratio being adopted in subsequent

model analysis.

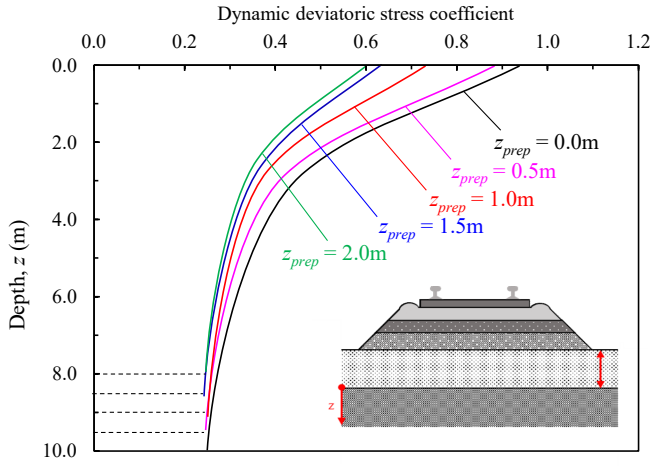

Figure 7.11: Influence of prepared subgrade thickness, z_{prep}, on the dynamic stress coefficient

7.3.4 Influence of Subgrade

The results presented for the variation of prepared subgrade depth, demonstrate the benefit of having a stiffer layer to mitigate against the loading of the train load under consideration, however as the focus of the studies presented have been focussed on the underlying clay subgrade it is important to consider the effects on this layer. Given this layer is examined with respect to partially drained conditions, one focus is the thickness of this layer and therefore the drainage distance for an element. The thickness of the layer with respect to the applied train load has been examined, considering no overlying prepared subgrade layer. The stress ratio is presented in Figure 7.12, demonstrating the greater the thickness of the layer, the greater the reduction in the stress induced by the train load. Considering a thickness of 5.0m, less reduction in stress occurs, however the total settlement of this layer will be influenced by the thickness with respect to pore pressure dissipation under consolidation.

As demonstrated in Section 7.3.3, having a layer of excavate and replace that is stiffer than the underlying strata results in a decrease in train load influence. Figure 7.13 presents the influence of the load with respect to variation in the

stiffness of the clay subgrade layer. For an increasing clay subgrade stiffness, the proportion of dynamic load taken by the soil marginally increases. However, in relation to the static strength of the soil, the cyclic stress ratio applied to the soil will therefore increase for the same load as the stiffness of the sample decreases. Similarly, the settlement accumulation would be greater the lower the stiffness of the material.

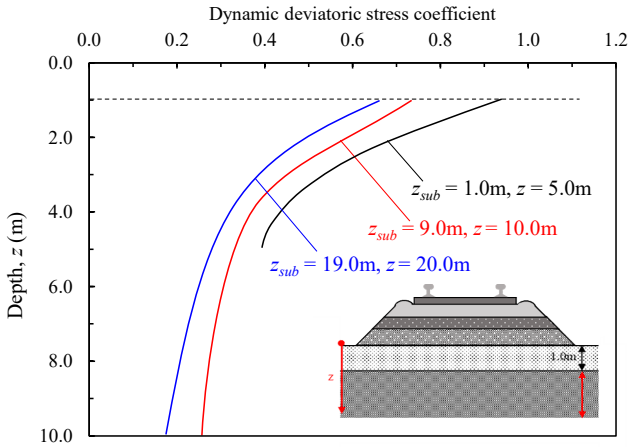

Figure 7.12: Influence of subgrade thickness, z_{sub}, on the dynamic stress coefficient

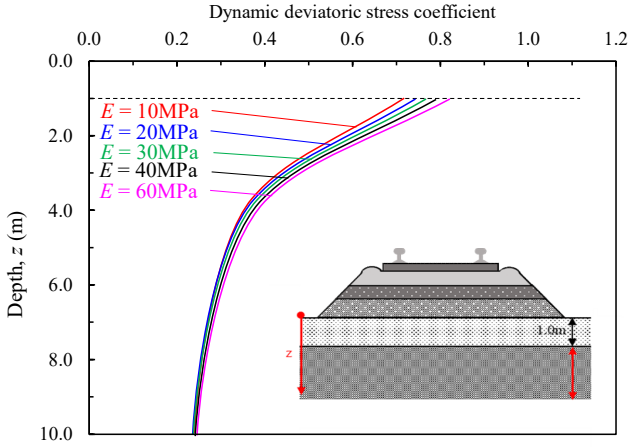

Figure 7.13: Influence of stiffness on the dynamic stress coefficient

7.3.5 Charts for Soil Type

The design charts presented for the dynamic stress have demonstrated the influence of train load, train speed and the depth and stiffness of prepared subgrade. As such, the dynamic stress imported in to the partially drained cyclic model has been determined. Based on determining a cyclic stress ratio, such that the undrained strength of the soil is also known, the strain accumulation can be determined.

The design charts presented in Figure 7.14 consider the results of the partially drained model for the soils considering typical properties based on soil classification, summarised in Table 7.8. The results of Figure 7.14 are presented considering the same void ratio of 1.5, such that under these conditions, the greater the clay content, the greater the accumulated strain. Figure 7.15 subsequently therefore presents the results for "CH" and "CL" clays considering a representative void ratio for that soil, where a larger void ratio is attributed to a soil with a greater clay fraction. In this case, "CH" was assigned a void ratio of 2.3.

Table 7.8: Summary of clay soil properties adopted for design charts

Soil Type	Plasticity index range, I_p	Representative I_p	c_v
CH	30 - 50%	50%	0.0004m^2/day
CL	10 - 30%	30%	0.0024m^2/day
MH	5 - 40%	20%	0.0064m^2/day
ML	0 - 15%	15%	0.0150 m^2/day

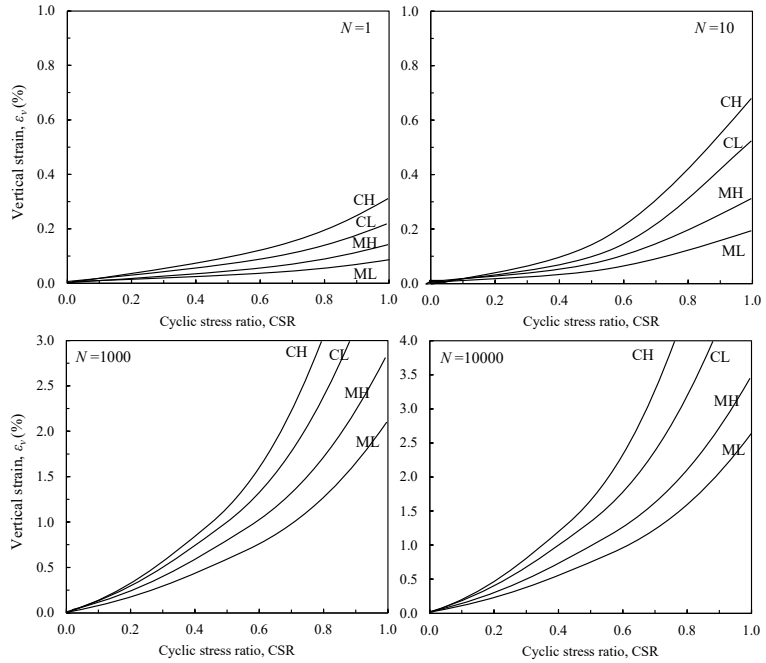

Figure 7.14: Design charts for the strain accumulation of typical clay soil types under slab track for a void ratio of 1.5

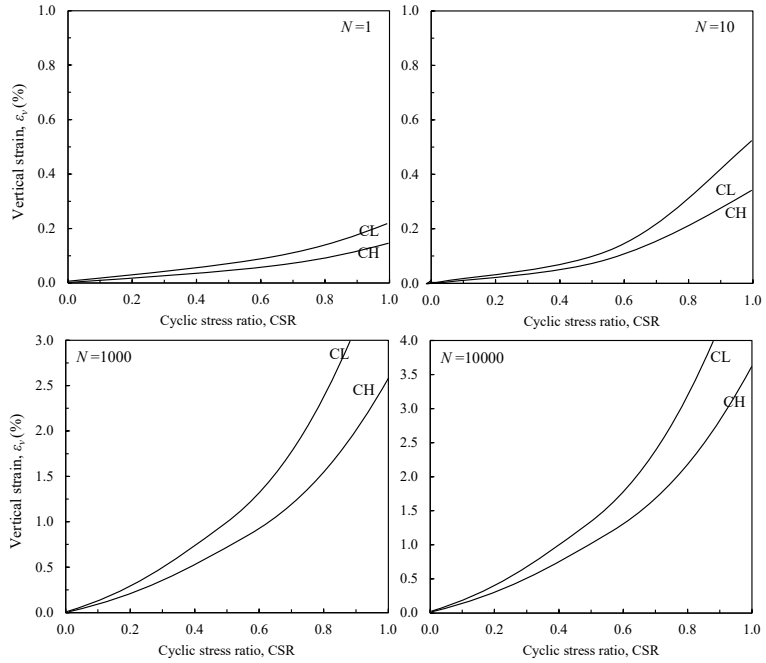

Figure 7.15: Design charts for the strain accumulation of typical clay soil types under slab track for a representative void ratio

7.4 Conclusions

This Chapter presents the results of the well-known case history of Ledsgård in which settlements occurred after the route opened to rail traffic, resulting in decreasing of line speed. The model considers the response of an organic soft clay deposit of high plasticity to determine the response under cyclic loading. To determine the cyclic deviatoric stress considered in the partially drained cyclic model, a FE analysis has been performed in ABAQUS that considers the rail-structure interaction and the change in stress induced in the underlying soil subgrade under the dynamic rail load. In this way, the rail system is modelled as a series of spring-dashpots considering the damping to better characterise the load applied at rail level, that is subsequently transmitted to the clay subgrade under consideration. The model under predicts the settlement of the system, where the difference can be attributed to the dynamic amplification of the displacements as a result of train speed relative to the speed at which dynamic waves are transmitted through the clay subgrade. Care should therefore be taken using the model for the case of high-speed rail systems overlying significantly soft deposits.

For the consideration of rail traffic loading of a slab track system, the system has been analysed in ABAQUS in a similar manner to the ballast track system adopted for Ledsgård. The influence of both train load and speed on the stress have been analysed and a dynamic load factor applicable for slab track stress is presented. Based on the change in stress obtained at clay subgrade layer, a series of design charts have been produced. Various clay subgrade properties have been analysed, representative of a "CH", "CL", "MH" and "ML" and the corresponding strain response summarised. Considering the same void ratio, the accumulation of strain is greater for high plasticity clays. As a result, a representative void ratio has been proposed for the clay layer and the design charts for "CH" and "CL" are presented.

Chapter 8

Conclusions

8.1 Introduction

Expansion of cities places greater demands on existing transport infrastructure. There are several ways in which this can be achieved; in the case of rail infrastructure this is done by increasing train capacity or increasing train frequency. An increase in capacity results in an increase in the magnitude of load applied to the soil, whilst increasing the train frequency results in an increase in the duration of traffic loading. In the case of road transport, this results in more frequent traffic loading. Similarly, as new transportation routes are created, they are governed by the availability of land, in some cases trafficking soil conditions that can be more compressible. Furthermore, new advances and developments in train and track technology mean the speeds at which these soils are trafficked are much greater. New rail infrastructure is also considering the adoption of slab track systems, rather than ballasted track arrangements, where the tolerances placed on these systems are more stringent.

Under the passage of a vehicle, a dynamic stress is applied to the soil subgrade. This causes an accumulation of permanent plastic displacement beneath the track. Excessive settlements can result in greater requirements for track maintenance and repairs, particularly for slab track. Therefore, the response of

a soft clay subgrade under traffic loading is of importance when considering the construction and maintenance of transport routes. This thesis examines the influence of various factors on the performance of clay deposits to cyclic loading. A body of monotonic, cyclic and post-cyclic triaxial tests under various conditions has been presented based on laboratory tests performed by the author. In Chapter 3, undrained monotonic and cyclic triaxial tests have been performed on laboratory prepared kaolin samples to determine the effects of frequency and magnitude of cyclic stress. Chapter 4 considers conditions representative of an in-situ soil element, namely the influence of preloading, a ground improvement technique adopted for soft soil deposits and examines the performance of the prepared kaolin samples under a condition of partial drainage. Chapter 5 summarises a cyclic model considering vertical drainage representative of a partially drained triaxial condition. This model is developed from Ni (2012), expanding the performance of the model considering overconsolidated samples. Chapter 6 extends the undrained cyclic triaxial tests to consider site-won Gault clay material whilst Chapter 7 subsequently examines the performance of the cyclic model, presenting a series of design charts for determining the dynamic stress and the strain response of typical clay soil subgrade classifications.

8.2 Influence of Load Magnitude

When a train or vehicle traffics a subgrade, the load is transmitted through rails and track system, or vehicle and road and pavement arrangement. A study of high speed trains has been summarised, determining their wheel load, where several empirical equations exist to consider the increase as a result of the dynamic effect. A limit has been identified based on existing literature and the study of small strain shear modulus, such that a threshold undrained shear strength of 66kPa is proposed for consideration. The cyclic stress ratio applied to samples has been defined as the ratio between the cyclic deviatoric stress applied to the sample and this threshold value under monotonic loading. Adopting a cyclic stress ratio in this manner facilitates the repeatability of the

cyclic undrained triaxial tests established in this study.

The influence of the cyclic stress ratio during undrained cyclic loading demonstrates the existence of a threshold value of cyclic stress, above which a sample will tend towards failure, demonstrated by the rapid accumulation of axial strain, and below which, the accumulation of axial strain gradually converges to a low level of strain, less than 5%. For samples that attained failure, the axial strain rapidly accumulated to 15%, defined from ASTM guidelines. This is observed in the hysteretic loops for one-way cyclic loading, where greater plastic strain accumulation is demonstrated by the greater opening of a load loop. This threshold value has been identified by a number of early studies by Seed et al. (1955) and Sangrey et al. (1969). This threshold for the kaolinite samples considered has been identified to exist between 0.6 and 0.8. For the Gault clay samples, it is shown to exist between 0.8 and 0.9. Supporting the conclusions of Sangrey et al. (1969) and Pillai et al. (2011). Adopting the shakedown concept to define the threshold for collapse, the threshold cyclic stress ratio was determined to be 0.71. An empirical model for axial strain has been proposed, where the axial strain is an exponential function of the number of load cycles provided the strain accumulation during the initial 10 cycles of load is accounted for. This intercept can be defined in terms of the cyclic stress ratio and the relationship agrees with observations for similar clays.

Considering the response of the Gault clay, the axial strain accumulation generated under an equivalent cyclic stress ratio is less than that obtained for the kaolin samples. This decrease in axial strain is attributed to the increased plasticity index.

Whilst failure of the samples could be observed from the accumulation of axial strain, it could not be observed from examination of the response of normalised excess pore pressure alone. Regardless of the cyclic stress ratio, the excess pore pressure rapidly accumulated before converging to a constant value. This value was dependent on the magnitude of cyclic load, and therefore cyclic stress ratio, applied to the sample. Hyde and Ward (1985) presented an empirical model to

describe the accumulation of excess pore pressure with respect to the number of cycles of load. The results of the undrained cyclic triaxial tests agree with the results of this solution, converging to values of 0.20, 0.45 and 0.67 for cyclic stress ratios of 0.4, 0.6 and 0.8 respectively.

8.3 Influence of Load Frequency

The response of both kaolin and Gault clay samples subjected to undrained cyclic loading was demonstrated to be independent of the load frequency for the consideration of traffic loading. Considering the results in terms of the number of load cycles, for a cyclic stress ratio of 0.8, the greater the frequency of load applied to the samples, the greater the number of load cycles a sample can withstand before failure. At lower frequencies, examination of an individual hysteretic loop showed that a greater permanent strain response occurred due to the increased load duration of a cycle. Ansal and Tuncan (1989) proposed that during the initial cycles, greater accumulation occurred, such that for samples with low frequency the permanent strain attains failure after fewer cycles. With respect to the duration of the test in terms of time, rather than number of cycles, the samples loaded at a lower frequency remain stable for a longer period of time. However, failure is attained irrespective of the frequency of loading.

Considering samples that attained a stable state upon cyclic loading, with a greater number of load cycles the influence of frequency on the axial strain and excess pore pressure accumulation becomes negligible. As such, for traffic loading, considering several hundred thousand cycles over the design life of the structure, the influence of frequency can be neglected.

8.4 Post-Cyclic Response

The post-cyclic response of an undrained normally consolidated sample under cyclic loading is such that the sample behaves as an overconsolidated clay,

exhibiting 'apparent' overconsolidation as determined by Pillai et al. (2014). The greater the cyclic stress ratio, and therefore reduction in effective stress due to excess pore pressure accumulation, the greater the reduction in undrained shear strength when sheared under undrained loading. The decrease in undrained shear strength is a maximum of around 15% considering the samples examined. Yasuhara et al. (1982) reported no decrease in strength whilst Ansal and Tuncan (1989) reported a decrease of upto 65%. The post-cyclic undrained shear strength tests on kaolin performed in this study exist within this range.

When drainage is permitted during post-cyclic shearing, reconsolidation is permitted resulting in the samples attaining a greater strength. The void ratio stress response that occurs during cyclic loading, followed by drainage is similar to the drainage path under partially drained cyclic loading. The volumetric strain attained during post-cyclic recompression can be described by a hardening function. Therefore, partially drained triaxial tests can be replicated by an undrained cyclic triaxial test followed by drainage prior to undrained monotonic shearing.

In the field, it is unlikely that complete reconsolidation will occur between train passages, particularly for clay soils. Considering varying degrees of reconsolidation, as the degree of consolidation increases the strength at failure increases. For the Gault clay, 75% reconsolidation would be required for the samples to attain their original undrained monotonic strength. Subsequently, stop-start triaxial tests have been performed, demonstrating the greater the duration of loading relative to no load, the less excess pore pressure dissipated and the greater the subsequent accumulation in the following cycle. Considering the analyses presented for different degrees of reconsolidation, the sample is capable of withstanding a greater magnitude of load in the next step, such that the axial strain accumulation is less.

8.5 Influence of Preloading

Preloading is often used as a ground improvement technique where soft soils can result in excessive settlements. A series of overconsolidated undrained monotonic and cyclic triaxial tests have been performed. At low to moderate degrees of overconsolidation, the axial strain accumulation decreases under cyclic loading. At higher degrees of overconsolidation, the excess pore pressure response suggests the sample dilates and the improvement in axial strain accumulation is incrementally less. The critical cyclic stress ratio for overconsolidated samples is still observed to be between 0.6 and 0.8 for the kaolin samples examined, whilst Meimon and Hicher (1980) demonstrated this threshold should increase.

Considering the post-cyclic monotonic undrained shearing of overconsolidated samples, the strength under cyclic loading is less than determined from the equivalent monotonic test. Mayne and Kulhawy (1982) proposed an equation determining the ratio between the normalised undrained shear strength of a normally consolidated and overconsolidated sample. This equation has been rephrased in terms of post-cyclic overconsolidated and the strength under these conditions can be determined from monotonic undrained tests and the swelling and compression indices of the soil.

The cyclic model presented by Ni (2012) has been considered in this study, extending its' performance to validate the model against the overconsolidated tests performed in the laboratory. The model shows good agreement with the results of the laboratory analysis for low overconsolidation ratios applicable to the consideration of preloading treatment. At higher overconsolidation ratios, such that the response is dilative, the model did not capture this behaviour and under-predicted the response observed in the laboratory.

8.6 Influence of Partial Drainage

A series of recommendations for performing partially drained triaxial tests in cyclic triaxial apparatus have been proposed, such that the vertical drainage lines remain open during cyclic loading of a clay sample. Sakai et al. (2003) presented a series of partially drained triaxial tests on Ariake clay samples that demonstrated a similar response to the kaolin samples examined in this study. The excess pore pressure accumulation under partial drainage can be defined in terms of a peak in excess pore pressure generation followed by subsequent dissipation to a constant value. As such as the excess pore pressure accumulate, simultaneous dissipation also occurs and volumetric strain is generated. The volumetric strain increases with respect to the magnitude of excess pore pressure generated, and therefore cyclic stress ratio. Care should be taken considering the repeatability of test results under partially drained conditions due to the lack of control over the test when drainage lines are open during cyclic loading.

The frequency of loading has also been examined. For a low frequency, greater excess pore pressure dissipation over a given number of cycles occurs due to a longer duration of load. This response has been demonstrated considering a critical state model for cyclic loading in which vertical drainage is permitted considering the theory of vertical consolidation. As such, the greater the coefficient of vertical consolidation, the greater the dissipation of excess pore pressure under cyclic loading. This model has been shown to reflect the cyclic triaxial tests performed on both kaolin samples and Gault clay as well as several case studies by Hyodo and Yasuhara (1988), Sakai et al. (2003) and Moses et al. (2003).

The cyclic stress ratio at which failure occurs exists between 0.6 and 0.8. Whilst authors including Ni (2012) have demonstrated the cyclic stress ratio under partial drainage to increase, this was not observed. However, compared to the equivalent undrained cyclic test, the sample is capable of withstanding a greater number of load cycles prior to failure.

8.7 Influence of Plasticity

Cyclic triaxial tests on Gault clay have been performed which generated a reduced axial strain accumulation compared to the kaolin samples. This difference in response can be attributed to the plasticity index of the sample which has been shown by Okur and Ansal (2007) to influence the stiffness degradation of a sample under cyclic loading. A higher plasticity index results in less degradation, where the sample has a higher specific surface such that cyclic loads are partially distributed to the water held within the soil skeleton, reducing the impact of the vertical load, also demonstrated by Soralump and Prasomsri (2016).

Post-cyclic monotonic tests considering both conditions of drainage and no drainage prior to undrained monotonic shearing demonstrate the strength reduction is less than for an equivalent kaolin sample, due to less degradation. However when drainage is considered, the strength improvement is also less, as the sample consolidation has resulted in a less dense sample with a greater void ratio than for the equivalent kaolin sample.

Under a condition of partial drainage, the accumulation of excess pore pressure is less for an increase in plasticity index. Subsequently, the low permeability and coefficient of vertical consolidation attributed to high plasticity soils inhibit the excess pore pressure dissipation. This has been presented in the partially drained cyclic model.

A finite element spring dashpot analysis has been employed to determine the deviatoric stress change that occurs as a result of the passage of a train over slab track and ballast track. The model is applicable to case studies where the undrained strength of the material exceeds the threshold determined from the review of literature such that dynamic amplification of displacements is minimal. Design charts have been developed demonstrating the influence of train load, train speed and subgrade conditions on the dynamic stress at the top of clay subgrade layer. Considering the stress developed beneath a slab track

system, a series of design charts are presented based on typical clay and silt soil classifications.

8.8 Recommendations for Future Work

Based on the analysis presented in this study, recommendations for further work are proposed;

- Preloading has been shown as an effective method for improving a soils resistance to cyclic loading. The energy concept presented graphically could be explored with respect to the triaxial tests performed, determining the energy to the system. Further analysis at low degrees of overconsolidation should also be examined in greater detail, to quantify the cost-improvement of cyclic load resistance. There is little available literature with respect to the cost of ground improvement, particularly considering preloading, and an improved body of research with respect to the economic considerations of this would also be beneficial. It was noted as high overconsolidation ratios, the model performance deviated from the laboratory observations, therefore examining the dilative cyclic response of the model would be a benefit to extend its' use.
- Stop-start cyclic loading tests have been performed, representative of the condition of train loading where periods of drainage occur without the application of a cyclic stress. It would be beneficial to explore this area in more detail, determining the effects on the stiffness of the material and its' resistance to cyclic load.
- Another consideration is the soil performance at small strains. This can be assessed by introducing LVDT or bender elements to the triaxial cell arrangement. Further studies could also be performed considering large scale triaxial samples. Characterising this response would provide an understanding of the stiffness degradation, including with respect to the plasticity of the samples that have been examined in this thesis.

- The values assigned to the degradation parameters were fitted based on the laboratory tests. Where predictions have been made, these have been fitted to the results. In the case of partially drained predictions, the equivalent undrained test was fitted or degradation parameters for a similar soil type have been adopted. As such, an improvement to the model would be to determine the values assigned to the degradation parameters for various soil types in order to facilitate its' wider use.

Chapter 9

Bibliography

Bibliography

H. Aboshi, H. Matsuda, and M. Okuda. Preconsolidation be separate-type consolidometer. In *Proc. 10th Int. Conf. on SMFE*, pages 19 – 22, 1981.

M. M. Agarwal. Indian railway track. *Prabha and Cooperation, A-68, NDSE Pt II, New Delhi-110049 India*, 1974.

ALSTOM. Case Study, NTV Nuovo Transporto Viaggiatori, AGV - Avelia range. 2016.

P. Alves Costa, R. Calçada, A. Silva Cardoso, and A. Bodare. Influence of soil non-linearity on the dynamic response of high-speed railway tracks. *Soil Dynamics and Earthquake Engineering*, 30(4):221–235, 2010.

American Society for Testing and Materials. Standard test method for load controlled cyclic triaxial strength of soil, ASTM D5311-92. *Annual Book of ASTM Standards*, 04.08(Reapproved 1996):1–10, 2004.

Amtrak. Amtrak Acela High Speed Trainset Mechanical Department Acela Trainset Typical Configuration Acela Data. 2013.

K. Andersen, J. Pool, S. Brown, and W. Rosebrand. Cyclic and static laboratory tests on Drammen clay. *Journal of the Geotechnical Engineering Division, ASCE*, 106(GT5):499 – 529, 1980.

A. M. Ansal and M. Tuncan. Consolidation in Clays due to Cyclic Stresses, 1989.

A. M. Ansal, R. Iyisan, and H. Yildirim. The cyclic behaviour of soils and effects of geotechnical factors in microzonation. *Soil Dynamics and Earthquake Engineering*, 21:445–452, 2001.

AREMA. *Manual for Railway Engineering*. American Railway Engineering and Maintenance-of-way Association Publishing Service, Washington, D.C., 2006.

A. Asaoka, M. Nakano, and M. Matsuo. Prediction of the partially drained behavior of soft clays under embankment loading. *Soils and foundations*, 32(1): 41–58, 1992.

R. Azeiteiro, P. Coelho, D. Taborda, and J. Grazina. Dissipated Energy in Undrained Cyclic Triaxial Tests. In *6th International Conference on Earthquake Geotechnical Engineering*, 2015.

A. Azzouz, R. Krizek, and R. Corotis. Regression analysis of soil compressibility. *Soils and foundations*, 16(2):19 – 29, 1976.

A. S. Azzouz, A. M. Malek, and M. M. Baligh. Cyclic behavior of clays in undrained simple shear. *Journal of Geotechnical Engineering, ASCE*, 115(5): 637–657, 1989.

Balfour Beatty Rail Technologies. Embedded Rail Slab Track 01. 44(September): 1–7, 2003.

P. K. Banerjee and N. B. Yousif. A plasticity model for the mechanical behavior of anisotropically consolidated clay. *Int. J. Numer. Anal. Meth. Geomech.*, 10: 521–541, 1986.

Banverket. *Evaluation and Analyses of Measurements from the West Coast Line at Ledsgard*. 1999.

S. Bhattacharya. *Design of Foundations for Offshore Wind Turbines*. 2019.

X. Bian, H. Jiang, Y. Chen, J. Jiang, and J. Han. A full-scale physical model test apparatus for investigating the dynamic performance of the slab track system of a high-speed railway. *Proceedings of the Institution of Mechanical Engineers, Part F: Journal of Rail and Rapid Transit*, 230(2):554–571, 2014.

X. Bian, H. Jiang, C. Chang, J. Hu, and Y. Chen. Track and ground vibrations generated by high-speed train running on ballastless railway with excitation of vertical track irregularities. *Soil Dynamics and Earthquake Engineering*, 2015.

X. Bian, H. Jiang, and Y. Chen. Preliminary Testing on High-speed Railway Substructure Due to Water Level Changes. *Procedia Engineering*, 143:769–781, 2016.

L. Bjerrum. Engineering Geology of Norwegian Normally-Consolidated Marine Clays as Related to Settlements of Buildings. *Géotechnique*, 17(2):83–118, 1967.

J. Black, S. Stanier, and S. Clarke. Shear wave velocity measurement of Kaolin during undrained unconsolidated triaxial compression. *Proceedings of the 62nd Canadian Geotechnical Conference*, 2009.

British Standard. BS1377:Part 5 British Standard Methods of test for Soils for civil engineering purposes Part 5. Compressibility, permeability and durability tests. Technical report, 1990.

S. F. Brown, A. K. F. Lashine, and A. F. L. Hyde. Repeated load triaxial testing of a silty clay. *Geotechnique*, 25(1):95–114, 1975.

S. F. Brown, B. V. Brodrick, N. H. Thom, and G. R. McDowell. The Nottingham railway test facility, UK. *Proceedings of the Institution of Civil Engineers - Transport*, 160(2):59–65, 2007.

BS EN ISO 14688-2. Geotechnical investigation and testing. Identification and classification of soil. Principles for a classification, 2018.

M. P. Burrow, D. Bowness, and G. S. Ghataora. A comparison of railway track foundation design methods. *Proceedings of the Institution of Mechanical Engineers, Part F: Journal of Rail and Rapid Transit*, 221(1):1–12, 2007.

Y. Cai, C. Gu, J. Wang, C. H. Juang, C. Xu, and X. Hu. One-Way Cyclic Triaxial Behavior of Saturated Clay: Comparison between Constant and Variable Confining Pressure. *Journal of Geotechnical and Geoenvironmental Engineering*, 139(5):797–809, 2013.

V. Carchiolo, M. Malgeri, G. Mangioni, and V. Nicosia. Evaluating the Dynamic Behaviour of Concrete Slab Track for High Sped Rail using Numerical Analysis. In M. Forde, editor, *Railway Engineering - 2017 .*, pages 904–915. Technics Press, 2017.

J. Carter, J. Booker, and C. Wroth. A critical state soil model for cyclic loading. In John Wiley & Sons, editor, *Soil mechanics - transient and cyclic loading*, pages 219–252. Chichester, 1982.

J. P. Carter, J. R. Booker, and C. P. Wroth. The Application of a Critical State Soil Model to Cyclic Triaxial Tests. In *Proc., 3rd Australia-New Zealand Conf. Geomech.*, pages 121 – 126, Wellington, N.Z., 1980.

H. B. Casal. Dynamic behaviour of high-speed railway bridges with ballastless track. 2010.

M. T. Čebašek, A. F. Esen, P. K. Woodward, O. Laghrouche, and D. P. Connolly. Full scale laboratory testing of ballast and concrete slab tracks under phased cyclic loading. *Transportation Geotechnics*, 17,33–40, 2018.

J.-C. Chai and N. Miura. Traffic-Load-Induced Permanent Deformation of Road on Soft Subsoil. *Journal of Geotechnical and Geoenvironmental Engineering*, 128 (11):907–916, 2002.

C. Chen. Use of prefabricated vertical drain to expedite the consolidation settlement. In *Seminar and Exhibition on Building on Geosynthetics, Kuala Lumpur, Malaysia, June-July.*, 2004.

C. Chen, Z. Zhou, L. Kong, X. Zhang, and S. Yin. Undrained dynamic behaviour of peaty organic soil under long-term cyclic loading, Part I: Experimental investigation. *Soil Dynamics and Earthquake Engineering*, 107:279–291, 2018a.

C. Chen, G. Xu, Z. Zhou, L. Kong, X. Zhang, and S. Yin. Undrained dynamic behaviour of peaty organic soil under long-term cyclic loading , Part II : Constitutive model and simulation. *Soil Dynamics and Earthquake Engineering*, 129: 105555, 2020.

R. Chen, X. Zhao, Z. Wang, H. Jiang, and X. Bian. Experimental study on dynamic load magnification factor for ballastless track-subgrade of high-speed railway. *Journal of Rock Mechanics and Geotechnical Engineering*, 5 (4):306–311, 2013.

W.-B. Chen, J.-H. Yin, W.-Q. Feng, L. Borana, and R.-P. Chen. Accumulated Permanent Axial Strain of a Subgrade Fill under Cyclic High-Speed Railway Loading. *International Journal of Geomechanics*, 18(5):04018018, 2018b.

C. W. Clarke. Track loading fundamentals–1 introduction: track and wheel loading. *Railway gazette*, 106:45–48, 1957.

D. Connolly, M. C. Forde, A. Giannopoulos, and P. K. Woodward. The effect of high speed rail embankments on vibration levels in the near and far field. *RRUKA Annual Conference*, (7 November):1–5, 2012.

D. P. Connolly. Ground borne vibrations from high speed trains. 2013.

D. P. Connolly, G. Kouroussis, P. K. Woodward, P. Alves Costa, O. Verlinden, and M. C. Forde. Field testing and analysis of high speed rail vibrations. *Soil Dynamics and Earthquake Engineering*, 67:102–118, 2014.

D. P. Connolly, P. Alves Costa, G. Kouroussis, P. Galvin, P. K. Woodward, and O. Laghrouche. Large scale international testing of railway ground vibrations across Europe. *Soil Dynamics and Earthquake Engineering*, 71:1–12, 2015.

X. Cui, N. Zhang, J. Zhang, and Z. Gao. In situ tests simulating traffic-load-induced settlement of alluvial silt subsoil. *Soil Dynamics and Earthquake Engineering*, 58:10–20, 2014.

B. Das. *Principles of Foundation Engineering*. Seventh Edition, 2007.

Department of Transport. Transport and Environment Statistics 2021 Annual report. Technical Report May, 2021.

S. E. Dickenson. *Dynamic response of soft and deep cohesive soils during the Loma Prieta Earthquake of October 17, 1989*. PhD thesis, 1994.

N. Doyle. *Railway Track Design - A review of current practice*. Australian Government Publishing Service, 1980.

E. C. Drumm, J. S. Reeves, M. R. Madgett, and W. D. Trolinger. Subgrade Resilient Modulus Correction for Saturation Effects. *Journal of Geotechnical and Geoenvironmental Engineering*, 123(7):663–670, 1997.

J. Duncan and S. G. Wright. *Soil Strength and Slope Stability*. 2005.

J. Eisenmann. Germans gain a better understanding of track structure. *Railway Gazette International*, 128(8), 1972. ISSN 0373-5346.

A. Erken and B. M. Can Ulker. Effect of cyclic loading on monotonic shear strength of fine-grained soils. *Engineering Geology*, 89(3-4):243–257, 2007.

C. Esveld. *Modern Railway Track*. MRT Productions, Zaltbommel, 2nd Edition, 2001. ISBN 9080032433.

S. Fan. Analysis on experiment of dynamic response in ballastless track subgrade of high speed rail- way. *China: Southwest Jiaotong University*, 9, 2010.

W. Q. Feng, B. Lalit, Z. Y. Yin, and J. H. Yin. Long-term Non-linear creep and swelling behavior of Hong Kong marine deposits in oedometer condition. *Computers and Geotechnics*, 84:1–15, 2017.

A. Forster, P. R. N. Hobbs, A. C. Cripps, C. D. Entwistle, S. M. M. Fenwick, M. R. Raines, J. R. Hallalll, L. D. Jones, S. J. Self, and J. L. Meakin. Technical Report WN/94/31 Engineering geology of British rocks and soils. Technical report, 1994.

J. W. France and D. A. Sangrey. Effects of Drainage in Repeated Loading of Clays. *Journal of the Geotechnical Engineering Division*, 103(7):769–785, 1977.

C. Fredrick and S. Newton. The relationship between traffic and track damage - The effect of vertical loads. Technical report, British Broad Research and Development Division, London, 1977.

M. W. Frost, P. R. Fleming, and C. D. F. Rogers. Cyclic triaxial tests on clay subgrades for analytical pavement design. *Journal of Transportation Engineering*, 130(GEOBASE):378–386, 2004.

L. Fu, J. Zhou, W. Wang, and J. Wang. A Double-layered Model for Highway Subgrade and its Dynamic Response due to Traffic Loads. *Procedia Engineering*, 143:795–802, 2016.

K. Fujikawa, N. Miura, and I. Beppu. Field Investigation on the Settlement of Low Embankment due to Traffic Load and Its Prediction. *Soils and Foundations*, 36(4):147–153, 1996.

H. Fujiwara and S. Ue. Effect of preloading on post-construction consolidation settlement of soft clay subjected to repeated loading. *Soils and foundations*, 30 (1):76–86, 1990.

C. Garrett and S. J. Barnes. The design and performance of the Dunton Green retaining wall. *Géotechnique*, 34(4):533–548, 1984.

A. Gluchowski and W. Sas. Impact of cyclic loading on shakedown in cohesive soils-simple hysteresis loop model. *Applied Sciences (Switzerland)*, 10(6), 2020.

P. Grabe. Effects of principal stress rotation on permanent deformation in rail track foundations. *Journal of Geotechnical and Geoenvironmental Engineering*, 135(4):555 – 565, 2009.

J. Graham and G. Houlsby. Anisotropic elasticity of a natural clay. *Géotechnique*, 33(2):165–180, 1983.

C. Gu, J. Wang, Y. Cai, Z. Yang, and Y. Gao. Undrained cyclic triaxial behavior of saturated clays under variable confining pressure. *Soil Dynamics and Earthquake Engineering*, 40:118–128, 2012.

C. Gu, Z. Gu, Y. Cai, J. Wang, and D. Ling. Dynamic modulus characteristics of saturated clays under variable confining pressure. 7(December):1–7, 2016.

D. A. Gunn and L. M. Nelder. Geophysical Monitoring of the Subgrade With Examples From Leominster. (McAnaw 2001), 2004.

L. Guo, J. Wang, Y. Cai, H. Liu, Y. Gao, and H. Sun. Undrained deformation behavior of saturated soft clay under long-term cyclic loading. *Soil Dynamics and Earthquake Engineering*, 50:28–37, 2013.

L. Guo, Y. Cai, R. J. Jardine, Z. Yang, and J. Wang. Undrained behaviour of intact soft clay under cyclic paths that match vehicle loading conditions. *Canadian Geotechnical Journal*, 55(1):90–106, 2018.

L. Guo, H. Jin, J. Wang, and L. Shi. Undrained monotonic shear behavior of marine soft clay after long-term cyclic loading. *Marine Georesources and Geotechnology*, 38(7):854–866, 2020.

A. M. Hanna and K. Javed. Design of Foundations on Sensitive Champlain Clay Subjected to Cyclic Loading. *Journal of Geotechnical and Geoenvironmental Engineering*, 134(7):929–937, 2008.

G. He. *Laboratory test and research on the settlement of soft foundation under low embankment considering the influence of traffic load.* PhD thesis, 2005.

D. Heath, J. Waters, M. Shenton, and R. Sparrow. DESIGN OF CONVENTIONAL RAIL TRACK FOUNDATIONS. *Proceedings of the Institution of Civil Engineers*, 51(2):251–267, 1972.

M. T. Hendry, C. D. Martin, and S. L. Barbour. Measurement of cyclic response of railway embankments and underlying soft peat foundations to heavy axle loads. *Canadian Geotechnical Journal*, 50(5):467–480, 2013.

K. Hirao and K. Yasuhara. Cyclic strength of underconsolidated clay. *Soils and Foundations*, 31(4):180–186, 1991.

G. Holm, B. Andréasson, P.-E. Bengtsson, A. Bodare, and H. Eriksson. Mitigation of track and ground vibrations by high speed trains at Ledsgard, Sweden. *Swedish Deep Stabilization Research Centre, Report*, 10:58, 2002.

R. Hosseini Kamal. Experimental Study of the Geotechnical Properties of UK Mudrocks. 2012.

B. Hough. *Basic soils engineering*. The Ronald Press Company, New York, 1st Edition, 1957.

C.-C. Hsu and M. Vucetic. Threshold Shear Strain for Cyclic Pore-Water Pressure in Cohesive Soils. *Journal of Geotechnical and Geoenvironmental Engineering*, 132 (10):1325–1335, 2006.

Y.-Y. Hu. Long-term settlement of soft subsoil clay under rectangular or semi-sinusoidal repeated loading of low amplitude. *Canadian Geotechnical Journal*, 47(11):1259–1270, 2010.

J. Huang, J. Chen, Y. Lu, S. Yi, H. Cheng, and L. Cui. Deformation Behaviors and Dynamic Backbone Curve Model of Saturated Soft Clay under Bidirectional Cyclic Loading. *International Journal of Geomechanics*, 20(4), 2020.

M. Huang, J. Li, and X. Li. Cumulative deformation behavior of soft clay in cyclic undrained test. *Chinese Journal of Geotechnical Engineering (in Chinese)*, 28(4):891–895, 2006.

A. F. Hyde, T. Higuchi, and K. Yasuhara. Postcyclic Recompression, Stiffness, and Consolidated Cyclic Strength of Silt. *Journal of Geotechnical and Geoenvironmental Engineering*, 133(4):416–423, 2007.

A. F. L. Hyde. *Repeated load triaxial testing of soils*. PhD thesis, University of Nottingham, 1974.

A. F. L. Hyde and S. J. Ward. A pore pressure and stability model for a silty clay under repeated loading. *Géotechnique*, 35(2):113–125, 1985.

B. A. F. L. Hyde, K. Yasuhara, and K. Hirao. One-Way Cyclic Loading. 119 (2904):1771–1789, 1994.

W. F. L. Hyde and S. F. Brown. The plastic deformation of a silty clay under creep and repeated loading. *Géotechnique*, 26(1):173–184, 1976.

M. Hyodo and K. Yasuhara. Analytical procedure for evaluating pore-water pressure and deformation of saturated clay ground subjected to traffic loads. In *Proceedings of the 6th International Conference on Numerical Methods in Geomechanics*, pages 653–658, Innsbruck, Austria, 1988.

M. Hyodo, K. Yasuhara, and K. Hirao. Prediction of clay behaviour in undrained and partially drained cyclic triaxial tests. *Soils and foundations*, 32(4):117–127, 1992.

Hyodo M., A. Hyde, Y. Yamamoto, and T. Fujii. Cyclic shear strength of undisturbed and remoulded marine clays. *Soils and Foundations*, 39(2):45–58, 1999.

I. M. Idriss, R. Dobry, and R. D. Singh. Nonlinear behaviour of soft clays during cyclic loading. *ASCE J Geotech Eng Div*, 104(12):1427 – 1447, 1978.

B. Indraratna, S. Nimbalkar, D. Christie, C. Rujikiatkamjorn, and J. Vinod. Field Assessment of the Performance of a Ballasted Rail Track with and without Geosynthetics. *Journal of Geotechnical and Geoenvironmental Engineering*, 136(7): 907–917, 2010.

B. Indraratna, J. Ni, C. Rujikiatkamjorn, and R. Zhong. A partially drained model for soft soils under cyclic loading considering cyclic parameter degradation. *Australian Geomechanics Journal*, 50(4):89–95, 2015.

B. Indraratna, T. Ngo, F. B. Ferreira, C. Rujikiatkamjorn, and A. Tucho. Large-scale testing facility for heavy haul track. *Transportation Geotechnics*, 28: 100517, 2021.

K. Ishihara and S. Yasuda. Cyclic Strength of Undisturbed Cohesive Soils of Wesiern Tokyo. In *Int. Sym. On Soils under Cyclic and Transient Loading*, pages 57 – 66, Swansea, 1980.

T. Ishikawa, E. Sekine, and S. Miura. Cyclic deformation of granular material subjected to moving-wheel loads. *Canadian Geotechnical Journal*, 48(5):691–703, 2011.

V. K. Jain and M. Dixit. Correlation of Plasticity Index and Compression Index of Soil. 5(3):263–270.

M. Jamiolkowski, C. C. Ladd, J. T. Germaine, and R. Lancellotta. New developments in field and laboratory testing of soils, 1985.

H. Jiang, X. Bian, C. Cheng, Y. Chen, and R. Chen. Simulating train moving loads in physical model testing of railway infrastructure and its numerical calibration. *Acta Geotechnica*, (11):231–242, 2016.

M. Karstunen and Z.-Y. Yin. Modelling time-dependent behaviour of Murro test embankment. *Géotechnique*, 60(10):735–749, 2010.

G. P. Karunaratne, S. H. Chew, S. L. Lee, and A. N. Sinha. Bentonite-Kaolinite Mix For GCLs, nov 2000.

H. J. Kim, K. H. Lee, J. C. Jamin, and J. L. C. Mission. Stochastic cost optimization of ground improvement with prefabricated vertical drains and surcharge preloading. *Geomechanics and Engineering*, 7(5):525–537, 2014.

K. Knight and G. E. Blight. Studies of some effects resulting from the unloading of soils. In *Proc. 6th International Conference on Soil Mechanics and Foundation Engineering, Montreal, Canada*, pages 103–107, 1965.

S. D. Koppula. Statistical estimation of compression index. *Geotechnical Testing*, 4(2):68 – 73, 1981.

L. Korkiala-Tanttu. Verification of rutting calculation for unbound road materials. *Proceedings of the Institution of Civil Engineers - Transport*, 162(2): 107–114, 2009.

G. Kouroussis, O. Verlinden, and C. Conti. Free field vibrations caused by high-speed lines: Measurement and time domain simulation. *Soil Dynamics and Earthquake Engineering*, 31(4):692–707, 2011.

V. V. Krylov. On the theory of railway-induced ground vibrations. *Journal De Physique*, 4(5 pt 2):769–772, 1994.

C. Ladd and D. DeGroot. Recommended practice for Casagrande, soft ground site characterization: Arthur Lecture. In *12th Panamerican Conference on Soil Mechanics and Geotechnical Engineering, MIT, USA*, 2003.

C. Ladd, R. Foot, K. Ishihara, F. Schlosser, and H. Poulos. Stress-deformation and strength characteristics. In *Proceedings of the 9th International Conference on Soil Mechanics and Foundation Engineering*, pages 421 – 494, Tokyo, 1977. Japanese Society of Soil Mechanics and Foundation Engineering,.

R. S. Ladd, R. Dobry, P. Dutko, F. Y. Yokel, and T. M. Chung. Pore-Water Pressure Buildup in Clean Sands Because of Cyclic Straining. *ASTM International, American Society for Testing and Materials*, 12(1):77–86, 1989.

T. Lambe and R. Whitman. *Soil Mechanics*. Wiley, New York, 1969.

H. Larew and G. Leonards. A repeated load strength criterion. *Proc. Highway Research Board*, 41:529–556, 1962.

R. Larsson and M. Mulabdic. Piezocone tests in clay. *Sgi Report*, (42):240, 1991.

A. Le Kouby, E. Bourgeois, and F. Rocher-Lacoste. Subgrade improvement method for existing railway lines - an experimental and numerical study. *Electronic Journal of Geotechnical Engineering*, 15 :1–34, 2010.

G. Lefebvre and D. LeBoeuf. Rate Effects and Cyclic Loading of Sensitive Clays. *Journal of Geotechnical Engineering*, 113(5):476–489, 1987.

G. Lefebvre and P. Pfendler. Strain Rate and Preshear Effects in Cyclic Resistance of Soft Clay. *Journal of Geotechnical Engineering*, 122(1), 1996.

H. Lei, B. Li, H. Lu, and Q. Ren. Dynamic Deformation Behavior and Cyclic Degradation of Ultrasoft Soil under Cyclic Loading. *Journal of Materials in Civil Engineering*, 28(11):04016135, 2016.

F. Lekarp, U. Isacsson, and A. Dawson. State of the Art. II: Permanent Strain Response of Unbound Aggregates. *Journal of Transportation Engineering*, 126 (1):76–83, 2000.

S. Leroueil. The isotache approach . Where are we 50 years after its development by Professor Šuklje ? (2006 Prof . Šuklje ' s Memorial Lecture). *13th Danube-European Conference on Geotechnical Engineering*, pages 13–46, 2006.

S. Leroueil, M. Kabbaj, F. Tavenas, and R. Bouchard. Stress–strain–strain rate relation for the compressibility of sensitive natural clays. *Géotechnique*, 35(2): 159–180, 1985.

D. Li and E. T. Selig. Cumulative plastic deformation for fine-grained subgrade soils. *Journal of Geotechnical Engineering*, 122(12):1006–1013, 1996.

L.-L. Li, H.-B. Dan, and L.-Z. Wang. Undrained behavior of natural marine clay under cyclic loading. *Ocean Engineering*, 38(16):1792–1805, nov 2011.

B. Lichtberger. *Track Compendium*. 2005.

J. Ling, W. Wang, and H. Wu. On residual deformation of saturated clay subgrade under vehicle load. *Journal - Tongji University*, 30(11):1315–1320, 2002.

X. Ling, P. Li, F. Zhang, Y. Zhao, Y. Li, and L. An. Permanent Deformation Characteristics of Coarse Grained Subgrade Soils under Train-Induced Repeated Load. *Advances in Materials Science and Engineering*, 2017.

G. Liu, M. Luan, X. Tang, Z. Wang, and Y. Guo. Critical cyclic stress ratio of undisturbed saturated soft clay in the yangtze estuary under complex stress conditions. *Transactions of Tianjin University*, 16(4):295–303, 2010.

J. Liu and J. Xiao. Experimental Study on the Stability of Railroad Silt Subgrade with Increasing Train Speed. *Journal of Geotechnical and Geoenvironmental Engineering*, 136(6):833–841, 2010.

S. Liu, H. S. Yu, J. Wang, and D. Wanatowski. Shakedown for slab track substructures with stiffness variation. *Geotechnical Research*, 5(1):31–38, 2018.

T. Liu, Y. Pei, and Q. Su. Field experimental study on the dynamic response of CRTS-I ballastless track subgrade of the Shanghai-Nanjing intercity high-speed railway during operation period. *IOP Conference Series: Earth and Environmental Science*, 508(1), 2020.

Z. Liu, J. Xue, and M. Yaghoubi. The effects of unloading on undrained deformation of a kaolin clay under cyclic loading. *Soil Dynamics and Earthquake Engineering*, 140(August 2020):106434, 2021.

K. Y. Lo. The pore pressure strain relationship of normally consolidated undisturbed clay. *Canadian Geotechnical Journal*, 6, 1969.

S. C. Loach. Repeated Loading of Fine Grained Soils for Pavement Design, 1987.

M. R. Lodahl. *Influence of smectite content on the deformation behaviour of clay*. 2017. ISBN 9788775074099.

M. S. Löfman, L. K. Korkiala-tanttu, M. S. Löfman, and L. K. Korkiala-tanttu. Georisk : Assessment and Management of Risk for Engineered Systems and Geohazards Transformation models for the compressibility properties of Finnish clays using a multivariate database multivariate database. *Georisk*, 0 (0):1–17, 2021.

P. C. Lombard. Track structure-optimization of design. *Civil Engineering= Siviele Ingenieurswese*, 20(9):231–238, 1978. ISSN 1021-2000.

Y. Lu, J. Chen, J. Huang, L. Feng, S. Yu, J. Li, and C. Ma. Post-cyclic mechanical behaviors of undisturbed soft clay with different degrees of reconsolidation. *Applied Sciences (Switzerland)*, 11(16):1–19, 2021.

Z. Luo, C. S. Ku, and L. Bu. Probabilistic model for long-term deformation of subgrade soil in upgrading-speed railway lines. *International Journal of Pavement Research and Technology*, 4(1):34–40, 2011.

T. Matsui, T. Ito, and H. Ohara. Cyclic stress–strain history and shear characteristics of clay. *Journal of Geotechnical Engineering*, 106(10):1101 – 1120, 1980.

T. Matsui, M. Bahr, and N. Abe. Estimation of shear characteristics degradation and stress-strain relationship of saturated clays after cyclic loading. *Soils and Foundations*, 32(1):161–172, 1992.

T. Matsui, Y. Nabeshima, and M. El Mesmary. Degradation in Cyclic Shear Behavior and Soil Properties of Saturated Clays. In *Proceedings of the Ninth (1999) International Offshore and Polar Engineering Conference*, volume I, page 880653, Brest, France, 1999.

P. W. Mayne. Cam-clay predictions of undrained strength. *Journal of the Geotechnical Engineering Division Proceedings of the American Society of Civil Engineers ASCE*, 106:1219 – 1242, 1980.

P. W. Mayne and F. H. Kulhawy. Ko-OCR relationships in soil. *J. Geotech. Eng. Div., Am. Soc. Civ. Eng.*, 108(6):851 – 872, 1982.

Y. Meimon and P. Hicher. *Mechanical behaviour of clays under cyclic loading*. 1980.

G. Michas. Slab Track Systems for High-Speed Railways. *MSc Thesis*, page 95, 2012.

G. A. Miller, S. Y. Teh, D. Li, and M. M. Zaman. Cyclic Shear Strength of Soft Railroad Subgrade. *Journal of Geotechnical and Geoenvironmental Engineering*, 126(2):139–147, 2000.

J. K. Mitchell and K. Soga. *Fundamentals of Soil Behavior*. John Wiley & Sons Inc., New York, 2005.

K. Miura, S. Miura, and S. Toki. Deformation behavior of anisotropic dense sand under principal stress axes rotation. *Soils and foundations*, 26(1):36–52, 1986.

N. Miura and S. Hayashi. Problems of subsidence and their mitigation in Saga Plain , Japan. In *Land Subsidence (Proceedings of the Fifth International Symposium on Land Subsidence*, number 234, pages 463–469, The Hague, 1995. IAHS.

N. Miura, J. C. Chai, T. Hino, and S. Shimoyama. Depositional environment and geotechnical properties of soft deposit in Saga plain. *Ind. Geotech. J.*, 28 (2):121 – 146, 1998.

C. Monismith, N. Ogawa, and C. Freeme. Permanent deformation characteristics of subgrade soils due to repeated loading. *Transportation Research Record*, (537), 1975.

A. R. Mortezaie and M. Vucetic. Effect of Frequency and Vertical Stress on Cyclic Degradation and Pore Water Pressure in Clay in the NGI Simple Shear Device. *Journal of Geotechnical and Geoenvironmental Engineering*, 139(10):1727–1737, 2013.

G. Moses, S. Rao, and P. Rao. Undrained strength behaviour of a cemented marine clay under monotonic and cyclic loading. *Ocean Engineering*, 30(14): 1765–1789, 2003.

D. Nash and M. Brown. A Comparison of Four Elastic Visco-Plastic Models for Soft Clay. *Constitutive Modeling of Geomaterials*, (1):121–124, 2013.

D. Nash, M. Lings, and C. Ng. Observed heave and swelling beneath a deep excavation in Gault clay. *Geotechnical Aspects of Underground Construction in Soft Ground*, pages 191–196, 1996.

NGI. Sustained Performance of Railway Tracks. Technical Report December, 2005.

J. Ni. *Application of geosynthetic vertical drains under cyclic loads in stabilizing tracks*. PhD thesis, University of Wollongong, 2012.

R.-s. Nie, W.-m. Leng, Q. Yang, Y. F. Chen, and F. Xu. Comparison and evaluation of railway subgrade quality detection methods. *Proceedings of the Institution of Mechanical Engineers, Part F: Journal of Rail and Rapid Transit*, 232(2):1–13, 2016.

S. Ohara and H. Matsuda. Study on the settlement of saturated clay layer induced by cyclic shear. *Soils and Foundations*, 28(3):103–113, 1988.

D. V. Okur and A. Ansal. Stiffness degradation of natural fine grained soils during cyclic loading. *Soil Dynamics and Earthquake Engineering*, 27(9):843–854, 2007.

ORE. Stresses in Rails, Question D17, Stresses in the Rails, the Ballast and the Formation Resulting from Traffic Loads. Technical report, 1965.

M. P. O'Reilly, S. F. Brown, and R. F. Overy. Cyclic Loading of Silty Clay with Drainage Periods. *Journal of Geotechnical Engineering*, 117(2):354–362, 1991.

K. Pan, X. M. Liu, Z. X. Yang, R. J. Jardine, and Y. Q. Cai. Undrained Cyclic Response of K0–Consolidated Stiff Cretaceous Clay under Wheel Loading Conditions. *Journal of Geotechnical and Geoenvironmental Engineering*, 147(8): 04021078, 2021.

Pandrol UK. Leading the way for high speed rail. 2014.

R. H. Parry. Short-term slipping of a shallow excavation in Gault clay. *Proceedings - Institution of Civil Engineers, Part 1*, 84(April):337–353, 1988.

R. H. G. Parry. Triaxial Compression and Extension Tests on Remoulded Saturated Clay. *Geotechnique*, 10(4):166–180, 1960.

M. Paul, R. B. Sahu, and G. Banerjee. Undrained Pore Pressure Prediction in Clayey Soil under Cyclic Loading. *International Journal of Geomechanics*, 15(5): 04014082, 2015.

M. Paul, R. B. Sahu, and G. Banerjee. A generalized consolidation model under cyclic loading. *International Journal of Geotechnical Engineering*, 14(5):497–513, 2020.

J. L. Paute, P. Hornych, and J. P. Benaben. Repeated load triaxial testing of granular materials in the French Network of Laboratories des Ponts et Chaussees. 1996.

R. J. Pillai, R. G. Robinson, and A. Boominathan. Effect of Microfabric on Undrained Static and Cyclic Behavior of Kaolin Clay. *Journal of Geotechnical and Geoenvironmental Engineering*, 137(4):421–429, 2011. .

R. J. Pillai, K. M. Nazeeh, and R. G. Robinson. Post-Cyclic Behaviour of Clayey Soil. *Indian Geotechnical Journal*, 44(1):39–48, 2014.

W. Powrie, L. Yang, and C. Clayton. Stress changes in the ground below ballasted railway track during train passage. *Proceedings of the Instituiton of Mechanical Engineering, Part F, J, Rapid Rail Transit*, 221(2):247 – 261, 2007.

K. S. Prakasha and V. S. Chandrasekaran. Behavior of Marine Sand-Clay Mixtures under Static and Cyclic Triaxial Shear. *Journal of Geotechnical and Geoenvironmental Engineering*, 131(2):213–222, 2005.

R. H. Prause, H. C. Meacham, H. D. Harrison, T. G. John, and W. A. Glaeser. Assessment of design tools and criteria for urban rail track structures. *Urban Mass Transit Administration, Report No. UMTA-MA-06-0025-74-3*, page 1, 1974.

D. C. Procter and J. H. Khaffaf. Cyclic Triaxial Tests on Remoulded Clays. *Journal of Geotechnical Engineering*, 110(10):1431–1445, 1984.

J. G. Qian, Z. B. Du, and Z. Y. Yin. Cyclic degradation and non-coaxiality of soft clay subjected to pure rotation of principal stress directions. *Acta Geotechnica*, 13(4):943–959, 2018.

Y. Qiu and Z. Sun. Permanent Deformation of Subgrade Soils in Flexible Pavement. *Journal of Southwest Jiaotong University*, 35(2):116 – 120 (in Chinese), 2000.

G. Rossato, N. Ninis, and R. Jardine. On Stress-Strain and Strength Properties of Model Soils. In *XIII ICSMGE*, pages 389–392, 1994.

J. Sadeghi. Experimental Evaluation of Accuracy of Current Practices in Analysis and Design of Railway Track Sleepers. *Canadian Journal of Civil Engineering*, 35:881 – 893, 2008.

J. Sadeghi and P. Barati. Evaluation of conventional methods in Analysis and Design of Railway Track System. *International Journal of Civil Engineering*, 8(1), 2010.

A. Sakai, L. Samang, and N. Miura. Partially-Drained Cyclic Behavior and Its Application to the Settlement of a Low Embankment Road on Silty-Clay. *Soils and Foundations*, 43(1):33–46, 2003.

L. Samang, N. Miura, and A. Sakai. Long-term Measurements of Traffic Load Induced Settlement of Pavement Surface in Saga Airport Highway, Japan. *Jurnal Teknic Sipil*, 12(4):275–286, 2005.

D. A. Sangrey, D. J. Henkel, and M. I. Esrig. The effective stress response of a saturated clay soil to repeated loading. *Canadian Geotechnical Journal*, 6:241 – 252, 1969.

D. A. Sangrey, W. S. Pollard, and J. A. Egan. Errors associated with rate of undrained cyclic testing of clay soils. *ASTM Special Technical Publication No.654*, 1978.

A. N. Schofield. Original cam-clay. *International Conference on Soft Soil Engineering*, 259(November), 1993.

G. Schramm. Permanent way techniques and permanent way engineering. *Otto Elsner Verlargs gersellashaft Darmitadt*, pages 66–70, 1961.

H. Seed and R. McNeill. Soil deformation in normal compression and repeated loading test. *Highway Research Board Bulletin*, 141:44–53, 1956.

H. Seed, C. Chan, and C. Monismith. Effects of repeated loading on the strength and deformation of compacted clay. *Highway Research Board Proceedings*, 34: 541–558, 1955.

Siemens AG. High speed train set Velaro CRH3 for the Chinese Ministry of Railways (MOR). 2013.

Siemens AG. Eurostar e320 high-speed trains for Eurostar International Limited. 2016.

A. Singh and J. K. Mitchell. General stress-strain-time function for soils. *J. Soil Mech. Found. Div., ASCE*, 94(1):21–46, 1968.

A. Skempton and O. Jones. Notes on compressibility of clays. *Quarterly Journal of the Geological Society London*, 100(2):119 – 135, 1944.

H. Song, X. Bian, Y. Chen, and J. Jiang. An analytical approach for slab track vibration with train-track-ground coupling effect. *Proceedings of the 8th International Conference on Structural Dynamics, EURODYN 2011*, (July): 852–858, 2011.

S. Soralump and J. Prasomsri. Cyclic Pore Water Pressure Generation and Stiffness Degradation in Compacted Clays. *Journal of Geotechnical and Geoenvironmental Engineering*, 142(1):04015060, 2016.

J. Spross and S. Larsson. Probabilistic observational method for design of surcharges on vertical drains. *Geotechnique*, 71(3):226–238, 2021.

A. S. J. Suiker, E. T. Selig, and R. Frenkel. Static and Cyclic Triaxial Testing of Ballast and Subballast. *Journal of Geotechnical and Geoenvironmental Engineering*, 131(6):771–782, 2005.

L. Sun. Strain Accumulation in Soft Marine Clay due to One-Way Cyclic Load with Variable Confining Pressure. *Advances in Civil Engineering*, 2021, 2021.

L. Sun, C. Gu, and P. Wang. Effects of cyclic confining pressure on the deformation characteristics of natural soft clay. *Soil Dynamics and Earthquake Engineering*, 78:99–109, 2015a.

L. Sun, Y. qiang Cai, C. Gu, J. Wang, and L. Guo. Cyclic deformation behaviour of natural K 0-consolidated soft clay under different stress paths. *Journal of Central South University*, 22(12):4828–4836, 2015b.

Q. Sun, B. Indraratna, and S. Nimbalkar. An Elasto-plastic Method for Analysing the Deformation of the Railway Ballast. *Procedia Engineering*, 143:954–960, 2016.

Q. Sun, Y. Cai, J. Chu, Q. Dong, and J. Wang. Effect of variable confining pressure on cyclic behaviour of granular soil under triaxial tests. *Canadian Geotechnical Journal*, 54(6):1–10, 2017.

M. Tafili, T. Wichtmann, and T. Triantafyllidis. Experimental investigation and constitutive modeling of the behaviour of highly plastic Lower Rhine clay under monotonic and cyclic loading. 1410(October 2020):1396–1410, 2021.

T. Takeda, M. Sugiyama, M. Akaishi, and H. W. Chang. Secondary compression behavior in one-dimensional consolidation tests. *Journal of GeoEngineering*, 7 (2):53–58, 2012.

Y. Q. Tang, J. Zhou, S. Liu, P. Yang, and J. X. Wang. Test on cyclic creep behavior of mucky clay in Shanghai under step cyclic loading. *Environmental Earth Sciences*, 63(2):321–327, 2011.

K. Terzaghi and R. Peck. *Soil mechanics in engineering practice*. 2nd Edition, 1967.

A. Thammathiwat and W. Chim-oye. Behavior of Strength and Pore Pressure of Soft Bangkok Clay under Cyclic Loading. *Thammasat International Journal of Science and Technology*, 9(4):21–28, 2004.

S. Y. Thian and C. Y. Lee. Cyclic stress-controlled tests on offshore clay. *Journal of Rock Mechanics and Geotechnical Engineering*, 9(2):376–381, 2017.

G. R. Thiers and H. B. Seed. Strength and Stress-Strain Characteristics of Clays Subjected to Seismic Loading Conditions. In A. S. f. T. and Materials, editor, *ASTM Special Technical Publication 450, Vibration Effects of Earthquakes on Soils and Foundations: A Symposium*, pages 3–56, San Francisco, California, 1968.

Z.-X. Tong, J.-M. Zhang, Y.-L. Yu, and G. Zhang. Drained Deformation Behavior of Anisotropic Sands during Cyclic Rotation of Principal Stress Axes. *Journal of Geotechnical and Geoenvironmental Engineering*, 136(11):1509–1518, 2010. .

UIC. Technical specification for the supply track support: rail, wooden, steel and concrete sleepers, broad-guage track and crossings. Technical report, 2004.

P. Ullditz. Mathematical model for pavement performance under moving wheel load. *Transp. Res. Rec. No. 1384, National Research Council, Transportation Research Board, Washington, D. C.*, 1993.

P. J. Vardanega and M. D. Bolton. Stiffness of Clays and Silts: Normalizing Shear Modulus and Shear Strain. *Journal of Geotechnical and Geoenvironmental Engineering*, 139(9):1575–1589, 2013.

P. J. Vardanega, B. H. Lau, S. Y. Lam, S. K. Haigh, S. P. Madabhushi, M. D. Bolton, and P. W. Mayne. Discussion: Laboratory measurement of strength mobilisation in kaolin: Link to stress history. *Geotechnique Letters*, 3 (JAN/MAR):16–17, 2013.

E. A. Voznesensky and S. Nordal. Dynamic instability of clays: An energy approach. *Soil Dynamics and Earthquake Engineering*, 18(2):125–133, 1999.

M. Vucetic. Cyclic threshold strains in soils. *Journal of Geotechnical Engineering, ASCE*, 120(12):2208 – 2228, 1984.

M. Vucetic and R. Dobry. Degradation of Marine Clays under Cyclic Loading. *Journal of Geotechnical Engineering*, 114(2):133–149, 1988.

M. Vucetic and R. Dobry. Effect if soil plasticity on cyclic response. *Journal of Geotechnical Engineering*, 117(1):89–107, 1991.

J. Wang, L. Guo, Y. Cai, C. Xu, and C. Gu. Strain and pore pressure development on soft marine clay in triaxial tests with a large number of cycles. *Ocean Engineering*, 74:125–132, 2013.

S. Wang, R. Luna, and S. Onyejekwe. Postliquefaction behavior of low-plasticity silt at various degrees of reconsolidation. *Soil Dynamics and Earthquake Engineering*, 75:259–264, 2015.

Y. Wang, D. Wu, Y. Qiu, and D. Wang. Experimental investigation on cyclic deformation behavior of soft marine clay involved principal stress rotation. *Marine Georesources and Geotechnology*, 35(4):571–577, 2017.

Y. Wang, J. Lei, Y. Wang, and S. Li. Post-cyclic shear behavior of reconstituted marine silty clay with different degrees of reconsolidation. *Soil Dynamics and Earthquake Engineering*, 116:530–540, 2019.

Y. Wang, Y. Wan, E. Wan, X. Zhang, B. Zhang, and Y. Zhong. The pore pressure and deformation behavior of natural soft clay caused by long-term cyclic loads subjected to traffic loads. *Marine Georesources and Geotechnology*, 39(4): 398–407, 2021.

W. A. Weiler. Small-Strain Shear Modulus of Clay. 1988.

T. Wichtmann and T. Triantafyllidis. Monotonic and cyclic tests on kaolin: a database for the development, calibration and verification of constitutive models for cohesive soils with focus to cyclic loading. *Acta Geotechnica*, 13(5): 1103–1128, 2018.

T. Wichtmann, A. Niemunis, and T. Triantafyllidis. On the influence of the polarization and the shape of the strain loop on strain accumulation in sand under high-cyclic loading. *Soil Dynamics and Earthquake Engineering*, 27(1): 14–28, 2007.

R. F. Woldringh and B. M. New. Embankment design for high speed trains on soft soils. *Geotechnical Engineering for Transportation Infrastructure*, pages 1–10, 1999.

P. K. Woodward, J. Kennedy, O. Laghrouche, D. P. Connolly, and G. Medero. Study of railway track stiffness modification by polyurethane reinforcement of the ballast. *Transportation Geotechnics*, 1(4):214–224, 2014.

C. P. Wroth and D. M. Wood. The correlation of index properties with some basic engineering properties of soils. *Canadian Geotechnical Journal*, 15(2):137–145, 1978.

J. Xiao, C. H. Juang, K. Wei, and S. Xu. Effects of Principal Stress Rotation on the Cumulative Deformation of Normally Consolidated Soft Clay under Subway Traffic Loading. *Journal of Geotechnical and Geoenvironmental Engineering*, 140 (4):04013046, 2014.

J. Xiao, B. Wang, C. Liu, and Z. Yu. Influences of Subgrade Form and Ground Stiffness on Dynamic Responses of Railway Subgrade under Train Loading: Field Testing Case Study. *Procedia Engineering*, 143:1185–1192, 2016.

Q. Yang, Y. Tang, B. Yuan, and J. Zhou. Cyclic stress–strain behaviour of soft clay under traffic loading through hollow cylinder apparatus: effect of loading frequency. *Road Materials and Pavement Design*, 20(5):1026–1058, 2019.

K. Yasuhara and K. H. Andersen. Effect of cyclic loading on recompresion of overconsolidated clay. In *Proceedings of the 12th International Conference on Soil Mechanics and Foundation Engineering*, pages 485–488, 1989.

K. Yasuhara and N. Toyota. Effects of initial static shear stress on post-cyclic degradation of a plastic silt, 1997.

K. Yasuhara, K. Hirao, and S. Kato. Swelling-recompression and change in shear strength of a saturated clay due to rebound. In *Proc. Of 16th Annual Meeting, JSSMFE (in Japanese)*, pages 257 – 260, 1981.

K. Yasuhara, T. Yamanouchi, and K. Hirao. Cyclic Strength and Deformation of Normally Consolidated Clay. *Soils and Foundations*, 22(3):77–91, 1982.

K. Yasuhara, K. Hirao, and M. Hyodo. Partial-drained behaviour of clay under cyclic loading. In *Proceedings of the 6th International Conference on Numerical Methods in Geomechanics*, pages 659–664, Innsbruck, Austria, 1988.

K. Yasuhara, S. Murakami, B.-W. Song, S. Yokokawa, and A. F. L. Hyde. Postcyclic Degradation of Strength and Stiffness for Low Plasticity Silt. *Journal of Geotechnical and Geoenvironmental Engineering*, 129(8):756–769, 2003.

H. Yildirim and H. Erşan. Settlements under consecutive series of cyclic loading. *Soil Dynamics and Earthquake Engineering*, 27(6):577–585, 2007.

J.-H. Yin and J. Graham. Viscous–elastic–plastic modelling of one-dimensional time-dependent behaviour of clays. *Canadian Geotechnical Journal*, 26(2): 199–209, 1989.

J.-H. Yin and J. Graham. Viscous–elastic–plastic modelling of one-dimensional time-dependent behaviour of clays: Reply. *Canadian Geotechnical Journal*, 27 (2):262–265, 1990.

J.-H. Yin and J. Graham. Equivalent times and one-dimensional elastic viscoplastic modelling of time-dependent stress–strain behaviour of clays. *Canadian Geotechnical Journal*, 31(1):42–52, 1994.

Z. Y. Yin, C. S. Chang, M. Karstunen, and P. Y. Hicher. An anisotropic elastic-viscoplastic model for soft clays. *International Journal of Solids and Structures*, 47(5):665–677, 2010.

Z.-Y. Yin, M. Karstunen, C. S. Chang, M. Koskinen, and M. Lojander. Modeling Time-Dependent Behavior of Soft Sensitive Clay. *Journal of Geotechnical and Geoenvironmental Engineering*, 137(11):1103–1113, 2011.

Z.-Y. Yin, Q. Xu, and C. Yu. Elastic-Viscoplastic Modeling for Natural Soft Clays Considering Nonlinear Creep. *International Journal of Geomechanics*, 15(5):1–10, 2015.

M. Zergoun and Y. P. Vaid. Effective stress response of clay to undrained cyclic loading. *Canadian Geotechnical Journal*, 31(5):714–727, 1994.

W. Zhai and C. Zhao. Frontiers and challenges of sciences and technologies in modern railway engineering. *Journal of Southwest Jiaotong University*, 51(2): 645–660, 2014.

W. Zhai, K. Wang, Z. Chen, S. Zhu, C. Cai, and G. Liu. Full-scale multi-functional test platform for investigating mechanical performance of track–subgrade systems of high-speed railways. *Railway Engineering Science*, 28(3):213–231, 2020.

J. Zhou and X. Gong. Strain degradation of saturated clay under cyclic loading. *Canadian Geotechnical Journal*, 38(1):208–212, 2001.

Appendix A

Determination of Confining Stress of a Soil Element as a Result of Slab Track Structure Components, after Ni (2012)

Ni (2012) previously determined the vertical stress for soil elements beneath ballasted track, demonstrating a depth of 4m should be adopted in cyclic triaxial tests such that additional dynamic stress attenuation induced as a result of train passage could be neglected. Using the same principle for consideration of slab track structures, the vertical stress applied to the soil element under consideration, shown in Figure Figure 3.21. as A, comprises three components; the additional stress from the slab track, the underlying sub-base material and the embankment. The applied vertical stress can subsequently be calculated based on the principle of superposition and elastic theory by sectioning the embankment, sub-base and slab into the following components and calculating the influence factor, I for each section whereby the vertical stress experienced is determined based on the factored pressure a section contributes:

$$\sigma_z' = Ip$$

Assuming the embankment slopes are at a distance such that they do not influence the stress distribution as a result of the track and sub-base structure, the pressure of the slab track structure per metre width of track can be determined:

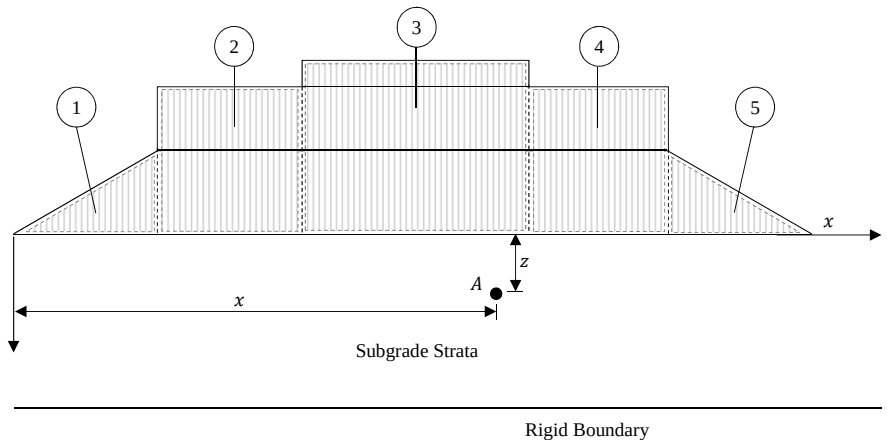

Figure A.1: Vertical stress components contributing to the vertical stress determination at point A

- The slab track comprises two components, the weight of the rail, defined as:

$$W_{rail}(\mathrm{N}) = 2 \times m_{rail}(\mathrm{kg/m}) \times g(\mathrm{m/s^2}) \times 1\mathrm{m} \tag{A.1}$$

The weight of the slab, defined as:

$$W_{slab}(\mathrm{N}) = \rho_{rail}(\mathrm{kg/m^3}) \times l_{slab}(\mathrm{m}) \times h_{slab}(\mathrm{m}) \times g(\mathrm{m/s^2}) \times 1\mathrm{m} \tag{A.2}$$

The total pressure due to the slab structure is therefore expressed as:

$$p_{slab}(\mathrm{kPa}) = \frac{W_{rail}(\mathrm{N}) + W_{slab}(\mathrm{N})}{l_{slab}(\mathrm{m}) \times 1\mathrm{m}} \tag{A.3}$$

- The sub-base comprises 5 sections, for Section 1 the pressure at the vertical edge is expressed as:

$$p_{SB1}(\mathrm{kPa}) = \rho_{LSB}(\mathrm{kg/m^3}) \times g(\mathrm{m/s^2}) \times H_{LSB}(\mathrm{m}) \tag{A.4}$$

For sections 2, 3 and 4, the pressure can be expressed as:

$$\begin{aligned} p_{SB2,3,4}(\mathrm{kPa}) = {} & (\rho_{LSB}(\mathrm{kg/m^3}) \times g(\mathrm{m/s^2}) \times H_{LSB}(\mathrm{m})) \\ & + (\rho_{USB}(\mathrm{kg/m^3}) \times g(\mathrm{m/s^2}) \times H_{USB}(\mathrm{m})) \end{aligned} \tag{A.5}$$

For section 5, the pressure at the vertical edge can be expressed as:

$$p_{SB5}(\text{kPa}) = \rho_{LSB}(\text{kg/m}^3) \times g(\text{m/s}^2) \times H_{LSB}(\text{m}) \tag{A.6}$$

- The additional vertical stress can be calculated:

$$\begin{aligned}\sigma'_{z,additional}(\text{kPa}) = {} & I_1\ p_{SB1}(\text{kPa}) + I_2\ p_{SB2}(\text{kPa}) \\ & + I_3\ (p_{SB13} + p_{slab})(\text{kPa}) + I_4\ p_{SB4}(\text{kPa}) + I_5\ p_{SB5}(\text{kPa})\end{aligned} \tag{A.7}$$

- The influence factors can be calculated as follows:

$$I_{SB1} = \frac{1}{\pi}\Big\{f_1\Big[\tan^{-1}\Big(\frac{f_1}{h_1}\Big) - \tan^{-1}\Big(\frac{f_1-1}{h_1}\Big)\Big] - \frac{(f_1-1)h_1}{(f_1-1)^2+(h_1)^2}\Big\}$$

$$\text{where } f_1 = \frac{x}{H_{LSB}\cot\delta} \text{ and } h_1 = \frac{z}{H_{LSB}\cot\delta} \tag{A.8}$$

$$I_{SB2} = \frac{1}{\pi}\Big\{\Big[\tan^{-1}\Big(\frac{f_2}{h_2}\Big) - \tan^{-1}\Big(\frac{f_2-1}{h_2}\Big)\Big] + \frac{f_2\,h_1}{f_2^2+h_2^2} - \frac{(f_2-1)h_2}{(f_2-1)^2+(h_2)^2}\Big\}$$

$$\text{where } f_2 = \frac{2(x - H_{LSB}\cot\delta)}{l_{SB}-l_{slab}} \text{ and } h_2 = \frac{2\,z}{l_{SB}-l_{slab}} \tag{A.9}$$

$$I_{SB3} = \frac{1}{\pi}\Big\{\Big[\tan^{-1}\Big(\frac{f_3}{h_3}\Big) - \tan^{-1}\Big(\frac{f_3-1}{h_3}\Big)\Big] + \frac{f_3\,h_3}{f_3^2+h_3^2} - \frac{(f_3-1)h_3}{(f_3-1)^2+(h_3)^2}\Big\}$$

$$\text{where } f_3 = \frac{2(x - H_{LSB}\cot\delta) - (l_{SB}-l_{slab})}{2\,l_{slab}} \text{ and } h_3 = \frac{z}{l_{slab}} \tag{A.10}$$

$$I_{SB4} = \frac{1}{\pi}\Big\{\Big[\tan^{-1}\Big(\frac{f_4}{h_4}\Big) - \tan^{-1}\Big(\frac{f_4-1}{h_4}\Big)\Big] + \frac{f_4\,h_4}{f_4^2+h_4^2} - \frac{(f_4-1)h_4}{(f_4-1)^2+(h_4)^2}\Big\}$$

$$\text{where } f_4 = \frac{2(x - H_{LSB}\cot\delta) - (l_{SB}+l_{slab})}{l_{SB}-l_{slab}} \text{ and } h_4 = \frac{2\,z}{l_{SB}-l_{slab}} \tag{A.11}$$

$$I_{SB5} = \frac{1}{\pi}\left\{ f_5 \left[\tan^{-1}\left(\frac{f_5}{h_5}\right) - \tan^{-1}\left(\frac{f_5 - 1}{h_5}\right)\right] - \frac{(f_5 - 1)h_5}{(f_5 - 1)^2 + (h_5)^2} \right\}$$

$$\text{where } f_5 = \frac{l_{SB} + 2\, H_{LSB} \cot\delta - x}{H_{LSB} \cot\delta} \text{ and } h_5 = \frac{z}{H_{LSB} \cot\delta} \tag{A.12}$$

- The total vertical stress experienced by soil element A at depth z is therefore:

$$\sigma'_z(\text{kPa}) = \gamma_{subgrade}(\text{kN/m}^3) \times z(\text{m}) \times \sigma'_{z,additional}(\text{kPa}) \tag{A.13}$$